Development of a Structural Fatigue Life Assessment Framework for High-Performance Naval Ships

by

Teresa Magoga, BEng (Aerospace)

National Centre for Maritime Engineering and Hydrodynamics

Australian Maritime College

Submitted in partial fulfilment of the requirements for the degree of Doctor of Philosophy

University of Tasmania

March 2019

[Page intentionally left blank]

Declarations

Authority of Access

The Commonwealth of Australia holds copyright of the papers comprising Chapters 2 and 4 to 8. Access to the material should be sought from the respective journals. The remaining non-published content of this thesis may be made available for loan and limited copying and communication in accordance with the Australian Copyright Act 1968.

Declaration of Originality

This thesis contains no material which has been accepted for a degree or diploma by the University or any other institution, except by way of background information and duly acknowledged in the thesis, and to the best of my knowledge and belief no material previously published or written by another person except where due acknowledgement is made in the text of the thesis, nor does the thesis contain any material that infringes copyright.

Signed: _____ Date: 29/3/2019

Statement of Co-authorship

The following people and institutions contributed to the publication of work undertaken as part of this thesis:

Candidate:	Ms Teresa Magoga	Australian Maritime College, University of Tasmania; Defence Science and Technology Group, Department of Defence, Australia
Author 1:	Dr Roberto Ojeda	Australian Maritime College, University of Tasmania
Author 2:	Dr Stuart Cannon	Australian Maritime College, University of Tasmania; Defence Science and Technology Group, Department of Defence, Australia
Author 3:	Prof Giles Thomas	University College London
Author 4:	Dr Seref Aksu	Defence Science and Technology Group, Department of Defence, Australia
Author 5:	Mr Karl Slater	Defence Science and Technology Group, Department of Defence, Australia
Author 6:	Mr Joshua Dawes-Lynch	QinetiQ Australia
Author 7:	Mr Michael Brincat	Defence Science and Technology Group, Department of Defence, Australia
Author 8:	Mr Dylan Dwyer	Defence Science and Technology Group, Department of Defence, Australia
Author 9:	Mr Brett Morris	Defence Science and Technology Group, Department of Defence, Australia

As part of this PhD investigation, the Candidate and the aforementioned authors produced peer-reviewed publications. The individual contributions to the work undertaken for each publication are detailed below:

1. Magoga, T., Aksu, S., Cannon, S., Ojeda, R., and Thomas, G., *The Need for Fatigue Life Prediction Methods Tailored to High-Speed Craft: A Technical Review*, in *Pacific 2015 International Maritime Conference*. 2015: Sydney, Australia.

The first publication is a conference paper that consists of a partial literature review that is also presented within Chapter 2 of the thesis. The Candidate was lead author and contributed 80% to the planning and execution of the research and resulting paper. Authors 1, 2, 3, and 4 contributed 5% each to the interpretation of the work and critical revision of the paper.

2. Magoga, T., Aksu, S., and Slater, K., *Proposed Implementation of Nominal Stress Approach for Fatigue Assessment of Aluminium Naval Ship Welded Details*. Part M: Journal of Engineering for the Maritime Environment, submitted for publication.

The second publication is presented within Chapter 4 of the thesis. The Candidate was lead author and contributed 85% to the planning and execution of the research and resulting paper. Authors 4 and 5 contributed 10% and 5%, respectively, to the interpretation of the work and critical revision of the paper.

3. Magoga, T., Aksu, S., Cannon, S., Ojeda, R., and Thomas, G., *Identification of Slam Events Experienced by a High-Speed Craft*. Ocean Engineering, 2017. 140: p. 309-321.

The third publication is presented within Chapter 5 of the thesis. The Candidate was lead author and contributed 80% to the planning and execution of the research and resulting paper. Authors 1, 2, 3, and 4 contributed 5% each to the interpretation of the work and critical revision of the paper.

4. Magoga, T., Aksu, S., Cannon, S., Ojeda, R., and Thomas, G.*, Comparison between Fatigue Life Values Calculated Using Standardised and Measured Stress Spectra of a Naval High Speed Light Craft*, in *13th International Symposium on the Practical Design of Ships and Other Floating Structures*. 2016: Copenhagen, Denmark.

The fourth publication is presented within Chapter 6 of the thesis. The Candidate was lead author and contributed 80% to the planning and execution of the research and resulting paper.

Authors 1, 2, 3, and 4 contributed 5% each to the interpretation of the work and critical revision of the paper.

5. Magoga, T., *Fatigue Damage Sensitivity Analysis of a Naval High Speed Light Craft via Spectral Fatigue Analysis*. Ships and Offshore Structures, submitted for publication.

The fifth publication is presented within Chapter 7 of the thesis. The Candidate was sole author of this paper.

6. Magoga, T., Aksu, S., Cannon, S., Ojeda, R., and Thomas, G., *Through-Life Hybrid Fatigue Assessment of Naval Ships*. Ships and Offshore Structures, published online 2019.

The sixth publication is presented within Chapter 8 of the thesis. The Candidate was lead author and contributed 80% to the planning and execution of the research and resulting paper. Authors 1, 2, 3, and 4 contributed 5% each to the interpretation of the work and critical revision of the paper.

7. Magoga, T., *Trials and Tribulations: Load and Structural Response Measurements of a Naval Semi-Planing Craft*, in Pacific 2017 International Maritime Conference. 2017, Sydney, Australia.

The seventh publication is presented within Appendix A of this thesis. The Candidate was sole author of this paper.

8. Dawes-Lynch, J. and Magoga, T., *HMAS Maryborough Hull Monitoring System: Data Processing and Analysis Methods*. 2017, Defence Science and Technology Group: Melbourne, Australia.

The eighth publication is presented within Appendix B of the thesis. The Candidate and Author 6 each contributed 50% to the report.

9. Magoga, T., Brincat, M., and Dawes-Lynch, J., *Verification of Pressure Sensors and Strain Gauges Installed Onboard HMAS Maryborough.* 2016, Defence Science and Technology Group: Melbourne, Australia.

The ninth publication is presented within Appendix C of the thesis. The Candidate, Author 6, and Author 7 each contributed one third to the report.

10. Magoga, T. and Dwyer, D., *Fatigue Life as a Variable in Assessing Naval Ship Flexibility*. Naval Engineers Journal, 2018. 130(3).

The tenth publication is presented within Appendix D of the thesis. The Candidate was lead author of this paper and contributed 60% to the planning and execution of the research and resulting paper, and the interpretation of the work. Author 8 contributed 40% to the planning and execution of the research and resulting paper, and the interpretation of the work.

11. Magoga, T. and Morris, B., *An Investigation into RAN Ship Structural Life-of-Type Management without Hull Monitoring Systems*. In review, DST-Group-TN-1826, Defence Science and Technology Group: Melbourne, Australia.

The eleventh publication is also presented within Appendix E of the thesis. The Candidate and Author 9 each contributed 50% to the report.

We the undersigned agree with the above stated 'proportion of the work undertaken' for each of the above publications that contribute to the thesis.

Signed: _____ Date: 26/3/19 Signed: _____ Date: 29/3/19

Dr Roberto Ojeda
Primary Supervisor
National Centre for Maritime
Engineering & Hydrodynamics
Australian Maritime College
University of Tasmania

Prof Shuhong Chai
Head of School
National Centre for Maritime
Engineering & Hydrodynamics
Australian Maritime College
University of Tasmania

Acknowledgements

My mum Faye Magoga and late dad Giordano Magoga taught me the value of hard-work. My sisters Angela and Lisa Magoga help me keep a sense of humour. My partner Johannes Straub is my rock.

I am grateful to Dr Roberto Ojeda, Dr Stuart Cannon, Prof Giles Thomas, and Dr Seref Aksu for their assistance during my candidature. I am also grateful to my colleagues from the Defence Science and Technology Group for their various contributions, from reviewing papers, showing me how to shunt-calibrate a strain gauge, and being a sounding board for my ideas and questions.

My PhD was supported by the Australian Defence Organisation. This research would not have been possible without the cooperation of the Royal Australian Navy and the Patrol Boat Program Systems Office.

Abstract

Navies around the world have been using High Speed Light Craft (HSLC) in a wider range of military roles and ocean environments than ever before. This increasing range of operations, use of lightweight scantlings, and susceptibility to slamming necessitates the development of improved structural fatigue assessment methods. These improved methods are required to ensure that a HSLC will meet its intended life, and to evaluate the impact of through-life modifications to the structure or operational profile.

This PhD thesis covers the development of an efficient structural fatigue life assessment framework for high-performance naval ships. The framework helps to inform risks through-life for decision-makers, by integrating real-world data and optimised tool selection.

The thesis begins with a critical review of available approaches to fatigue assessment and their associated merits and limitations when applied to naval aluminium HSLC. The review is followed by fatigue analyses of a naval HSLC using the different approaches, to establish their accuracy, fidelity, and expense. This part of the research includes the utilisation of full-scale measurements to quantify and explore the characteristics of slam events. The significant contribution of slamming to the fatigue damage is also demonstrated.

Though the S-N curve concept in fatigue analysis is commonly used in the maritime industry, there are diverse specifications for its use which leads to different fatigue life estimates. Therefore, a new implementation of the nominal stress approach to assess the fatigue life of different welded details on the naval HSLC is presented.

In the later stage of the thesis, a robust, easily implemented hybrid method for naval HSLC fatigue assessment is presented. The method uses a tailored combination of in-service data, fleet maintenance reports, and Finite Element Analysis to predict ongoing fatigue life and hence support the management of the remaining service life of a ship. The merit of the framework is demonstrated through the determination of the optimum approach to providing advice regarding the structural Life of Type (LOT) of naval HSLC for decision-makers. This includes identification of the variables that reduce the confidence limits of the LOT answer.

The impact of the research includes improved understanding of the uncertainties and interdependencies between the fatigue life and capability aspects of naval ships, and the establishment of an evidence-base for setting testable requirements for new ships to support both the fleet-in-being and naval shipbuilding.

Table of Contents

Chapter 1. Introduction **1**

1.1 General 1

1.2 Research Objective 4

1.3 Research Questions 4

1.4 Outcomes 5

1.5 Scope and Limitations 5

1.6 Thesis Organisation 7

Chapter 2. Need for Fatigue Life Prediction Methods Tailored to High-Speed Light Craft: A Technical Review **9**

2.1 Introduction 10

2.2 Loads and Structural Responses 10

2.3 Classification Societies' Rules 11

2.4 Fatigue Assessment Approaches 13

2.4.1 Applications 13

2.4.2 Challenges 15

2.5 What is Needed? 17

2.6 Conclusion 18

Where to Next? 19

Chapter 3. Materials and Methods **20**

3.1 Introduction 20

3.2 Armidale Class Patrol Boat 20

3.3 Hull Monitoring Systems 22

3.3.1 HMAS Glenelg HMS 22

3.3.2 HMAS Maryborough HMS 24

3.3.3 Signal Conditioning and Data Analysis 25

3.4 Fleet Maintenance Data 25

3.5 Finite Element Model 25

3.6 Cumulative Damage Theory 28

3.6.1 S-N Curve Concepts 29

3.7 Sources of Stress Spectra for Marine Structures 31

3.7.1 Simplified Fatigue Analysis 31

3.7.2 Spectral Fatigue Analysis 31
3.7.3 Rainflow Counting 32
3.8 Eurocode 9 33
Where to Next? 35

Chapter 4. Proposed Implementation of Nominal Stress Approach for Fatigue Assessment of Aluminium Naval Ship Welded Details 37
4.1 Introduction 38
4.2 Analysis and Results 39
4.2.1 Finite Element Analysis 40
4.3 Long-Term Stress Distributions 41
4.4 Fatigue Life Calculation 43
4.5 In-Service Experience – Maintenance Data 44
4.6 Sensitivity of Fatigue Life Calculation to S-N Curve and Stress Parameter 46
4.6.1 Stress Distributions at Structural Details of Interest (Step A) 48
4.6.2 Stress Range as a Function of Distance from Weld Seam/Intersection (Step B) 50
4.6.3 Eurocode 9 Details / S-N curves (Step C) 51
4.6.4 Comparison of Fatigue Life Values (Step D) 52
4.7 Discussion 54
4.8 Conclusion 56
Where to Next? 57

Chapter 5. Identification of Slam Events Experienced by a High-Speed Craft 58
5.1 Introduction 59
5.2 Hull Monitoring System 60
5.3 Decomposition of wave and whipping stress from total response 62
5.4 Importance of Slamming 67
5.5 Slam Identification 69
5.5.1 Stress Criterion 70
5.5.2 Stress Rate Criterion 71
5.5.3 Visual Inspection 72
5.5.4 Criterion Based on Fatigue Damage 75
5.5.5 Summary of Results 77
5.6 Discussion 77

5.7 Conclusion and Further Work 78
5.8 Acknowledgements 79
Where to Next? 79

Chapter 6. Comparison between Fatigue Life Values Calculated Using Standardised and Measured Stress Spectra of a Naval High Speed Light Craft 80
6.1 Introduction 81
6.2 Analysis 82
6.2.1 Sensitivity of Fatigue Life to Fitted Spectra 85
6.2.2 Sensitivity of Fatigue Life Estimation to Standardised Lifetime Spectra 86
6.2.3 Relationship between Fatigue Life and Design Loads 89
6.3 Discussion 90
6.4 Conclusion 91
Where to Next? 92

Chapter 7. Fatigue Damage Sensitivity Analysis of a Naval High Speed Light Craft via Spectral Fatigue Analysis 93
7.1 Introduction 94
7.2 Spectral Fatigue Analysis 95
7.2.1 Finite Element Model 96
7.3 HMAS *Maryborough* Sea Trials 97
7.3.1 Uncertainties 98
7.4 Validation of SFA 101
7.5 Sensitivity Analyses 105
7.5.1 Model Uncertainty Analysis 107
7.5.2 Sensitivity Analysis 108
7.6 Implications of Results 112
7.7 Conclusion 114
7.8 Acknowledgements 115
Where to Next? 115

Chapter 8. Through-Life Hybrid Fatigue Assessment of Naval Ships 116
8.1 Introduction 117
8.2 Proposed Through-Life Hybrid Fatigue Assessment Method 118

8.3 Application 120
8.3.1 Finite Element Analysis 120
8.3.2 Fleet Maintenance Data 120
8.3.3 Collection of Full-Scale Data and Derivation of Stress Spectra 120
8.3.4 Fatigue Life Estimation 122
8.3.5 Fatigue Life Results 122
8.3.6 Validation 123
8.3.7 Feedback to Platform Management 124
8.4 Discussion 125
8.5 Conclusion 127
Where to Next? 127

Chapter 9. Approach to Provide Advice Regarding Fatigue Life for Decision-makers 128
9.1 Introduction 128
9.2 Qualitative Analysis of Fatigue Life Evaluation Approaches 129
9.2.1 Data Review 130
9.2.2 Codification 130
9.2.3 Comparative Analysis 131
9.3 Quantitative Analysis of Fatigue Life Variables 134
9.3.1 Analysis of Maryborough HMS Data 135
9.3.2 Multi-Factorial Numerical Experiment Based on SFA Results 141
9.3.3 Sensitivity Analysis with Inclusion of Slam Correction 146
9.3.4 Discussion 147
9.4 Material Factors 150
9.5 Conclusion 151
9.6 Acknowledgements 153

Chapter 10. Main Conclusions and Further Work 154
10.1 Summary of Work Completed 154
10.2 Main Conclusions 155
10.3 Value Proposition 157
10.4 Further Work 158

Chapter 11. References 160

Appendix A 185
A.1 Recommendations 186

Appendix B 187

Appendix C 188

Appendix D 189

Appendix E 190
E.1 Integrated Platform Management System 191
E.2 Digital Twin 192

Appendix F Measurement Period for Fatigue Life Prediction 193

List of Figures

Figure 1-1: Comparison between Australian Defence CLC and Blanchard and Fabrycky's [10] Life Cycle 2
Figure 1-2: Activities that need to be performed to answer research questions 6
Figure 1-3: Schematic of mapping of chapters to research questions 7
Figure 2-1: Photograph of cracking on web frame of an aluminium HSLC 10
Figure 2-2: Wave-induced and whipping stress components [39] 10
Figure 2-3: A slam event experienced by an Armidale Class Patrol Boat – photograph on left shows bow emerging from water, and on right shows boat impacting water on re-entry [40] 11
Figure 3-1: Armidale Class Patrol Boat 20
Figure 3-2: Profile view of analysed strain gauge locations installed on HMAS *Glenelg* 23
Figure 3-3: Type and approximate locations of sensors comprising HMAS *Maryborough's* HMS 24
Figure 3-4: Global FE model of ACPB (origin located at transom, underside of keel, and centreline) 26
Figure 3-5: Fine mesh model containing welded detail of interest a) ID-1, b) ID-2, c) ID-3, d) ID-4, and e) ID-5 27
Figure 3-6: Schematic showing different stress types for fatigue analysis 29
Figure 3-7: Illustration of a) a stress time history, and b) rainflow counting of time history [121] 33
Figure 3-8: A generic Δσ-N curve as defined by Eurocode 9 [102] 34
Figure 4-1: Normalised vertical bending moment distributions of Wave Crest Landing and Wave Hollow Landing conditions 41
Figure 4-2: Approximate locations of strain gauges and details of interest in global FEA model 42
Figure 4-3: HMAS *Glenelg's* speed profile between August 2012 and February 2014 42
Figure 4-4: Derived normalised stress spectra at strain gauge locations 42
Figure 4-5: Histogram of ACPB fleet time at sea as a fraction of calendar time since commissioning 45
Figure 4-6: Example schematic of a pillar joined to an end plate, with stress concentration at top of pillar. Stresses are recovered at varying distances along length of pillar 47

Figure 4-7: Workflow for study on sensitivity of calculated fatigue life to S-N curve and derivation of stress parameter 47
Figure 4-8: Distribution of normal stress in y-direction under Wave Crest Landing condition at detail of interest ID-1 48
Figure 4-9: Distribution of normal stress in x-direction under Wave Crest Landing condition at detail of interest ID-2 48
Figure 4-10: Distribution of normal stress in x-direction under Wave Crest Landing condition at detail of interest ID-3 49
Figure 4-11: Distribution of normal stress under Wave Crest Landing condition at detail of interest ID-4 49
Figure 4-12: Distribution of normal stress in longitudinal direction under Wave Crest Landing condition at detail of interest ID-5 50
Figure 4-13: Stress range as a function of distance from intersection (d/t) between welded members for each welded detail of interest 50
Figure 4-14: FL_p/FL_m as a function of d/t at detail of interests a) ID-1, b) ID-2, c) ID-4, and d) ID-5 52
Figure 4-15: FL_p/FL_d as a function of d/t at detail of interest ID-3 53
Figure 5-1: Stress measured by strain gauge D, heading, and, vessel speed during Set 1, Set 2, and Set 3 61
Figure 5-2: Spectral density estimation of a one hour time record at strain gauge location D .. 62
Figure 5-3: Comparison of spectral density estimation during five different hours at strain gauge locations D, E, and F 63
Figure 5-4: Two-node mode shape of ACPB (scaled x1000) 63
Figure 5-5: Three-node mode shape of ACPB (scaled x1000) 63
Figure 5-6: RMS of difference between total and wave-induced stress (residual) at strain gauge location D 64
Figure 5-7: Sensitivity of wave-induced and whipping stresses to $\beta = 2$ and 11 ($F_c = \beta F_e$), for $F_e = 0.18$ Hz 65
Figure 5-8: Sample stress record from Set 1 hour 1 at strain gauge location D, E, and F 66
Figure 5-9: Hourly fatigue damage incurred at different strain gauge locations, estimated using total and wave-induced stress time records 68
Figure 5-10: Sample of slam detection using total stress rate threshold at strain gauge location A (peak of slam event depicted by cross) and whipping stress component 70

Figure 5-11: Sample of slam detection using stress magnitude threshold at strain gauge location D (peak and trough depicted by cross and asterisk) 71
Figure 5-12: Sample of slam detection using stress rate threshold at strain gauge location A (peak and trough depicted by cross and asterisk) 72
Figure 5-13: Histogram of wave-induced and total stress spectra at strain gauge location D during set 1 hour 1 76
Figure 5-14: No. slams detected at strain gauge location D using different approaches 77
Figure 6-1: Comparison of strain gauge A derived and assumed stress spectra 84
Figure 6-2: Comparison of strain gauge B derived and assumed stress spectra 84
Figure 6-3: Comparison of strain gauge C derived and assumed stress spectra 85
Figure 6-4: Standard stress range spectra given by GL 86
Figure 6-5: Standardised Linear and Convex stress range spectra, with n_{min} equal to 10^{0}, 10^{-2}, and 10^{-4} 87
Figure 6-6: $\Delta\sigma/\Delta\sigma_{design}$ versus n_i/N_i based on a) derived stress spectrum, and standardised linear spectra with n_{min} equal to b) 10^{0}, c) 10^{-2}, and d) 10^{-4}, at detail ID-1. Note y-axis scale of plot a differs from b, c and d 89
Figure 6-7: Relationship between FL based on standardised linear spectra and $\Delta\sigma_{design}$ at details ID-1, ID-2 and ID-3. Values of FL are normalised by that based on the derived spectrum, for each detail 90
Figure 7-1: Example fine mesh model (underside of aft main deck) in vicinity of a strain gauge. Positive x-direction is towards bow, positive z-direction is to starboard 97
Figure 7-2: Profile view of approximate locations of analysed strain gauges installed onboard HMAS *Maryborough* 98
Figure 7-3: $H_{1/3}$ versus computed σ_{RMS} with line of best fit at s.3.1.2, for v = 15 kn, χ = 180 deg, and T_z = 4 s 100
Figure 7-4: Comparison between calculated and measured spectral response at strain gauge s3.1.2 over four different conditions 102
Figure 7-5: Measured σ_{RMS} versus computed σ_{RMS} results, with linear model and line of exact agreement, at strain gauge locations (N_{runs} = 13). Note differing y-axis scales 104
Figure 7-6: HMAS *Maryborough* speed profile for speeds greater than 1 kn, over approximately 9200 hours 107
Figure 7-7: PDF, cumulative probability, and mean of D_i at strain gauge locations a) s3.1.2, and b) s6.4.2 107

Figure 7-8: μ_D and variance of μ_D as function of number of fatigue damage samples at strain gauge locations a) s3.1.2, and b) s6.4.2. Note differing y-axis scales..... 108
Figure 7-9: Relationship between fatigue damage and wave scatter, summed across the speed range, for equal distributions of all parameters at a) s3.1.2, and b) s6.4.2..... 111
Figure 7-10: Relationship between fatigue damage and wave scatter, summed across the speed range, for unique distributions of input parameters at a) s3.1.2, and b) s6.4.2 111
Figure 7-11: Polar plot of fatigue damage (radius) at T_z = 6.5 s and $H_{1/3}$ = 3.5 m at a) s3.1.2, and b) s6.4.2. Note differing radial axis scales 112
Figure 7-12: Polar plot of fatigue damage (radius) at T_z = 6.5 s and $H_{1/3}$ = 2.5 m at a) s3.1.2, and b) s6.4.2. Note differing radial axis scales 112
Figure 8-1: Process to estimate and update fatigue life 119
Figure 8-2: Normalised stress spectra derived from strain measurements (stress ranges at strain gauge A in vertical direction, and at B and C in longitudinal direction) 121
Figure 8-3: Comparison between fatigue damage at details of interest and respective reference locations..... 123
Figure 8-4: FL_p of details of interest, normalised by FL_p of detail ID-1..... 123
Figure 8-5: Difference between fatigue life values based on derived stress spectra and maintenance records as ratio of design fatigue life of patrol boat..... 124
Figure 8-6: Change in FL_p with change in K applied to reference stress spectra at detail of interest ID-1..... 124
Figure 9-1: Qualitative analysis process and inputs and outputs at each step..... 130
Figure 9-2: Schematic of hull cross-section showing *Maryborough* strain gauge locations listed in Table 9-4 137
Figure 9-3: Comparison between normalised speed histograms from 522 hour subset and 9200 hours (speed greater than 1 kn) 138
Figure 9-4: D_{total} at s3.1.2 versus N_{slam}, v_{ave}, $\Delta\sigma_{1/3}$ at s2A5.2, $\Delta\sigma_{1/3}$ at s3.1.2, D_{total} at s2A.5.2, and D_{total} at s3.1.2 over 522 hours in which *Maryborough* was at sea..... 140
Figure 9-5: Uniform, non-uniform1, and non-uniform2 heading distributions 142
Figure 9-6: Boxplot of fatigue damage versus wave scatter at s3.1.2 and s2.5.2 143
Figure 9-7: Boxplot of fatigue damage versus wave energy spectrum at s3.1.2 and s2.5.2 144
Figure 9-8: Boxplot of fatigue damage versus speed distribution at s3.1.2 and s2.5.2..... 144
Figure 9-9: Boxplot of fatigue damage versus heading distribution at s3.1.2 and s2.5.2 144
Figure 9-10: Comparison between histograms of D for *Maryborough* 'full' speed profile and Pierson-Moskowitz wave spectrum..... 144

Figure 9-11: Lower CI, mean, and upper CI (90%) of D for wave scatter, wave spectrum, and heading-speed distributions for s3.1.2 145
Figure 9-12: Lower CI, mean, and upper CI (90%) of D for wave scatter, wave spectrum, and heading-speed distributions for s2A.5.2 145
Figure 9-13: Scatter plot of v, χ, and $H_{1/3}$ with colourbar scaled by D. Unfilled circles denote samples without slam correction, and filled circles denote samples with slam correction 147
Figure 9-14: Number of slam events versus D_{total} at s3.1.2, grouped by trip, with two-term power curves of best fit 149
Figure 9-15: Number of slam events versus D_{wave} at s3.1.2, grouped by trip, with two-term power curves of best fit 149
Figure F-1: Annual distribution of *Glenelg* operational time over 3.5 year period [87] 194

List of Tables

Table 2-1: Review of Classification Society Rules on Fatigue Assessment for HSLC 12
Table 2-2: Application of fatigue assessment methods to HSLC 14
Table 2-3: Matrix of possible data available at different stages of a ship's CLC[v] 18
Table 3-1: Armidale Class Patrol Boat principal particulars 21
Table 3-2: Nominal material properties 21
Table 3-3: Requirements for patrol boat capability 21
Table 3-4: Description of strain gauge locations installed on HMAS *Glenelg* 24
Table 3-5: Eurocode 9 details [102] 36
Table 4-1: Description and figure of each detail of interest 40
Table 4-2: Reference strain gauges 43
Table 4-3: Fleet average FL_m at each detail of interest normalised by that of ID-1 45
Table 4-4: E9 details and their consistency with details of interest 51
Table 4-5: d/t at $FL_p/FL_m = 1$ for each detail of interest 54
Table 4-6: K_g, K_{te}, K, and FL_p/FL_M and FL_p/FL_M for each detail of interest 54
Table 5-1: Comparison of Computed and Measured Wet Mode Vibration Frequencies 64
Table 5-2: Detail categories of strain gauge locations 67
Table 5-3: Comparison of visual inspection, whipping stress magnitude, and whipping stress rate approaches to define slam events based on strain gauge D data 74
Table 5-4: Comparison of visual inspection, and the whipping stress rate approach to define slam events based on strain gauges B and C data from Set 3 75
Table 5-5: Number of half cycles in wave-induced and total stress spectra above fatigue limit at strain gauge location D 76
Table 6-1: Individual and aggregate coefficients of Linear, Gaussian and Weibull models, for each derived stress spectrum, based on stress cycles normalised by $\Delta\sigma_{design}$ 84
Table 6-2: Comparison between R^2 values of Linear, Gaussian and Weibull fits of stress spectra using individual and aggregate coefficients 84
Table 6-3: Fatigue life estimates using different stress spectrum models, normalised by fatigue life values based on derived spectra 85
Table 6-4: Percentage fatigue life based on standardised linear and convex spectra, relative to that based on derived spectra, for each detail of interest 87
Table 7-1: Approximate locations of analysed strain gauges on HMAS *Maryborough* 98

Table 7-2: Uncertainties related to data collected during sea trials 99
Table 7-3: Ratio between calculated and measured σ_{RMS} and D at s3.1.2 for four conditions 102
Table 7-4: Comparison of calculated and measured σ_{RMS} (N_{runs} = 13)..... 105
Table 7-5: Fatigue damage model input parameters 106
Table 7-6: Correlation coefficients between v, χ, $H_{1/3}$, T_z, $\Delta\sigma_L$, and D at s3.1.2 – input variables uniformly distributed 109
Table 7-7: Correlation coefficients between v, χ, $H_{1/3}$, T_z, $\Delta\sigma_L$, and D at s6.4.2 - input variables uniformly distributed..... 109
Table 7-8: Correlation coefficients between v, χ, $H_{1/3}$, T_z, $\Delta\sigma_L$, and D at s3.1.2 – input variables have unique probability distributions..... 110
Table 7-9: Correlation coefficients between v, χ, $H_{1/3}$, T_z, $\Delta\sigma_L$, and D at s6.4.2 - input variables have unique probability distributions 110
Table 7-10: Comparison of s3.1.2 and s6.4.2 as a 'fatigue meter' 114
Table 9-1: Identified key attributes of a fatigue analysis of a welded hull structure 131
Table 9-2: Comparison of extents that different approaches to fatigue life analysis achieve key attributes 132
Table 9-3: Known/definable variables in fatigue life prediction for each approach..... 135
Table 9-4: Analysed strain gauge locations on HMAS *Maryborough*..... 136
Table 9-5: D_{total} during monitoring period and period in which slamming occurred..... 136
Table 9-6: τ correlation coefficients between hourly N_{slam}, average vessel speed at instances of slams v_{slam}, slam severity, D_{wave}, and D_{total} at s3.1.2 (522 observations)..... 138
Table 9-7: p-values for results in Table 9-6 139
Table 9-8: Coefficients with confidence intervals for Equation 25 139
Table 9-9: Fatigue damage model input variables 142
Table 9-10: τ correlation coefficients between slam correction, v, χ, $H_{1/3}$, T_z and D at s3.1.2 147
Table 9-11: p-values of results in Table 9-10 147
Table 9-12: Coefficients and R^2 values for best fits of N_{slam} versus D_{total} and D_{wave} 150
Table 9-13: Summary of variables in fatigue analysis, and ways to obtain information to reduce related uncertainty 152
Table F-1: Factors in determining if full-scale dataset is sufficiently extensive to derive long-term stress distribution (for example case of HMAS *Glenelg*) 194

Abbreviations

2D	Two-dimensional
3D	Three-dimensional
ABS	American Bureau of Shipping
ACPB	Armidale Class Patrol Boat
ADF	Australian Defence Force
ADO	Australian Defence Organisation
AMC	Australian Maritime College
ASI	Aircraft Structural Integrity
ASIMP	Aircraft Structural Integrity Management Plan
ASIP	Aircraft Structural Integrity Program
BV	Bureau Veritas
CDT	Cumulative Damage Theory
CL	Centreline
CLC	Capability Life Cycle
CRS	Cooperative Research Ships
DNV	Det Norske Veritas
DRDC	Defence Research and Development Canada
DST	Defence Science and Technology
E9	Eurocode 9
FE	Finite Element
FEA	Finite Element Analysis
FFT	Finite Fourier Transform
FP	Forward Perpendicular
GL	Germanischer Lloyd
GLE	HMAS *Glenelg*
GPS	Global Positioning System
GSA	Global sensitivity analysis
HMAS	Her Majesty's Australian Ship
HMS	Hull Monitoring System
HSC	High Speed Craft
HSLC	High Speed Light Craft

IMO	International Maritime Organization
IQR	Interquartile Range
LOT	Life of Type
LR	Lloyd's Register
LSA	Local sensitivity analysis
MAR	HMAS *Maryborough*
MRU	Motion Reference Unit
NAW	Northern Australian Waters
NSP	Naval Shipbuilding Plan
OSI	Operating and Support Intent
PDF	Probability density function
P-W	Pierson-Moskowitz
RAN	Royal Australian Navy
RAO	Response Amplitude Operator
RC	Rainflow Counting
SEIO	South East Indian Ocean
SFA	Spectral Fatigue Analysis
S-N	Fatigue strength curve
SO	Southern Ocean
TTCP	The Technical Cooperation Program
US	United States
USN	United States Navy
UTAS	University of Tasmania

Nomenclature

$\bar{a}$	S-N curve parameter	
A	Fatigue crack growth rate material constant	
c_1	Coefficient of linear equation	
c_2	Coefficient of linear equation	
CV(RMSD)	Coefficient of variation of root mean square deviation	
d	Distance from joint intersection	[mm]
D	Fatigue damage	
e	Maximum misalignment between plates	
E	Modulus of Elasticity	[GPa]
e_0	Misalignment inherent in S-N data for butt welds	
e_t	Eccentricity due to change in thickness	
F_c	Cut-off frequency [Hz]	
F_e	Average encounter wave frequency	[Hz]
FL	Fatigue Life	[years]
FL_d	Design fatigue life	[years]
FL_m	Time from commissioning to discovery of first crack	[years]
FL_p	Predicted fatigue life	[years]
F_s	Sample rate [Hz]	
F_{valley}	Frequency of valley between first 2 peaks in a spectral response	[Hz]
G_1, G_3, G_3	Coefficients of Gaussian function	
$H_{1/3}$	Significant wave height	[m]
i	Sample	
k	Number of stress ranges	
K	Stress range ratio	
K_{gt}	Geometric stress concentration factor	
L_1, L_2	Coefficients of linear function	
L_{WL}	Waterline length	[m]
m	Inverse slope of S-N curve	
m_crack	Crack growth rate exponent	
m_{0ij}	Zero spectral moment of stress response process	
m_1	First S-N inverse slope gradient	

m_2	Second S-N inverse slope gradient	
N	Number of stress cycles to failure	
n	Number of stress cycles	
N_samples	Number of samples	
N_C	$2x10^6$ cycles	
N_D	$5x10^6$ cycles	
Ni	Predicted number of cycles to failure of a stress range $\Delta\sigma_i$	
N_L	10^8 cycles	
N_{load}	Number of load conditions	
n_{min}	Probability of exceedance of occurrence of maximum stress range	
N_{runs}	Number of trials runs	
p_n	Fraction of design life in load condition	
r	Pearson correlation coefficient	
R^2	Coefficient of determination	
r_{ij}	Number of stress cycles in short-term condition i,j	
RMS	Root mean square	
S_σ	Stress energy spectrum	
S_ζ	Wave energy spectrum	
SD	Standard deviation	
t	Thickness	[mm]
T_1	Mean centroid wave period	[s]
t_1	Thickness of thinner plate	[mm]
t_2	Thickness of thicker plate	[mm]
T_d	Design life in seconds	[s]
T_z	Wave period	[s]
v	Speed	[kn]
v_{ave}	Average speed	[kn]
W_1	Scale parameter of Weibull function, independent of exponent	
W_2	Scale parameter of Weibull function	
W_3	Shape parameter of Weibull function	

Γ	Gamma function	
χ	Ship heading relative to wave direction	[deg]
ω	Wave frequency	[rad/s]
α	Coefficient of power equation	
ϕ	Coefficient of power equation	
η	Coefficient of power equation	
ρ	Density	[kg/m^3]
τ	Kendall's rank correlation coefficient	
β	Multiplication factor	
ν	Poisson's ratio	
σ	Stress	[MPa]
$\Delta\sigma$	Stress range	[MPa]
ζ_α	Wave amplitude	[m]
$\Delta\sigma/S$	Stress range	[MPa]
$\Delta\sigma_L$	Fatigue limit	[MPa]
$\Delta\sigma_{max}$	Maximum stress cycle	[MPa]
$\Delta\sigma_R$	Reference fatigue stress	[MPa]
ν_0	Long-term average response zero-crossing frequency	[rad/s]
σ_{crest}	Stress under design crest landing condition	[MPa]
μ_D	Mean of total damage	[MPa]
σ_{hollow}	Stress under design hollow landing condition	[MPa]
σ_K	Stress intensity range	[MPa]
σ_{RMS}	Root mean square of stress	[MPa]
σ_{yield}	Yield strength	[MPa]
σ/σ_{allow}	Stress non-dimensionalised by allowable stress	
$\Delta\sigma_C$	Reference value of fatigue strength at $2x10^6$ cycles	
$\Delta\sigma_{design}$	Range between maximum and minimum stresses resulting from maximum and minimum relevant seaway induced loads	[MPa]
$\Delta\sigma_i$	Stress range in construction detail for n_i cycles	[MPa]
$\Delta\sigma_L$	Cut-off below which stress cycles are considered non-damaging	[MPa]

[Page intentionally left blank]

Chapter 1. Introduction

1.1 General

In recent years, the Governments of Australia, Canada and the United Kingdom have embarked upon enterprise approaches to naval shipbuilding [1-3]. Such approaches aim to build and sustain naval capabilities and maximise industry participation. The United States Navy (USN) is also planning for the most significant fleet size increase in over 30 years [4].

In the Australian Government's Naval Shipbuilding Plan (NSP) [1], the need for the Royal Australian Navy (RAN) to have operational flexibility to deal with evolving requirements was identified. In addition, the significant acquisition costs of naval ships and budgetary constraints necessitate the effective management of the structural Life of Type of the fleet-in-being to maintain maritime capability [5, 6].

Another objective of the NSP is the Continuous Shipbuilding Program, which involves management of the production tempo in a strategic manner and facilitation of the construction of warships in batches[i]. With each batch new technologies and systems are integrated into the original design as operational requirements evolve [7], and to permit improvements to the production process.

In 2018, the United States Government Accountability Office [4, p. 7] reported that 'Navy shipbuilding programs under construction during the last 10 years have often not achieved their cost, schedule, quality, and performance goals'. In Australia, the early decommissioning of HMAS *Manoora* and the unavailability of HMA Ships *Kanimbla* and *Tobruk* lead to the landmark Rizzo review [8]. The review determined that through-life approaches to managing the structural integrity of surface ships were needed. With naval shipbuilding ramping up around the world, and to ensure the operational availability of the current fleet, it is imperative that lessons learned from both domestic and international experience are implemented.

The life cycle of a major defence capability is comprised of different phrases. The Australian Defence Capability Life Cycle (CLC) [9] is shown in Figure 1-1. To contextualise

[i] An example of batch building is the production of the US Navy Arleigh Burke class of guided missile destroyers. The class is comprised of four flights: I, II, IIA, and III. The flights differ in length, displacement, and warfare suites.

the problem space for a wide audience, the CLC is compared to a generic life cycle after Blanchard and Fabrycky [10].

The phases of the Australian Defence CLC are:

- Strategy and Concepts - identification of capability needs that are informed by assessments of the ability to meet the Defence missions set out in strategic guidance.
- Risk Mitigation and Requirement Setting - the development and progression of capability options through the investment approval process. The outcome of this phase leads to a government approval to proceed to acquisition.
- Acquisition - executing a contract with industry to acquire the asset, and then introducing the capability into service.
- In-service and Disposal – through-life sustainment of the asset, withdrawal from service of the asset, and management of the transition to a replacement as required.

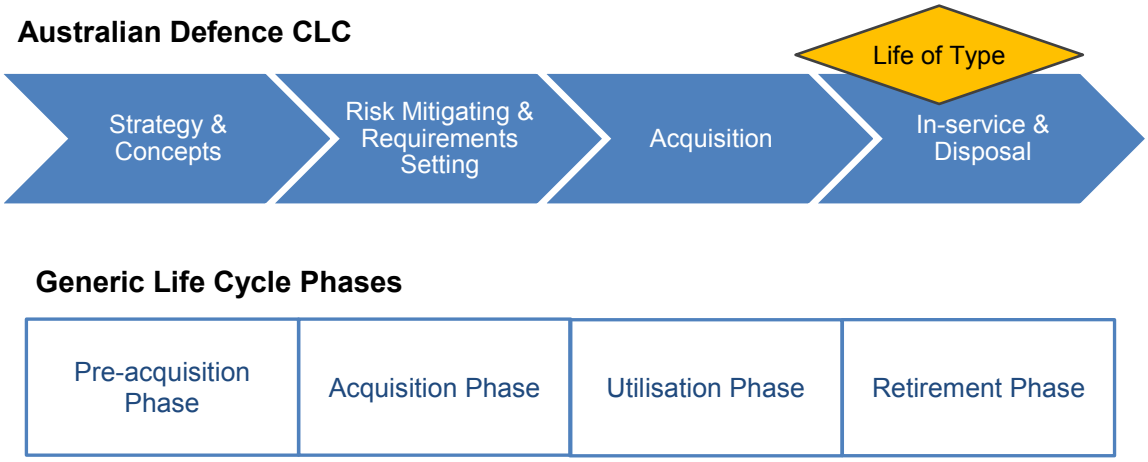

Figure 1-1: Comparison between Australian Defence CLC and Blanchard and Fabrycky's [10] Life Cycle

The Life of Type (LOT) of a capability describes how long it will remain in-service whilst being cost-effective, before it is required to be upgraded or replaced. A LOT review, which is a typical activity in the In-service & Disposal phase of the CLC, takes into account the resources needed to maintain the asset, the cost of replacement, changes in operational requirements, and obsolescence of parts and technology [9].

The LOT of a naval ship can be dictated by the structural fatigue life. Fatigue damage of a structure occurs under the exposure to numerous cycles of stress peaks and troughs. The fatigue damage accumulates until the load-bearing capacity of the structural item falls below the applied load. Sources of cyclic loads experienced by a ship structure include wave action,

inertial reactions from contents, hydrodynamic loads from appendages and propulsive devices, rotating machinery, and transient vibration induced by impact loads such as slamming [11].

Fatigue analysis is an important part of the structural design of weight-optimised ships as they are often constructed from aluminium alloys or high tensile steel. Due to the low fatigue strength of these metals the welded joints are vulnerable to fatigue cracking [12, 13]. Fatigue cracking of the structure can lead to costly repairs and reduction of availability of the ship. In addition, ship structural performance is one of several factors that is critical to the overall function and performance of a maritime mission or support system [14].

The LOT of a naval ship is often extended beyond the original design life [15-17]. Owing to operational requirements such as fast transport of troops and equipment and improved interception and apprehension capability, High Speed Light Craft (HSLC) are being increasingly used in naval applications [18, 19]. Fatigue damage to naval HSLC can be exacerbated by:

- The relatively low stiffness of the weight-optimised structural design and high wave encounter frequency due to the high operational speed [20].
- The increase in the typical vessel size, together with the requirement of increased operational roles suggesting exposure to increasingly harsher lifetime seaway loads [21].
- The applied loads can feature a high degree of non-linearity due to their hullform, operation in semi-planing or planing modes and their susceptibility to slamming. Slamming loads and associated responses of HSLC can have a significant impact on the stress magnitudes experienced in the structure and in turn the fatigue life [20, 22].

The motivation for this PhD is to improve the management of the operational availability of the current RAN fleet, and to support the requirement for operational flexibility of ships as identified in the NSP. Thus, the general question the thesis will answer is how stakeholders can better understand and manage uncertainties related to the different approaches to, and source and accuracy of variables in, the fatigue life analysis of naval HSLC.

This chapter introduces the research objective, over-arching questions, outcomes, scope, and organisation of the thesis.

1.2 Research Objective

The overarching objective of the present research project is:

> *To develop a framework for efficient structural fatigue life assessment of high-performance naval ships. The framework helps to inform risks through-life to stakeholders, by integrating real-world data and optimised tool selection.*

1.3 Research Questions

In order to achieve the research objective, the following research questions must be answered:

1. *Which available tools can be combined to progress structural LOT assessment of naval HSLC?*

   This question comprises identification of available methods to understand and predict the fatigue life of ship structures, and subsequent assessment of their applicability to HSLC.

2. *What are suitable enhancements to fatigue life assessment methods applied to naval HSLC?*

   Given that naval HSLC can experience a high degree of non-linear loads and flexure, fatigue life calculations are particularly sensitive to assumptions based on conventional ships. The source and accuracy of variables in fatigue assessment, use of measured strains versus computed stress, and detailed versus simplified load characterisation is a balance between the maturity of the method, available resources and data, and the need for accuracy. This implies that a balanced or hybrid approach that leverages the benefits of different methods and sources of data may be valid.

3. *What is the optimum approach to provide advice regarding the structural LOT of naval HSLC for decision-makers?*

   This question considers the availability and fidelity of available data, the level of uncertainty associated with a fatigue life answer, and how the uncertainty changes with different operational profiles and the stage in the CLC of the ship.

1.4 Outcomes

The outcomes of the research include:

1. Provision of evidence-based advice regarding the structural LOT of naval HSLC at the different stages of the CLC.
2. Improved management of the operational availability of the fleet.
3. Improved understanding of the structural performance of naval HSLC, to enable informed decision-making regarding operational and technology changes through-life.
4. Support to the Australian NSP.

The beneficiaries of the outcomes include Government, Navy as the owner and operator, classification societies, and maintenance providers.

1.5 Scope and Limitations

The activities that need to be performed to answer the research questions are listed in Figure 1-2. The activities are undertaken for the Royal Australian Navy (RAN) Armidale Class Patrol Boat (ACPB) described in Section 3.2. Although the research is focused on an in-service aluminium HSLC, most of the developed methods and knowledge gained are applicable to other current and future naval ships.

The objective of the thesis is to develop a framework for efficient structural fatigue life assessment. As stated by Hess *et al.* [16, p. 7], 'integrated approaches for future maritime design and operations … factoring in uncertainty, likelihood, reliability, consequence and risk can better inform the owner/operator of the asset's health and provide a route for managing that health efficiently and effectively.' Thus, stakeholder involvement is needed. In this regard, the S-N curve concept for fatigue analysis, rather than fracture mechanics, underpins the present research project. Fracture mechanics (discussed further in Section 3.6) allows detailed fatigue life analysis by taking into account the initial crack size, the crack size at failure, and the load sequence. However, it requires considerably more computational effort than the S-N curve concept and as such tends to be used for a limited number of structural locations [23]. In comparison, the S-N curve concept is widely accepted in the maritime industry [24-26]. Therefore, the use of fracture mechanics is outside of the scope of the PhD.

Although other material degradation effects, such as corrosion, metal sensitisation, the heat affected zone, and welding-induced plate and stiffener imperfections are important in ship structural integrity, incorporation of these factors to any meaningful degree would require effort that extends beyond the time constraints of the candidature. In addition, research on these

material degradation effects is prevalent in the literature (for example, refer to [27-32]). Similarly, ultimate strength and other limit states have been studied elsewhere (for example refer to [33-35]) and the related classification society rules are generally quite prescriptive.

Figure 1-2: Activities that need to be performed to answer research questions

Scale model testing is a popular method to inform loading predictions of different types of ships particularly in the design stages. However, questions about the usability of the results in structural assessment are raised from:

- For experiments conducted in regular waves – the extrapolation of the results to higher sea states, particularly for HSLC.
- For experiments conducted in irregular waves – the determination of the wave conditions to be tested (that is, knowledge of the likelihood that particular conditions will be encountered during the service life of the ship).

These concerns are avoided by using full scale data. Thus, model testing is not one of the project activities.

1.6 Thesis Organisation

This thesis is comprised of ten chapters mainly compiled from three published journal articles, two peer-reviewed conference papers, and one journal articles currently under review. The relevant publishing details are given at the beginning of each chapter. The chapters are mapped to the research questions as illustrated in Figure 1-3.

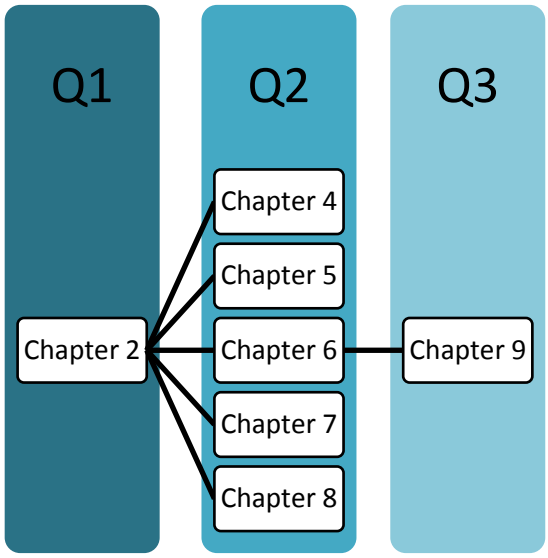

Figure 1-3: Schematic of mapping of chapters to research questions

The outline of the chapters is as follows:

- Chapter 2 presents a literature review concerning the general problem, which includes review of available approaches to fatigue assessment and their associated merits and limitations applied to naval HSLC. That is, the knowledge gaps and possible means to solve the research problem are identified.
- Chapter 3 discusses the materials and methods used in the research. In particular, the ACPB and acquisition of in-service information are described.
- Chapter 4 proposes efficient implementation of the S-N curve concept applied to real joints typical of naval HSLC.
- Chapter 5 establishes the significance of the contribution of slamming to the fatigue damage incurred on a naval HSLC, and proposes a method to detect slams.

- Chapter 6 investigates the applicability of simplified fatigue analysis (an industry approach) to naval HSLC.
- Chapter 7 presents an investigation into the sensitivity of the fatigue damage of a naval aluminium HSLC to various input parameters, using a spectral-based method that is partially validated against sea trials data.
- Chapter 8 proposes a new through-life hybrid fatigue assessment method that combines measured full-scale data, survey reports, and numerical tools in a practical manner. The method is applied to a naval HSLC to demonstrate its merit.
- Chapter 9 articulates the level of confidence associated with the accuracy/fidelity of fatigue analysis input parameters.
- Chapter 10 presents the main research conclusions and recommendations.

The appendices contain abstracts for supplementary publications, which present:

- Sea trials undertaken on a patrol boat (Appendix A).
- The approach to analyse full-scale data from a RAN vessel (Appendix B).
- The verification of sensors that were installed on-board a RAN vessel (Appendix C).
- Work towards improving understanding of the uncertainties and interdependencies between the fatigue life and capability aspects of naval ships (Appendix D).
- A preliminary study on the considerations, assumptions, and options for managing the structural LOT of new RAN ships (Appendix E).

In addition, the process used to determine if a set of data is long enough to appropriately quantify the distribution of stress ranges is elaborated in Appendix F.

Chapter 2. Need for Fatigue Life Prediction Methods Tailored to High-Speed Light Craft: A Technical Review

The work presented in this chapter was accepted in a peer-reviewed conference paper presented at the Pacific 2015 International Maritime Conference. The paper has been edited for inclusion into this thesis to avoid repetition and to improve readability. The citation is:

Magoga, T., Aksu, S., Cannon, S., Ojeda, R., and Thomas, G., *The Need for Fatigue Life Prediction Methods Tailored to High-Speed Craft: A Technical Review*, in *Pacific 2015 International Maritime Conference*. 2015: Sydney, Australia.

Chapter 2 has been removed for copyright or proprietary reasons.

Chapter 3. Materials and Methods

3.1 Introduction

In Chapter 2, it was determined that a hybrid approach to fatigue assessment of HSLC, which combines measured data, survey reports and numerical procedures, is worthy of investigation. The materials and methods used in the different steps of the investigation are described in the present chapter. The study platform is the Armidale Class Patrol Boat (ACPB), described in Section 3.2. Hull Monitoring Systems were implemented on two ACPBs. The systems, and signal conditioning and analysis of the collected data, are discussed in Section 0. Further in-service information is available in the form of hull survey reports (refer to Section 3.4). Finite Element (FE) modelling and stress analysis of the ACPB is performed throughout the investigation. The FE tool used and model are presented in Section 3.5. As the investigation is scoped to the use of Cumulative Damage Theory, which is described further in Section 3.6, it is necessary to obtain stress spectra (Section 3.7) and to select appropriate fatigue resistance data or S-N curves. The selected S-N curves are from the fatigue design code Eurocode 9, which is introduced in Section 3.8.

3.2 Armidale Class Patrol Boat

Fourteen ACPBs were commissioned into the RAN between June 2005 and February 2008. The youngest of class, HMAS *Glenelg*, is shown in Figure 3-1.

Figure 3-1: Armidale Class Patrol Boat

The ACPBs were designed and built by Austal Ships, Western Australia and classed by DNV to be compliant with High Speed, Light Craft and Naval Surface Craft rules [44] supplemented by naval technical regulatory and safety rules as required. They were designed using the allowable stress approach, and should maintain operations in Sea State 5 and to survive cyclonic conditions up to Sea State 9 [76]. The ACPBs feature a deep-vee, hard-chine, semi-planing hullform, as they can operate with a Froude number of 0.57 [77]. The principal particulars of the ACPB are given in Table 3-1.

Table 3-1: Armidale Class Patrol Boat principal particulars

Length overall	56.8 m
Beam overall	9.7 m
Draught	2.7 m
Displacement (standard)	300 t

The hull and superstructure of the patrol boat were constructed from aluminium alloy 5083-H321/H116 for plating, and aluminium alloy 6082-T5/T6 for rolled sections and bars. The nominal material properties are given in Table 3-2.

Table 3-2: Nominal material properties

	5083-H321	**6082-T6**
Modulus of Elasticity, E [GPa]	70.3	69
Density, ρ [kg/m^3]	2660	2700
Yield Strength, σ_{yield} [MPa]	215	250
Poisson ratio, ν	0.33	0.33

The pertinent operational requirements of the ACPBs are listed in Table 3-3. As of December 2018, the average age of the patrol boat fleet is 12 years. In 2014, the Defence Minister David Johnston said that the boats 'have had an enormous output and work rate' [78].

Table 3-3: Requirements for patrol boat capability

Operational role	Fisheries protection, immigration, customs and drug law enforcement
Primary operating area	Northern Australian Waters (NAW)
Service life	15 years, with option for 5 year extension
Maximum availability	3000 days per year, plus a surge capacity of 600 days per year [79]
Class notation	1A LC Naval Support Patrol EO NAUT NV CRANE

3.3 Hull Monitoring Systems

One approach to obtain information on the long-term fatigue loads to which the ships are exposed, required for accurate and through-life LOT analysis and risk management, is implementation of a Hull Monitoring System (HMS) [41, 80-84]. A HMS is a ship-board system that can monitor the hull response, sea state, and operational parameters of a ship. Examples of the utilisation of HMS data include the demonstration of an approach for reliability analysis and damage detection of a naval aluminium catamaran [85], validation of analytical approaches to structural management, and in the development of better designs [84].

In 2009, the Defence Science and Technology (DST) Group collaborated with Austal Ships to develop and install an innovative HMS onboard the ACPB HMAS *Glenelg*. The aims of the project were to initiate development of an improved capability for structural fleet management and service life assessment, and to demonstrate the application of a versatile network using specialised sensors on a naval platform [86]. The HMS operated until 2014. From the experience with this HMS recommendations were made, including [87]:

- Determination and management of the sources of noise and error present in the different signals.
- Increased sample rate of the strain signals to improve the accuracy of the subsequent structural analysis.
- Measurement of the hydrodynamic pressures acting on the hull, via hull-mounted pressure transducers, to enable improved modelling of the loads and understanding of the vessel's subsequent behaviour (refer to Appendix A).
- Installation of strain gauges in the bow thruster compartment (void 2) to allow investigation of the stresses induced in this area.

Subsequently, a modified HMS was commissioned on-board HMAS *Maryborough* in 2015.

3.3.1 HMAS Glenelg HMS

Glenelg's HMS was based on a network of specialised circuit boards that returned data from several sensors to an embedded personal computer. The sensors included accelerometers, strain gauges, torsion meters to measure shaft power, a six degree of freedom rigid body motion reference unit (MRU), and a Global Positioning System (GPS) [86]. The sensors were programmed to continuously collect and return data to the computer for storage.

In the original arrangement of the system, strain gauges were located to measure both global and local strains. Global stresses were measured using strain gauges at three longitudinal sections; forward, towards midships, and aft. To detect large strains due to slamming, strain rosettes were located on the keel and several metres up from the keel. In general, locations that were predicated to be relatively highly stressed and with a uniform stress distribution, were instrumented [86]. In 2012, additional strain gauges at various locations in the engine room (void 6) were installed to better understand stresses induced in pillars and supporting structure items.

In general, the HMS remained on, including when *Glenelg* was wharf-side. However, the collection of data was not continuous due to system defects, and maintenance of the vessel requiring power to the HMS to be switched off. Nonetheless, in excess of 14,000 hours of data for some sensors was recorded.

A profile view and description of strain gauge locations installed on *Glenelg* that are analysed in the thesis are provided in Figure 3-2 and Table 3-4, respectively. The sample rates (F_s) and measured strain directions of the gauges are also provided in Table 3-4.

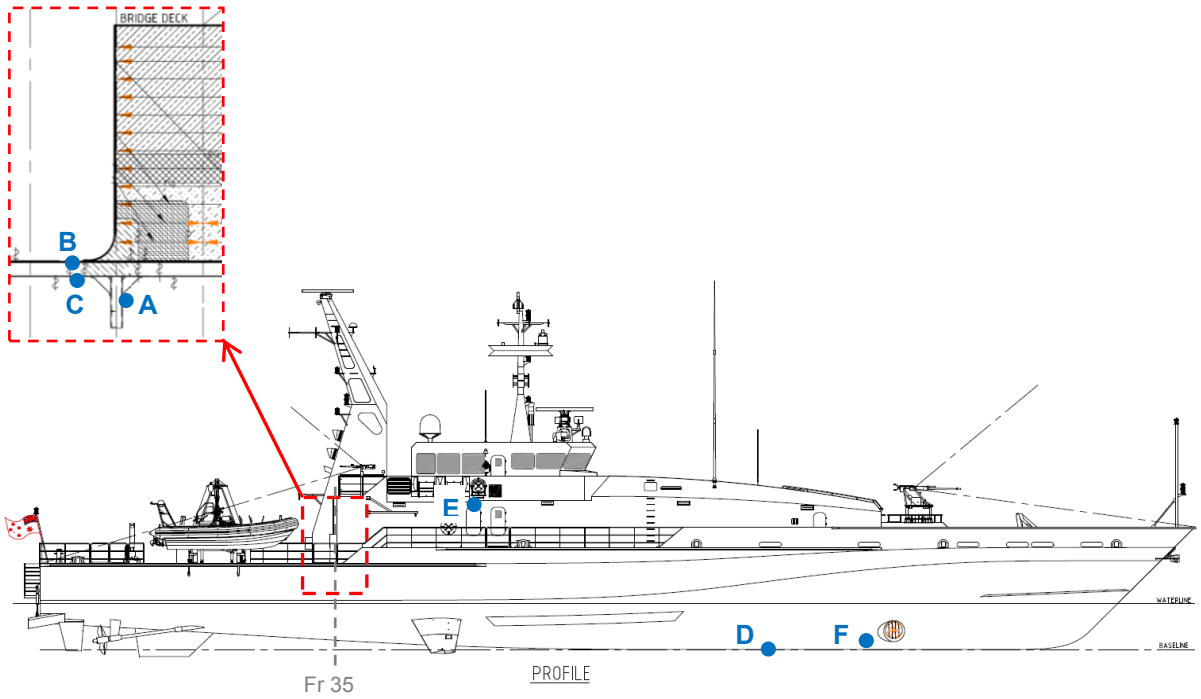

Figure 3-2: Profile view of analysed strain gauge locations installed on HMAS *Glenelg*

Table 3-4: Description of strain gauge locations installed on HMAS *Glenelg*

Strain Gauge ID	Side	Approximate Location	F_s [Hz]
A	Stbd	On Frame 35 pillar, 0.033 m below forward bracket at top of pillar	50
B	Stbd	On deck plating 42.6 m aft of FP, approximately 0.45 m inboard from deck edge (between two outermost stiffeners)	50
C	Stbd	On centre of flange of stiffener underside of main deck, 3.65 m off CL, 42.6 m aft of FP (and 0.6 m aft of a pillar)	50
D	CL	On centre of flange of bottom centreline girder, 19.8 m aft of forward perpendicular (FP)	50
E	Port	On sideshell plating 0.2 m below bridge deck, 33.8 m aft of FP	20
F	Port	On centre of flange of 4th stiffener from CL girder on port side, 20 m aft of FP	20

CL = Centreline
FP = Forward perpendicular
Stbd = Starboard

3.3.2 HMAS Maryborough HMS

A schematic of *Maryborough's* HMS is shown in Figure 3-3.

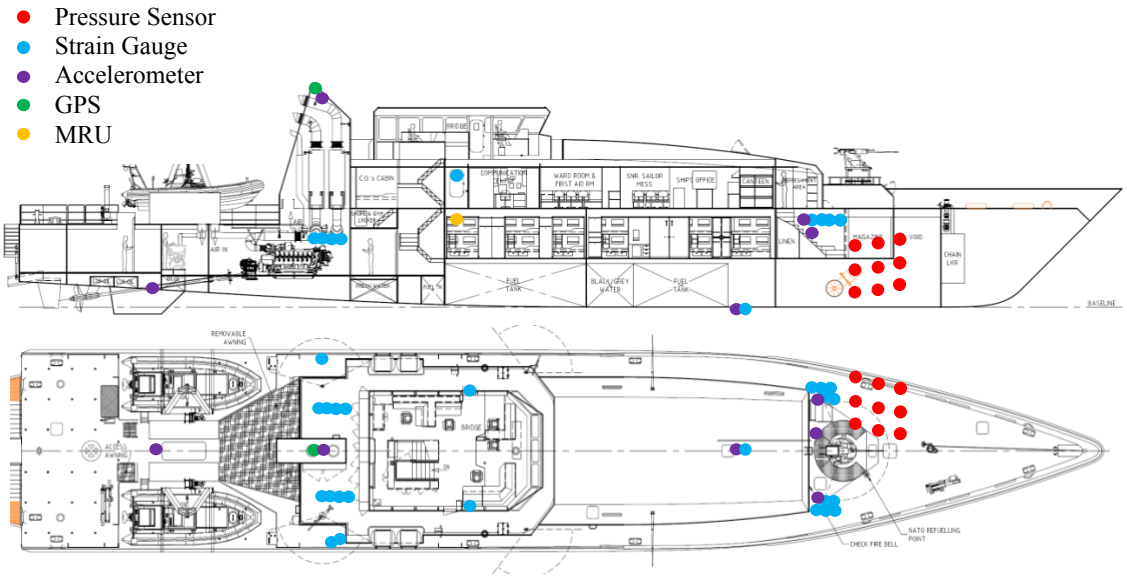

Figure 3-3: Type and approximate locations of sensors comprising HMAS *Maryborough's* HMS

The HMS was an advanced version of that installed on *Glenelg*. The sensors included foil-based strain gauges, pressure transducers, accelerometers, an external GPS receiver, and a MRU. The strain gauges were located to understand the loading in fatigue-prone areas of the ACPB and to compare strains with those measured on *Glenelg*. The HMS remained on,

including when *Maryborough* was wharf-side. However, as with the *Glenelg* HMS, there are some interruptions in the data due to system defects and ship maintenance that required power to the HMS to be switched off.

3.3.3 Signal Conditioning and Data Analysis

Data processing routines were developed in MATLAB [88] to convert and filter the raw strain data to stress. Due to the susceptibility of strain measurements to electrical interference from surrounding equipment, spikes are present in the raw data. Spikes are considered short duration electrical transients in voltage and are not representative of a continuous process such as seaway loading. As such, the data processing routines include the removal of spikes. High frequency noise is attenuated by applying a low-pass Chebyshev filter at 8 Hz, which is greater than the three-node bending vibration frequency of 5 Hz of the hull girder [89].

The Candidate co-authored a DST Group report [90] that describes a systematic approach developed to utilise HMS data (refer to Appendix B).

3.4 Fleet Maintenance Data

ACPB hull survey reports [91] are available to the Candidate.

Inspection of an in-service vessel provides information on the state of a structure. Thus, it is crucial input to maintenance and operational decision-making. Whilst wear-in failures can be expected, severe failure of primary structural items due to fracture demands scrutiny. Maintenance reports have been utilised to optimise repair duration and intervals [92], and to devise techniques aimed at reducing the risk of structural failure [93]. The benefit of survey reports is that they are an actual account of fatigue damage incurred in a ship. However, the data quality must be acceptable for the reports to be of value [94, 95].

Using search terms such as ‘crack’ and ‘fracture’, reports of cracking were found. Only the first discovered crack per ship at a location of interest is regarded. The time between repair and any subsequent defect is not included, to preclude introduction of uncertainty associated with the effectiveness of the repair.

3.5 Finite Element Model

An FE model of the patrol boat, shown in Figure 3-4, has been constructed in the commercially available package MAESTRO 11.4.9 [96]. The model is comprised of 169,775 nodes and

268,422 4-node shell and 2-node beam elements. The sign convention used is positive x-direction towards the bow, positive y-direction is up, and positive z-direction is to starboard.

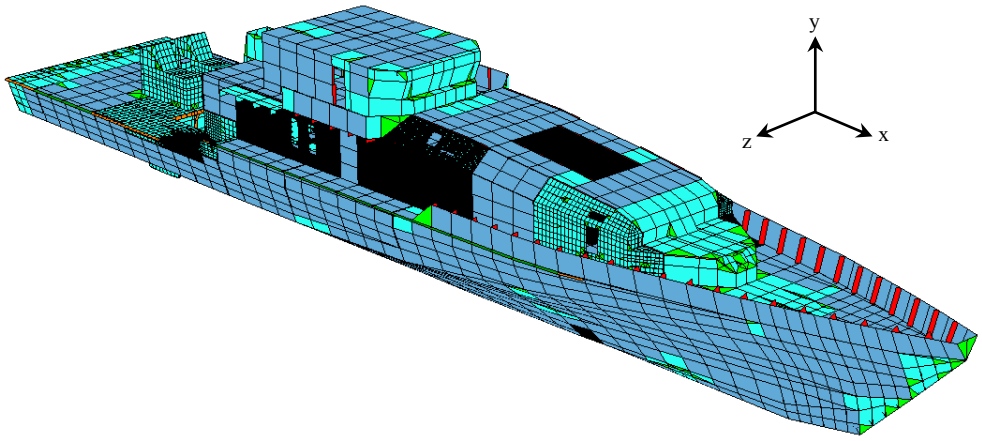

Figure 3-4: Global FE model of ACPB (origin located at transom, underside of keel, and centreline)

The model was developed and verified by the Candidate [97] before the commencement of the PhD candidature, though has been updated to meet the analytical requirements of the present research.

The mesh is relatively coarse to compute the global stress distribution of primary members of the hull. In general, the element length in the global model is one frame spacing.

Fine mesh models, shown in Figure 3-5, have been embedded into the global model. The mesh density at the refined areas is approximately one thickness of the material, which provides acceptable stress resolution. CQUAD4R 4-noded flat shell elements are mainly used in the fine mesh models. The CQUADR element has a linear strain variation with 6 degrees of freedom stiffness. An in-plane rotational stiffness is part of the formulation. The CQUAD4R element allows the recovery of the stress at its centroid. The global mesh model and the fine mesh models are connected by Rspline elements that provide a 'restraint' stiffness matrix added into the global stiffness matrix. Thus, the global model and fine mesh models are solved together so that the results are coupled [96].

The assumption of linear elasticity is used in the FEA. Linear elastic FEA is the most commonly used approach to model the ship structure, has been extensively benchmarked to cover a range of typical problems and requirements encountered in real-life, and provides a good description of the stress state [98].

Other assumptions include the use of isotropic materials and that the scantlings are accurate (that is, no real-life configuration changes from the build drawings). As the weld

profile is taken into account in the fatigue analysis (described in Sections 3.6.1 and 3.8), welding-induced imperfections, residual stresses, and the heat affected zone are not modelled.

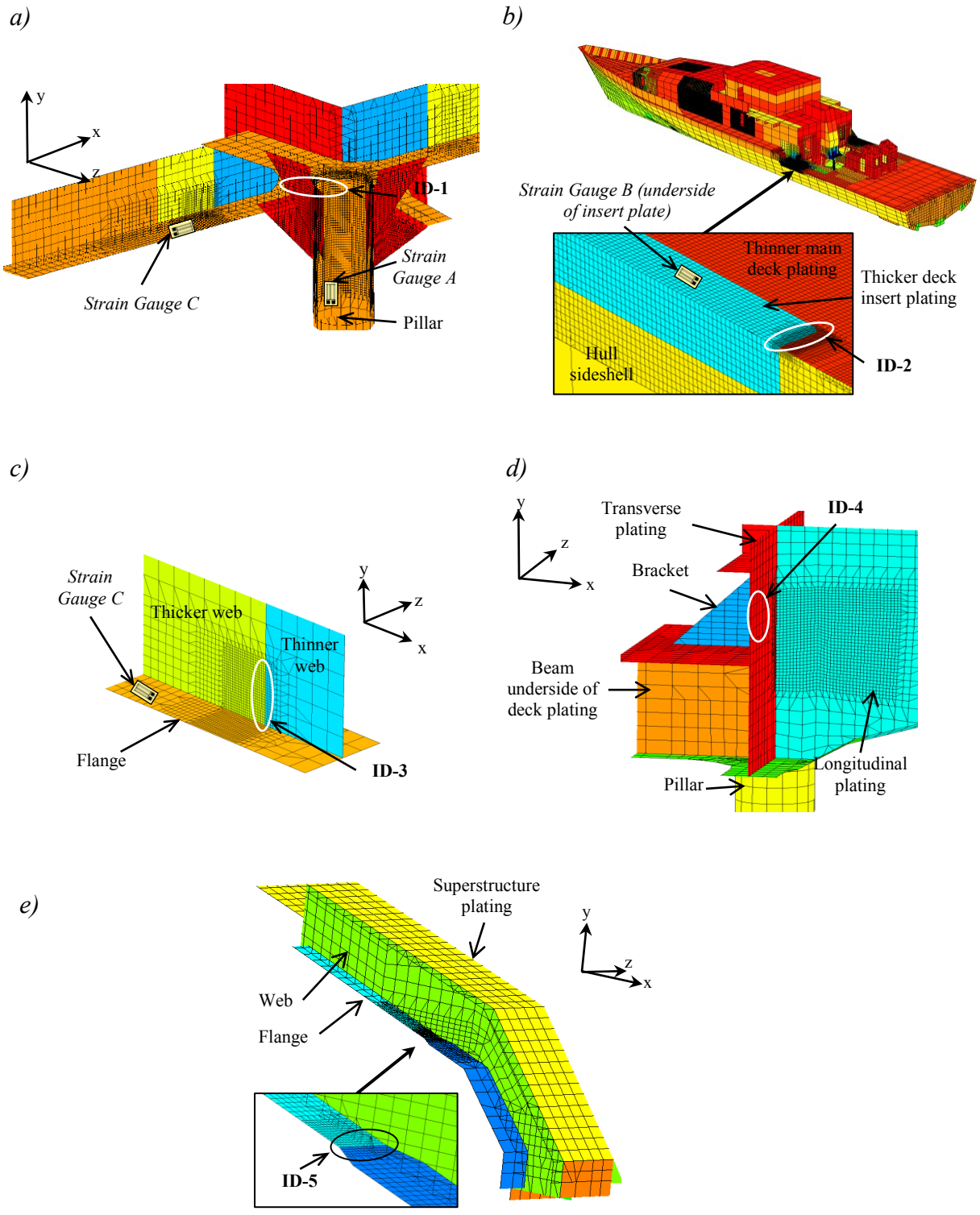

Figure 3-5: Fine mesh model containing welded detail of interest a) ID-1, b) ID-2, c) ID-3, d) ID-4, and e) ID-5

3.6 Cumulative Damage Theory

Cumulative Damage Theory (CDT) coupled with the S-N curve method is used to estimate the fatigue life of the aluminium welded joints. CDT, also known as the Palmgren–Miner rule [99], calculates the fatigue damage from each interval of the applied stress range as the ratio of the number of cycles (n) to the number of cycles (N) to failure. N is determined from an S-N curve. Though CDT coupled with the S-N curve method is widely accepted in the maritime industry [24-26, 100] and in fatigue design codes [101, 102], there are differing views regarding its accuracy.

CDT assumes that the fatigue strength is dependent only on the stress range, and the effect of mean stress can be ignored. There is no interaction between the applied stress cycles, and the cycles can be linearly summed. The latter assumption is an important difference to crack growth modelling. Zhang and Maddox [103] suggest that the most significant effect on the fatigue behaviour is the stress cycle interaction, and that long and/or multiple crack paths that develop can significantly vary the fatigue life of full-scale structures. Hodapp *et al.* [25] and Cui *et al.* [104] criticise the sizeable uncertainty/error in the fatigue life values of a simple ship detail evaluated via industry approaches that employ CDT, due partly to the effects of the load sequence and initial flaw size being ignored. In addition, Ravi Chandran *et al.* [105] argue that the traditional single S-N curve oversimplifies the diverse fatigue failure behaviour of metals. The authors' showed that the difference in fatigue lives between the types of crack initiation could be one or more orders of magnitude. In comparison, Cosso, Rizzo and Servetto [106] assessed the fitness-for-service of welded joints, representative of those found in ship and bridge structures, using scale-model experiments. The authors showed that the examined butt and cruciform joints behaved in accordance with the relevant detail design categories based on good fabrication. Of particular relevance to the present study, in 2000 the Ship Structures Committee reported that CDT 'provides a reasonably accurate, cost-effective result that is consistent with the level of available information in the high-speed craft industry' [107, p. 28]. 17 plus years later, CDT is still seen as fit-for-purpose for calculating the consumed fatigue life of an aluminium high-speed craft [108], and to calculate the fatigue life of a United States Coast Guard Cutters based on measured strains [109]. In addition, Neuberg and Drimer [110] used the S-N curve in the development of a direct calculation method to address the fatigue limit state of an aluminium planing boat, because it is effective, well established, and applied by the Eurocode; the detail categories in Eurocode 9 are characterised partly by the crack initiation site [102].

Ultimately, for practical purposes, a fatigue assessment approach must be chosen. In light of the known shortfalls of CDT the presented method treats the fatigue life as a dynamic value, rather than a static value assumed or calculated during the design stage of the ship life-cycle.

In CDT [99], the damage D caused by all cycles is calculated using Equation 2:

$$D = \sum_{i=1}^{k} \frac{n_i}{N_i} = \frac{1}{\bar{a}} \sum_{i=1}^{k} n_i \left(\Delta\sigma_i\right)^m \qquad \textbf{Equation 2}$$

Where k is the number of stress ranges, $\bar{a}$ and m are S-N curve parameters, and n_i and N_i are the number of actual cycles experienced and cycles to failure for the i^{th} stress range increment, respectively.

The fatigue life (FL) of a structural detail is the ratio of the service life, in years, to the fatigue damage. If the fatigue damage is less than unity, the structure has a fatigue life longer than the service life:

$$FL\ [years] = \frac{\text{Service life}}{D} \qquad \textbf{Equation 3}$$

3.6.1 S-N Curve Concepts

A schematic of the nominal stress, hot-spot stress, and effective notch stress at a welded joint is shown in Figure 3-6.

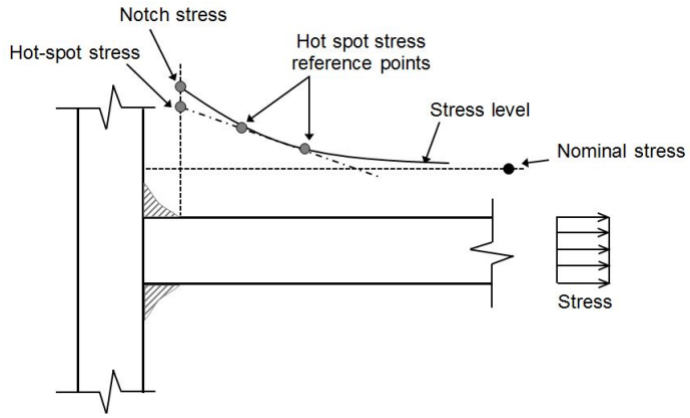

Figure 3-6: Schematic showing different stress types for fatigue analysis

The nominal stress is the stress in the sectional area under consideration. The hot-spot stress is the surface stress at the weld toe that includes the stress raising effects due to structural discontinuities. Both the nominal stress and the hot-spot stress disregard the stress raising effects of the weld. In contrast, the effective notch stress is the total stress at the root or toe of a weld; the weld contour and the non-linear material behaviour at the notch are calculated.

The nominal stress approach for calculating the fatigue life of a welded structural detail is commonly practiced in the maritime industry [55, 71, 111]. This method uses the stress acting on the location to be assessed, neglecting the stress concentration arising from both the structural configuration and the weld. These effects are inherently taken into account in the S-N curves for each specific type of structural connection/detail. Structural design codes that allow for the effects of a corrosive environment and the aluminium alloy series are available (for example, Eurocode 9). This is important to consider because the fatigue strength of a typical alloy used in the construction of marine vessels (5083-H111) is reduced due to constant or intermittent immersion in saltwater [112]. If the structural connection/detail of interest is represented in a fatigue design standard then use of the nominal stress approach is valid. However, difficulty with the selection of a suitable reference detail, and workability with structures characterised by complex geometry and/or load combinations, has been noted [55, 71, 113-115].

The hot-spot stress approach is argued to overcome some of the shortfalls of the nominal stress approach [55, 101, 114]. Fatigue tests inclusive of hot-spot stress analysis of some aluminium details have been published, for example, by the International Institute of Welding. Notwithstanding, concerns about this technique have been raised as follows:

- It is difficult to define the hot-spot, due to the strong dependence of the calculated local stress at the weld on the mesh size for FEA [12]. Methods that mitigate this issue are viewed by some as time-intensive and complicated [114].
- Different stress extrapolation techniques continue to be the subject of review [114-118].
- There is large variability of both the recommendations for, and results from, hot-spot analysis for steel and aluminium ship details [13, 114].

The development of the effective notch stress approach for aluminium alloys has been limited [26], and it is considered unsuitable for design and in-service assessment [111]. Hence, it is not discussed further.

3.7 Sources of Stress Spectra for Marine Structures

Among sources of stress spectra for fatigue analysis of marine structures are simplified fatigue analysis, spectral fatigue analysis, and rainflow counting of a stress history.

3.7.1 Simplified Fatigue Analysis

Simplified fatigue analysis assumes a stress history or spectrum at the detail, characterised by the shape, mean and maximum of the stress cycles. An appropriate probability level is allocated to a reference stress. Stresses are generally based on rule loads and may be calculated by an analytical approach or FEA.

3.7.2 Spectral Fatigue Analysis

Spectral Fatigue Analysis (SFA) uses a database of stress Response Amplitude Operators (RAOs) or transfer functions for the vessel to calculate fatigue damage. The RAOs are used to transform an input wave spectrum into a response spectrum [119].

The wave energy spectrum S_ζ, defined as Equation 4, where ω is the wave frequency and ζ_α is the wave amplitude:

$$S_\zeta(\omega)\cdot d\omega = \frac{1}{2}\zeta_\alpha^2(\omega) \qquad \textbf{Equation 4}$$

Similarly, the energy spectrum of the stress response $\sigma(\omega, t)$ can be defined by:

$$S_\sigma(\omega)\cdot d\omega = \frac{1}{2}\sigma_\alpha^2(\omega)$$

$$S_\sigma(\omega)\cdot d\omega = \left|\frac{\sigma_\alpha}{\zeta_\alpha}(\omega)\right|^2 \frac{1}{2}\zeta_\alpha^2(\omega)$$

$$S_\sigma(\omega)\cdot d\omega = \left|\frac{\sigma_\alpha}{\zeta_\alpha}(\omega)\right|^2 S_\zeta(\omega)\cdot d\omega \qquad \textbf{Equation 5}$$

Thus, the stress response spectrum can be found by using the RAO of the stress motion (Equation 5) and the wave spectrum (Equation 4):

Equation 6

$$S_{\sigma}(\omega) = \left| \frac{\sigma_{\alpha}}{\zeta_{\alpha}}(\omega) \right|^{2} S_{\zeta}(\omega)$$

Using SFA, a vessel's lifetime exposure at sea is divided into 'cells'. Each cell represents a particular combination of sea state, ship heading with respect to the waves, and speed. By locking these variables, the stochastic response in the cell becomes statistically stationary.

3.7.3 Rainflow Counting

Rainflow counting reduces a stress time history into a histogram of stress reversals or cycles. Matsuishi and Endo [120] introduced the first accepted method to extract closed uni-axial load cycles. The rainflow process described below is extracted from Lee *et al.* [121]:

1. Rotate the stress history, in Figure 3-7a, 90° so that the time axis is vertical (Figure 3-7b).
2. Designate A as the first extreme point, the largest peak in this load time history.
3. Identify the first largest reversal A–D as the flow of rain starts at A and falls off the second extreme point D, the smallest valley in this load time history.
4. Identify the second largest reversal D–A as the flow initiates at D and ends at the other extreme point, which is A.
5. In the first largest reversal A–D,
    a. Identify a reversal B–C as the rain starts flowing at B and terminates at C because D is a larger maximum than B.
    b. Identify a reversal C–B as the rain starts flowing at C and meets a previous flow at B.
    c. Complete all the points in the first large reversal A–D.
6. In the second largest reversal D–A,
    a. Identify a reversal E–H as the rain starts flowing at E and falls off the roof at H.
    b. Identify a reversal H–E as the rain starts flowing at point H and meets a previous flow at E.
    c. Identify a reversal F–G as the rain starts flowing at F and terminates at G because H is a larger maximum than F.
    d. Identify a reversal G–F as the rain starts flowing from the successive extreme point G and meets a previous flow at F.

e. Complete all the points in the second largest reversal D–A.

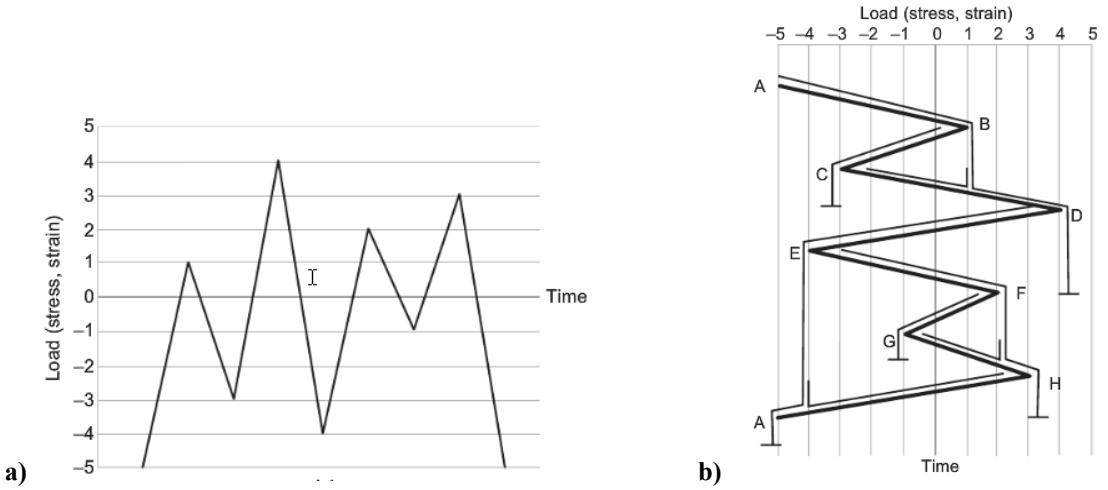

Figure 3-7: Illustration of a) a stress time history, and b) rainflow counting of time history [121]

3.8 Eurocode 9

The aluminium structural design code Eurocode 9 [102] is employed throughout the thesis.

The European Commission conducted a detailed program of work over 30 years with an aim to harmonise technical specifications in the design of construction works that resulted in establishing a number of design codes, known as Eurocodes. Eurocode 9 is developed for the design of aluminium structures.

Eurocode 9 fatigue strength curves are based on estimates of the mean and standard deviation, assuming a normal distribution, of observed logarithmic cycles for given logarithmic stress values. These statistics are used to obtain a characteristic regression line for a probability of survival of approximately 97.7% from the mean. This is less than 80% of the corresponding mean strength value, and allows for wider variations in production than can be expected in a set of fatigue specimens. This is relevant because the welding procedure in a shipyard is different from that in a strictly controlled laboratory [122].

Most of the S-N curves for welded joints in Eurocode 9 have three slopes, as shown in Figure 3-8, where:

- Ni is the predicted number of cycles to failure of a stress range $\Delta\sigma_i$.
- N_C is defined as $2x10^6$ cycles.
- N_D is defined as $5x10^6$ cycles.
- N_L is defined as 10^8 cycles.

- $\Delta\sigma_i$ is the constant stress range for the principal stresses in the construction detail for n_i cycles.
- $\Delta\sigma_C$ is the reference value of fatigue strength at $2x10^6$ cycles.
- $\Delta\sigma_L$ is the lower cut off limit, below which stress cycles are considered non-damaging.
- m_1 is the inverse slope of the log $\Delta\sigma$ – log N fatigue strength curve for $N_i \leq N_D$ detail category (first S-N inverse slope gradient).
- m_2 is the inverse slope of the log $\Delta\sigma$ – log N fatigue strength curve for $N_D \leq N_i \leq N_L$ (second S-N inverse slope gradient).

The effect of the marine environment and alloy can be taken into account by adjusting the $\Delta\sigma$-N curve. For example, for a 6xxx series aluminium welded joint in a severe marine environment, the detail category is reduced by one and the $\Delta\sigma$-N curve is adjusted such that N_D is increased from $5x10^6$ cycles to 10^7 cycles.

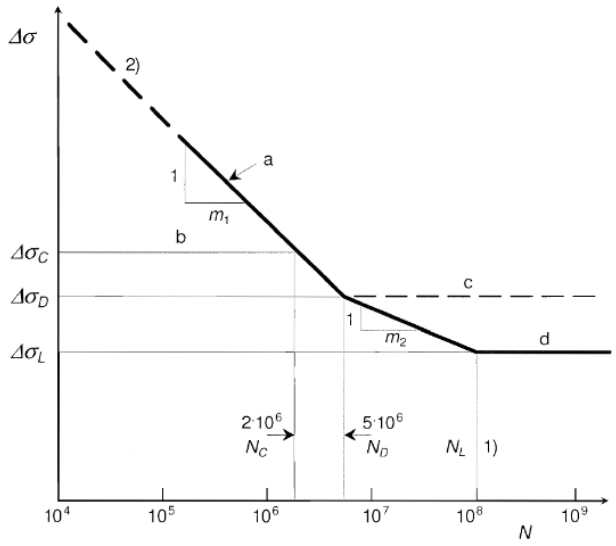

Figure 3-8: A generic $\Delta\sigma$-N curve as defined by Eurocode 9 [102]

The S-N curves were derived for a stress ratio[vi] not less than +0.5 (tension-tension fatigue testing). The effect of welding residual stress has traditionally been taken into account by assuming the mean stress, due to residual stress, to be large and tensile. This may be overly conservative for marine structures, as they are subjected to random loading and possible

[vi] The ratio between that maximum stress and minimum stress in a constant amplitude stress history, or a cycle derived from a variable amplitude stress history.

shakedown of residual stresses [123][vii]. In Eurocode 9, there is provision for application of an enhanced fatigue strength factor when the stress ratio is less than +0.5. For a specific welded connection, it is necessary to conduct experiments to accurately ascertain its sensitivity to the presence of static stresses. However, the sensitivity of a real structure may differ in the presence of non-zero mean stresses. In practice, complex aluminium welded joints are usually designed by taking the enhancement factor equal to unity [124]. As the mean stress of the joints of the ACPB cannot be reliably ascertained without significant additional expense, an enhancement factor equal to unity is assumed in the present research.

A detail category refers to the designation given to a particular fatigue initiation site for a given direction of stress fluctuation, to indicate the applicable fatigue strength curve for fatigue assessment. The category, crack initiation site, type of weld, and $\Delta\sigma_L$ for the Eurocode 9 (E9) details used in the thesis are presented in Table 3-5.

Where to Next?

This chapter has described the materials and methods used in the research. As noted in Section 3.6, there is uncertainty associated with using CDT coupled with the S-N curve approach. Therefore, there is a need to assess the applicability of different S-N curves to welded aluminium ship structures in the context of in-service experience. This requires a refinement of an S-N curve approach. As such, Chapter 4 proposes a refinement of the nominal stress approach for joints typical of aluminium welded ship details, which leverages in-service maintenance reports and stress spectra derived from HMS data.

[vii] It is generally accepted that fatigue and crack propagation only occur when the material is in tension. Residual compressive stresses are beneficial to a detail by reducing the overall tensile stress developed locally. Conversely, residual tensile stresses are detrimental to the fatigue life because they add to the nominal tensile stresses through the detail [31].

Table 3-5: Eurocode 9 details [102]

E9 Detail	Category	Crack initiation site	Type of weld	$\Delta\sigma_L$ [MPa]
5.5	Members with longitudinal weld	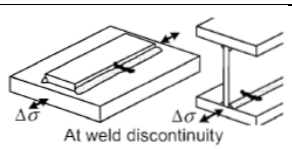	Continuous fillet weld	20.1
7.2.1	Butt-welded joint between members	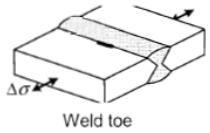	Welded from both sides, full penetration, flat solids	25.1
7.2.2			Welded from both sides, full penetration, open shape	14.5
7.4.3		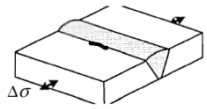	Welded one side only, full penetration without backing, open shapes, hollow, tubular	14.0
7.5		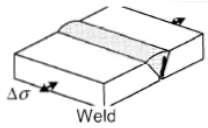	Partial penetration	7.9
7.6		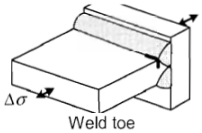	Full penetration	15.8
9.1	Fillet-welded joint between members	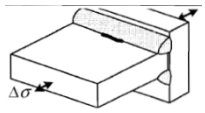	Double fillet weld partial penetration, toe crack	12.3
9.2		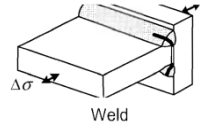	Double fillet weld partial penetration, root crack	11.0
9.3		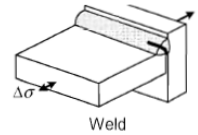	One sided fillet weld	5.3
11.3	Crossing welds on built-up beams	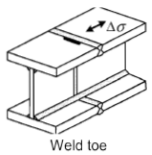	Double sided butt weld, full penetration	15.8

Chapter 4. Proposed Implementation of Nominal Stress Approach for Fatigue Assessment of Aluminium Naval Ship Welded Details

The work presented in this chapter has been submitted for publication in Part M: Journal of Engineering for the Maritime Environment. The paper has been edited for inclusion into this thesis to avoid repetition and to improve readability. The citation for this research article is:

Magoga, T., Aksu, S., and Slater, K., *Proposed Implementation of Nominal Stress Approach for Fatigue Assessment of Aluminium Naval Ship Welded Details*. Part M: Journal of Engineering for the Maritime Environment, submitted for publication.

4.1 Introduction

Methods to assess the fatigue strength of welded joints include the nominal stress approach, hot-spot stress approach, effective notch stress approach, fracture mechanics, and component testing. The first three methods are categories of the S-N curve concept (discussed in Section 3.6.1), which is the most commonly used in the design of ship structures [55, 71].

Following an industry recognised structural design code to conduct fatigue analysis often requires some interpretation by the analyst. For example, Eurocode 9 [102] (introduced in Section 3.8) prescribes the use of modified nominal stresses where the crack initiation site is near a gross change in cross section, or the joint misalignment is greater than that defined in the detail categories. However, if the crack initiation site is a weld toe and the nominal stresses in the joint are not clearly defined, the hot-spot stress approach is preferable though hot-spot S-N curves must be available. If not all of the conditions for use of the modified nominal stress or the hot-spot stress are met, the analyst must find an alternative way to interpret the guidelines. In addition, to derive the modified nominal stress using FEA, the mesh size should be sufficiently fine to resolve the stress field. Eurocode 9 does not specify a required mesh resolution, and how to obtain the modified nominal stress.

The applicability of the nominal stress based methods to design aluminium welded joints against fatigue has been previously considered. Al Zamzami and Susmel [124] conducted a comparative assessment of different approaches based on extensive experimental data. The authors found that the application of industry design curves with the nominal stress approach provided an adequate level of accuracy. Soliman *et al.* [55] presented an approach to utilise strain monitoring data for the service life prediction of an aluminium catamaran. Fatigue analysis of a member with a longitudinal fillet weld was conducted using the hot-spot stress approach, with the justification that many of the construction details have no direct match in design guides. Tveiten *et al.* [114] demonstrated the variability in the stress levels at highly stressed locations with different FEA models and stress extrapolation techniques. Further, the various applications of the nominal stress and hot-spot stress concepts share the issue that there are numerous variants in modelling and procedures [125].

Both ship designers and in-service managers require reliable fatigue evaluation approaches that are sufficiently accurate but also time-efficient to minimise costs. Therefore, the aim of this work is to propose a refinement of the nominal stress approach for joints typical of aluminium welded ship details. The refinement process leverages both in-service maintenance reports and stress spectra derived from long-term strain measurements acquired

from the *Glenelg* HMS (Section 3.3.1). To provide a basis for judging the applicability of different S-N curves to welded aluminium ship structures, key features are compared and assessed in the context of in-service experience. That is, the sensitivity of the predicted fatigue life of welded details to the choice of S-N curve, available from a structural design code, and stress parameter extraction is investigated.

4.2 Analysis and Results

The analysed details are shown in photographs and as schematics in Table 4-1. These details were chosen because they represent many of the types of joints found on the vessel.

Table 4-1: Description and figure of each detail of interest

ID	Description	Photograph of Detail	Weld Schematic
1	A pillar (hollow tube) joined to an end plate by a 45° bevel-butt circumferential weld		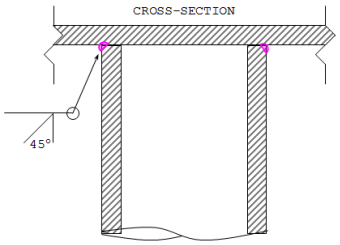
2	A butt weld between a relatively thick insert and thinner deck plating		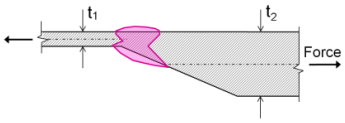
3	A built-up longitudinal beam comprised of web plating of different thickness joined by a butt weld and a flange joined by a continuous weld (photo of similar joint)		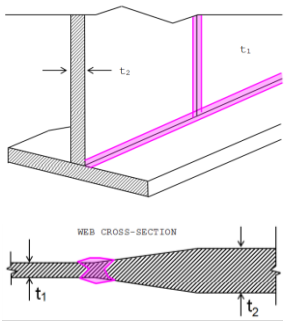
4	Longitudinal plating joined to transverse plating via a double fillet weld	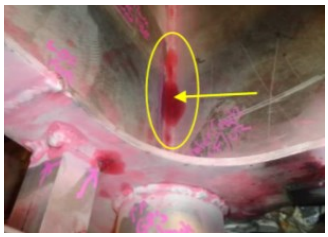	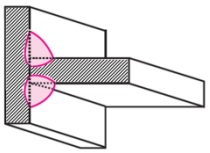
5	Butt weld in girder flange, between different thicknesses	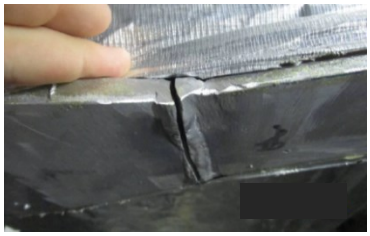	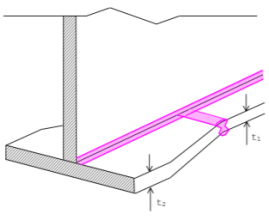

4.2.1 Finite Element Analysis

An FE model of the patrol boat is available, as detailed in Section 3.5. Two load cases are considered in the FEA, and are representative of the design Wave Crest Landing and Wave

Hollow Landing conditions defined in DNV HSLC rules [44]. Figure 4-1 shows the corresponding vertical bending moment distributions normalised by the maximum Wave Hollow Landing bending moment.

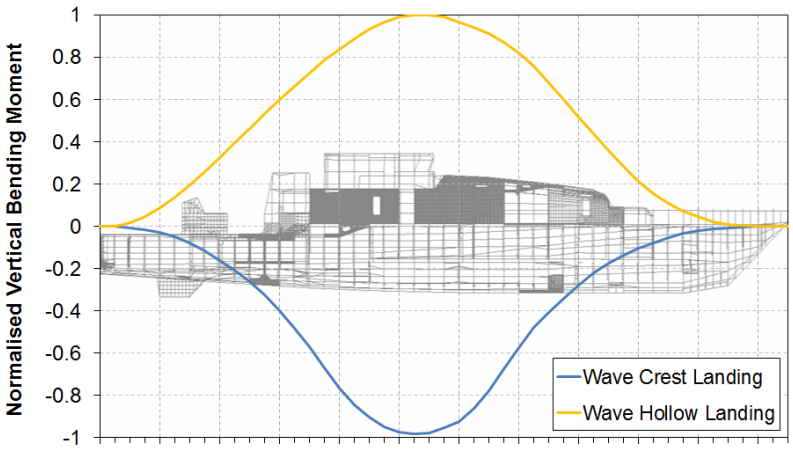

Figure 4-1: Normalised vertical bending moment distributions of Wave Crest Landing and Wave Hollow Landing conditions

4.3 Long-Term Stress Distributions

Uni-axial stress spectra at four of the strain gauge locations on *Glenelg* are considered in the present chapter. The locations of these gauges, and the details of interest, are displayed in Figure 4-2. The locations of strain gauges A, B and C are also indicated on the local FEA models in Figure 3-5a, b, and c.

The monitoring period considered in this chapter is approximately 4500 hours, and *Glenelg* was at sea two thirds of this time. The speed profile for this period is shown in Figure 4-3. The normalised stress spectra at the strain gauge locations are presented in Figure 4-4. The direction of the stresses measured by strain gauges B, C, and D is longitudinal (x-direction). The direction of the stress measured by strain gauge A is vertical (y-direction). These directional stresses are the responses to the dominant loads experienced in the structure at the strain gauge locations, which was verified via FEA. Further information about the derivation of the stress spectra is provided in [86, 126].

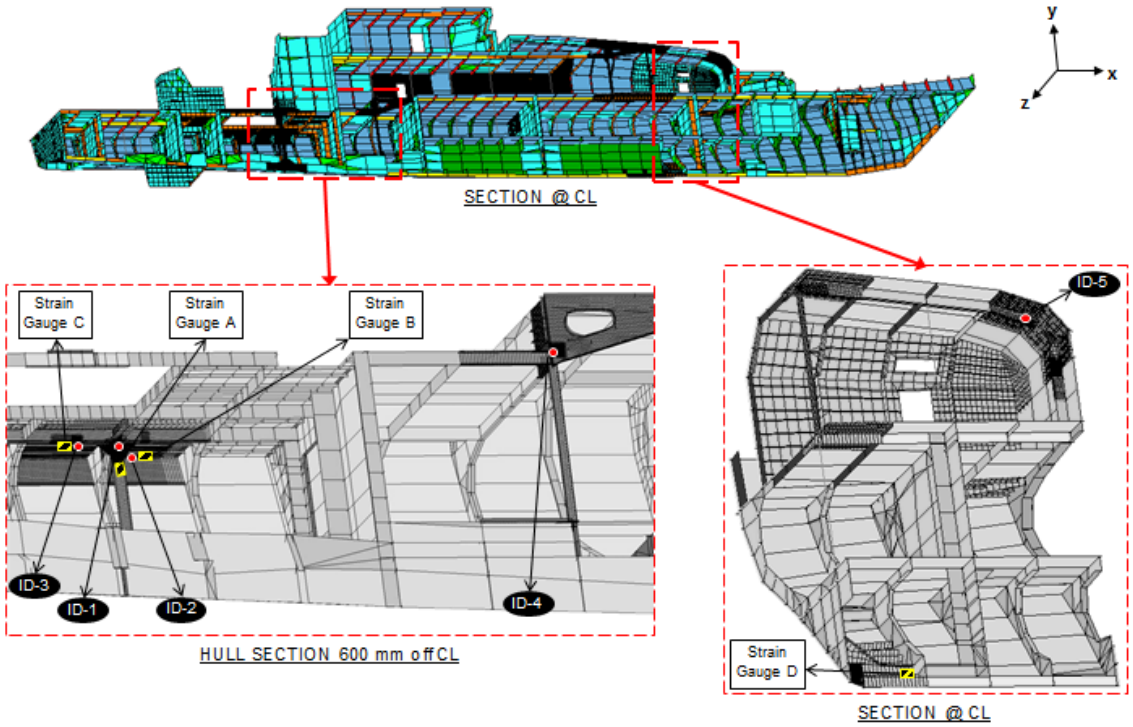

Figure 4-2: Approximate locations of strain gauges and details of interest in global FEA model

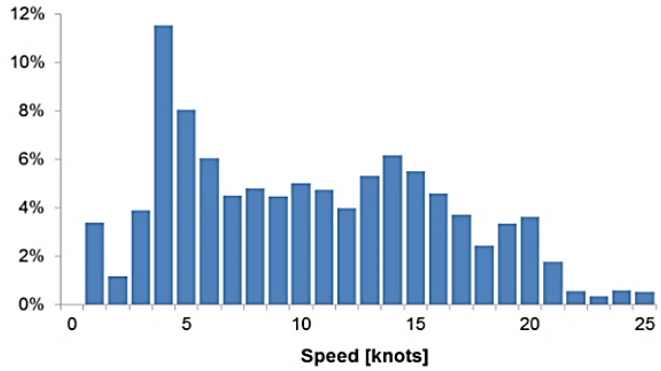

Figure 4-3: HMAS *Glenelg's* speed profile between August 2012 and February 2014

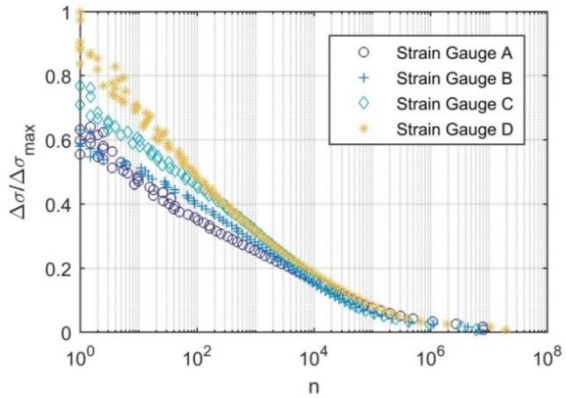

Figure 4-4: Derived normalised stress spectra at strain gauge locations

4.4 Fatigue Life Calculation

Eurocode 9 [102] provides the so-called 'Hot-spot reference detail method'. In this method, the 'hot-spot stresses' at the two locations are determined from FEA under a unit load; in this case, the loads applied are the design Wave Crest Landing and Wave Hollow Landing conditions. The fatigue damage at the detail is then assessed using the ratio of the stress ranges at the two locations. In this analysis the ratio between $\Delta\sigma_{max}$ at the detail of interest to that of the reference location, is applied to the reference stress spectrum. The ratio is denoted by K_g:

$$K_g = \frac{(\sigma_{crest} - \sigma_{hollow})_{detail\ of\ interest}}{(\sigma_{crest} - \sigma_{hollow})_{reference\ location}} = \frac{(\Delta\sigma_{max})_{detail\ of\ interest}}{(\Delta\sigma_{max})_{reference\ location}} \quad \textbf{Equation 7}$$

The strain gauge locations are considered as reference details, as defined in Table 4-2 (the suitability of reference locations is discussed in Section 8.3.4.)

Table 4-2: Reference strain gauges

Location	Strain Gauge	Stress Direction
ID-1	Strain gauge A	Vertical
ID-2	Strain gauge B	Longitudinal
ID-3	Strain gauge C	Longitudinal
ID-4	Strain gauge B	Longitudinal
ID-5	Strain gauge D	Longitudinal

The FEA accounts for effects due to the local geometry such as gross geometric changes and attachments, though not eccentricities. Given that the stress spectra used in the fatigue life calculations are uni-directional, the stress parameter of a particular detail is regarded as the normal stress in the same direction as that of the reference stress spectrum.

Eccentricity in butt welded joints is also considered (applicable only to detail of interest ID-2 of the details considered in this chapter). The stress concentration factor due to eccentricity K_{te} between welded plates of different thickness is calculated using the formula for butt welds available in DNV Classification Note No. 30.7 [60]:

$$K_{te} = 1 + \frac{6(e + e_t - e_0)}{t_1\left[1 + \frac{t_2^{1.5}}{t_1^{1.5}}\right]} \quad \textbf{Equation 8}$$

The thickness of the thinner plate is denoted by t_1, t_2 is the thickness of the thicker plate, e is the maximum misalignment between the plates, e_t is the eccentricity due to the change in thickness (half of the difference between the two thicknesses), and e_0 is misalignment inherent in the S-N data for butt welds (assumed to be 0.1t).

K_g and K_{te} are multiplied to obtain a single factor K:

$$K = K_g \times K_{te} \qquad \textbf{Equation 9}$$

The fatigue damage is predicted using CDT (refer to Section 3.6). To estimate the fatigue damage at a detail of interest, the reference stress spectrum is multiplied by K as per Equation 10.

$$D_{detail} = \frac{1}{\bar{a}} \sum_{i=1} n_i \left(K \times \Delta\sigma_i \right)^m \qquad \textbf{Equation 10}$$

The fatigue life (FL) is the ratio of the service life in years to the fatigue damage, calculated using Equation 3.

4.5 In-Service Experience – Maintenance Data

The International Association of Classification Societies [127] use 'damage experience', or the number and location of cracks related to the fleet, as the main source of information for maintenance planning. Similarly, the presence or absence of a crack at a construction detail can be interpreted as a sample of the corresponding fatigue life [15].

The maintenance records of each patrol boat were reviewed to obtain the time from commissioning to first discovery of a crack (FL_m) at various locations (refer to Section 3.4). Importantly, the cracks at the specified locations were fleet-wide occurrences rather than defects or manufacturing errors isolated to a single vessel.

Table 4-3 presents the fleet-wide average and standard deviation (assuming a normal distribution, which is reasonable for most situations [128]) of FL_m for each structural detail of interest, normalised by that of ID-1. On average, cracking was first discovered at ID-2 followed by ID-1, ID-4, and ID-5. At the time of the analysis, no defects had been observed at ID-3. The standard deviation was greatest at ID-2 (31%) followed by ID-1 (25%), ID-5 (10.3%), and ID-4 (9.3%).

Table 4-3: Fleet average FL_m at each detail of interest normalised by that of ID-1

Detail	Fleet average FL_m normalised by FL_m of ID-1	Standard deviation
ID-1	1.0	25%
ID-2	0.72	31%
ID-3	N/A – no defects reported	
ID-4	1.2	9.3%
ID-5	1.7	10.3%

The fatigue life of a detail of interest is described by the time from commissioning to first failure discovery (calendar time) rather than operating time. The safe life approach (described in Section 2.4) was assumed in the design of the ACPBs. The Candidate understands that the maintenance strategy for the ACPBs is time-based[viii], although unplanned or event-driven maintenance occurs. Thus, it may be misleading to express defects in terms of operational time because it implies a level of usage monitoring that is not practiced. In addition, other than the GPS data from *Glenelg* and *Maryborough*, the information available to the Candidate is limited to daily fleet activities. From this information, a histogram of the estimated time at sea as a fraction of calendar time since commissioning, over several years, is generated (Figure 4-5). The time at sea of most of the vessels was similar, and the variance is not greater than that suggested in the statistics of the defect data in Table 4-3.

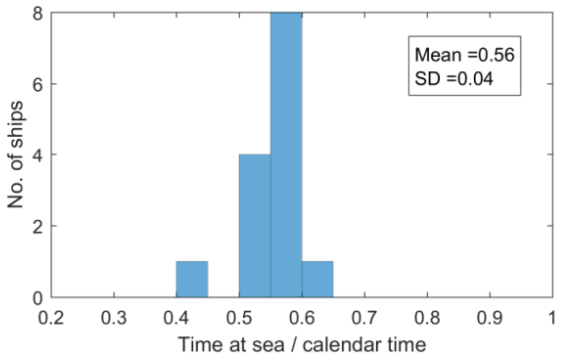

Figure 4-5: Histogram of ACPB fleet time at sea as a fraction of calendar time since commissioning

The level of variation in the results in Table 4-3 is considered reasonable, as maintenance data often suffers from issues with accuracy and completeness [94, 95]. However, the results in Table 4-3 should be understood to be somewhat optimistic as they rely on

[viii] Time-based maintenance refers to maintenance activities being carried out periodically. It is assumed that equipment failure is predictable based on failure rate trends [129].

average behaviour of the fatigue life. In addition, the variation of FL_m may be due to difficulties with accessing some parts of the structure (for example, behind insulation), inconsistent defect reporting, and variability in the usage of the ships [130]. From discussion with the maintenance contractor, it is understood that a crack may have been reported up to 6 weeks after it was detectable due to the nature of fleet activities. Notwithstanding the ease of inspection of detail of interest ID-2 (at a point of embarkation at the aft deck and thus very visible), the standard deviation of the fatigue life is the largest.

Manufacturing and the degree of quality control can also have a major influence on fatigue strength. Welded structures contain pre-existing cracks or crack-like flaws associated with abrupt change in section, weld toes, weld stop/starts, porosity, inclusions, oxides, and lack of fusion [102, 122]. The effect of the manufacturing process on the fatigue life of aluminium HSLC is studied at a first-order level in this research project. The fabrication quality is taken into account, to an extent, with the selection of an appropriate E9 detail category (in Section 3.8) that corresponds to a welding execution quality according to ISO 10042:2005 [131]. Thus, it is also assumed that appropriate welding techniques and quality management was applied during the construction of the ACPBs.

4.6 Sensitivity of Fatigue Life Calculation to S-N Curve and Stress Parameter

Selection of an applicable detail or S-N curve, from a fatigue design code, for a complex structure can be challenging and somewhat subjective. It has been demonstrated that the data used to develop Eurocode 9 does not reflect some of the structural details used in the construction of high-performance aluminium vessels [48]. It is not clear how to determine the stress parameter when using fatigue resistance data expressed in terms of the nominal stress, particularly when both complex geometry and stress fields are present. In the fatigue analysis of trapezoidal joints in a fast ferry, Garbatov *et al.* [132] assumed that the neighbouring 'low-gradient' is the nominal stress though no further guidance is provided. Therefore, it is necessary to determine the distance from the intersection between structural members (weld seam) to be determined. This involves:

1. Deciding the number of elements, parallel to the weld seam, from which the stress is recovered. For this purpose, the total length of the elements parallel to the weld seams is chosen to be equal to double the thickness of the structural member. This means that the stress parameter will be taken as the average of the stresses recovered from the

centroid of a minimum of two elements, which allows the central tendency of the stress response to be represented.

2. Recovery the stresses at varying distances from the weld seam. Figure 4-6 shows an example schematic of a pillar joined to an end plate with a circumferential weld. A stress concentration occurs at the top of the pillar. The stresses are recovered at a distance of, for example, 1t (one thickness), 2t, and 3t along the length of the pillar from the stress concentration.

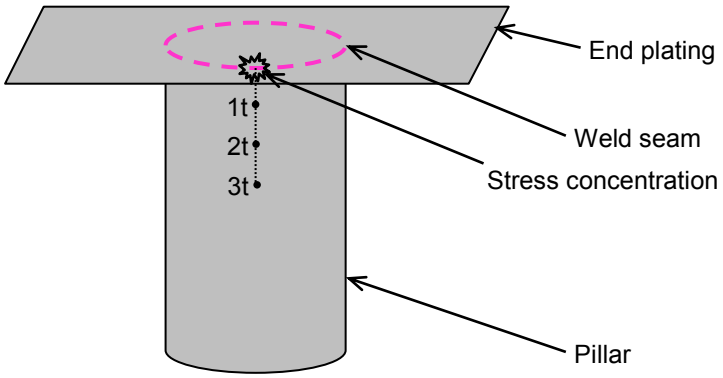

Figure 4-6: Example schematic of a pillar joined to an end plate, with stress concentration at top of pillar. Stresses are recovered at varying distances along length of pillar

The steps to investigate the sensitivity of the calculated fatigue life to the choice of the S-N curve and derivation of the stress parameter are outlined in Figure 4-7. With respect to step C, in the first instance the most applicable detail category (S-N curve) is considered. However, the effect of the selection of potentially unsuitable details is also evaluated.

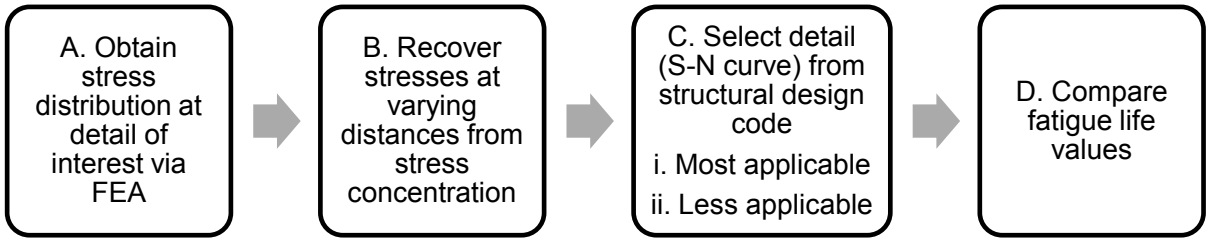

Figure 4-7: Workflow for study on sensitivity of calculated fatigue life to S-N curve and derivation of stress parameter

The category, crack initiation site, type of weld, and fatigue limit $\Delta\sigma_L$ for the Eurocode 9 (E9) details used in the present chapter are given in Table 3-5.

4.6.1 Stress Distributions at Structural Details of Interest (Step A)

The nominal stresses at the strain gauge locations are taken directly from the model. The mesh density is approximately equal to the size of a strain gauge.

The normal stress distribution in the vertical direction at detail of interest ID-1, under the Wave Crest Landing condition, is shown in Figure 4-8. For brevity, only the results for the Wave Crest Landing condition are shown (under the Wave Hollow Landing condition, though the stress is in the opposite direction the distribution is similar to that under the Wave Crest Landing condition). As shown in Figure 4-8 there is a significant stress concentration at the top of the pillar that exceeds the yield stress of the material (given in Table 3-2). Also, it is within the breadth of weld. Due to the presence of the bracket, there is no clear nominal stress in the pillar. This result exemplifies the need to use the modified nominal stress.

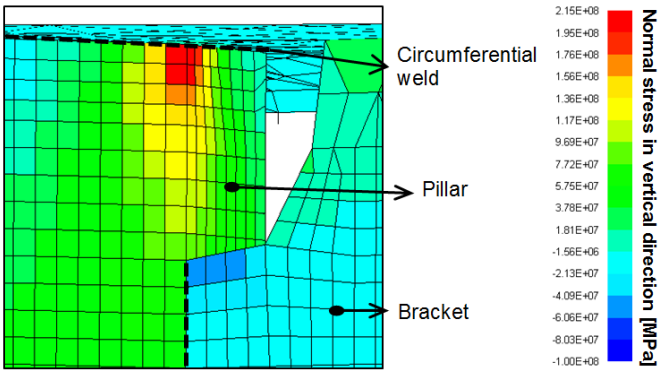

Figure 4-8: Distribution of normal stress in y-direction under Wave Crest Landing condition at detail of interest ID-1

The normal stress distribution in the longitudinal direction at detail of interest ID-2, under the Wave Crest Landing condition, is shown in Figure 4-9. The stresses are greatest in the thinner (main deck) plating adjacent to the corner of the insert plate and deck edge.

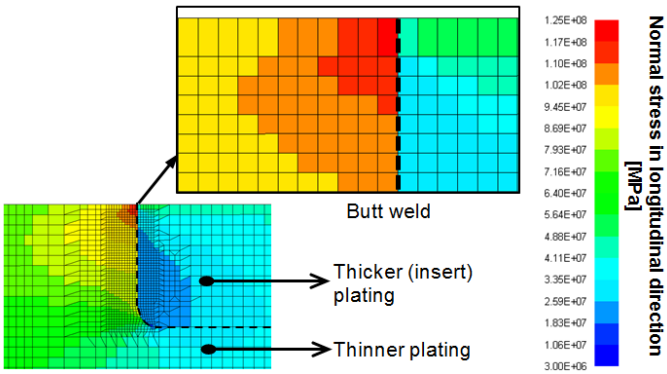

Figure 4-9: Distribution of normal stress in x-direction under Wave Crest Landing condition at detail of interest ID-2

Detail of interest ID-3 is a butt weld between relatively thin and thick plating that make up the web of a fabricated beam. The flange of the beam is joined to the web via a double sided continuous weld. Figure 4-10 displays the normal stress distribution in the longitudinal direction at detail of interest ID-3, under the Wave Crest Landing condition. A stress concentration in the thinner web plating, adjacent to the flange, is apparent. In addition, it is assumed that the beam is restricted in out-of-plane movement. Thus, the stress concentration factor due to eccentricity between the plates is equal to one [133].

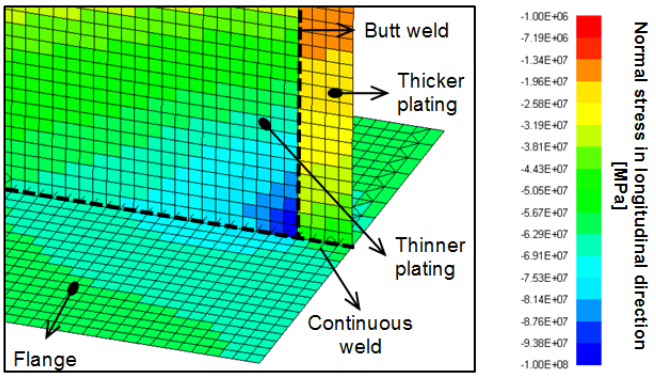

Figure 4-10: Distribution of normal stress in x-direction under Wave Crest Landing condition at detail of interest ID-3

The load paths at detail of interest ID-4 are complex. The pillar supports loads in the vertical direction, the transverse plating supports transverse loads, and both the longitudinal plating and beam underside of deck plating support the longitudinal loads. Figure 4-11 presents the directional stress distribution at detail of interest ID-4, under the Wave Crest Landing condition. The stress concentration (normal stress in the longitudinal direction) occurs at the junction of the longitudinal plating, the deck plating, and the transverse plating.

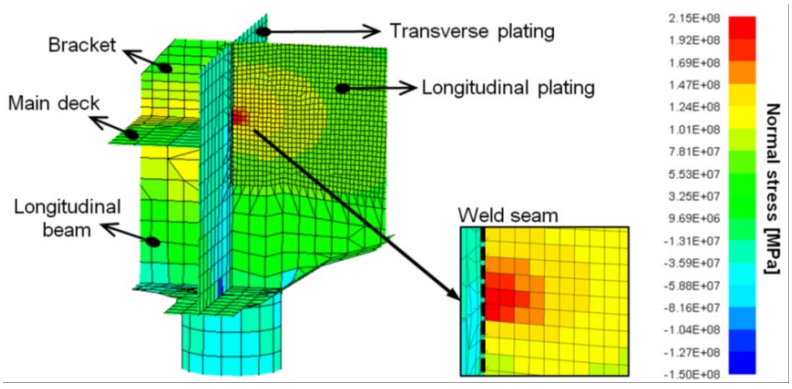

Figure 4-11: Distribution of normal stress under Wave Crest Landing condition at detail of interest ID-4

As shown in Table 4-1, detail of interest ID-5 is a butt weld between thinner and thicker plating that comprise the flange of a longitudinal beam. The width of the thicker plating is tapered to the narrower section of the flange. Relatively high stress magnitudes in the thinner section of the flange are visible in the normal stress distribution under the Wave Crest Landing condition as shown in Figure 4-12.

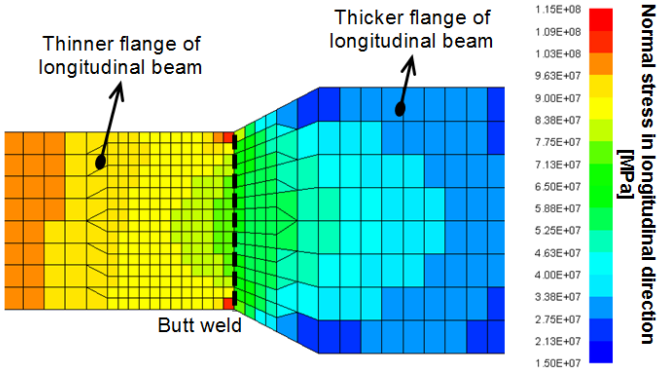

Figure 4-12: Distribution of normal stress in longitudinal direction under Wave Crest Landing condition at detail of interest ID-5

4.6.2 Stress Range as a Function of Distance from Weld Seam/Intersection (Step B)

For each detail of interest the stresses are recovered at increasing increments of distance from the weld seam, as illustrated in Figure 4-6. The stress range under the design load cases $\Delta\sigma_{max}$ as a function of the ratio between the distance from the intersection and the thickness of the structural member (d/t) are presented in Figure 4-13. The values of $\Delta\sigma_{max}$ are normalised by $\Delta\sigma_{max}$ at detail of interest ID-4. Though values of d/t less than 0.5 are plotted, they are disregarded in the remaining analysis as they are assumed to be within the weld. At details of interest ID-1, ID-3, and ID-5, the stress range decreases non-linearly with d/t. In comparison, the stress range at ID-2 and ID-3 decreases approximately linearly with increasing d/t.

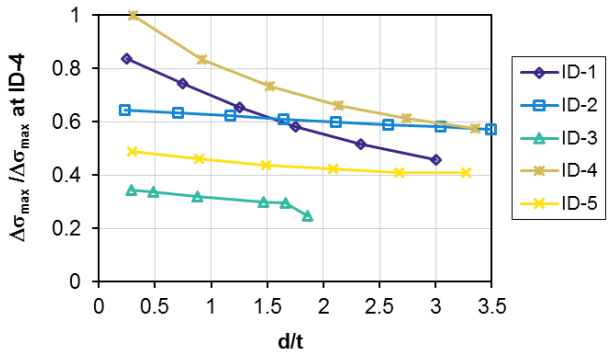

Figure 4-13: Stress range as a function of distance from intersection (d/t) between welded members for each welded detail of interest

4.6.3 Eurocode 9 Details / S-N curves (Step C)

The E9 details considered in the fatigue life estimation for each detail of interest are given in Table 4-4. At least two E9 details are considered per detail of interest; the first E9 detail is judged the most applicable, and the second (and third) are potential alternatives.

Table 4-4: E9 details and their consistency with details of interest

ID	E9 detail	Rank	Consistency between E9 category and welded detail of interest			
			Weld category	Weld type (penetration, single/double sided)	Geometry	Loading direction
1	7.4.3	1st	✓	○	✓	✓
	7.5	2nd	✓	✓	×	✓
	9.3	3rd	×	✓	×	✓
2	7.2.1	1st	✓	✓	✓	✓
	7.2.2	2nd	✓	✓	×	✓
3	11.3	1st	✓	✓	✓	✓
	5.5	2nd	○	×	✓	✓
4	7.6	1st	✓	✓	✓	✓
	9.1	2nd	○	○	✓	✓
	9.2	3rd	○	○	✓	✓
5	11.3	1st	✓	✓	✓	✓
	7.2.1	2nd	○	✓	○	✓
	7.2.2	3rd	○	✓	○	✓

✓ = consistent
○ = somewhat consistent
× = not consistent

Table 4-4 also summarises the factors in determining the most applicable E9 detail for each welded detail of interest. For example:

- For detail of interest ID-1, E9 detail 7.4.3 is judged applicable because it is also a butt welded joint between two members; the geometry (hollow section) and the loading direction are consistent. However, ID-1 features a partial penetration weld (refer to Table 4-1) whereas E9 detail 7.4.3 is a full penetration weld. Thus, although the geometry differs from ID-1, E9 detail 7.5 may be appropriate because it is a partial penetration butt weld. Still, ID-1 could be construed as a one-sided fillet weld with a bevel that is analogous to E9 detail 9.3.

- For detail of interest ID-4 E9 detail 7.6 is judged applicable because it is double-sided butt welded joint between two members, and the geometry as well as the loading direction are consistent. From the maintenance records, it is understood that the fracture of the weld in the transverse plating (shown in Table 4-1) is suspected to be due partly to a stress concentration in way of the adjoining deck that corresponds to the FEA results displayed in Figure 4-11. However, if the crack initiation site was above the junction of the main deck, E9 details 9.1 or 9.2 may be applicable as fillet welds are used. Both E9 detail 9.1 and 9.2 pertain to a double fillet weld with partial penetration, though the crack initiates in the weld toe of the former and in the weld root of the latter.

4.6.4 Comparison of Fatigue Life Values (Step D)

The predicted fatigue life FL_p of each detail of interest is calculated using Equations 4 and 5 for varying d/t. Figure 4-14a, b, c, and d display the variation of FL_p, normalised by the fatigue life indicated by the maintenance records FL_m (given in Table 4-3), with varying d/t for welded details of interest ID-1, ID-2, ID-4, and ID-5, respectively. For ID-3, as FL_m is not applicable, FL_p is normalised by the design life FL_d as given in Figure 4-15.

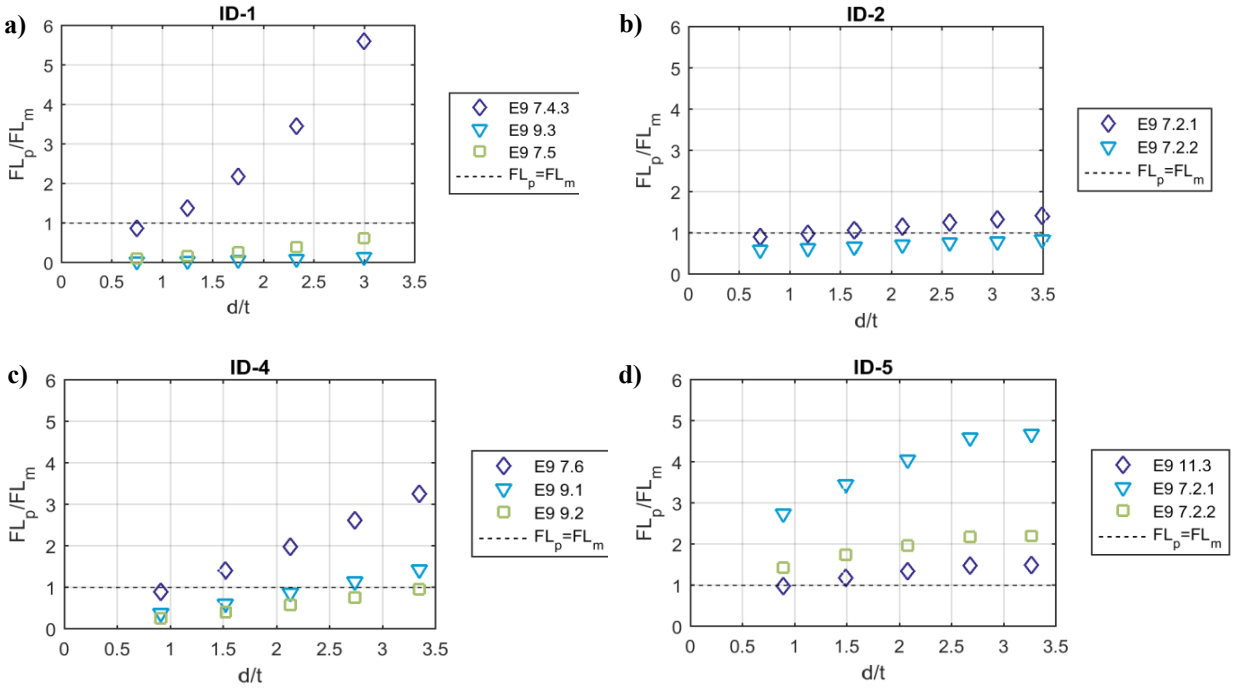

Figure 4-14: FL_p/FL_m as a function of d/t at detail of interests a) ID-1, b) ID-2, c) ID-4, and d) ID-5

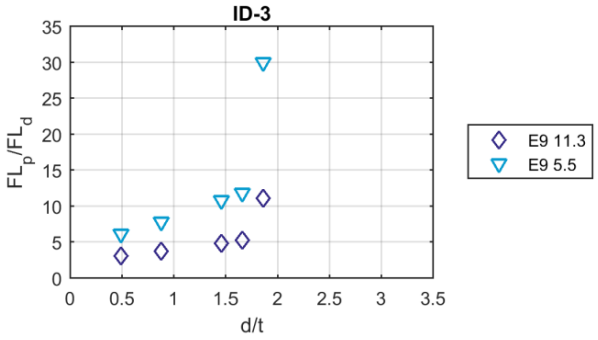

Figure 4-15: FL_p/FL_d as a function of d/t at detail of interest ID-3

For each relationship between FL_p/FL_m and d/t shown in Figure 4-14 a one-term power model, given by Equation 11 (where α and ϕ are coefficients), was fitted in MATLAB [88] using the non-linear least squares approach.

$$\frac{FL_p}{FL_m} = \alpha\left(\frac{d}{t}\right)^{\phi}, \text{ for } \frac{d}{t} > 0 \qquad \textbf{Equation 11}$$

The corresponding values of α, ϕ, and the coefficient of determination R^2 are given in Table 4-5. All of the R^2 values are greater than 0.96. Therefore, the power models explain most of the variability of the data.

The suitable distance from the intersection from which to recover the stresses (that is, to define the extraction of the stress parameter) is established by assuming that FL_p/FL_m is equal to one. That is, the maintenance data is used to calibrate the stress parameter extraction process. Using Equation 11, d/t was solved for FL_p/FL_m equal to one for each detail of interest; the results are given in Table 4-5.

The results shown in Figure 4-14 suggest that the first choice E9 detail provide reasonable fatigue life predictions, with respect to those indicated by the maintenance records. In addition, there is a level of agreement between the values of d/t across the different details of interest when FL_p/FL_m equals one; that is, the average of d/t is 1.0 ± 0.2. Based on this finding, the values of K_g (Equation 7), K_{te} (Equation 8, applicable to ID-2), and K (Equation 9), most applicable E9 detail, and FL_p/FL_m are presented in Table 4-6. Also presented are the values of FL_p normalised by FL_m at detail of interest of ID-1.

Table 4-5: d/t at $FL_p/FL_m = 1$ for each detail of interest

ID	E9 detail	Rank	α	ϕ	R^2	d/t at $FL_p/FL_m = 1$
1	7.4.3	1st	0.92	1.6	0.99	1.1
	7.5	2nd	0.030	1.4	0.99	> 5
	9.3	3rd	0.12	1.5	0.99	4.3
2	7.2.1	1st	0.95	0.31	0.97	1.2
	7.2.2	2nd	0.61	0.25	0.97	> 5
3	11.3	1st	N/A	N/A	N/A	N/A
	5.5	2nd				
4	7.6	1st	0.92	1.0	0.99	1.1
	9.1	2nd	0.39	1.1	0.99	3.5
	9.2	3rd	0.27	1.1	0.99	2.4
5	11.3	1st	1.0	0.34	0.98	0.74
	7.2.1	2nd	2.9	0.42	0.98	< 0.5
	7.2.2	3rd	1.5	0.34	0.98	< 0.5

Table 4-6: K_g, K_{te}, K, and FL_p/FL_M and FL_p/FL_M for each detail of interest

ID	K_g	K_{te}	K	E9 Detail	FL_p/FL_m at d/t = 1	FL_p/FL_m at ID-1
1	3.3	1.0	3.3	7.4.3	0.9	0.9
2	2.8	1.8	5.0	7.2.1	1.0	0.7
3	1.7	1.0	1.7	11.3	4.0*	13.0
				5.5	1.6*	5.0
4	3.5	1.0	3.5	7.6	0.9	1.1
5	2.7	1.0	2.7	11.3	1.1	1.9

*FL_p/FL_d is used instead of FL_p/FL_m

4.7 Discussion

Based on the results presented in Figure 4-14 as well as Tables 4-5 and 4-6, it is proposed that the nominal stress parameter can be extracted by averaging the normal stresses recovered at a distance of 1t from the weld/intersection for the analysed structural details. As revealed in Table 4-6, the estimated fatigue life values range between 90% and 110% of those derived from the maintenance records. As shown in Figure 4-15, the predicted fatigue life at detail of interest ID-3 is greater than the design life, and no cracks have been reported at this location. In addition, the values of FL_m and FL_p normalised by FL_m at ID-1, from Table 4-3 and Table 4-6 respectively, are also comparable. Thus, the predicted order of the fatigue cracking in the patrol boat structure is realistic.

It is acknowledged that the proposed application of the nominal stress approach is dependent on the appropriate selection of the E9 detail, combined with the influence of the stress distribution at the welded detail. For example, as shown in Figure 4-14a, selection of E9 detail 7.5 for ID-1 results in an overly conservative fatigue life prediction. If E9 detail 7.5 was nonetheless used, based on extrapolation of the power model of the relationship between FL_p/FL_m and d/t (Equation 11), the stress parameter would need to be extracted at a distance substantially greater than 5t from the weld for the fatigue life prediction to realistic (refer to Table 4-5). In this case, recovery of the stresses at this location would be inappropriate, as it is within the weld seam of the bracket to the pillar (refer to Figure 4-8). On the other hand, it is observed from Figure 4-14a that the fatigue life at detail of interest ID-2 is less sensitive to d/t in comparison to the other details of interest. At this detail the stress range decreases approximately linearly, and with a relatively small gradient, with increasing d/t (refer to Figure 4-13). Thus, the uncertainty associated with the fatigue life predictions varies across the different welded details.

As noted in Section 4.5, the results in Table 4-3 should be understood to be somewhat optimistic as they rely on average behaviour of the fatigue life. Also, a crack most likely propagated to a critical length, in terms of requiring defect rectification, some time before being reported. However, the contribution of each of the different variables (operational usage, weld quality, defect detection and reporting) in FL_m is very difficult to quantify. For example, although detail of interest ID-2 is easy to inspect (at a point of embarkation at the aft deck), the standard deviation of the fatigue life derived from the maintenance data is the largest. Thus, the fatigue life at this detail may be more sensitive to the effect of weld quality or load history. At the same time, the degree and sources of conservatism/optimism in the parameters and proposed modified stress approach to predict the fatigue life differ. For instance, the E9 S-N curves correspond to the mean life curve minus two standard deviation from the experimental data to allow for wide variations in production [102]. At the minimum, the analyst should be aware of the above complexity in the imprecise data. Future valuable work, to build confidence in both the maintenance data and the proposed modified stress approach, would be to utilise Monte Carlo concepts for statistical estimations of the variables in FL_m and FL_p [134].

Nonetheless, there is a way forward when expert judgment, FEA, and in-service information are used to substantiate the fatigue assessment process. The requirement for expert judgment in the design and through-life management of structures is by no means a new concept. Expert judgement is often required when applying a factor to account for uncertainty of the applied loads in the structural reliability assessment of bridges with respect to the fatigue

failure. This is despite reasonable accuracy of the load measurements [135]. Similarly, sound judgement based on the analyst's practical experience is needed to define the long-term seaway loads that sufficiently represent the fatigue demand that the ship structure will experience, and to design some welded details [136, 137].

Uncertainty in the fatigue capacity of welded joints under constant amplitude loading, relating to geometrical and material parameters, has been recognised over several decades [138-140]. This uncertainty is compounded when variable amplitude loading is applied to the joint. Moreover, the fatigue life of the welded joints is a function of the fourth power of the stress range [126]. Given that a predictive method cannot be expected to produce estimates that are less uncertain than the information used to verify the method, the accuracy of the predicted fatigue life values is satisfactory. In addition, the process to validate the proposed implementation of the nominal stress approach is considered an improvement on that of a comparative study of the fatigue assessment of a pad detail on a containership, which used the design life as the baseline [13].

The study presented compliments the work of Al Zamzami and Susmel [124], which was based on experimental data, because the nominal stress concept was assessed in the context of in-service experience. Soliman *et al.* [55] scoped their research to the fatigue life evaluation of one detail on an aluminium vessel by means of the hot-spot stress concept. Their work is expanded in the present study as five different welded details were analysed, and the applicability of a structural design code was specifically investigated. In addition, a modified nominal stress extraction process has been detailed, which extends upon the guidance provided by Eurocode 9.

It is recommended that the proposed implementation of the nominal stress approach be supported through undertaking a controlled experimental and/or simulation program. In addition, the work presented in the chapter may be extended by investigating similar aluminium welded joints, at other locations, to test the robustness of the findings.

4.8 Conclusion

Both naval ship designers and in-service managers require reliable fatigue evaluation approaches that are sufficiently accurate but also time-efficient to minimise costs. Therefore, this chapter proposed a refinement of the nominal stress approach for joints typical of aluminium welded ship details. The refinement process leverages both in-service maintenance reports and stress spectra derived from long-term strain measurements acquired from a hull

monitoring system onboard a 56 m aluminium patrol boat. In addition, a modified nominal stress extraction process was detailed that extends upon guidance provided by Eurocode 9.

Where to Next?

The nominal stress approach proposed in this chapter is utilised in the subsequent chapters of the thesis.

In Chapter 2 evidence of the considerable influence of slamming on the fatigue life of HSLC, when compared to accounting for the global wave induced stresses alone, was uncovered. Similarly, it is necessary to investigate the contribution of slamming to the fatigue damage incurred in the studied naval HSLC as part of improving fatigue life assessment. This requires the development of a method to identify slam events experienced by the naval HSLC, which is presented in Chapter 5.

Chapter 5. Identification of Slam Events Experienced by a High-Speed Craft

The work presented in this chapter was published in Ocean Engineering. The paper has been edited for inclusion into this thesis to avoid repetition and to improve readability. The citation is:

Magoga, T., Aksu, S., Cannon, S., Ojeda, R., and Thomas, G., *Identification of Slam Events Experienced by a High-Speed Craft.* Ocean Engineering, 2017. **140**: p. 309-321.

5.1 Introduction

As noted in Chapter 2, slamming loads and associated responses of HSLC have been known to have a significant impact on the stress magnitudes experienced in the structure [20, 22]. In order to improve understanding of the influence of slamming on the fatigue life of HSLC, the definition of a slam event needs to be established.

Treating slamming- and wave-induced stress components separately can also be practical in structural integrity assessments performed analytically or numerically. Similarly, the contributions of wave-induced and whipping stresses to the total stress can be related in a probabilistic manner. The peak values of the wave- and slamming-induced (whipping) loads may be asynchronous; the relationship between wave and slamming effects is dependent on the sea state, vessel speed, and wave frequency [39, 141]. Therefore, slam event identification can be used to establish both the requirement and a practical approach to account for slamming loads in ship structural assessment based on a fatigue criterion.

Slam detection is also useful information in structural health monitoring and operational guidance. This can take the form of a slam avoidance system that predicts the possibility of a vessel approaching operating conditions that could induce slamming. Alternatively, a slam monitor can also indicate the trend over time in relation to impacts that exceeds warning levels. Colwell and Stredulinsky [142] discussed the development of polar plots to indicate which combinations of vessel speed and heading can lead to a high probability of exceedance levels for slamming loads on the KINGSTON Class Maritime Coastal Defence Vessel. The authors also examined ways to provide real time operator guidance to enable informed evaluation of the risk of severe slamming versus the urgency of the mission. Part of this work was selection of an appropriate parameter to indicate slam severity, such as centreline vertical bow acceleration or structural response provided by strain gauges. Even so, efforts to improve operational advice regarding slamming and its effects on the structure have tended to be focused on larger vessels. Barhoumi and Storhaug [54] presented an assessment of whipping and springing of a large container vessel. Data from a HMS was used to study fatigue damage rates with respect to re-routing and speed reduction and the associated whipping contribution. Nielsen *et al.* [41] outlined a procedure for hull-girder fatigue damage rate prediction, taking into account whipping stresses, for hypothetical changes in ship course and speed. The proposed spectral method was verified against full-scale results of a container ship analysed by the rainflow counting method.

As driven by the need to improve fatigue life prediction of relatively HSLC, this chapter presents an investigation of different approaches to characterise and count slam events using full-scale measurement data from an ACPB. Attention is directed to determining a robust method to decompose stress time records into its wave and whipping stress parts, indicative fatigue damage induced by slamming, and slam event definition and detection.

5.2 Hull Monitoring System

The following analysis utilises data acquired from the *Glenelg* HMS (Section 3.3.1). Five of the strain gauge locations, displayed in Figure 3-2 and described in Table 3-4, are analysed. These strain gauges are B through F.

The ACPBs' primary operational area is the North-West of Australia. Sea state information relating to this area has been sourced through the RAN Meteorology and Oceanography Office. From significant wave height statistics over a 2.5 year period, it is deduced that *Glenelg* may have been operated 86% of the time in seas up to the top of Sea State 4, 13% in Sea State 5, and 1% in Sea State 6. *Glenelg's* speed profile features two speed ranges in which the vessel operates over 25% of the time; 4 to 6 knots, and 13 to 17 knots [143].

Three sets of five consecutive hours in which *Glenelg* experienced relatively high stresses due to operating in significant sea states have been extracted. This data is used to investigate slam detection. From satellite hindcast data of the significant wave heights covering the area of operations, the vessel encountered Sea State 5 during Sets 1 and 2, and Sea State 4 during Set 3. The stress measured by strain gauge D, vessel heading, and speed during each dataset are shown in Figure 5-1.

During most of the duration of Set 1 the vessel was heading West at approximately 14 knots, though changed heading to East and dropped speed for a portion of the fourth hour. During most of the duration of Set 2, the vessel was heading South-South-West at approximately 16 knots. However, for parts of the second and third hours the vessel changed direction to East and dropped speed. Noticeable in both of these sets, at strain gauge location A the changes in the encounter wave frequency and speed reduction resulted in a substantial decrease in stress magnitudes. In addition, the vessel speed features some variability that is attributed to involuntary speed reduction caused by the relatively severe sea state. During most of the duration of Set 3 the vessel was heading East at approximately 15 knots.

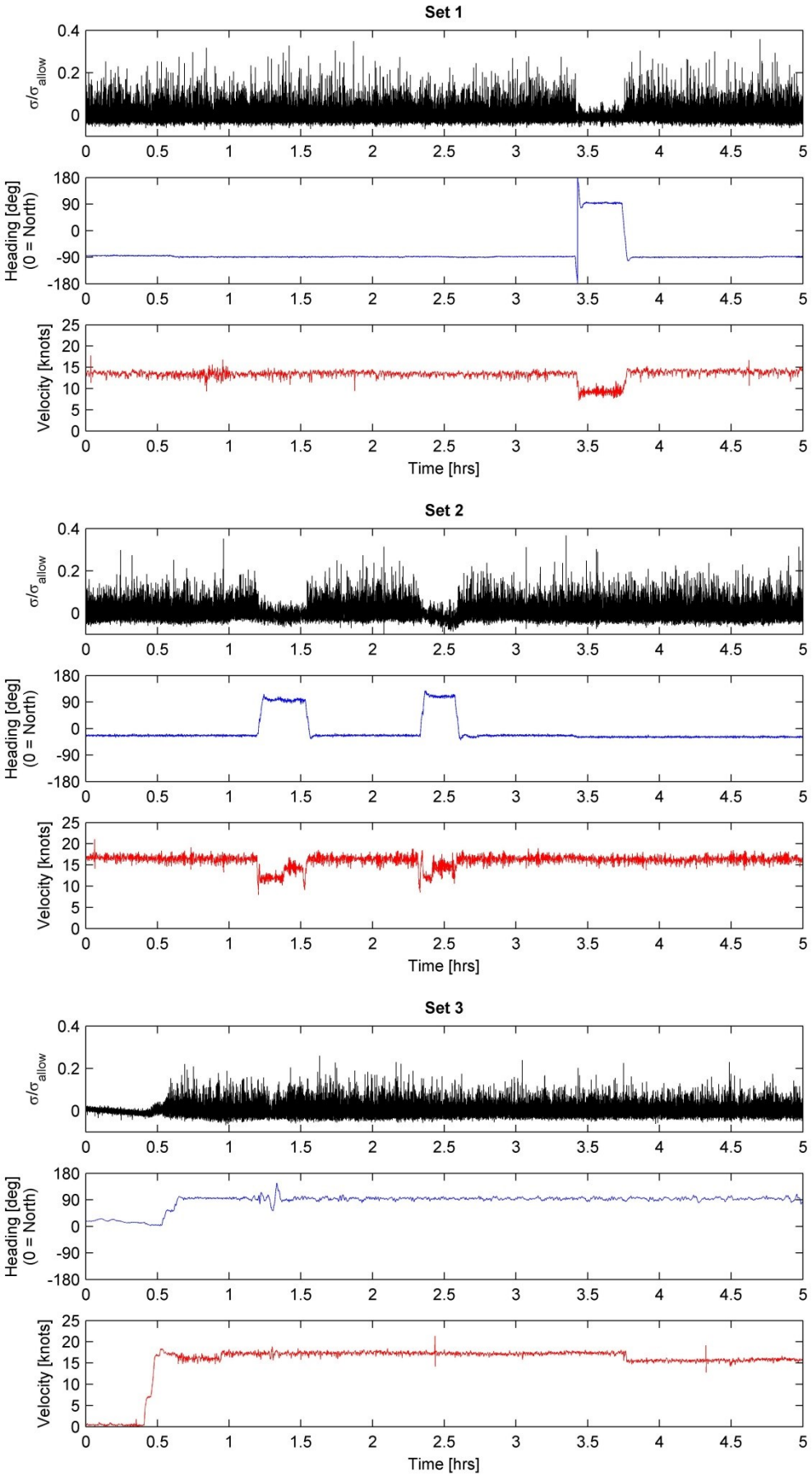

Figure 5-1: Stress measured by strain gauge D, heading, and, vessel speed during Set 1, Set 2, and Set 3

5.3 Decomposition of wave and whipping stress from total response

As previously mentioned, the decomposition of the slamming and wave-induced contributions from the total measured stress is important for the calibration of numerical models, and to gain a better understanding of the contribution of the individual stress components to fatigue [41, 144, 145]. The structural response to slamming loads usually occurs at a higher frequency than the wave-induced response. To decompose the stress time record into its wave- and slam-induced constituents, the cut-off frequency that differentiates the low and high frequency signals is required to be found.

Spectral density estimates of the stress records are used to identify the cut-off frequency. A spectral density function of a time record provides a measure of the strength of its component frequencies. The ensemble-averaged spectral density estimates of the digitised stress record are computed using finite Fourier transforms, and a Hamming window is applied to the data to reduce spectral leakage.

As an example, Figure 5-2 shows the spectral density estimate of a one-hour time record at strain gauge location D. The largest response of the structure is to wave-induced loading between 0 and 1.8 Hz. The next two peaks in the response at approximately 2.5 and 5 Hz are the two-node and three-node natural modes of the ACPB structure. At approximately 13.6 Hz there is a sharp peak, which is believed to be due to machinery vibrating near the strain gauge.

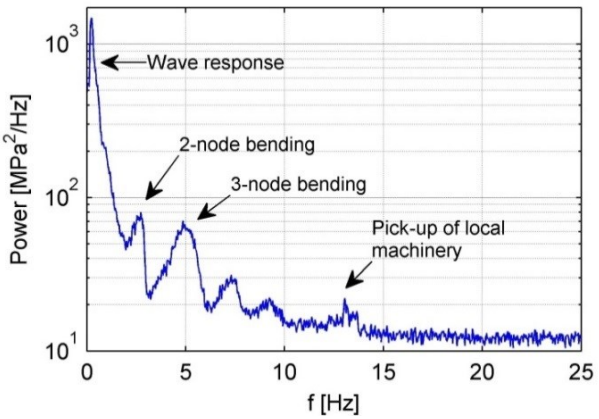

Figure 5-2: Spectral density estimation of a one hour time record at strain gauge location D

The spectral density estimates of each hour of response data in Set 1, up to 10 Hz, at strain gauge locations D, E, and F are compared in Figure 5-3. As expected, the frequencies at which peaks occur are similar.

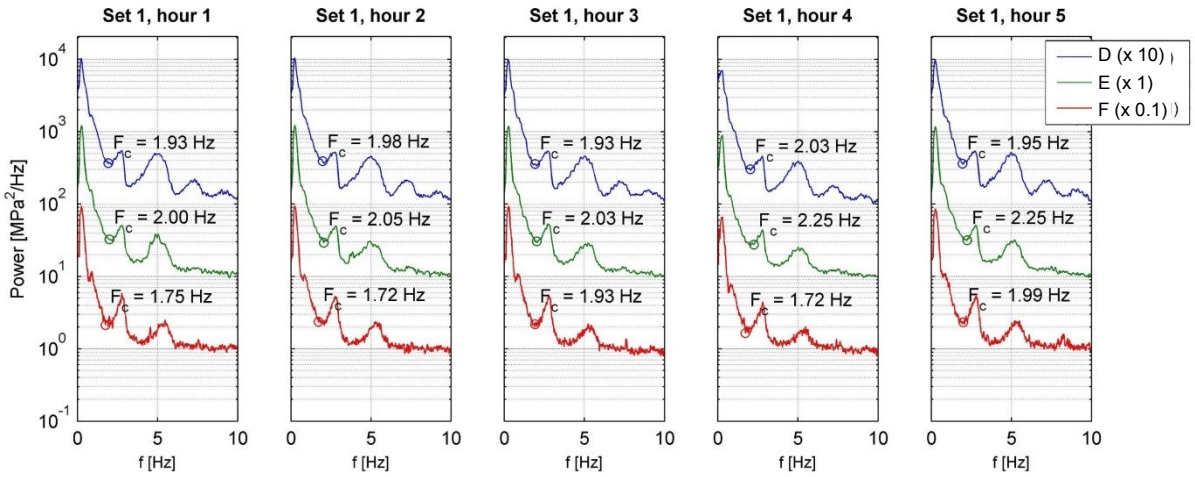

Figure 5-3: Comparison of spectral density estimation during five different hours at strain gauge locations D, E, and F

The observations from the spectral density estimations of the measured strain records are verified by comparison to the results of natural frequency analysis of a finite element model of the ACPB. The natural frequency analysis was performed in MAESTRO [96]. A displacement likely to be the operational condition of the ACPB was assumed, and stillwater conditions were used. In MAESTRO, fluid added mass is generated for all wettable elements (hull plating) below the waterline using a panel method. The mode extraction method selected was Subspace [146].

The two-node and three-node mode shapes of the ACPB calculated using finite element analysis, in wet mode, are displayed in Figure 5-4 and Figure 5-5 respectively. A summary of the computed and measured two-node and three-node vibration frequencies is provided in Table 5-1. The values are comparable, and verify the natural frequencies found in the measured data. The small differences between the measured and computed frequencies are attributed to the numerical method used to calculate the mass of the seawater in the finite element software. In addition, as the vessel moves through waves it will heave and pitch the positions of the bending nodes move longitudinally.

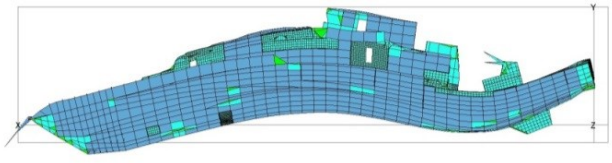

Figure 5-4: Two-node mode shape of ACPB (scaled x1000)

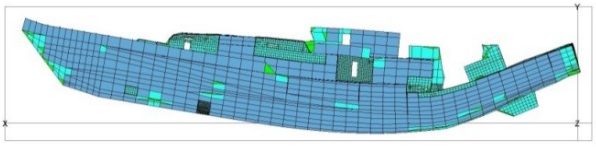

Figure 5-5: Three-node mode shape of ACPB (scaled x1000)

Table 5-1: Comparison of Computed and Measured Wet Mode Vibration Frequencies

	Computed	Measured	Difference
2-node [Hz]	2.4	2.5	4%
3-node [Hz]	4.6	5.0	7%

The sensitivity of the cut-off frequency F_c on the resulting isolated wave-induced and whipping stresses is assessed to ensure that an appropriate value is used. For a high-speed catamaran, F_c has been defined as the frequency where half the signal is attenuated, or double the average encounter wave frequency F_e [58]. Alternatively, the cut-off between the wave frequency and the high frequency response has been represented by the valley between the first and second peaks in the power spectral density [22, 41, 145]. As an indicator of the effect of F_c, Figure 5-6 shows the sensitivity of the Root Mean Square (RMS) of the difference between the total and wave-induced stresses (residual) to F_c at strain gauge location D during sets 1 and 2. F_c is expressed as F_e multiplied by a factor β. For all hours the residual decreases as F_c increases, though becomes asymptotical. A similar trend was reported by French [58]. In Figure 5-7 the sensitivity of the decomposition of the total stress to F_c is illustrated in the time domain via samples of the total, wave-induced and whipping stress (non-dimensionalised by the allowable stress σ_{allow} of the ACPB) for β values of 2 and 11. When F_c is double F_e, though the residual is reduced by approximately 40% (see Figure 5-6), the underlying wave response does not match large rises and falls in the total response. On the other hand when β is 11, and almost coincides with frequency at which the valley between the first two peaks in the spectral response occurs F_{valley}, the residual is reduced by approximately 85% and the wave-induced stress time record better follows the behaviour of the total stress. Therefore, to ensure that the wave and whipping responses are appropriately isolated, F_c for the ACPB is defined as F_{valley}.

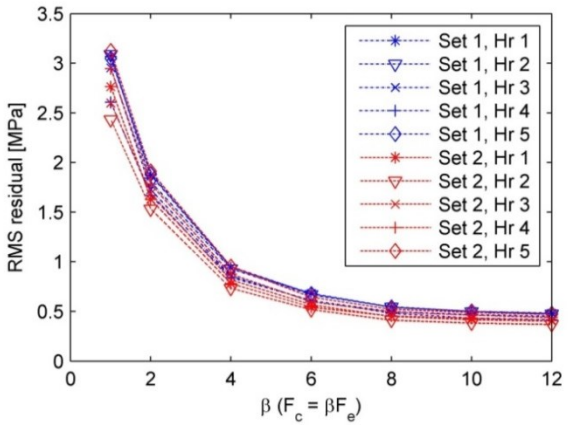

Figure 5-6: RMS of difference between total and wave-induced stress (residual) at strain gauge location D

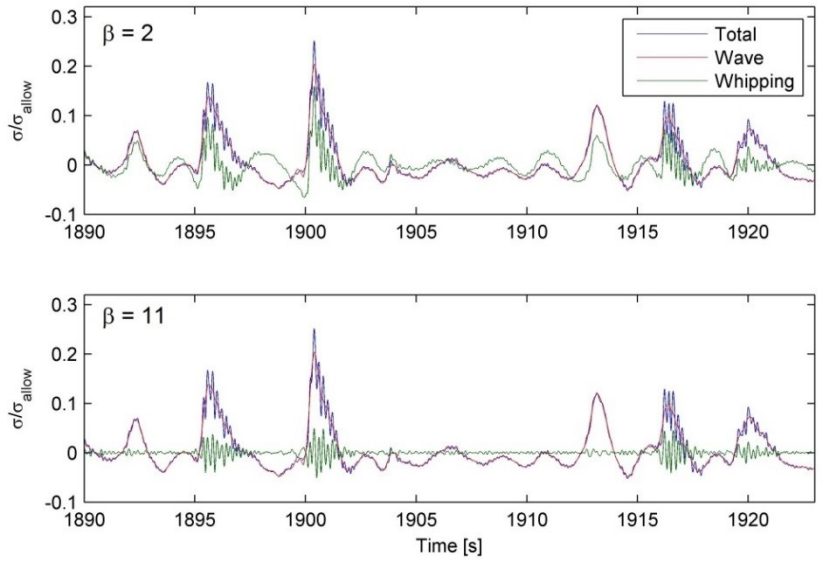

Figure 5-7: Sensitivity of wave-induced and whipping stresses to β = 2 and 11 ($F_c = \beta F_e$), for F_e = 0.18 Hz

Based on the above results, the wave-induced and whipping stress components are obtained using steps consistent with those outlined in [22, 41, 145]. The structural response is assumed the measurement of strain below 7.5 Hz; vibration modes greater than 7.5 Hz die out quickly because of strong structural damping characteristics. As such, the signal above 7.5 Hz is truncated by applying a Chebyshev low pass filter to produce the filtered 'total' stress record. The cut-off between the wave frequency and the high frequency response is represented by the valley between the first and second peaks in the power spectral density. As evidenced in Figure 5-3 F_c varies with the location due to proximity to a node or anti-node. Further, F_c is influenced by wave heading, wave period and displacement of the vessel. As such, F_c is determined for each hour of strain data for each gauge. The whipping component of the stress record is obtained by applying a Chebyshev band pass filter between the valley and 7.5 Hz. The wave-induced component can also be determined by applying the Chebyshev band pass filter between zero and F_c.

The location of F_c is shown in the hourly spectral density estimates for Set 1 in Figure 5-3. The value of F_c varies slightly per hour.

Figure 5-8 shows a sample of the total stress record, and its associated wave-induced and whipping components, at strain gauge locations D, E, and F. This section of the time record is highlighted because at approximately 1900 s the vessel responded to a relatively severe slam impact. This is exhibited by a relatively large increase in the total stress. The impulsive loading of the slam imparted sufficient energy at the bottom forward section of the

hull to excite transient vibration, as evidenced by the large oscillations in the slamming-induced stress component beginning at approximately 1900 s at strain gauge location A. The whipping persisted for about three seconds before being damped so that only the underlying wave response remained. In contrast, there are fewer whipping oscillations visible at strain gauge location E than at the bottom gauges. One possible explanation for this is that the energy of the slam, propagating from the bottom forward section of the hull through the structure, is dampened by the hull-girder. This results in reduced frequency vibration further aft and on the superstructure.

Particularly perceptible at strain gauge location D, the magnitude of the peak and the trough of the wave-induced stress during the slam event at 1900 s were significantly large compared to those of the proceeding and subsequent wave encounters. That is, the contribution of the whipping stress alone does not account for the large stress rise and magnitude of the total stress in the slam event. When the vessel encounters a relatively large wave, the energy from the heavy slam impact is partly absorbed by the forward, bottom section of the hull. This manifests as a significant stress rise generally in the sagging condition, in addition to excitation of bending modes. As such, there is distinctive asymmetry in the stress response between the sagging and hogging conditions.

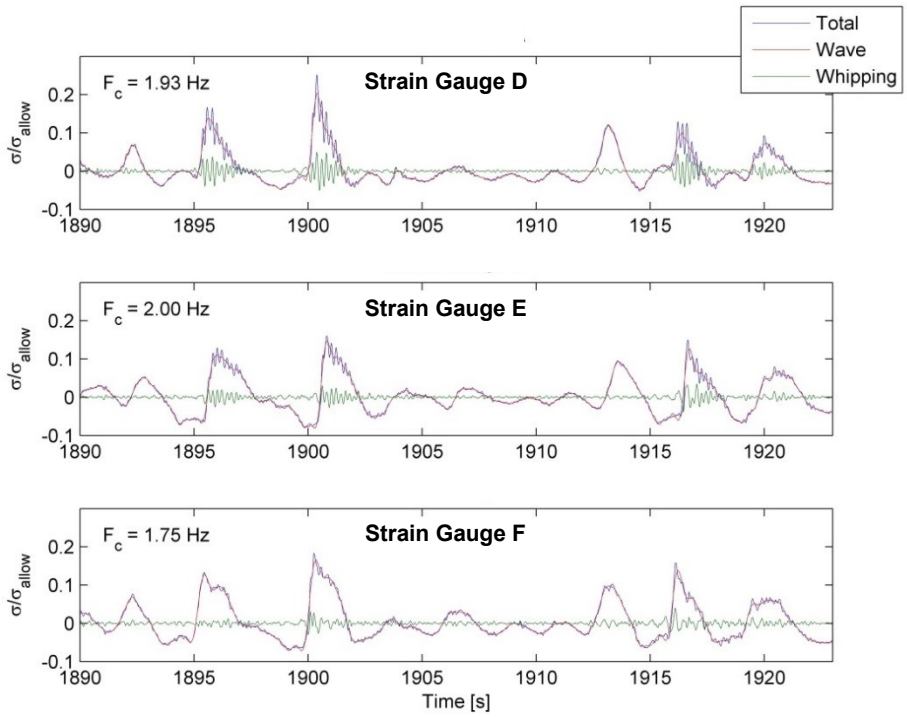

Figure 5-8: Sample stress record from Set 1 hour 1 at strain gauge location D, E, and F

5.4 Importance of Slamming

Fatigue loading is the ensemble of different structural load variations of particular magnitude and occurring in a certain sequence. The loading of the structure depends on its modes of operation; for ships, this is characterised by sea state and speed.

To demonstrate the importance of the high frequency hull-girder response in fatigue damage estimation of the ACPB, a counting procedure and cumulative damage theory are applied to the stress measurements. The stress records were reduced into spectra of cycles using the rainflow counting method (Section 3.7.3). The Palmgren-Miner rule [99] is used to calculate the fatigue damage (Section 3.6).

Eurocode 9 construction details and fatigue resistance data [102] are available for use in fatigue analysis (Section 3.8). The construction details selected for this analysis are given in Table 5-2.

Table 5-2: Detail categories of strain gauge locations

Strain Gauges	Eurocode 9 Detail Type	Fatigue limit [MPa]	Justification
D & E	7.2.1 - welded from both sides using full penetration welding on flat solid	25.1	Strain gauges are on plating, in the vicinity of butt-welded joints that are assumed to be welded from both sides. A crack that initiates is assumed to be due to a flaw or discontinuity in the weld.
C, D, & F	5.5 – continuous fillet weld	20.1	Strain gauges are located on the flange of longitudinal girders, joined to the web of the girders using a continuous fillet weld. The dominant load direction (longitudinal) is in-line with the weld. Again, a crack that initiates is assumed to be due to a flaw or discontinuity in the weld.

To appreciate the contribution of the high frequency slamming response to fatigue damage in the ACPB structure, plots of the fatigue damage estimated using the total stress and wave-induced component of the stress time records for the five strain gauges considered are provided in Figure 5-9. Time records for strain gauges D and E were available for all sets. However, strain gauge F was damaged before the time covered in Set 3 and as such fatigue damage values are unavailable. In addition, strain gauges B and C were installed at a later stage and thus the respective fatigue damage values are only available for Set 3.

To derive the fatigue damage accumulated due to slamming, it is assumed that the slam-induced component is the difference between the total fatigue damage and that derived from the wave-induced component. This definition has been used in estimations of the fatigue damage of a container ship based on full-scale measurements of hull girder stresses [41, 147].

As indicated by the difference in the fatigue damage estimated using the total stress and wave-induced stress component from Figure 5-9, the contribution of slamming to the fatigue damage is generally considerable at all strain gauge locations. During Set 1 the average contribution of slamming to the fatigue damage at strain gauge location D was 46%, at E 35%, and at F 37%. The slamming contribution during Set 2 was similar; 48% at strain gauge location D, 36% at E, and 35% at F. For Set 3 the average contribution of slamming to the fatigue damage at strain gauge location D was 50%, at E 40%, at B 49%, and at C 57%.

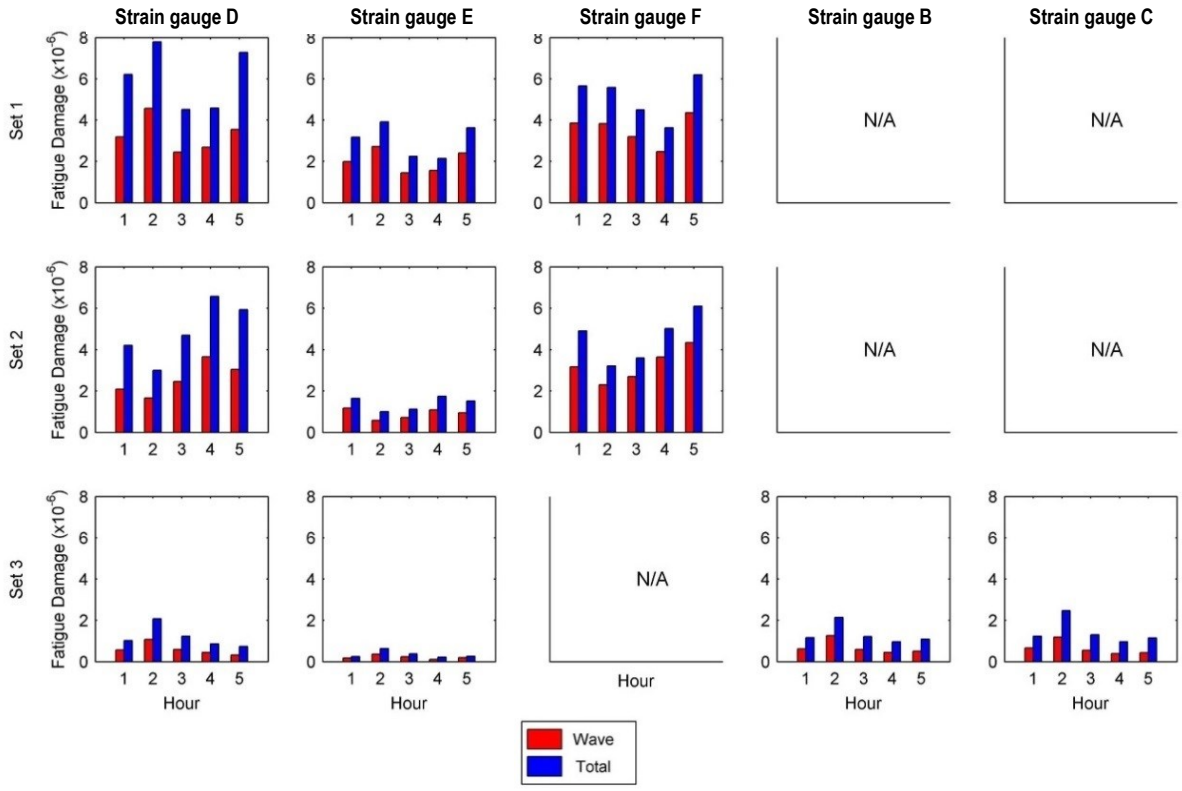

Figure 5-9: Hourly fatigue damage incurred at different strain gauge locations, estimated using total and wave-induced stress time records

During Sets 1 and 2, the largest fatigue damage occurred at strain gauge location D. However, during Set 3 the largest fatigue damage was incurred at strain gauge location C. It should be noted that stresses at these strain gauge locations do not necessarily represent the largest stresses observed in the structure, as the strain gauges were located in relatively easily accessible areas and away from major stress concentrations.

Figure 5-9 also illustrates that the period in which the vessel sustained the most fatigue damage was Set 1.

5.5 Slam Identification

Approaches to establish a ship-specific slam event definition by interpreting structural response data have been investigated. Ochi [148] concluded that two conditions were necessary for slamming to occur; the relative motion must exceed the sectional draft, and the relative velocity at the instant of re-entry must exceed a threshold magnitude specific to a vessel. However, Dessi and Ciappi [63] found that in segmented-hull model testing, slam events that did not satisfy the Ochi velocity threshold were responsible for large vertical bending moments. As such the authors proposed a slam event identification method labelled the whipping criterion, whereby the whipping response in the form of the high frequency contribution to the total vertical bending moment was set. Thomas *et al.* [22] used a stress derivative threshold as a criterion for slamming detection. The definition is independent of strain gauge location and sea state conditions. Alternatively, the damage incurred in the structure due to slamming can be considered. Thomas *et al.* [20] proposed a criterion based on fatigue damage. The stress level at which the fatigue resistance curve of a particular material and structural detail provides a criterion for defining a threshold above which slam events are significant.

Given that no universally accepted criterion for identification of slams exists in the open literature, a slam criterion for the ACPB based on the measurement data is investigated. The approaches considered are; application of a stress magnitude threshold, application of a stress rate threshold, and fatigue damage contribution of slam events.

Thomas *et al.* [22] examined thresholds applied to the total stress to detect slam events experienced by a catamaran. The suitability of applying a total stress threshold was investigated for the present vessel, at strain gauge location D. As illustration, for a given threshold and sample time record shown in Figure 5-10 there are six peaks above the threshold. These peaks are identified as slams. In contrast to the first, third, fourth, and fifth slams which feature relatively significant whipping, the second and sixth “slams” induced relatively minor whipping and are thus not true slam events. In other words, it is possible for the magnitude of the total stress to exceed the defined target without excitation of transient vibration. Therefore, it is concluded that a target defined in terms of the isolated whipping stress is suitable, and algorithms to detect slams have been developed accordingly.

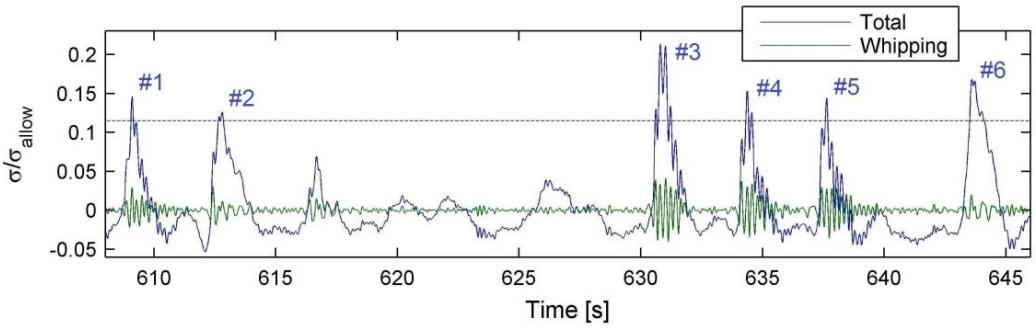

Figure 5-10: Sample of slam detection using total stress rate threshold at strain gauge location A (peak of slam event depicted by cross) and whipping stress component

As discussed by Colwell and Stredulinsky [142], the provision of effective operator guidance regarding slam severity is dependent on the selection of an appropriate indicator (location and type of sensor). Based on the sample stress time record shown in Figure 5-8, strain gauge E is not a good candidate for slam detection because the high frequency component of the stress does not feature the multiple oscillations and decay of typical slam events. However, a strain gauge located on the forward section of the centreline girder (strain gauge D) is an effective reference. As this part of the structure experiences the slam impact, and is on the centreline, addressing complexities such as structural damping and asymmetry in the response can be avoided.

5.5.1 Stress Criterion

Application of a stress magnitude threshold involves determining if the whipping stress within one slam event exceeds a defined target stress, for example a percentage of the allowable stress $\sigma_{allow.}$ The magnitude of the target stress was chosen by conducting a sensitivity analysis that gauged the effect that the variation of the percentage of σ_{allow} had in the number of slams detected. Stress threshold values between 1.45% and 2.45% of σ_{allow} in 0.25% increments were set in order to compute the number of slams at strain gauge location D.

A sample total stress time record and the corresponding slam-induced component with detected slam events is provided in Figure 5-11. The stress peaks and troughs of the slams are denoted by crosses and asterisks.

For the timeframe shown in Figure 5-11, four slams were detected at strain gauge location D. Interestingly, though a relatively large peak in the total stress occurred at approximately 1913 s it was not counted as a slam event because the whipping response was below the threshold. A similar total stress peak at approximately 1916 s was identified as a

slam event as the whipping response exceeded the defined threshold. The magnitude, temporal and spatial distributions of wave and slamming loads have different dependencies to the encountered wave height and frequency and vessel speed. Given the probabilistic nature of wave and slam loads, it can be expected that the whipping stress relative to the total stress can vary from one wave encounter to the next.

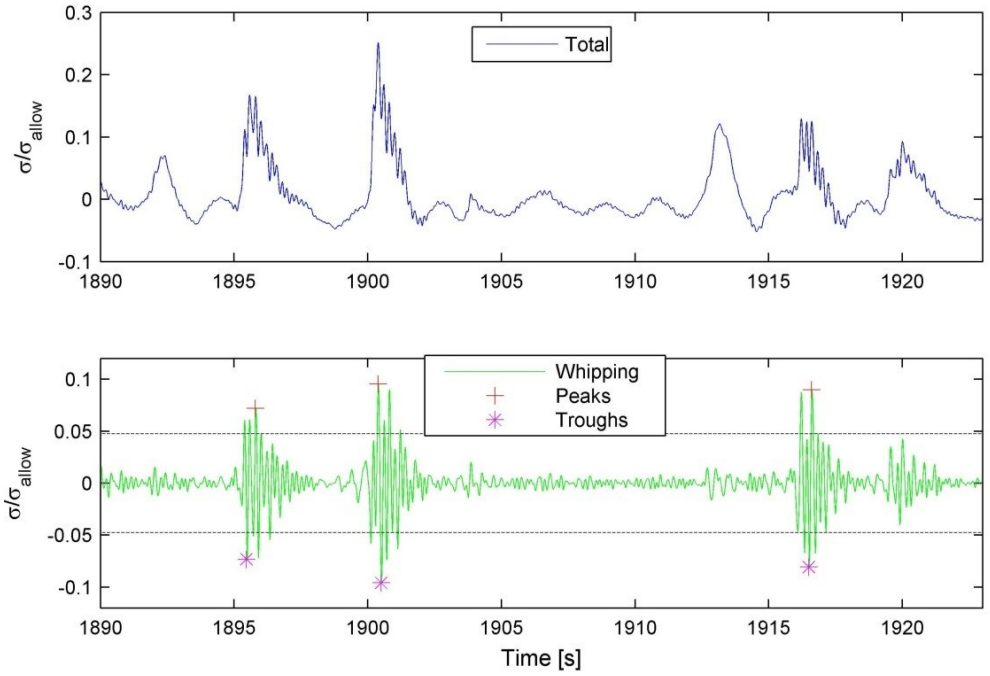

Figure 5-11: Sample of slam detection using stress magnitude threshold at strain gauge location D (peak and trough depicted by cross and asterisk)

5.5.2 Stress Rate Criterion

Application of a stress rate threshold involves determining if the derivative of the whipping stress within one slam event exceeds a defined target. This method is proposed to be favourable over the stress magnitude criterion, because the threshold values need to be modified as the sea conditions (sea state) change, and slowly changing stress peaks with large magnitude are identified but small and quickly changing slam events are not [20].

For consistency in the units, the threshold value for the stress rate approach is taken as σ_{allow}/dt, where dt is $1/F_s$. Again, a sensitivity analysis of the effect of varying the stress rate threshold between 3.75% and 4.75% of σ_{allow}/dt in 0.25% increments on slam occurrence (see Section 5.3 for further verification). A sample whipping stress time record measured at strain gauge A, and its derivative, is presented in Figure 5-12.

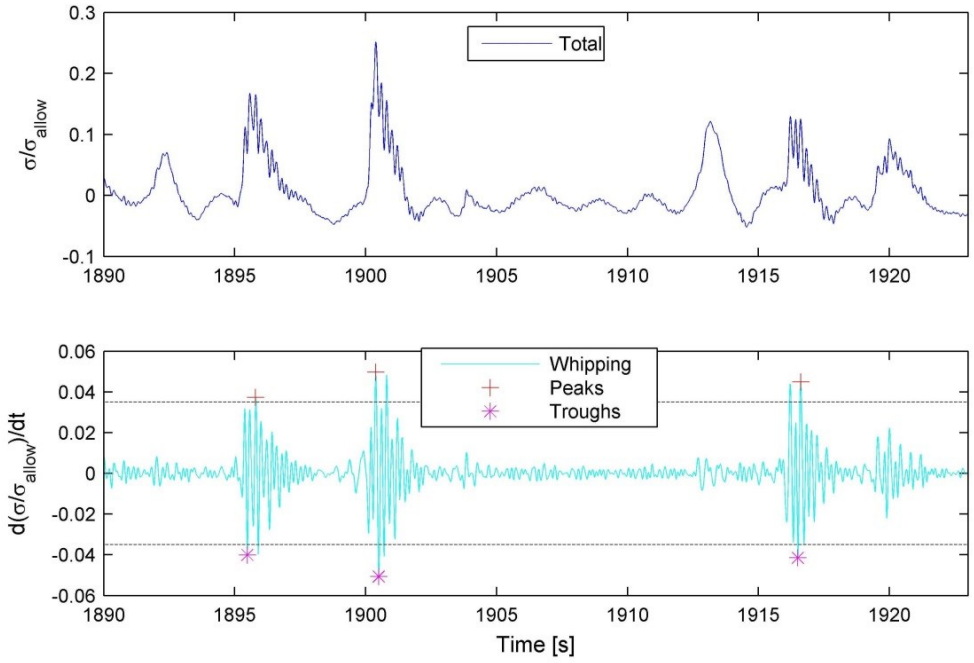

Figure 5-12: Sample of slam detection using stress rate threshold at strain gauge location A (peak and trough depicted by cross and asterisk)

5.5.3 Visual Inspection

As a means of verification of the whipping stress magnitude and rate approaches, and their associated threshold values, the stress time records measured at strain gauge location D were visually inspected. Visual inspection encompasses judging the stress record on the significance of the high frequency component and the decay after several oscillations.

Checks between the slam event times detected by each approach (in an algorithm) and by visual inspection were performed:

- i = the number of slams in common
- ii = the number of slams that were detected by the algorithm but not visually.
- iii = the number of slams that were detected visually but not by the algorithm.

Further, the success of the whipping stress magnitude and derivative approaches was measured via an "efficiency metric", defined as the difference between the number of slams in common (i) and the number of slams that were found not to be in common (ii + iii) divided by the number of slams that were visually detected: efficiency = (i – ii – iii)/(no. slams visually detected).

The results of the visual inspection, and the sensitivity of the slam occurrence to variation of the stress magnitude and rate thresholds, are presented in Table 5-3. For example, during the first hour in Set 1, 95 slam events were distinguishable by visual inspection. With

the whipping stress magnitude threshold set to 1.95% of σ_{allow} the algorithm detected 91 of these slams, though found an additional 25 slams and missed four slams. As such the efficiency for this threshold type and value was 0.65. In comparison, using the whipping stress derivative criterion set to 4% of σ_{allow}/dt the algorithm found 90 of the visually distinguishable slams, detected an additional 15 slams, and missed five slams. The efficiency for this threshold type and value was 0.76.

In Table 5-3, the threshold for each criterion type that was the most efficient in detecting the slam occurrence for each hour is highlighted. In general, the whipping stress derivative was more efficient than the whipping stress magnitude at detecting slams, and the optimum threshold varied less with each hour. Overall, the optimum threshold of the whipping stress magnitude was 2.2% of σ_{allow}. The optimum whipping stress rate threshold was 4% of σ_{allow}/dt.

The approaches for slam identification presented in this chapter are specific to one strain gauge in a certain vessel. This is because the structural response and operational profile of naval HSLC, such as the ACPB, are quite distinct from conventional vessels (as discussed in Chapter 2). In addition, the structural response to slamming varies at different locations. To further demonstrate that the selection of the sensor location is important for slamming detection, the whipping stress rate approach has been applied to the data measured by strain gauges B and C and the results are given in Table 5-4. As can be seen, the algorithm when applied to this response data does not successfully detect slams. For example, for the first hour 37 slams were visually distinguishable. With decreasing whipping stress rate threshold, though there is more commonality between the number of slams detected by both the algorithm and by eye, there are substantially more slams that are erroneously picked by the algorithm. This result is attributed to the relatively small dynamic response of the structure further aft and at main deck level.

Table 5-3: Comparison of visual inspection, whipping stress magnitude, and whipping stress rate approaches to define slam events based on strain gauge D data

Set	Hour	Check Type	Whipping stress magnitude (% of σ_{allow})					Whipping stress derivative (% of σ_{allow}/dt)					Visual detection
			2.45%	2.20%	1.95%	1.70%	1.45%	4.75%	4.50%	4.25%	4.00%	3.75%	
1	1	i	59	76	91	94	95	59	67	75	90	93	95
		ii	4	11	25	42	89	2	4	9	13	21	
		iii	36	19	4	1	0	36	28	20	5	2	
		Efficiency	*0.20*	*0.48*	*0.65*	*0.54*	*0.06*	*0.22*	*0.37*	*0.48*	*0.76*	*0.74*	
	2	i	52	67	78	80	82	54	59	71	78	80	82
		ii	2	6	22	44	85	1	2	4	11	21	
		iii	30	15	4	2	0	27	22	11	4	2	
		Efficiency	*0.24*	*0.56*	*0.63*	*0.41*	*-0.04*	*0.32*	*0.43*	*0.68*	*0.77*	*0.70*	
	3	i	40	46	56	60	61	40	46	56	60	61	63
		ii	2	2	5	12	20	2	2	5	12	20	
		iii	23	17	7	3	2	23	17	7	3	2	
		Efficiency	*0.24*	*0.43*	*0.70*	*0.71*	*0.62*	*0.24*	*0.43*	*0.70*	*0.71*	*0.62*	
	4	i	36	41	47	49	52	36	41	47	49	52	52
		ii	0	0	4	6	14	0	0	4	6	14	
		iii	16	11	5	3	0	16	11	5	3	0	
		Efficiency	*0.38*	*0.58*	*0.73*	*0.77*	*0.73*	*0.38*	*0.58*	*0.73*	*0.77*	*0.73*	
	5	i	54	61	65	72	76	54	61	65	72	76	77
		ii	2	4	5	10	20	2	4	5	10	20	
		iii	22	16	12	5	1	22	16	12	5	1	
		Efficiency	*0.39*	*0.53*	*0.62*	*0.74*	*0.71*	*0.39*	*0.53*	*0.62*	*0.74*	*0.71*	
2	1	i	22	29	37	37	37	21	26	28	32	34	37
		ii	2	5	23	40	81	2	4	4	11	21	
		iii	15	8	0	0	0	16	11	9	5	3	
		Efficiency	*0.14*	*0.43*	*0.38*	*-0.08*	*-1.19*	*0.08*	*0.30*	*0.41*	*0.43*	*0.27*	
	2	i	18	23	24	25	25	19	20	23	24	25	25
		ii	0	2	7	24	64	0	2	2	5	8	
		iii	7	2	1	0	0	6	5	2	1	0	
		Efficiency	*0.44*	*0.76*	*0.64*	*0.04*	*-1.56*	*0.52*	*0.52*	*0.76*	*0.72*	*0.68*	
	3	i	27	38	46	48	48	25	32	38	44	47	48
		ii	0	2	11	27	61	0	1	3	3	10	
		iii	21	10	2	0	0	23	16	10	4	1	
		Efficiency	*0.13*	*0.54*	*0.69*	*0.44*	*-0.27*	*0.04*	*0.31*	*0.52*	*0.77*	*0.75*	
	4	i	32	45	54	58	60	35	40	47	56	58	61
		ii	4	8	16	41	82	1	1	4	6	11	
		iii	29	16	7	3	1	25	21	14	5	3	
		Efficiency	*-0.02*	*0.34*	*0.51*	*0.23*	*-0.38*	*0.15*	*0.30*	*0.48*	*0.74*	*0.72*	
	5	i	48	63	72	73	73	45	52	60	68	73	73
		ii	2	6	25	63	118	2	3	4	10	23	
		iii	25	10	1	0	0	28	21	13	5	0	
		Efficiency	*0.34*	*0.77*	*0.75*	*0.16*	*-0.74*	*0.25*	*0.46*	*0.70*	*0.87*	*0.82*	
3	1	i	8	12	12	12	12	9	10	12	12	12	37
		ii	1	1	5	10	23	1	1	1	2	4	
		iii	4	0	0	0	0	3	2	0	0	0	
		Efficiency	*0.25*	*0.92*	*0.58*	*0.17*	*-0.92*	*0.42*	*0.58*	*0.92*	*0.83*	*0.67*	
	2	i	28	41	46	48	49	26	35	40	44	45	25
		ii	0	0	8	28	68	0	0	0	3	8	
		iii	21	8	3	1	0	23	14	9	5	4	
		Efficiency	*0.14*	*0.67*	*0.71*	*0.39*	*-0.39*	*0.06*	*0.43*	*0.63*	*0.73*	*0.67*	
	3	i	11	15	23	23	23	11	14	16	21	23	48
		ii	0	3	11	31	69	0	1	2	4	9	
		iii	12	8	0	0	0	12	9	7	2	0	
		Efficiency	*-0.04*	*0.17*	*0.52*	*-0.35*	*-2.00*	*-0.04*	*0.17*	*0.30*	*0.65*	*0.61*	
	4	i	9	14	18	18	18	8	11	13	17	18	61
		ii	0	0	6	29	57	0	0	0	3	6	
		iii	9	4	0	0	0	10	7	5	1	0	
		Efficiency	*0.00*	*0.56*	*0.67*	*-0.61*	*-2.17*	*-0.11*	*0.22*	*0.44*	*0.72*	*0.67*	
	5	i	7	10	16	18	19	7	8	10	14	15	73
		ii	0	1	4	22	52	0	0	1	1	4	
		iii	12	9	3	1	0	12	11	9	5	4	
		Efficiency	*-0.26*	*0.00*	*0.47*	*-0.26*	*-1.74*	*-0.26*	*-0.16*	*0.00*	*0.42*	*0.37*	

Table 5-4: Comparison of visual inspection, and the whipping stress rate approach to define slam events based on strain gauges B and C data from Set 3

Set	Hour	Check Type	Strain gauge D, whipping stress derivative (% of σ_{allow}/dt)					Strain gauge E, whipping stress derivative (% of σ_{allow}/dt)					Visual detection
			4.75%	4.50%	4.25%	4.00%	3.75%	4.75%	4.50%	4.25%	4.00%	3.75%	
3	1	i	2	2	3	5	6	3	3	4	6	7	37
		ii	1	1	1	1	4	2	2	5	8	12	
		iii	10	10	9	7	6	9	9	8	6	5	
		Efficiency	*-0.75*	*-0.75*	*-0.58*	*-0.25*	*-0.33*	*-0.67*	*-0.67*	*-0.75*	*-0.67*	*-0.83*	
	2	i	7	12	13	16	20	3	6	9	17	19	25
		ii	4	5	8	12	21	4	6	11	20	26	
		iii	32	27	26	23	19	36	33	30	22	20	
		Efficiency	*-0.74*	*-0.51*	*-0.54*	*-0.49*	*-0.51*	*-0.95*	*-0.85*	*-0.82*	*-0.64*	*-0.69*	
	3	i	3	3	5	9	10	2	5	6	9	13	48
		ii	2	2	3	5	12	1	3	5	10	20	
		iii	20	20	18	14	13	21	18	17	14	10	
		Efficiency	*-0.83*	*-0.83*	*-0.70*	*-0.43*	*-0.65*	*-0.87*	*-0.70*	*-0.70*	*-0.65*	*-0.74*	
	4	i	4	5	6	7	9	0	1	2	5	6	61
		ii	0	0	2	2	6	1	2	4	6	12	
		iii	14	13	12	11	9	18	17	16	13	12	
		Efficiency	*-0.56*	*-0.44*	*-0.44*	*-0.33*	*-0.33*	*-1.06*	*-1.00*	*-1.00*	*-0.78*	*-1.00*	
	5	i	3	3	4	5	6	1	3	7	8	10	73
		ii	1	1	3	6	11	0	4	7	11	21	
		iii	16	16	15	14	13	18	16	11	11	9	
		Efficiency	*-0.74*	*-0.74*	*-0.74*	*-0.79*	*-0.95*	*-0.89*	*-0.89*	*-0.58*	*-0.74*	*-1.05*	

5.5.4 Criterion Based on Fatigue Damage

Similar to that proposed by Thomas *et al.* [20], a slam criterion based on the fatigue damage incurred in a structural item is proposed. This method identifies the number of slam events that occurred during a period by calculating the difference in the number of stress cycles, above the fatigue limit of a structural item, between the total and wave-induced stress spectra. The number of slams is rounded to the nearest integer. The value of this method is that it is based on the effect of the slam on fatigue damage, rather than the dynamic response.

As an example, the wave-induced and total stress spectra at strain gauge location D during the first hour of Set 1 is presented in Figure 5-13. The fatigue limit of the construction item is also indicated in this figure.

The fatigue damage criterion has been applied at all three datasets. The resulting number of wave-induced and total stress half-cycles, truncated below the fatigue limit, is provided in Table 5-5. For the first hour in Set 1, there were 19 more stress half-cycles above the fatigue limit in the total stress spectrum than in the wave-induced stress spectrum. Therefore, as the total stress spectrum includes whipping stresses, the estimated number of slam events that induced fatigue damage at strain gauge D location was rounded to nine.

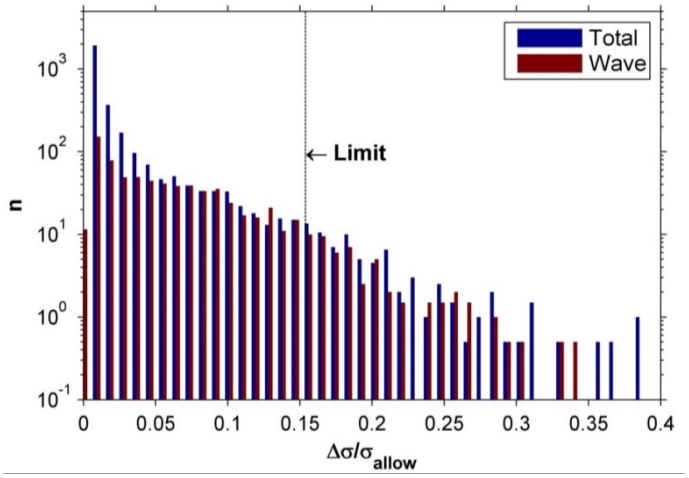

Figure 5-13: Histogram of wave-induced and total stress spectra at strain gauge location D during set 1 hour 1

Table 5-5: Number of half cycles in wave-induced and total stress spectra above fatigue limit at strain gauge location D

$\Delta\sigma/\sigma_{allow}$	Set 1, Hour 1		Set 1, Hour 2		Set 1, Hour 3		Set 1, Hour 4		Set 1, Hour 5	
	Wave stress n	Total stress n	Wave stress n	Total stress n	Wave stress n	Total stress n	Wave stress n	Total stress n	Wave stress n	Total stress n
0.18	30	37	23.5	30.5	25.5	36.5	22	18.5	25	34.5
0.23	6.5	15	8	12	7.5	9	4.5	13.5	7.5	8.5
0.28	5	5.5	5.5	5.5	2.5	5.5	3	4	6	6.5
0.32	1.5	2.5	1.5	4.5	1.5	3.5	2	3	2	4.5
0.37	0	2	2	1	0	0	0	1	0	1.5
0.41	0	0	0	1.5	0	0	0	0	0	1
SUM	43	62	40.5	55	37	54.5	31.5	40	40.5	56.5
DIFF.	*19*		*14.5*		*17.5*		*8.5*		*16*	

$\Delta\sigma/\sigma_{allow}$	Set 2, Hour 1		Set 2, Hour 2		Set 2, Hour 3		Set 2, Hour 4		Set 2, Hour 5	
	Wave stress n	Total stress n	Wave stress n	Total stress n	Wave stress n	Total stress n	Wave stress n	Total stress n	Wave stress n	Total stress n
0.18	20.5	31	17	21.5	19.5	27.5	27	36.5	35	39.5
0.23	3.5	8.5	5.5	7.5	8	12	5.5	7.5	11.5	19
0.28	1	1	2.5	3	1.5	3.5	2	3.5	2.5	6.5
0.32	0.5	1	0	2	1	1	0	1	1	2
0.37	1	1	0	0.5	0.5	1	2.5	2.5	0	1
0.41	0	1	0	0	0	0.5	0	0	0	0
SUM	26.5	43.5	25	34.5	30.5	45.5	37	51	50	68
DIFF.	*17*		*9.5*		*15*		*14*		*18*	

$\Delta\sigma/\sigma_{allow}$	Set 3, Hour 1		Set 3, Hour 2		Set 3, Hour 3		Set 3, Hour 4		Set 3, Hour 5	
	Wave stress n	Total stress n	Wave stress n	Total stress n	Wave stress n	Total stress n	Wave stress n	Total stress n	Wave stress n	Total stress n
0.18	6	9.5	18.5	28	12	13.5	6.5	12	7	11
0.23	3.5	2	3.5	6.5	1	6.5	2.5	1.5	0.5	2.5
0.28	0.5	2.5	1.5	2	0.5	1.5	0	1	0.5	1
0.32	0	0	0	1	0	0	0	0.5	0	0
0.37	0	0	0	0	0	0	0	0	0	0
0.41	0	0	0	0	0	0	0	0	0	0
SUM	10	14	23.5	37.5	13.5	21.5	9	15	8	14.5
DIFF.	*4*		*14*		*8*		*6*		*6.5*	

5.5.5 Summary of Results

A plot of the number of slams detected at strain gauge location D using the three approaches, and by visual inspection, for each hour considered is given in Figure 5-14. The number of slam events identified by the different methods varied. For the time records examined, the whipping stress magnitude of 2.2% of σ_{allow} resulted in the detection of 17% more slam events than found by visual inspection. Using the whipping stress rate threshold of 4% of σ_{allow}/dt, the difference in the slam occurrence relative to visual observation was 6%. The fatigue damage criterion was the least successful, finding only 13% of the slams found visually.

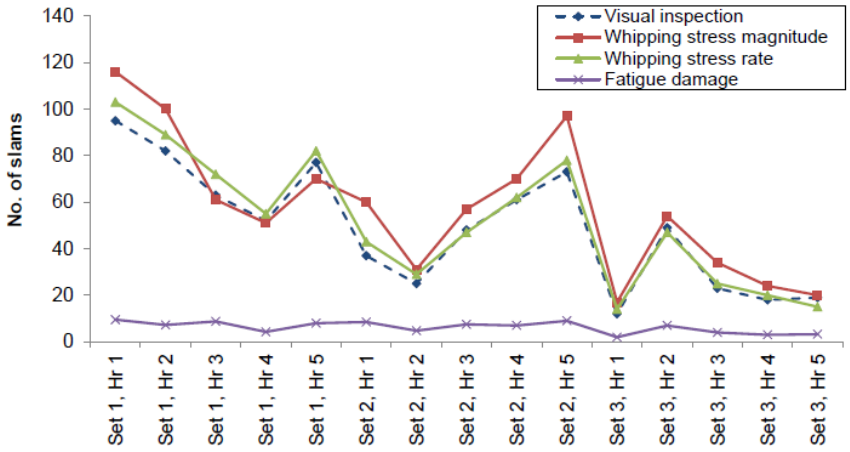

Figure 5-14: No. slams detected at strain gauge location D using different approaches

5.6 Discussion

The benefit of slam identification methods based on stress magnitude and stress rate is that the time at which a slam event is known, and it can be implemented as near real-time structural response feedback to the operator. Therefore, the effect of parameters such as speed, heading, and wave height on the number and severity of individual slam events can be related. However, the threshold values chosen result in a subset of data being treated as slam events. For use of this subset to characterise slam events (for example, in terms of severity and damping), it is possible that a different threshold would produce different results. On the other hand the fatigue damage criterion is based on a defined limit, providing that the fatigue strength and construction detail of a structural item are known. At this stage, the fatigue damage method is limited to computing the number of slams occurring in a given period, the severity of the stress cycle rather than the stress magnitude, and it assumes that one fatigue-contributing stress cycle equates to one slam event. That is, the method does not account for several stress oscillations exceeding the fatigue limit within one slam event. With incorporation of a technique to time-

stamp stress half-cycles that contribute to fatigue, it may be possible to better characterise slam events differentiated via fatigue damage induced by the high frequency response.

Though sets of data representative of different vessel speeds, headings, encounter frequency and sea state were analysed, the applicability of the thresholds to all operational conditions has not been tested. A next step is to use the slam detection approach to investigate the sensitivity of both slam occurrence and severity to encounter frequency, speed, and wave height.

As the approaches considered rely on measured response data, sources of uncertainty are introduced by the measurement process. A level of broad spectrum noise appears to be present in the strain data, which varies from gauge to gauge, and may be attributed to noise in the amplification system. There is also a contribution to the signal from induced electrical noise.

5.7 Conclusion and Further Work

This chapter has presented an investigation into different approaches to identify slam events using strain measurement data of an in-service naval HSLC. Hull monitoring data measured onboard a RAN ACPB, during which the vessel experienced relatively high stresses, were considered. To examine the individual stress components, the total stress was decomposed into the wave- and slam-induced (whipping) contributions. Using spectral density estimations of the measured strain records at four strain gauge locations, the wave-induced and whipping were separated by the cut-off frequency between the low and high frequency response. Differences in the whipping component of the stress time records were observed at different locations. At the bottom gauge locations, the impulsive loading of the slam imparted sufficient energy to excite high-frequency stress oscillations. In demonstrating the importance of high frequency hull-girder response for fatigue damage estimation of the ACPB, it was found that the contribution of whipping stresses to the fatigue damage ranged from 35% to 57% for the hourly records and strain gauges analysed.

Three ship-specific approaches to identify slam events in the measured strain data were examined against visual inspection, or judging the stress record on the significance of the high frequency component and the decay after several oscillations. In general, for the hull monitoring data considered it was found that the most successful criterion for slam detection was that based on the whipping stress rate.

5.8 Acknowledgements

The assistance of Austal Ships, the Patrol Boat Systems Program Office, and DST Group staff involved with the HMS is greatly appreciated.

Where to Next?

This chapter proposed a method to identify slam events experienced by the naval HSLC, and demonstrated the importance of the high frequency hull-girder response for fatigue damage estimation of the ACPB. This work feeds into Chapters 8 and 9.

As per research question #2, in order to identify and develop suitable enhancements to fatigue life assessment methods applied to naval HSLC, it is necessary to first test the applicability of different methods. Accordingly, the next chapter of the thesis is concerned with simplified fatigue analysis (described in Section 3.7.1).

Chapter 6. Comparison between Fatigue Life Values Calculated Using Standardised and Measured Stress Spectra of a Naval High Speed Light Craft

The work presented in this chapter was accepted in a peer-reviewed conference paper presented at the 13th International Symposium on the Practical Design of Ships and Other Floating Structures. The paper has been edited for inclusion into this thesis to avoid repetition and to improve readability. The citation is:

Magoga, T., Aksu, S., Cannon, S., Ojeda, R., and Thomas, G., *Comparison between Fatigue Life Values Calculated Using Standardised and Measured Stress Spectra of a Naval High Speed Light Craft*, in *13th International Symposium on the Practical Design of Ships and Other Floating Structures*. 2016: Copenhagen, Denmark.

6.1 Introduction

With increasing use of semi-planing and planing hullforms and lightweight materials such as marine-grade aluminium, in addition to examples of fatigue failures in such craft, the need to develop rigorous lifetime load spectra has been recognised [19, 71, 149]. Options to establish a lifetime fatigue load spectrum, required in fatigue life evaluation, include spectral analysis, time-domain analysis, and simplified analysis. Spectral analysis considers the operational conditions of a ship by dividing different operational modes by speed, heading, and significant wave height for a specific wave scatter diagram. Typically, this method assumes linear load effects and is performed in the frequency domain. However, its utilisation to accurately estimate load distributions and actual stress ranges of HSLC is restricted due to the difficulty in predicting the highly nonlinear relationship between applied loading and fatigue life [44, 71]. In comparison, there are time-domain seakeeping codes available to calculate nonlinear loads to be transferred to structural models. However, coupled hydrodynamic-structural analysis is very time intensive, has tended to be limited to assessment of details, and requires validation via full-scale trials data [42, 72]. In view of the above issues, it is suggested that practical procedures to generate standardised load histories for implementation in simplified fatigue life prediction of HSLC may be of benefit [107].

Simplified fatigue analysis is described in Section 3.7.1. As summarised by Horn *et al.* [111], many classification societies assume that the long term distributions of stress ranges at local details are described by the Weibull distribution. This interpretation differs from a study of strain measurements of commercial ships, which demonstrated that the long-term distribution of cyclic stresses induced by wave loads is largely linear [150]. The latter approach is provided in Germanischer Lloyd's (GL) Rules for Classification and Construction – Seagoing Ships [151].

Nonetheless, from a review of the literature and classification rules by the authors, there appears to be little information on the applicability of standardised stress spectra for HSLC. Design guidance for fatigue life estimation of HSLC receives less support than for steel ships [55]. As such, there is a level of uncertainty associated with use of simplified fatigue analysis for HSLC, especially for naval vessels operating in demanding environments.

This chapter presents a comparative study between assumed stress spectra and derived stress spectra from strain measurements, with respect to the fatigue life at three structural details of a naval aluminium HSLC. Using the results from FEA and HMS data, the accuracy of Linear, Gaussian and Weibull modelling of the derived stress spectra is investigated in two

ways; firstly via goodness of fit, and secondly by comparing the fatigue life at the three details based on the derived and modelled spectra. The fatigue life is estimated using the Palmgren-Miner rule applied to fatigue resistance data for welded aluminium structures (using the nominal stress approach described in Chapter 4). This is followed by an examination of the sensitivity of fatigue analysis to standardised stress spectra, characterised by the maximum and number of stress cycles. Finally, recommendations for further work are proposed. The results of this study inform the selection of the service life stress spectrum for use in LOT evaluation of naval HSLC with demanding operational requirements.

6.2 Analysis

The study platform is the ACPB, described in Section 3.2. The FE model of the ACPB (refer to Section 3.5), and data acquired from the *Glenelg* HMS (refer to Section 3.3.1), are utilised.

Analysis of the HMS data has allowed development of a reliable operational profile of the ACPB fleet. *Glenelg* is considered representative of the class. Each ACPB was built over a period of three years in the same shipyard, out of the same material, and to effectively the same design. As *Glenelg* is the last of class, it would be expected that any structural modifications introduced during the build period were included on the vessel. In addition, *Glenelg* is based in Darwin along with the majority of the ACPBs[ix] (four boats are based in Cairns).

In this chapter, approximately 4500 hours of data from strain gauges A, B, C, which were installed on *Glenelg* (refer to Sections 3.3.1 and 4.3), is utilised. The locations of these gauges are displayed in Figure 3-2 and described in Table 3-4.

To investigate the accuracy of form fitting of each of the derived stress spectra, the spectra have been modelled using the linear (Equation 12), Gaussian (Equation 13), and Weibull (Equation 14) functions:

$$\Delta\sigma = L_1 \log(n) + L_2 \qquad \textbf{Equation 12}$$

$$\Delta\sigma = G_1 e^{\left(-\left(\frac{\log(n)-G_2}{G_3}\right)^2\right)} \qquad \textbf{Equation 13}$$

[ix] It is noted that ships of the same class will be operated differently depending on the required, or acceptable or desirable, levels of safety, comfort, and speed. Also, it is understood that the speed profiles of *Glenelg* and one of the Cairns-based boats, over approximately 3.5 years, were comparable. However, the Cairns-based boat undertook more frequent high-speed transits to/from Darwin.

$$\Delta\sigma = W_1 W_2 W_3 \log(n)^{(W_3-1)} e^{(-W_3 \log(n))}$$ **Equation 14**

Where L_1 and L_2 are the coefficients of the linear function, and G_1, G_3, and G_3 are the coefficients of the Gaussian function. The scale and shape parameters of the Weibull function are denoted by W_2 and W_3 respectively, and W_1 is a scale parameter independent of the exponent term. The form fitting is conducted by the method of least squares.

The stress cycles are normalised by the design stress range $\Delta\sigma_{design}$, which differs at each strain gauge location. The values of $\Delta\sigma_{design}$ are computed using FEA under the design conditions (refer to Section 4.2.1).

The coefficients of the Linear, Gaussian and Weibull models of the stress spectra for each strain gauge individually and combined (aggregate) are given in Table 6-1. The intention of the aggregate coefficients is to provide rationalised stress spectra for structural details indicative of those near the strain gauge locations (that is, pillars and supporting structural items). The goodness of fit R^2 values, shown in Table 6-2, indicate that the stress spectra are best approximated by a Gaussian model. Although the R^2 values of the Weibull models are also relatively high, there is non-physical decay at small values of n.

The derived and assumed stress spectra, using the aggregate coefficients, for strain gauges A, B, and C are compared in Figure 6-1, Figure 6-2, Figure 6-3, respectively. As the stress spectra follow distributions, and there is reasonable coverage of the speed range, the measurement period is considered to provide an adequate long-term distribution of stress cycles[x] (this is discussed further in Appendix F).

[x] In the design stage, if analytical data is being used, a sufficiently large amount of time should be evaluated to ensure that the lifetime values are being captured.

Table 6-1: Individual and aggregate coefficients of Linear, Gaussian and Weibull models, for each derived stress spectrum, based on stress cycles normalised by $\Delta\sigma_{design}$

Function		Strain Gauge			Aggregate
		A	B	C	
Linear	L_1	-0.180	-0.174	-0.186	-0.180
	L_2	1.000	1.000	1.000	1.000
Gaussian	G_1	1.000	1.000	1.000	1.000
	G_2	-1.338	-0.700	-0.898	-0.979
	G_3	4.401	4.138	4.055	4.198
Weibull	W_1	0.366	0.360	0.367	0.364
	W_2	1.072	1.234	1.148	1.152
	W_3	2.800	3.011	2.791	2.867

Table 6-2: Comparison between R^2 values of Linear, Gaussian and Weibull fits of stress spectra using individual and aggregate coefficients

Function	R^2	Strain Gauge		
		A	B	C
Linear	Original	0.915	0.967	0.959
	Aggregate	0.915	0.964	0.956
	Difference	0%	0.30%	0.31%
Gaussian	Original	0.986	0.984	0.991
	Aggregate	0.979	0.956	0.990
	Difference	0.70%	2.8%	0.10%
Weibull	Original	0.983	0.977	0.975
	Aggregate	0.961	0.942	0.973
	Difference	2.2%	3.7%	0.23%

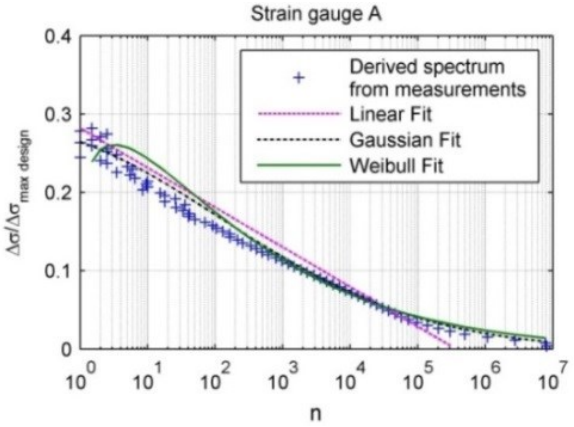

Figure 6-1: Comparison of strain gauge A derived and assumed stress spectra

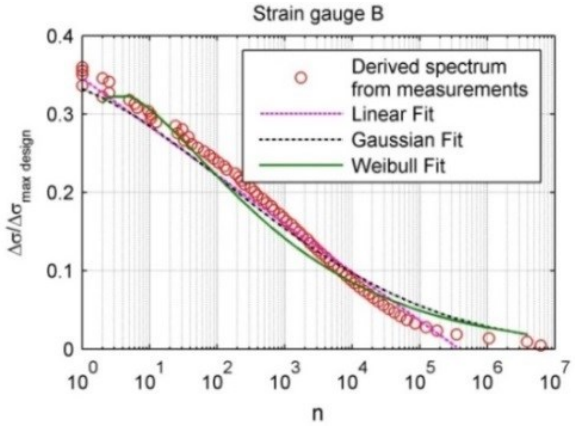

Figure 6-2: Comparison of strain gauge B derived and assumed stress spectra

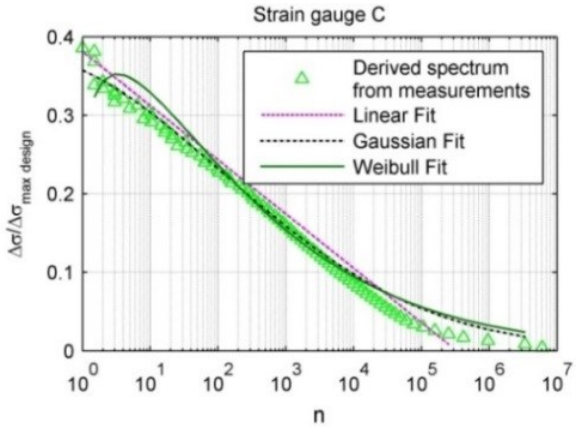

Figure 6-3: Comparison of strain gauge C derived and assumed stress spectra

6.2.1 Sensitivity of Fatigue Life to Fitted Spectra

The fatigue lives at structural details of interest ID-1, ID-2 and ID-3, shown in Table 4-1, are analysed. Fatigue resistance data from Eurocode 9 (Section 3.8) is utilised. The reference gauges are selected due to the close vicinity to the location of interest, consistency of the dominant load direction, and similarity of construction detail (discussed in Sections 4.4 and 8.3.4).

The spectra are based on stress cycles incurred over approximately 4500 hours. Thus, to calculate the fatigue life considering a service period of 20 years, the spectra are linearly extrapolated.

Table 6-3 provides the estimated fatigue life, using the process described in Chapter 4, for details ID-1, ID-2, and ID-3 based on the derived, Linear, Gaussian and Weibull spectra.

Table 6-3: Fatigue life estimates using different stress spectrum models, normalised by fatigue life values based on derived spectra

Detail	Spectrum			
	Derived	**Linear**	**Gaussian**	**Weibull**
1D-1	1.00	0.738	0.980	0.767
ID-2	1.00	0.841	1.35	1.31
ID-3	1.00	0.565	0.907	0.872

The results given in Table 6-3 indicate that when a Linear model is used to represent the stress spectra at the strain gauge locations, the corresponding fatigue life estimates are smaller than those based on the derived spectra by an average of 29%. The Weibull model performs better, as the average difference (absolute) between the fatigue life estimates is 22%.

In comparison, the fatigue life estimates based on the Gaussian spectra are most comparable with those based on the derived spectra, as the average difference is 15% (absolute).

6.2.2 Sensitivity of Fatigue Life Estimation to Standardised Lifetime Spectra

As discussed in the introduction, in the absence of detailed long term distributions of stresses, an approach provided by GL's Rules for Classification and Construction – Seagoing Ships [151] is to use standardised linear spectra as shown in Figure 6-4. Convex spectra can also be used with agreement from the society. The stresses range between the maximum and minimum stresses resulting from the maximum and minimum relevant seaway induced load effects ($\Delta\sigma_{design}$).

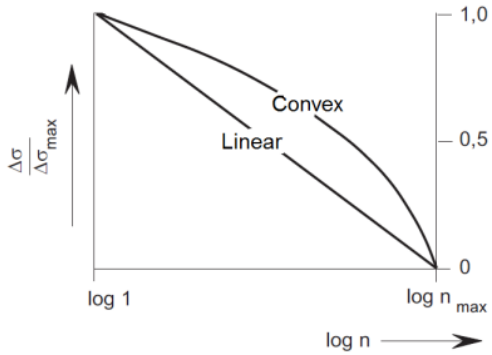

Figure 6-4: Standard stress range spectra given by GL

To test the applicability of standardised lifetime spectra to the three details of interest, the linear and convex spectra with the maximum stress range considered to occur once are used to estimate the fatigue life. That is, the probability of exceedance (n_{min}) is 10^0. It is generally assumed that the number of stress cycles that a ship structure will experience over its life is 10^8 stress cycles. As such, when generating a spectrum the sum of the number of cycles considered is 10^8 occurring during the design life of 20 years. In addition the number of stress increments needs to be sufficiently large to ensure reasonable numerical accuracy and should not be less than 20 [133]. In this analysis 60 increments are used.

Table 6-4 shows the fatigue life based on the standardised linear and convex spectra with n_{min} equal to 10^0 at each detail of interest, as a percentage of the fatigue life based on the derived spectra. For details ID-1, ID-2, and ID-3 the fatigue life estimates based on the standardised linear spectra are 4.1%, 2.8% and 4.9% of the fatigue life based on the derived spectra, respectively. Using the standardised convex spectra the fatigue life estimates at all

three details are less than 1% of those based on the derived spectra. The standardised convex spectrum features more significant stress cycles over a greater range of n. Thus, its use leads to more conservative fatigue life estimates than the standardised linear spectra. However, for n_{min} equal to 10^0 both standardised spectra result in considerably smaller fatigue life values than those predicted using the measured strain data.

Table 6-4: Percentage fatigue life based on standardised linear and convex spectra, relative to that based on derived spectra, for each detail of interest

Detail	Spectrum	Probability of exceedance (n_{min})		
		10^0	10^{-2}	10^{-4}
ID-1	Linear	4.1%	9%	18%
	Convex	0.59%	1.2%	2.2%
ID-2	Linear	2.8%	6.4%	13%
	Convex	0.41%	0.8%	1.5%
ID-3	Linear	4.9%	11%	23%
	Convex	0.69%	1.4%	2.6%

When n_{min} is equal to 10^0, it is accepted that the structure will sustain the design loads once in its lifetime. Thus, application of standardised spectra with n_{min} equal to 10^0 is unrealistic. Therefore, standardised spectra with probabilities of 10^{-2} and 10^{-4} of the structure sustaining the design loads are additionally considered as plotted in Figure 6-5.

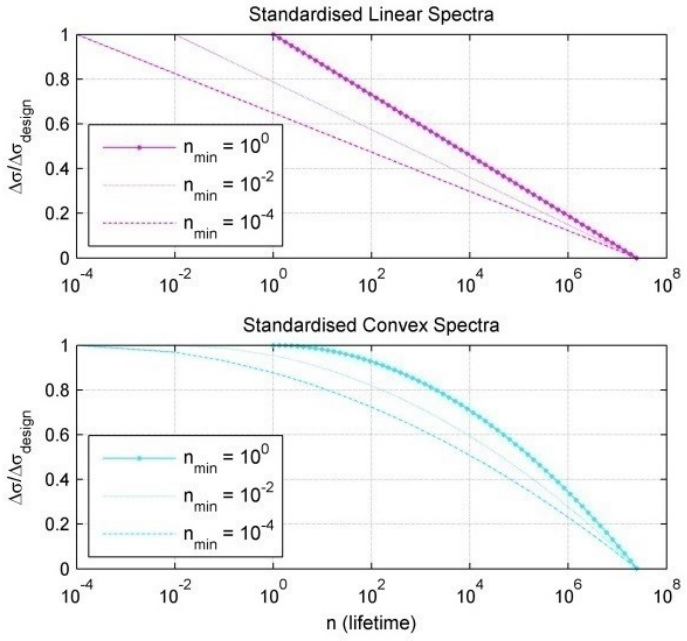

Figure 6-5: Standardised Linear and Convex stress range spectra, with n_{min} equal to 10^0, 10^{-2}, and 10^{-4}

To check the validity of defining the standardised spectra by smaller probabilities of the structure sustaining the design loads, the subsequent relationships between increments of n_i/N_i ($D_i = n_i/N_i$) and $\Delta\sigma/\Delta\sigma_{design}$ are compared to those based on the derived spectra. For example, for detail ID-1, Figure 6-6a, b, c, and d display the relationship between n_i/N_i and $\Delta\sigma/\Delta\sigma_{design}$ based on the derived spectrum of the reference strain gauge, the linear spectrum with n_{min} equal to 10^0, n_{min} equal to 10^{-2}, and n_{min} equal to 10^{-4}, respectively. Note that the y-axis scale of the derived spectrum plot (Figure 6-6a) is smaller than the y-axis scale of the linear spectra plots (Figure 6-6b, c and d) because the measurement period, and hence number of cycles, was considerably less than assumed during the design life used to generate the linear spectra.

Figure 6-6a reveals that at detail ID-1 the combination of the fatigue resistance data for E9 construction detail 9.1 (refer to Table 3-5) and the distribution of the stress cycles measured at reference strain gauge A results in the largest contribution to fatigue damage (n_i/N_i) occurring at approximately 7% of $\Delta\sigma_{design}$. For the linear spectra with n_{min} equal to 10^0, 10^{-2}, and 10^{-4} the fatigue damage peaks occur at 20%, 16%, and 13%, respectively, of $\Delta\sigma_{design}$ (refer to Figure 6-6b, c and d). For all spectra n_i/N_i increases relatively steeply until the maximum, and then decreases gradually with increasing $\Delta\sigma$. Thus, both the shape and location of the peak of the $\Delta\sigma/\Delta\sigma_{design}$ versus n_i/N_i curve of the linear spectrum with n_{min} equal to 10^{-4} are the most analogous to those of the derived spectrum.

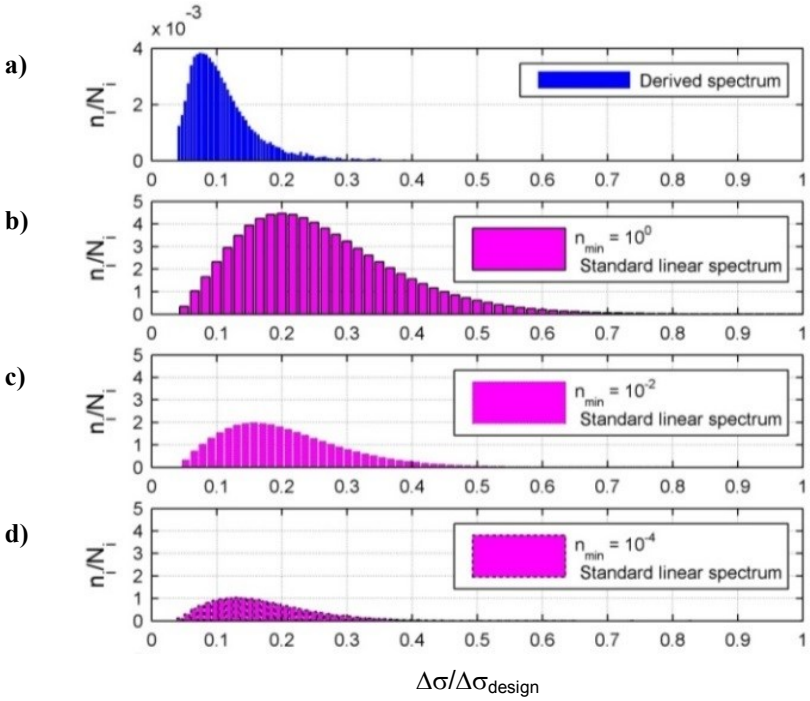

Figure 6-6: $\Delta\sigma/\Delta\sigma_{design}$ versus n_i/N_i based on a) derived stress spectrum, and standardised linear spectra with n_{min} equal to b) 10^0, c) 10^{-2}, and d) 10^{-4}, at detail ID-1. Note y-axis scale of plot a differs from b, c and d

The fatigue life estimates based on the standardised linear and convex spectra with n_{min} equal to 10^{-2} and 10^{-4} at each detail of interest, as a percentage of the fatigue life estimates based on the derived spectra, are also given Table 5. For the three details of interest, the fatigue life values based on the standardised linear spectrum with n_{min} equal to 10^{-4} ranged between 18% and 23% of those of the derived spectrum.

6.2.3 Relationship between Fatigue Life and Design Loads

In an analysis of fatigue damage incurred in a US Coast Guard Cutter, Stambaugh *et al.* [81] concluded that it is important to monitor impact loading because the fatigue damage accumulated is proportional to the third power of the stress range. In line with this finding, the relationship between the design stress range $\Delta\sigma_{design}$ and the fatigue life at the three details of interest of the ACPB is quantified. For this exercise the fatigue life is estimated using the standardised linear spectra characterised by a 10^0 probability of the vessel sustaining between 30% and 100% of the design loads. The subsequent fatigue life estimates for each percentage of $\Delta\sigma_{design}$, normalised by that based on the derived spectrum, are plotted in Figure 6-7. Power functions are fitted to each detail's set of fatigue life values, and Equation 15 is the average of the three functions. In Equation 15 the power term of the inverse stress range is 3.9.

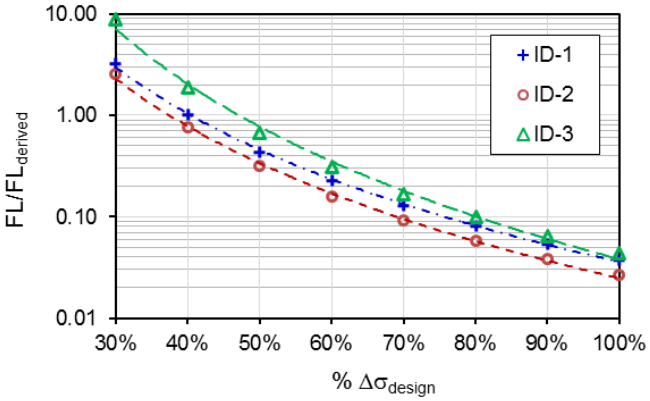

Figure 6-7: Relationship between FL based on standardised linear spectra and $\Delta\sigma_{design}$ at details ID-1, ID-2 and ID-3. Values of FL are normalised by that based on the derived spectrum, for each detail

$$\frac{FL}{FL_{derived}} = 0.033\left(\frac{1}{\Delta\sigma_{design}}\right)^{3.9} \qquad \textbf{Equation 15}$$

6.3 Discussion

Based on the above analysis, valuable further work includes establishment of the probability of exceedance of fatigue loads in the area of operations of the naval HSLC of concern. This would be similar to the approach employed in the Common Structural Rules (CSR) for Bulk Carriers and Oil Tankers [127], in that dynamic sea pressures or fatigue loads are based on a 10^{-4} probability level of exceedance for the North Atlantic Wave Environment. However, naval HSLC operate in various wave environments and thus the probability of exceedance of fatigue loads vary. Also, in the CSR the characteristic load for fatigue assessment is an average value representing the expected load history reduced from the design load by a knock-down factor, rather than the maximum and minimum relevant seaway induced load effects. Given that the analysis presented is this chapter indicates that the use of the stress range corresponding to design sagging and hogging load cases leads to conservative fatigue life estimates, even when a 10^{-4} probability of sustaining the design loads is considered, it is concluded that characteristic fatigue loads for naval HSLC are required.

From Equation 15 it is inferred that when the design loads are reduced by, for example, 10% the estimated fatigue life of the analysed details increase by approximately 50% assuming a linear stress spectrum. As the fatigue life is proportional to approximately the fourth power of the inverse stress range, it is important to predict and/or monitor the accumulation of fatigue damage over the lifetime of the vessel.

Clearly analysis of the fatigue life at the details of interest is heavily dependent on the

representation of stress ranges, as well as other parameters. Thus, understanding of uncertainties in the analysis is critical. The uncertainties include:

- Applicability of rules-based design loads to determine the design stress ranges. The loads applied to the HSLC can feature a high degree of nonlinearity due to their hullform, operation in semi-planing or planing modes, and susceptibility to slamming.
- The dynamic behaviour of the structure, that is, variation in the response frequencies and structural damping.
- Use of the structural stress approach in the fatigue evaluation at the details of interest, which is a compromise between accuracy and ease of use [111].
- Assumption of linear scalability of the number of stress cycles incurred during the strain measurement period to the service life. This premise neglects the random nature of ocean waves over time. Strain monitoring during the entire life of the ship would be one way to mitigate this simplification.
- Uncertainty in the measurement of strains, due to uncertainty in the calibration of the strain gauges, induced electrical noise, and noise in the amplification system.

The three details analysed are part of the ACPB engine room structure close to a pillar. As such, further investigation is required to broaden the presented findings for reliable fatigue life evaluation at other structural areas. In addition, extending these findings to other classes with different missions, geographic locations, and seakeeping performance forms valuable future work.

As discussed in Section 6.2, it is considered that *Glenelg* is representative of the class and the measurement period sufficiently characterises the long-term operational profile and load distribution. It is acknowledged that increased variability on individual ships, which can be expected as more maintenance on the aging fleet is required and mission requirements evolve [152, 153], will affect the relevance of the conclusions drawn. Thus, an analytical procedure can be utilised in combination with information on the ship speed and encountered wave environment within a hybrid framework (this is discussed further in Chapter 8).

6.4 Conclusion

Strain gauge data obtained from a hull monitoring system installed onboard a naval HSLC has been used to investigate stress spectra assumptions required in simplified fatigue analysis. Form fitting was performed to find the best model of the measured stress range data normalised

by the design stress ranges. Then, using the structural stress approach, the fatigue life based on the derived and modelled stress spectra was calculated at three details of interest. It was found that, in comparison to the Linear and Weibull models, the fatigue life estimates based on Gaussian model correlated best to those of the derived spectra and fleet maintenance data. In addition, aggregate coefficients of the models are provided in order to inform the generation of stress spectra at structural details indicative of the joints of pillars and supporting structural items. Finally, it is recommended that strategies to better describe stress spectra, which include determination of characteristic fatigue loads and probabilities in the area of operations, are needed.

Where to Next?

As per research question #2, in order to identify and develop suitable enhancements to fatigue life assessment methods for naval HSLC, it is necessary to first test the applicability of different methods. This chapter was concerned with simplified fatigue analysis. The investigation of the suitability of this method was somewhat inconclusive, partly due to the underlying assumptions being based on conventional ships. In the next chapter of the thesis, the applicability of Spectral Fatigue Analysis, a direct fatigue analysis approach, is examined. Use of this method also allows a sensitivity study of the fatigue damage to different variables to be performed.

Chapter 7. Fatigue Damage Sensitivity Analysis of a Naval High Speed Light Craft via Spectral Fatigue Analysis

The work presented in this chapter has been accepted for publication in Ships and Offshore Structures. The paper has been edited for inclusion into this thesis to avoid repetition and to improve readability. The citation for this research article is:

Magoga, T., *Fatigue Damage Sensitivity Analysis of a Naval High Speed Light Craft via Spectral Fatigue Analysis*. Ships and Offshore Structures, 2019.

7.1 Introduction

Representative fatigue life assessment methods include simplified fatigue analysis and spectral fatigue analysis (SFA) [154]. In simplified fatigue analysis, the dominant loads that determine the stress range of the detail to be assessed are determined via empirical equations. It is typically assumed that the long-term distribution of stress ranges is of Weibull or Gaussian form [60, 127]. In contrast, SFA is a direct calculation method that explicitly includes a proposed operational profile and encountered wave environment. This is advantageous to understanding the effect of changing operational profile and area on the fatigue life of ships [153, 155]. By implementing a spectral method, the fatigue analysis is treated as a linear process and it is assumed that non-linear effects can be neglected; this is often considered adequate [156, 157]. However, the use of a linear (frequency domain) approach to estimate the load distributions of HSLC is not always appropriate due to differences in the characteristics and magnitudes of hydrodynamic loads at higher forward speeds and the relatively larger motions in waves [55, 62]. For HSLC nonlinearities become significant in relatively moderate waves due to their greater susceptibility to slamming [158]. However, in the absence of knowledge of the actual loads encountered during the operational life of a HSLC, and during early design phases as well as concept studies, SFA can be a functional tool [159]. This is because SFA allows fatigue screening of any part of the ship structure, is quicker than time-domain simulations, and is an approach accepted by the industry and used by classification societies [59, 133].

In any modelling effort, validation is crucial. Typically, a numerical approach is validated against experimental data. However, the uncertainties, assumptions, and errors inherent in the datasets obtained from modelling and measurement of a ship's structural responses coupled to the operational environment differ in source and magnitude.

There are various sources of uncertainty in the calculation of the fatigue life of a ship, such as the assumed operational environment and in the calculation of structural responses to wave encounters. The fatigue damage incurred in a ship structure is affected by several variables including the fatigue resistance of the structural details, the operational area, and the operational profile. Modelling steps, such as the discretisation of a physical system and the calculation of the structural responses and the fidelity of the simulation are also influential. Thompson [160] summarised the simplified aspects of SFA; they include, but are not limited to, representation of the seaway, modelling of the ship's hydrodynamic and structural behaviour, fatigue resistance of the welded joints, and stress concentration factors.

This chapter presents an investigation into the effects of the various inputs to the SFA of a naval aluminium HSLC, the RAN ACPB. The aim is to address the following questions:

1. Which parameter(s) should be used for validation of SFA?
2. Which are the most influential input factors to the predicted fatigue damage incurred at structural details on an aluminium naval vessel?
3. If the input factors were weighted (that is, probability distributions were applied), which factors should be focused on with a view to reducing the fatigue damage?

The first question is addressed by reviewing the literature and comparing different parameters derived from SFA and available ACPB sea trials data [77]. The second and third questions are resolved by conducting a sensitivity analysis of the fatigue damage estimated via SFA at two structural details on the patrol boat.

By achieving the above aim, the effectiveness of SFA as a way to explore the sensitivity of input parameters to the estimated fatigue damage incurred in a naval ship is demonstrated. This is of relevance to the through-life management of naval ship structures; the method and results enables informed decision-making regarding design and operations [153, 161].

7.2 Spectral Fatigue Analysis

The commercial FEA package MAESTRO 11.2.2 [146] is used in the present study. MAESTRO has a hydrodynamic analysis module called MAESTRO-Wave, and a SFA module. SFA is described in Section 3.7.2.

MAESTRO-Wave includes an implementation of strip theory that computes both panel pressures and sectional loads. Strip theory formulates the motion of the fluid on slender bodies as a 2-D problem. The equations of motion are formulated based on the structural mesh, allowing equilibrium of the applied pressure and inertial force. Based on the panel pressure integration, the vertical bending moment, vertical shear force, longitudinal torsional moment, horizontal bending moment, and horizontal shear force are computed [162]. MAESTRO-Wave also includes the option ‘strip theory, 2.5D, high speed’, which uses a Rankine Source method with a forward speed correction term in the free surface computation [163]. This option is recommended when running cases with a Froude number greater than 0.4.

The SFA module within MAESTRO calculates the fatigue damage based on cumulative damage theory. After the computation of stresses, the expected values of short-term stress

ranges are determined from an assumed Rayleigh distribution. The total fatigue damage is found by summing the fatigue damage resulting from each short-term stress prediction, weighted by the corresponding occurrence probability of the operational (speed and heading) and environmental (wave height and period) conditions. When a single-slope S-N curve (curve that relates the nominal applied cyclic stress ranges (S) to the corresponding number of cycles to failure (N)) is used, the fatigue damage D for each short-term stress prediction is given by Equation 16 [164]:

Equation 16

$$D = \frac{\nu_0 T_d}{\bar{a}} \Gamma\left(1+\frac{m}{2}\right) \sum_{n=1}^{N_{load}} p_n \cdot \sum_{i=1,j=1}^{\substack{\text{all sea states} \\ \text{all headings}}} r_{ijn} \left(2\sqrt{2m_{0ijm}}\right)^m$$

N_{load} is the total number of load conditions, T_d is the design life in seconds, $\Gamma(1+m/2)$ is a Gamma function, r_{ij} is the number of stress cycles in the short-term condition i,j, ν_0 is the long-term average response zero-crossing frequency, p_n is the fraction of the design life in the load condition, and m_{0ij} is the zero spectral moment of the stress response process. When a two-slope S-N curve is selected, a modified version of Equation 11 is used. When a three-slope S-N curve is selected, MAESTRO divides the stress spectrum into a number of stress bins and then uses cumulative damage theory to compute the fatigue damage (described in Section 3.6).

7.2.1 Finite Element Model

The global FE model of the patrol boat is shown in Figure 3-4. Fine mesh models to recover the stresses at strain gauge locations for each load case were embedded in the global model. The mesh density of the local models ranged between half the thickness of the material to approximately the size of a strain gauge (~11 mm). An example local model is shown in Figure 7-1.

For the hydrodynamic analysis of the patrol boat 2D strip theory was used for speeds equal to or less than 15 kn. For speeds greater than 15 kn, 2.5D strip theory was used.

As the S-N curve concept is adopted in the SFA, it is necessary to select appropriate detail categories/types from a structural design code. In this analysis Eurocode 9 is utilised (Section 3.8).

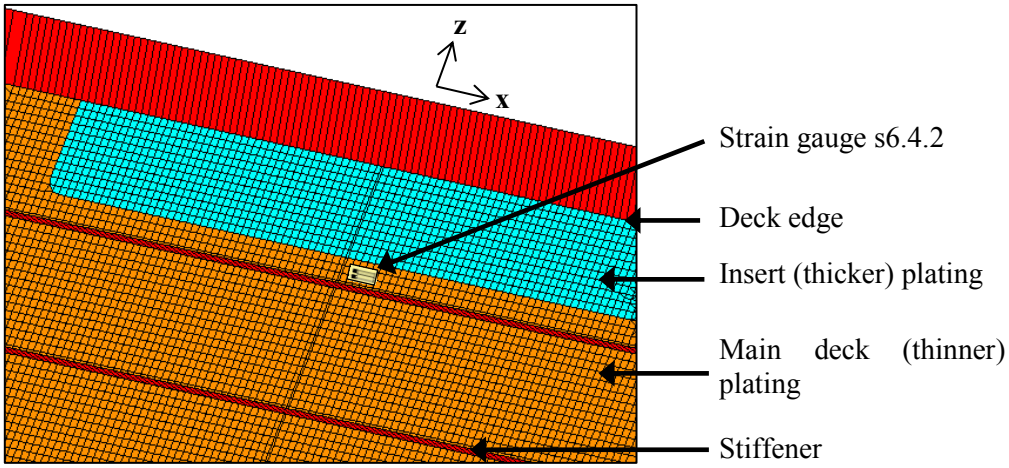

Figure 7-1: Example fine mesh model (underside of aft main deck) in vicinity of a strain gauge. Positive x-direction is towards bow, positive z-direction is to starboard

7.3 HMAS *Maryborough* Sea Trials

Dedicated sea trials were conducted with *Maryborough* in mid-2016. The purpose of the trials was to obtain a full-scale dataset related to the wave environment via wave buoy measurements [77].

Several trials runs were performed over two days in waters offshore from the Northern Territory, Australia. The runs were defined by vessel speed (v) and heading relative to the dominant wave direction (χ). The speeds ranged between 10 kn and 25 kn, in 5 kn increments. The headings ranged between head seas (180 deg) and following seas (0 deg) in 45 deg increments. During the sea trials, the bottom of sea state 3 to the bottom of sea state 4 was encountered. Consequently, linear motions and loads dominated [77]. This result partly justifies the comparison of the linear SFA against the trials data.

The locations of the strain gauges analysed in this chapter are given in Table 7-1 and shown in Figure 7-2.

Table 7-1: Approximate locations of analysed strain gauges on HMAS *Maryborough*

ID	Longitudinal position (% of L_{WL}[#] forward of transom)	Vertical position (% of L_{WL} upwards of baseline)	Location details
s2A.1.3 ●	79%	10%	Middle of flange of stiffener 3340 mm off CL
s2A.5.2 ■	79%	10%	Underside of main deck plating 2925 off CL
s2A.5.3 ◆	80%	10%	Middle of flange of stiffener 2850 mm off CL
s3.1.2 ▲	70%	0%	Middle of flange of centreline girder (keel)
s6.3.3 ●	29%	8%	Middle of flange of stiffener 3600 off CL
s6.4.2 ■	30%	8%	Underside of main deck plating, between weld seam of insert plating and outermost stiffener
s6.4.3 ◆	30%	7%	Internal side shell plating, 70 mm below weld seam of insert plating

[#]L_{WL} = waterline length

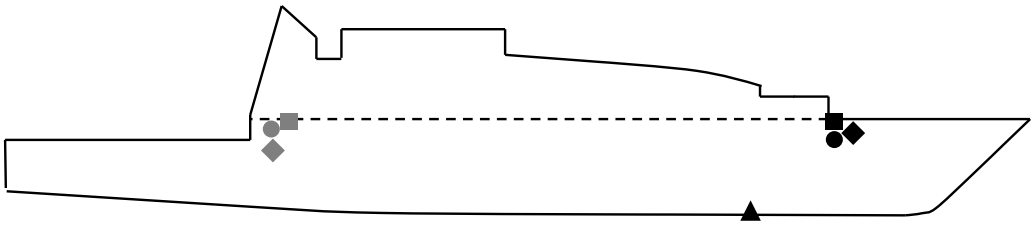

Figure 7-2: Profile view of approximate locations of analysed strain gauges installed onboard HMAS *Maryborough*

7.3.1 Uncertainties

When using measurements to validate a numerical model, it is necessary to have knowledge of the uncertainties inherent in the measurements to establish the accuracy of the validation. In an uncertainty analysis of ship performance modelling, one of main sources of uncertainty identified was instrument uncertainty [161]. Similarly, some of the uncertainties related to measurements taken during *Maryborough's* sea trials are listed in Table 7-2.

Table 7-2: Uncertainties related to data collected during sea trials

#	Variable	Precision	Source
1	Strain gauge misalignment (for uni-axial loading), for example by 10 deg	±8%	Magoga *et al.* [165]
2	Strain gauge gain	±2.5%	Magoga *et al.* [165]
3	Use of longitudinal stress for comparison (strain measured by uni-axial strain gauges)	Depends on location	Discussed by Thompson [160]
4	Wave height measured by wave buoy	±0.2 m	QinetiQ North America [166]
5	Dominant wave direction (not easy to detect on day that 20 kn and 25 kn runs were completed)	10 deg	Observation during sea trial - estimated
6	Ship displacement	±10 t	Estimated
7	Speed (from Global Positioning System)	±0.2 kn	GPS datasheet

A limited estimation of the effects of uncertainty in the strain measurement is performed via a propagation of errors analysis, which combines uncertainties from multiple variables.

A result 'x' is dependent on the addition/subtraction of variables 'a', 'b', and 'c', as follows:

$$x = a + b + c \qquad \textbf{Equation 17}$$

Each measurement of 'a', 'b' and 'c' has an uncertainty about its mean. Thus, the standard deviation (SD) of 'x' can be expressed as:

$$SD_x = \sqrt{SD_a^{\,2} + SD_b^{\,2} + SD_c^{\,2}} \qquad \textbf{Equation 18}$$

Using Equation 18, and considering only the uncertainty of variables #1 and #2 in Table 7-2, the error in the stress measurement is estimated as follows:

$$SD_{\sigma\_measured} = \sqrt{0.08^2 + 0.025^2} \qquad \textbf{Equation 19}$$
$$SD_{\sigma\_measured} = 0.084$$

The uncertainties inherent in variables #3 to #5 in Table 7-2 affect the input parameters in the SFA, to match the trials conditions:

- Variable #3 - the longitudinal and perpendicular stresses (transverse or vertical depending on location) predicted by MAESTRO at the strain gauge locations were recovered. On average, across all strain gauges, the transverse root mean square (RMS) of the stress σ_{RMS} was 2.5% of the longitudinal σ_{RMS}.
- Variable #4 - the computed σ_{RMS} is assumed to be directly proportional to $H_{1/3}$, as shown in Figure 7-3, which illustrates the approximately linear relationship between $H_{1/3}$ and the computed σ_{RMS} at s.3.1.2 for 15 kn, head seas, wave period of 4 s, and Bretschneider wave spectrum [167]. Since the smallest encountered $H_{1/3}$ during a trials run was 1.0 m, a conservative maximum error of 20% of the σ_{RMS} is assumed.
- Variable #5 - the inaccuracy in the estimation of the ship's heading relative to the dominant wave direction is similar to that of variable #1. As per Table 7-2, it is estimated that the precision is 8%.

The Bretschneider wave spectrum [167] is suited for open sea areas, and is given mathematically by Equation 20 (where T_1 is the mean centroid wave period):

$$S_\varsigma(\omega) = \frac{173 \cdot H_{1/3}^2}{T_1^4} \cdot \omega^{-5} \cdot e^{\frac{-692}{T_1^4} \cdot \omega^{-4}}$$

Equation 20

Using Equation 18, and considering the assumed uncertainties of variables #3 to #5, the error in the computed σRMS is estimated as follows:

$$SD_{\sigma\_SFA} = \sqrt{0.025^2 + 0.2^2 + 0.08^2}$$
$$SD_{\sigma\_SFA} = 0.22$$

Equation 21

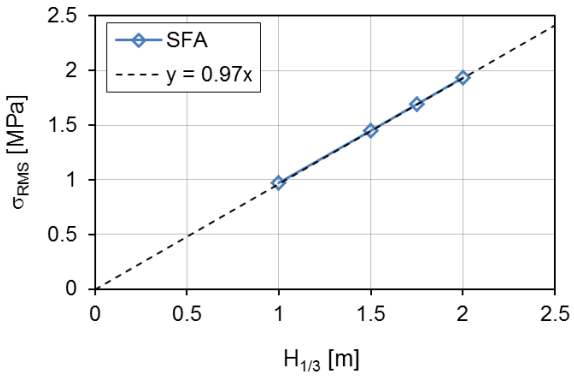

Figure 7-3: $H_{1/3}$ versus computed σ_{RMS} with line of best fit at s.3.1.2, for v = 15 kn, χ = 180 deg, and T_z = 4 s

7.4 Validation of SFA

Before using SFA to conduct a sensitivity analysis of the estimated fatigue damage in the patrol boat structure, it is necessary to establish confidence in the results generated by the tool. Thompson [160] assessed the accuracy of a SFA software tool by comparing the σ_{RMS}, zero-upcrossing frequency, and fatigue damage D with those derived from strains measured during a naval vessel sea trial. Li *et al.* [168] validated a proposed spectral approach by comparing the computed fatigue damage to that obtained via the rainflow counting method (described in Section 3.7.3) [164], which reduces a stress history into a spectrum of stress ranges, applied to full-scale measurements of a container ship. The authors concluded that the accuracy of the model was very good, as the maximum error from the model was approximately 20 %. Interestingly, this is very similar to the maximum error of the computed σ_{RMS} due to uncertainty in the input parameters from the sea trials (refer to Equation 21).

In an evaluation of the frequency domain approach to fatigue damage estimation of a large offshore platform, a numerically intensive, full-scale time domain fatigue assessment was regarded as the benchmark [169]. The authors used σ_{RMS} and D as the metrics for comparison between the two approaches. However, due to the stationary nature of the analysed structure the authors did not need to consider forward speed. Also, for time-domain problems the simulation time is very long so that it is usually only possible to conduct analysis for a limited set of conditions.

All of these approaches to validating or assessing the applicability of SFA for marine structures contain some degree of assumptions, data reduction, and convolution. For example, applying a window function in the calculation of the Fourier transform of a stress record, to obtain the stress power density, affects the resulting σ_{RMS} and zero crossing period. The number of increments of the wave period used in the SFA also affects the spectral characteristics. Of course, it is necessary to make assumptions in SFA. A thorough investigation of this matter is outside of the scope of this chapter, though the number of cells of the operational profile used in the SFA is part of the model uncertainty analysis in the following section. Notwithstanding, the effect of some of the assumptions is demonstrated in the context of validation of SFA.

Example comparisons between the calculated and measured spectral response at strain gauge s3.1.2 (on the keel, refer to Table 7-1), for four trials runs, are displayed in Figure 7-4. The Bretschneider spectrum is assumed in the SFA, and the wave-spreading is limited to long-crested seas. The measured stress has been filtered, using the process outlined by Magoga *et al.*

[89], so that the RMS of the 'wave-only' component is compared to the calculated σ_{RMS}. The associated ratios between the calculated and measured σ_{RMS} and D are given in Table 7-3; the latter values determined using the process described by Magoga *et al.* [170]. At s3.1.2, the Eurocode 9 S-N curve 36-3,4 and a stress ratio of 2.6 are assumed, and the stress cycles are relatively small. By applying the stress ratio the stress spectra is effectively translated to another detail [170] (butt weld in a flange).

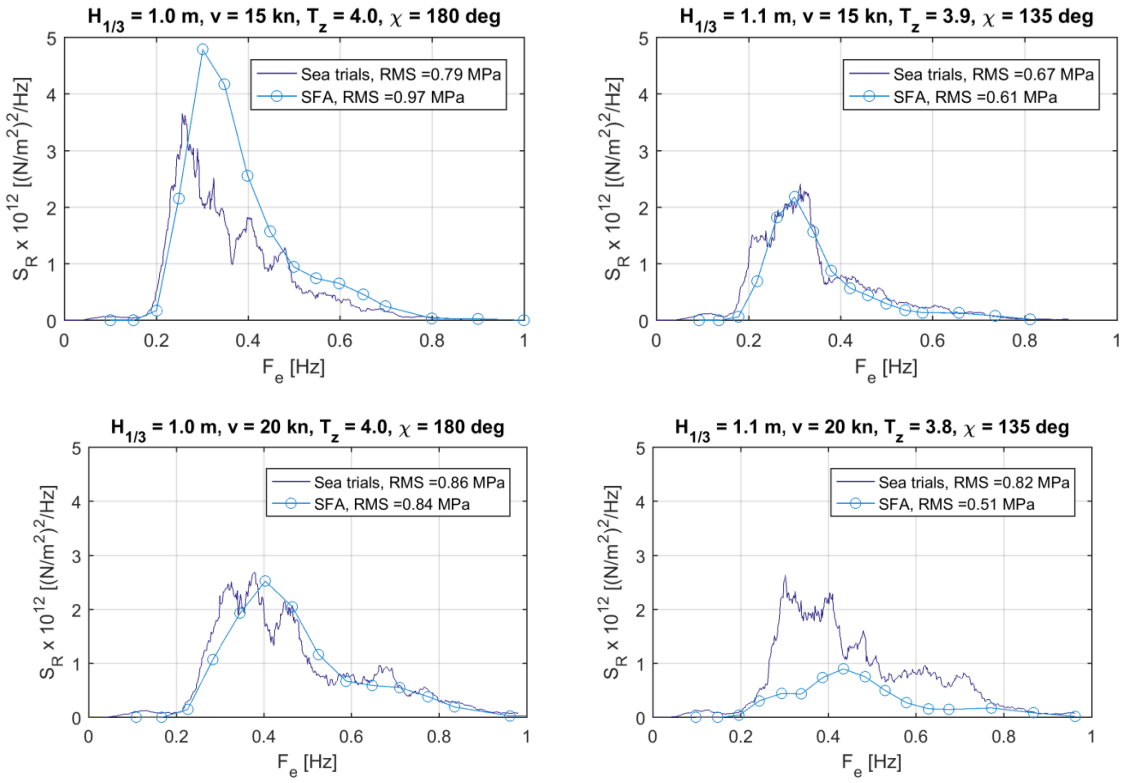

Figure 7-4: Comparison between calculated and measured spectral response at strain gauge s3.1.2 over four different conditions

Table 7-3: Ratio between calculated and measured σ_{RMS} and D at s3.1.2 for four conditions

Condition	Figure	$\frac{\text{SFA}\,\sigma_{RMS}}{\text{Sea trials}\,\sigma_{RMS}}$	$\frac{\text{SFA D}}{\text{Sea trials D}}$
$H_{1/3}$ = 1.0 m, v = 15 kn, T_z = 4.0 s, χ = 180 deg	Figure 7-4a	1.23	1.8
$H_{1/3}$ = 1.1 m, v = 15 kn, T_z = 3.9 s, χ = 135 deg	Figure 7-4b	0.98	0.50
$H_{1/3}$ = 1.0 m, v = 20 kn, T_z = 4.0 s, χ = 180 deg	Figure 7-4c	0.92	0.66
$H_{1/3}$ = 1.1 m, v = 20 kn, T_z = 3.8 s, χ = 135 deg	Figure 7-4d	0.62	0.005

The effect of filtering the measured stress is assessed by comparing the RMS values of the wave-only stress and total stress for the four trials runs described in Table 7-3. The RMS of

the wave-only stress ranges between 91% and 93% of the RMS of the total stress. As well as the high-frequency response, the difference between the RMS values is attributed to the attenuation of a greater range of broadband noise that is present in the strain signal. Therefore, the significance of the high-frequency stress response is minor.

The results in Table 7-3 indicate that whilst there is relatively good agreement between the calculated and measured σ_{RMS}, the agreement between the D values is relatively poor. The fatigue life of the aluminium welded joints, typical of naval HSLC, has been found to be a function of approximately the fourth power of the stress range [126]. As such, the estimated error propagation in the fatigue damage is four-fold the error in the stress range. In addition, the duration of the trial runs, though meeting International Towing Tank Committee guidelines (2014), is unlikely to be sufficient for insightful fatigue damage assessment. Therefore, σ_{RMS} is taken as the discriminating metric.

Stress transfer functions for each strain gauge location were generated in MAESTRO for each of the combinations of speed and heading that characterised the sea trials runs. The computed and measured values of σ_{RMS} were then compared in two ways:

- Linear regression to determine line of best fit and the coefficient of determination R^2.
- Coefficient of variation of the root mean square deviation CV(RMSD), calculated using Equation 22 (where N_{runs} is the number of trials runs):

$$\mathrm{CV(RMSD)} = \frac{\sqrt{\frac{\sum_{i=1}^{N_{runs}} (\mathrm{Calculated} - \mathrm{Measured})^2}{N_{runs}}}}{\mathrm{Mean\ of\ measured\ parameter}} \qquad \textbf{Equation 22}$$

The σ_{RMS} values from the measurements taken during the trials are plotted against the σ_{RMS} values from SFA in Figure 7-5, for each strain gauge location. The largest stresses occurred at s6.4.3, and the smallest at s3.1.2. Linear curves of best fit are also shown Figure 7-5.

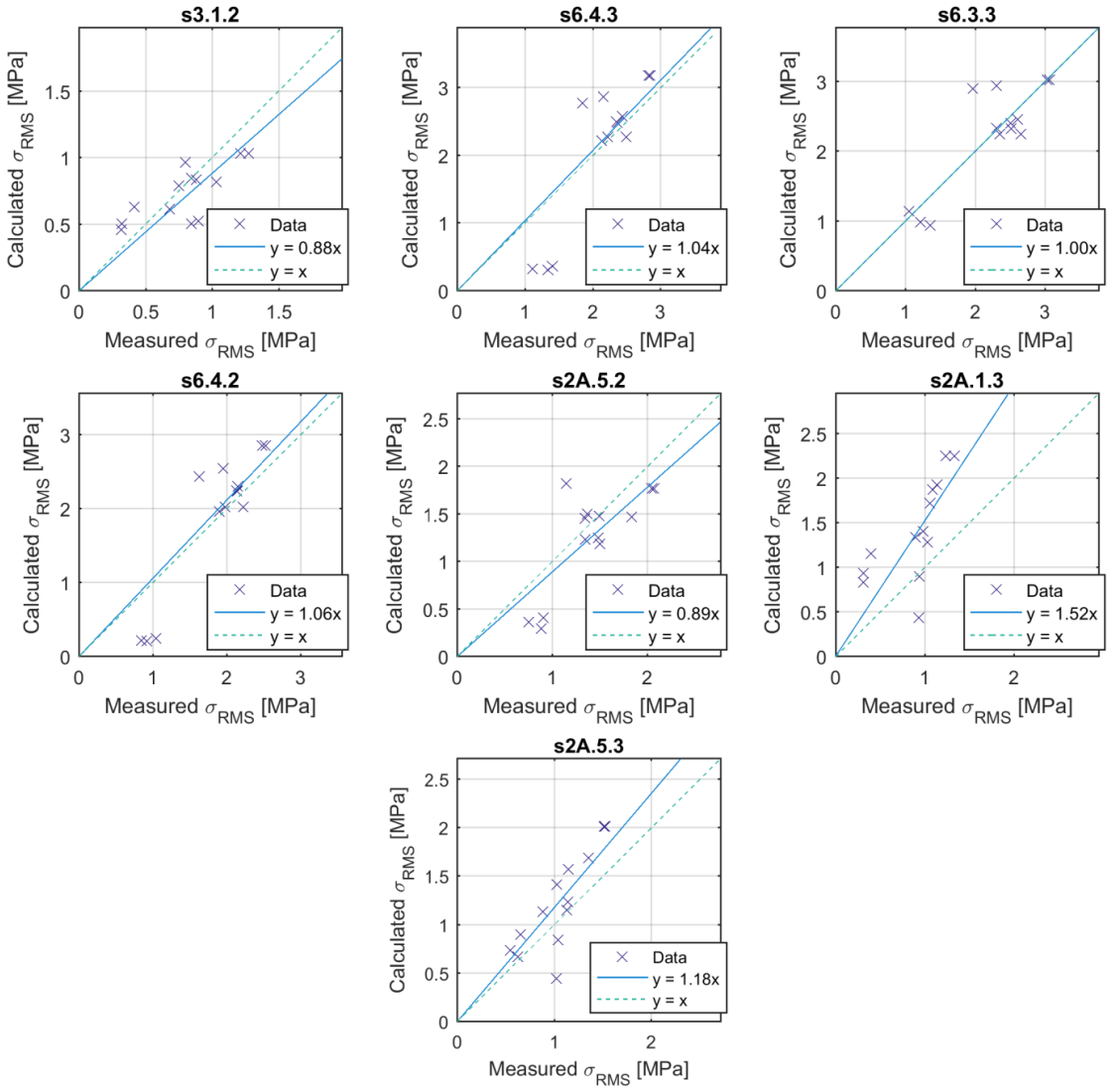

Figure 7-5: Measured σ_{RMS} versus computed σ_{RMS} results, with linear model and line of exact agreement, at strain gauge locations (N_{runs} = 13). Note differing y-axis scales

The calculated and measured σ_{RMS}, R^2, and CV(RMSD) values are compared in Table 7-4. The calculated σ_{RMS} is on average 8% greater than the measured σ_{RMS}, though the difference ranged between -12% and 52%. The CV(RMSD) values reveal that the level of variation in the predictions ranged between 0.17 and 0.46; the smaller the value, the better the predictions agree with the measurements. This range is consistent with that reported for the validation of SFA of a Canadian naval vessel against full-scale measurements [160]. Therefore, considering the uncertainties associated with both the strain measurements and the SFA results, and for conditions dominated by linear motions and loads, SFA applied to the patrol boat is deemed appropriate for the following sensitivity analysis.

Table 7-4: Comparison of calculated and measured σ_{RMS} (N_{runs} = 13)

Strain Gauge	Regression slope	R^2	CV(RMSD)
s3.1.2	0.88	0.23	0.26
s6.4.3	1.04	0.67	0.29
s6.3.3	1.00	0.74	0.17
s6.4.2	1.06	0.76	0.27
s2A.5.2	0.89	0.61	0.24
s2A.1.3	1.52	0.41	0.46
s2A.5.3	1.18	0.67	0.29
Average	*1.08*	*0.59*	*0.28*

7.5 Sensitivity Analyses

The sensitivity of the fatigue damage to different model parameters is investigated using both local and global sensitivity analyses.

Local sensitivity analysis (LSA) is a one-at-a-time technique. It involves examination of the effect of one parameter on the cost function at a time, whilst keeping the other parameters fixed. Whilst LSA allows ready visualisation of the influence of the individual parameters on the cost function, it does not provide insight about the interactions between the parameters. Also, usually only a small part of the 'design space' or damage function is explored [172].

Conversely, global sensitivity analysis (GSA) describes techniques that vary all parameters simultaneously. Thus, GSA is multivariate and allows evaluation of the parameter interactions. One GSA approach is the use of a Monte Carlo technique to represent a global set of samples, followed by correlation between the parameters [172].

The fatigue damage incurred over the patrol boat's service life at two locations, strain gauges s3.1.2 and s6.4.2, is calculated using SFA. The model input parameters are given in Table 7-5. There are combinations of $H_{1/3}$ and T_z that are very unlikely (for example, T_z of 4 s and $H_{1/3}$ of 7.5 m), and they are excluded from the analysis. Thus, the total number of combinations is 11,520. The vessel's displacement, the Bretschneider wave energy spectrum, and stress ratio K are held constant (the effect of different S-N curves and varying stress ratios on the fatigue damage estimated at five structural details on the patrol boat has been investigated by Magoga *et al.* [170]). Both unweighted and weighted multivariate sensitivity analyses of the fatigue damage are performed:

- In the unweighted analysis, the variables are uniformly distributed.

- In the weighted analysis, in general, the variables have probability distributions that are representative of operational conditions.
    - The speed profile, shown in Figure 7-6, is derived from in-service measurements of *Maryborough* over approximately 9200 hours. The vessel was at sea approximately 30% of this time.
    - The wave scatter diagram (combined probability of $H_{1/3}$ and T_z) is for Northern Australian Waters.
    - The heading distribution is uniformly distributed (this is assumed in the absence of operational information).

Two different joint categories or S-N curves per location are analysed, with equal probability of occurring, to simulate varying weld quality. For example, as shown in Table 7-5, the Eurocode 9 [102] weld categories considered for s6.4.2 are 50-4,3 and 40-3,4. These categories are both a full penetration double-sided butt weld between structural members; the former relates to a weld with relativity good quality surface and geometry and the latter to a weld of relativity poor quality. Accordingly, the fatigue limits $\Delta\sigma L$ of 50-4,3 and 40-3,4 are 25.1 MPa and 17.5 MPa, respectively.

Table 7-5: Fatigue damage model input parameters

Parameter	**Range**		**Number**
v [kn]	5:5:25		5
χ [deg]	0:15:345		24
$H_{1/3}$ [m]	0.5:1.0:7.5		Up to 8
T_z [s]	4.0, 4.5, 5.5, 6.5, 7.5, 8.5, 9.5, 10.5, 11.5		Up to 9
Joint category; $\Delta\sigma_L$	Strain gauge s3.1.2	40-3,4; 17.5 MPa	2
		36-3,4; 15.8 MPa	
	Strain gauge s6.4.2	50-4,3; 25.1 MPa	
		40-3,4; 17.5 MPa	
Total			*11520*

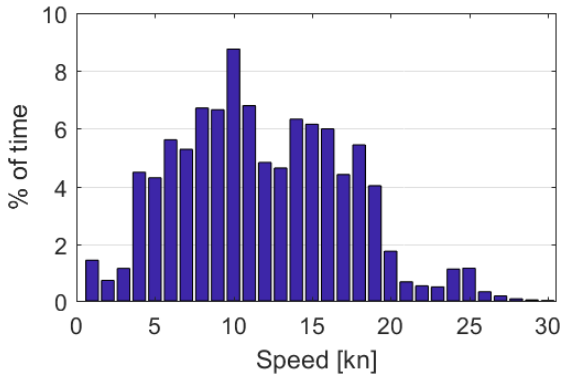

Figure 7-6: HMAS *Maryborough* speed profile for speeds greater than 1 kn, over approximately 9200 hours

7.5.1 Model Uncertainty Analysis

Among different types of uncertainty in modelling and analysis is the simplification of the physical problem. The probability density function (PDF) is a way to describe the uncertainty of the model output. Figure 7-7a and b show the PDF, cumulative probability, and mean of the fatigue damage samples D_i (for the i^{th} $\Delta\sigma$, or each combination of input parameters) at strain gauge locations s3.1.2 and s6.4.2, respectively. At these locations, the vast majority of the damage samples are relatively small.

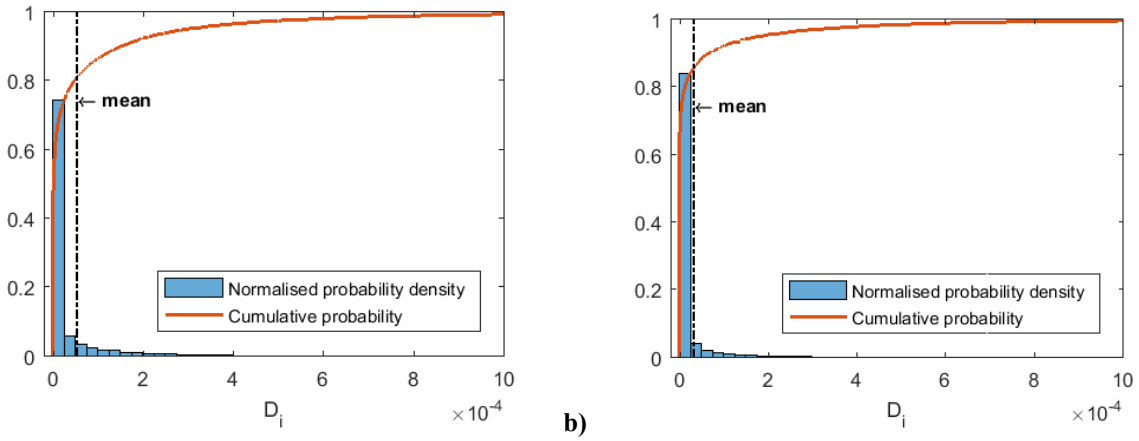

Figure 7-7: PDF, cumulative probability, and mean of D_i at strain gauge locations a) s3.1.2, and b) s6.4.2

The stability, and fidelity, of the model is ascertained by plotting both the mean of the total damage μ_D and the variance of μ_D as a function of the number of samples (or discretisation of the operational profile), as given in Figure 7-8a and b for s3.1.2 and s6.4.2 respectively. The plots indicate that the variance of μ_D quickly diminishes with increasing number of samples, and μ_D converges to approximately 5.5×10^{-5} at s3.1.2 and 3.2×10^{-5} at s6.4.2.

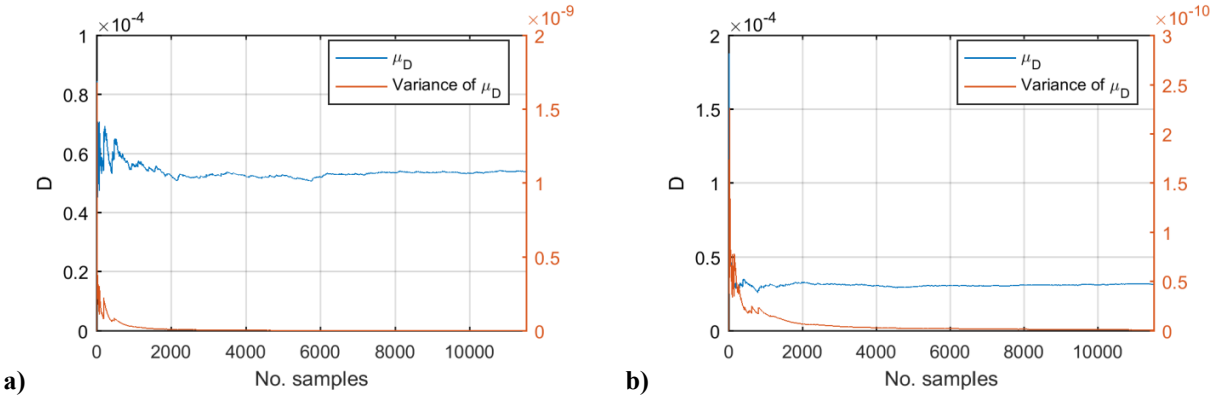

Figure 7-8: μ_D and variance of μ_D as function of number of fatigue damage samples at strain gauge locations a) s3.1.2, and b) s6.4.2. Note differing y-axis scales

7.5.2 Sensitivity Analysis

The Pearson correlation coefficient is used to establish the linear correlation between the significant wave height, wave period, ship heading relative to the dominant wave direction, fatigue resistance of the detail, and the fatigue damage. This correlation represented by r is given by Equation 23, where X_i and Y_i are the individual sample points indexed by i, $\overline{X}$ and $\overline{Y}$ are the mean of the X and Y samples, and n_samples is the sample size:

$$r = \frac{\sum_{i=1}^{n\_samples}\left(X_i - \overline{X}\right)\left(Y_i - \overline{Y}\right)}{\sqrt{\sum_{i=1}^{n\_samples}\left(X_i - \overline{X}\right)^2}\sqrt{\sum_{i=1}^{n\_samples}\left(Y_i - \overline{Y}\right)^2}}$$

Equation 23

The values of r for s.3.1.2 and s6.4.2, for the case that each parameter is equally distributed, are presented in Table 7-6 and Table 7-7 respectively. It is observed that:

- For both locations, the largest absolute value of the correlation coefficient is between $H_{1/3}$ and D. Thus, relative to the other parameters considered, fatigue damage is most sensitive to the increasing tendency of the significant wave height.
- The second largest absolute value of the correlation coefficient is between T_z and D for s3.1.2, and between χ and D for s6.4.2. Whilst s3.1.2 is located on the bottom centreline girder (the keel), s6.4.2 is located approximately 3340 mm off the centreline. Thus, the fatigue damage incurred at s6.4.2 is more sensitive to changes in heading than the wave period relative to s3.1.2.

- The negative correlation coefficient between T_z and D implies that as the wave period decreases, the fatigue damage tends to increase. This is interpreted to mean that the magnitude of the vertical bending moment (global load) decreases for longer wavelengths relative to the length of the ship. Also, the larger the wave period, the smaller the number of load cycles in a given period. In turn, the fatigue damage is expected to be smaller.
- The relative significance of speed to the fatigue damage incurred at both locations is similar. However, whilst v has more influence on D than $\Delta\sigma_L$ at s6.4.2, at s3.1.2 $\Delta\sigma_L$ is of greater significance than v.
- Not surprisingly, there is interdependency between T_z and $H_{1/3}$.

Table 7-6: Correlation coefficients between v, χ, $H_{1/3}$, T_z, $\Delta\sigma_L$, and D at s3.1.2 – input variables uniformly distributed

	$\Delta\sigma_L$ [MPa]	v [kn]	χ [deg]	$H_{1/3}$ [m]	T_z [s]	**D**
$\Delta\sigma_L$ [MPa]	1					
v [kn]	0	1				
χ [deg]	0	0	1			
$H_{1/3}$ [m]	0	0	0	1		
T_z [s]	0	0	0	0.285	1	
D	**-0.077**	**0.109**	**0.090**	**0.403**	**-0.136**	**1**

Table 7-7: Correlation coefficients between v, χ, $H_{1/3}$, T_z, $\Delta\sigma_L$, and D at s6.4.2 - input variables uniformly distributed

	$\Delta\sigma_L$ [MPa]	v [kn]	χ [deg]	$H_{1/3}$ [m]	T_z [s]	**D**
$\Delta\sigma_L$ [MPa]	1					
v [kn]	0	1				
χ [deg]	0	0	1			
$H_{1/3}$ [m]	0	0	0	1		
T_z [s]	0	0	0	0.285	1	
D	**-0.115**	**0.105**	**0.186**	**0.320**	**-0.128**	**1**

The values of r for s.3.1.2 and s6.4.2, for the case that each parameter has a unique probability distribution, are given in Table 7-8 and Table 7-9. When applying probability distributions that are indicative of operational conditions, in comparison to the input parameters being uniformly distributed (Table 7-6 and Table 7-7), the results suggest that:

- The influence of the wave period, speed, and fatigue resistance of the detail on the fatigue damage, incurred at both locations, is more significant. In contrast, the correlation between $H_{1/3}$ and D is weaker. This is likely to be due to the vessel encountering, statistically, slight sea states more of the time.
- At s6.4.2, D is more dependent on $\Delta\sigma_L$ than the wave scatter (T_z and $H_{1/3}$).

Table 7-8: Correlation coefficients between v, χ, $H_{1/3}$, T_z, $\Delta\sigma_L$, and D at s3.1.2 – input variables have unique probability distributions

	$\Delta\sigma_L$ [MPa]	v [kn]	χ [deg]	$H_{1/3}$ [m]	T_z [s]	**D**
$\Delta\sigma_L$ [MPa]	1					
v [kn]	0	1				
χ [deg]	0	0	1			
$H_{1/3}$ [m]	0	0	0	1		
T_z [s]	0	0	0	0.285	1	
D	**-0.112**	**0.194**	**0.091**	**0.135**	**-0.167**	**1**

Table 7-9: Correlation coefficients between v, χ, $H_{1/3}$, T_z, $\Delta\sigma_L$, and D at s6.4.2 - input variables have unique probability distributions

	$\Delta\sigma_L$ [MPa]	v [kn]	χ [deg]	$H_{1/3}$ [m]	T_z [s]	**D**
$\Delta\sigma_L$ [MPa]	1					
v [kn]	0	1				
χ [deg]	0	0	1			
$H_{1/3}$ [m]	0	0	0	1		
T_z [s]	0	0	0	0.285	1	
D	**-0.159**	**0.165**	**0.201**	**0.125**	**-0.147**	**1**

The relationship between the predicted fatigue damage and wave scatter (T_z and $H_{1/3}$) for uniform distributions of all parameters at s3.1.2 and s6.4.2 is visualised in Figure 7-9a and b, respectively. The fatigue damage is accumulated over one year at sea. Each data point is the summation of the fatigue damage across the speed range. At both locations, the fatigue damage is greatest when T_z is 6.5 s and $H_{1/3}$ is 6.5 m. However, when applying probability distributions that are indicative of operations the results differ; Figure 7-10a and b indicate that the largest fraction of the fatigue damage is incurred when T_z is 6.5 s and $H_{1/3}$ is 3.5 m. If the vessel operator was to encounter a seaway characterised by these values it may be possible to change vessel speed and/or heading, depending on the mission requirements.

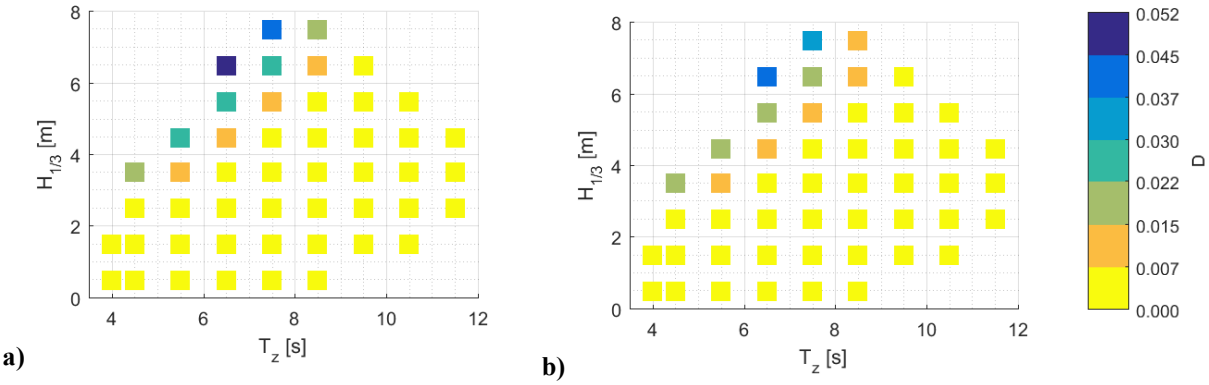

Figure 7-9: Relationship between fatigue damage and wave scatter, summed across the speed range, for equal distributions of all parameters at a) s3.1.2, and b) s6.4.2

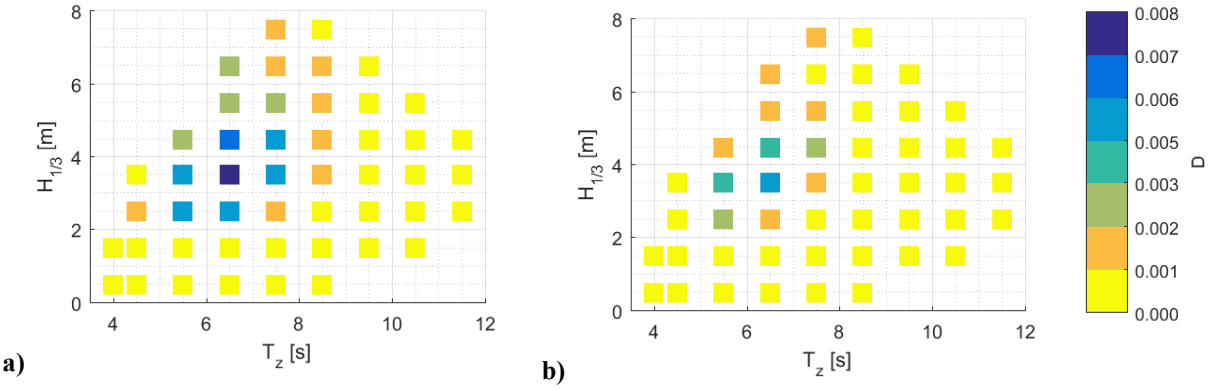

Figure 7-10: Relationship between fatigue damage and wave scatter, summed across the speed range, for unique distributions of input parameters at a) s3.1.2, and b) s6.4.2

The associated effect on the fatigue damage is explored by conducting a local sensitivity analysis. Figure 7-11a and b present polar plots of the fatigue damage, for T_z equal to 6.5 s and $H_{1/3}$ equal to 3.5 m at s3.1.2 and s6.4.2, respectively (each D_i is accrued over the same period). For example, if the vessel is travelling at 15 kn in head seas (180 deg), and the speed is then reduced to 10 kn, the fatigue damage incurred would decrease by 30%. Similarly, Figure 7-12a and b display polar plots of the fatigue damage for T_z equal to 6.5 s and $H_{1/3}$ equal to 2.5 m at s3.1.2 and s6.4.2, respectively. With the drop in $H_{1/3}$ by 1 m, the fatigue damage incurred is an order of magnitude smaller at both locations. Again, if the vessel is travelling at 15 kn in head seas, and the sea state subsided, it may be acceptable to increase the speed (this will depend on the previous usage, or remaining life, of the vessel).

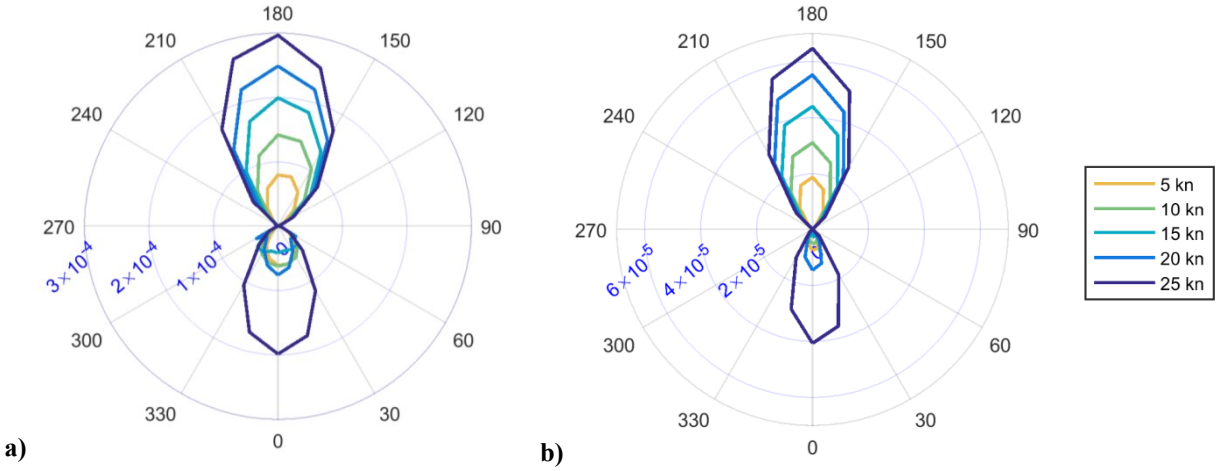

a) b)

Figure 7-11: Polar plot of fatigue damage (radius) at T_z = 6.5 s and $H_{1/3}$ = 3.5 m at a) s3.1.2, and b) s6.4.2. Note differing radial axis scales

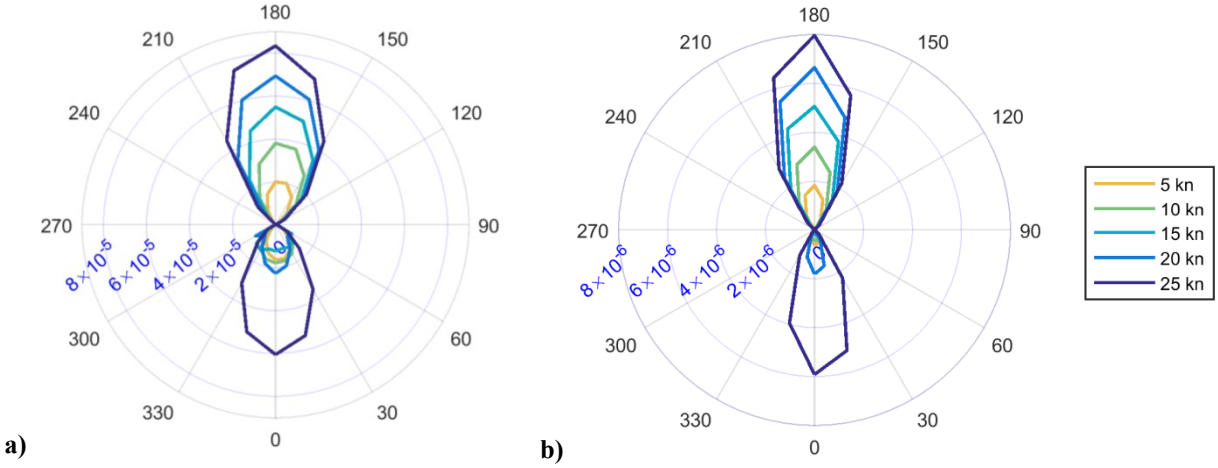

a) b)

Figure 7-12: Polar plot of fatigue damage (radius) at T_z = 6.5 s and $H_{1/3}$ = 2.5 m at a) s3.1.2, and b) s6.4.2. Note differing radial axis scales

7.6 Implications of Results

The results of the fatigue damage modelling uncertainty and sensitivity analyses can be utilised for the service life management and operations of naval HSLC.

Given that the fatigue damage incurred in the patrol boat is most sensitive to the increasing tendency of the significant wave height, it is important to have accurate wave height data during design and to monitor encountered environmental conditions during service:

- The former is emphasised by the notable differences between the $H_{1/3}$ probability density functions based on the Northern Australian Waters wave scatter diagram (assumed during design) and satellite measurements of the patrol boat's operational area [153].

- The latter is particularly important when it is impractical or cost-prohibitive to implement a HMS on a naval ship. That is, in the absence of in-service strain measurements, a numerical tool can be used to estimate the accrued, and future, fatigue damage. Cannon *et al.* [173] highlighted the paucity of long-term wave statistics for the winter months in the Southern Ocean, which lead to the under-representation of the global bending moments experienced by a typical frigate.

Presentation of fatigue damage polar plots for a targeted condition - when the largest fraction of the fatigue damage is likely to occur - may be a good addition or alternative to a speed-wave height limiting curve as operator guidance on the bridge. This is because operational conditions are explicitly linked to structural fatigue damage; the operator can recognise the impact of course and/or speed changes on the structural integrity of the hull.

When the input factors to the SFA were weighted their relative significance to the fatigue damage varied between the two locations strain gauge locations. Thus, the identification of the factor(s) that should be focused on with a view to reducing the fatigue damage is not immediately clear. One may argue that all factors should be monitored. However, for example, it may be desirable to utilise one strain gauge as a 'fatigue meter'. A fatigue meter is a simple and cheap monitoring tool, analogous to a g-meter used in military aviation [174]. Factors in the selection of the optimal location for a fatigue meter include ease of validation of data, magnitude and type of responses, proximity to fatigue-critical areas of the structure, and significance of different parameters to D. Based on the results presented in this chapter, and previous work, some of the advantages and disadvantages of using strain gauges positioned at s3.1.2 and s6.4.2 as a fatigue meter are identified in Table 7-10.

The contribution of slamming to the fatigue damage incurred in an aluminium patrol boat can be significant depending on the encountered wave environment [89]. SFA assumes linear loads; thus, non-linear effects such as those due to slamming are neglected.

A simplified way to include the contribution of non-linear loads in SFA may be to identify the missing 'non-linear loads variable' through regression analysis between the measured strain and other parameters. Long-term strain measurements acquired from the HMS onboard *Maryborough* are available. The 'non-linear loads variable' could then be used to calibrate the results of the SFA. Such an approach may be in a similar vein to a correlation analysis between wave and whipping bending moments [155].

In addition, methods to include slamming loads in spectral approaches to fatigue analysis have been proposed [175, 176]. There is merit in incorporating such a method in future analyses.

Table 7-10: Comparison of s3.1.2 and s6.4.2 as a 'fatigue meter'

Issue	Strain Gauge	
	s3.1.2	**s6.4.2**
Comparability to other testing/simulation (for example SFA results - Table 7-4)	CV(RMSD) similar to average of all strain gauge locations	R^2 of linear fit relatively high, and CV(RMSD) similar to average of all strain gauge locations
Magnitude and type of responses	Strain gauge location similar to another instrumented on a different patrol boat, which has been shown to be good location to detect slamming [89] though stresses are relatively small (refer to Figure 7-5a)	Relatively large stresses (refer to Figure 7-5d)
Strain gauge in proximity to fatigue-critical areas of the structure?	No (to best knowledge)	Yes [170] – may be more informative, and can be correlated with hull survey reports [177]
Average absolute difference between r values for weighted and 'unweighted' inputs	43%	36%

7.7 Conclusion

This chapter has presented an investigation into the sensitivity of the fatigue damage of a naval aluminium HSLC to various input parameters. The work has been motivated by the need to manage the operational availability of naval ships cost-effectively, particularly in the context of changing mission requirements and uncertainties associated with structural service life prediction. Spectral Fatigue Analysis (SFA), implemented in MAESTRO, was deemed appropriate for use in the sensitivity analysis. This was based on validation of the SFA against sea trials data during which linear motions and loads dominated.

A linear correlation analysis between the significant wave height, wave period, ship heading, fatigue resistance of the detail, and the fatigue damage at two structural locations was performed. It was determined that the fatigue damage is most sensitive to the increasing

tendency of the significant wave height. When the input parameters were weighted by probabilities indicative of operational conditions, the relative importance of the speed and heading increased. In addition, the results of the SFA helped to identify the combination of significant wave height and wave period in which, statistically, the largest fraction of the fatigue damage would be incurred. For this condition, a local sensitivity analysis was performed to illustrate the variation of the fatigue damage with heading and speed. This is a means of providing operational guidance as part of management of the structural integrity of the fleet.

7.8 Acknowledgements

The assistance provided by the following individuals and organisations is acknowledged: Defence Science and Technology Group colleagues, including Mr Michael Brincat, Mr Peter Vincent, Mr Peter Graham, Dr Peter Dennis, Dr John Wharington, Mr Mario Selvestrel, Dr Seref Aksu, Dr Stuart Cannon, Mr Andrew Tynan, Ms Zenka Mathys, and Dr David Kershaw.

Where to Next?

In Chapters 6 and 7, suitable enhancements to simplified fatigue analysis and SFA of naval HSLC were identified and developed. This involved the discovery of how these methods can be utilised in through-life fatigue assessment, and their limitations. This work feeds into the next chapter of the thesis; a new through-life hybrid fatigue assessment method is proposed, and the utility of HMS data is demonstrated.

Chapter 8. Through-Life Hybrid Fatigue Assessment of Naval Ships

The work presented in this chapter has been published online in Ships and Offshore Structures. The paper has been edited for inclusion into this thesis to avoid repetition and to improve readability. The citation for this research article is:

Magoga, T., Aksu, S., Cannon, S., Ojeda, R., and Thomas, G., *Through-Life Hybrid Fatigue Assessment of Naval Ships*. Ships and Offshore Structures, published online 2019.

8.1 Introduction

The service life of a ship can be dictated by its structural fatigue life. Fatigue is defined as the weakening of a structural part through crack initiation and propagation, caused by repeated stress fluctuations under cyclic loads.

Fatigue analysis is generally conducted using fracture mechanics or the S-N curve approach. Fracture mechanics concerns modelling of the growth of cracks after initiation, based on an empirical relationship between the stress intensity factor range and the crack growth. The main input parameters are the crack dimensions, the material crack growth data, and the applied stress ranges or spectrum. The S-N curve approach is currently the preferred approach in the design of ship structures [55, 71, 178].

In the design of ship structures, factors such as construction quality, operational loads, material performance, and maintenance quality are assumed. These factors change over the life of a ship, which in turn affect the accuracy of the structural service life estimated during design [179]. An additional source of variability for many naval ships is the operational profile [84]. Safety factors and margins are typically used to account for differences between the actual operational conditions and those assumed during design. However, the application of margins in ship design may not be a suitable means to allow for changing operational requirements through-life [153, 180]. Further, with the exception of the hull girder capacity and material allowances, it is difficult to identify the safety factors in classification society rules because they are often implicit within empirical equations.

In military aviation, Aircraft Structural Integrity (ASI) management has been a core part of platform and operational safety for several decades [174]. ASI management is the basis for fleet availability and realisation of the design life without major unforeseen remediation [181, 182]. Both the safe-life and damage tolerance philosophies are accepted. Effective fatigue management includes, but is not limited to, the measurement of in-service loads and environmental conditions, cataloguing information on the structural configuration and maintenance, and regular operator feedback [174].

In the maritime industry, lifecycle assessment and management is less prolific. It is generally recognised that integrated approaches, which take into account uncertainty, can better inform decision-makers about a ship's structural health. However, for widespread adoption of technology and methods that support through-life structural integrity management a change in culture is needed [129].

The operational costs arising from maintenance activities can be significant in asset-intensive industries [94]. For naval ships, an unplanned failure of a critical component can manifest as increased cost of ownership, reduced operational availability, or a condition of class enforced by the regulatory body. At the same time, fiscal and/or political constraints are placing smaller navies under pressure to extend the longevity of their ships [6, 129]. Whilst full-scale fatigue prototypes and destructive testing of platforms removed from service is common in military aviation, it is impractical for ships due to the scale and associated costs [21]. Accordingly, data collection and fatigue analysis of ship structures should be efficient. However, research has tended to be focused on increasing the modelling accuracy and fidelity. The approaches also tend to be validated via other numerical methods and experimental data [115, 116, 118, 183-185]. In comparison, use of in-service load and response data combined with survey reports to update service life predictions has been limited. Although a number of techniques have been developed, little work has been completed on compiling the information from analyses and inspections [95].

Therefore, the aim of this work is to propose a new through-life hybrid fatigue assessment method. This method combines measured full-scale data, survey reports, and numerical tools in a practical manner. The method is applied to a naval HSLC to demonstrate its merit.

8.2 Proposed Through-Life Hybrid Fatigue Assessment Method

The key steps of the proposed through-life hybrid fatigue assessment method are depicted in Figure 8-1.

The design fatigue life of a ship can be implied or estimated from classification society rules, or a direct fatigue analysis. The design life assumptions include the construction quality, loads, material performance, operational area, and operational profile. However, the ‘as-built’ configuration of the vessel and the actual operational profile are very likely to differ from those specified. In the proposed method, in-service data, fleet maintenance reports, and FEA are incorporated to predict the remaining service life of a ship. Via an on-board hull monitoring system, data including the structural responses (strains), speed profile, and area of operations is collected. The S-N curve approach can then be applied to stress distributions or spectra derived from the strain data to perform direct fatigue analysis of critical details.

It is necessary to calibrate models that predict structural defects using expert judgement and in-service information, as this information leads to changes of the variables incorporated

into the prediction [95]. That is, real-world experience is utilised for continuous validation of the predictive model. Ships provide a number of innate indicators of degradation, such as cracks, that can be taken as a record of the structural condition [15]. Therefore, the validity of the updated (predicted) fatigue life is established via comparison to hull survey reports.

Feedback can then be provided to the operator. Variations in the usage of different ships, and between the usage assumed during design and the actual operational profile, can be highlighted. This information provides a sound basis for maintenance practices and through-life cost savings, by avoiding unnecessary inspections of low risk areas and earlier detection of defects in high risk areas [84].

The predicted service life is periodically updated as the structural configuration and vessel's operations change, and with targeted monitoring and inspection. Also, with increasing data there is an opportunity to improve the fidelity of the modelling.

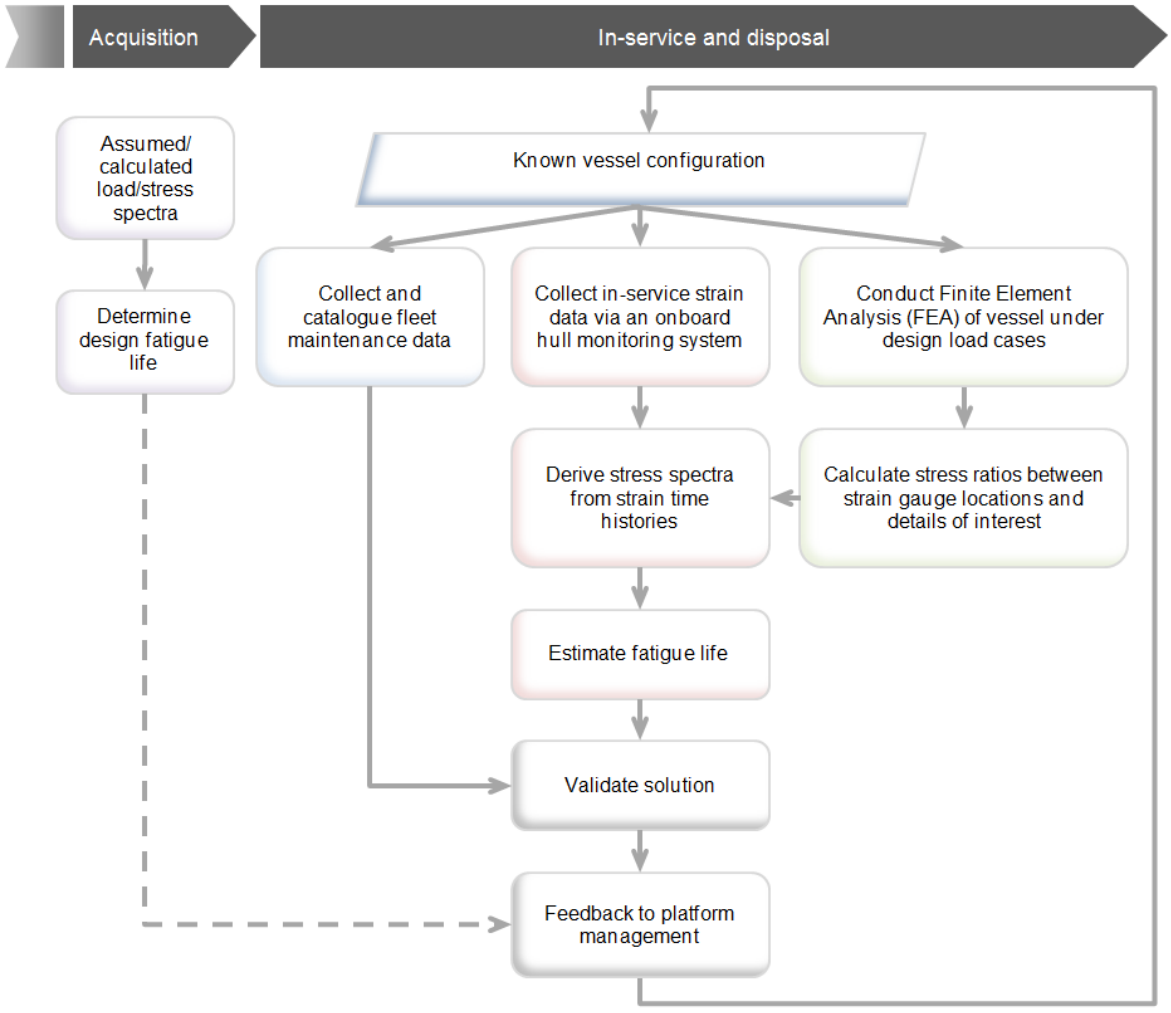

Figure 8-1: Process to estimate and update fatigue life

Although long-term strain monitoring is arguably the best way to determine the long-term stress distribution of the ship structure, in its absence a spectral (direct) procedure can be utilised (described in Section 3.7.2 and Chapter 7). Thus, if information on the ship speed and encountered wave environment are obtained, these parameters can be input into the spectral approach within the proposed through-life hybrid fatigue assessment method.

8.3 Application

The method described in the previous section is applied to the ACPB. Four welded details found on the patrol boat are considered in this chapter:

1. A pillar (hollow tube) joined to an end plate by a bevel-butt circumferential weld.
2. A butt weld between a relatively thick insert and thinner deck plating.
3. A built-up longitudinal beam comprised of web plating of different thickness joined by a butt weld and a flange joined by a continuous fillet weld.
4. Longitudinal plating joined to transverse plating via a double fillet weld.

8.3.1 Finite Element Analysis

Stress analysis of the patrol boat is performed using FEA implemented in the commercial package MAESTRO [96]. The FE model of the ACPB is discussed in Section 3.5. The load cases are considered in the FEA as described in Section 4.2.1.

8.3.2 Fleet Maintenance Data

Maintenance reports of cracking are used to validate the predicted fatigue life, as discussed in Section 4.5. Table 4-3 presents the fleet-wide average and standard deviation of FL_m for each structural detail of interest, normalised by that of ID-1.

8.3.3 Collection of Full-Scale Data and Derivation of Stress Spectra

Data acquired from strain gauges A, B, and C, which were installed onboard *Glenelg*, is utilised in the present chapter (Section 3.3.1).

Data processing routines were developed in MATLAB [88] to convert and filter the raw strain data to stress (refer to Section 3.3.3). The stress signal was reduced to cycles using the rainflow counting method (described in Section 3.7.3).

The stress spectra derived at strain gauge locations A, B, and C, normalised by the maximum measured stress range, are presented in Figure 8-2. The stresses measured by strain

gauge A are in the vertical direction and by strain gauges B and C in the longitudinal direction. The most severe spectrum occurred at strain gauge C, in the global longitudinal direction of a major load-bearing girder underside of the main deck in the engine room.

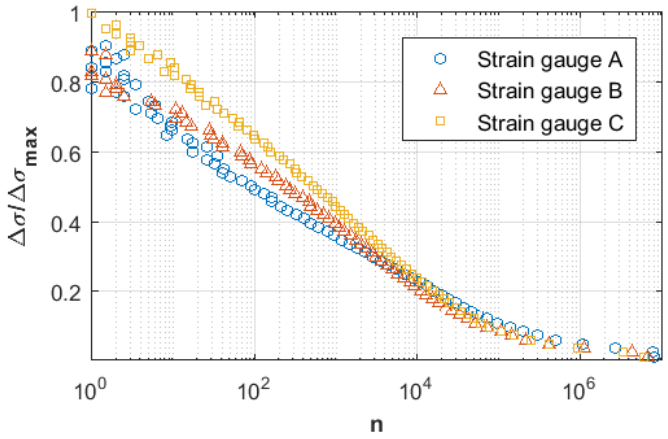

Figure 8-2: Normalised stress spectra derived from strain measurements (stress ranges at strain gauge A in vertical direction, and at B and C in longitudinal direction)

8.3.3.1 General Recommendations for Configuration of HMSs installed on Naval Ships

When planning installation of a HMS on-board a naval platform it is important that sensors are specified and located to meet the aims of the HMS. The following are general recommendations [84, 89]:

- To use the global wave loading as a hull-girder fatigue indicator, install strain gauges along the length of the vessel. Further, these strain gauges should be located away from bending nodes to ensure that appreciable structural excitation is detected. This can be checked via natural frequency analysis (generally, the first and second modes are sufficient).
- To understand localised fluctuating stresses that induce fatigue damage, install strain gauges in proximity to highly stressed or cracking-prone details. However, care should be taken to ensure that placement of strain gauges is not unduly influenced by stress concentrations or stress gradients. This can be checked via FEA.
- The results from monitoring stresses at one location should be able to be related to the structural response at other locations.
- The design of a HMS should factor in ease of access to the structure, weight limitations, and potential interference with on-board activities.
- Consideration should be given to designing redundancy into the system and the reliability and longevity of the sensors.

For fatigue monitoring, data integrity, volume, retrieval, and sampling frequency are important factors [174].

Inevitably, the costs associated with setting-up and maintaining hardware as well as processing and analysing large quantities of data, and the complexity of the system, need to be balanced.

8.3.4 Fatigue Life Estimation

The fatigue life values of the patrol boat details of interest are predicted using the nominal stress approach combined with CDT (process proposed in Chapter 4), with the stress spectra displayed in Figure 8-2. It is assumed that the fatigue strength of the examined details is represented by analogous details found in Eurocode 9 [102].

A limitation of the nominal stress approach in fatigue assessment is that only uni-directional stresses can be incorporated in details provided in Eurocode 9. However, this assumption does not hold true in actual operational conditions. In the proposed method, a three-dimensional (3D) global FE model of the vessel was developed and the subsequent stress analysis considering design load cases. This enables stresses in all three directions to be resolved. The dominant stress, usually aligned with the direction of the reference stress, is then used to determine the stress ratio between the reference sensor location and the location of interest. Thus, the effect of this limitation is somewhat reduced. In addition, the interpretation of the stress directions incurred in the structure, with respect to the ship heading relative to the principal wave direction, is important. As such, as best as possible, the gauges were adhered to the structure so that the direction of the associated measured stresses were aligned with the estimated dominant stress/load direction. This was verified via 3D stress analysis.

The selected Eurocode 9 detail categories for the details of interest and K factors are given in Table 4-6. The reference locations are given in Table 4-2.

8.3.5 Fatigue Life Results

Figure 8-3 presents a comparison between the fatigue damage D predicted at the details of interest and the reference locations. The largest fatigue damage was incurred at ID-2. Interestingly, its reference location (strain gauge B) incurred the smallest fatigue damage. The smallest fatigue damage at a detail of interest was predicted at ID-3. However, the fatigue damage at its reference location (strain gauge C) was the greatest. These results highlight that

the structure near a strain gauge that measures relatively large stresses may not be the most fatigue-critical.

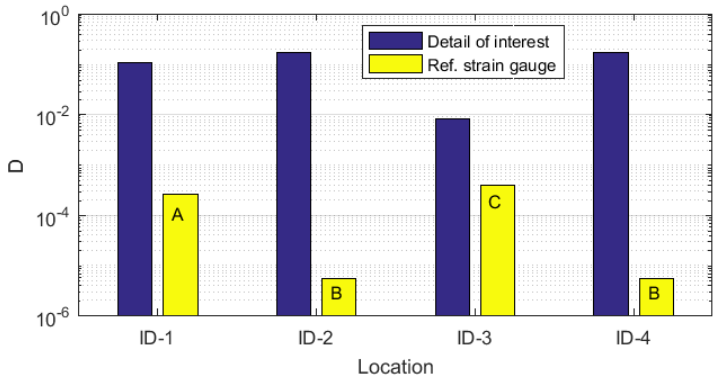

Figure 8-3: Comparison between fatigue damage at details of interest and respective reference locations

Figure 8-4 shows the predicted fatigue life, FL_p of each detail of interest normalised by FL_p at detail ID-1. The fatigue life was smallest at ID-2, followed by ID-4, ID-1, and ID-3. The values of FL_p are relatively similar. The exception is FL_p at ID-3, which is approximately fourteen times greater than FL_p of ID-1, and fatigue cracking would not be expected to occur at this location.

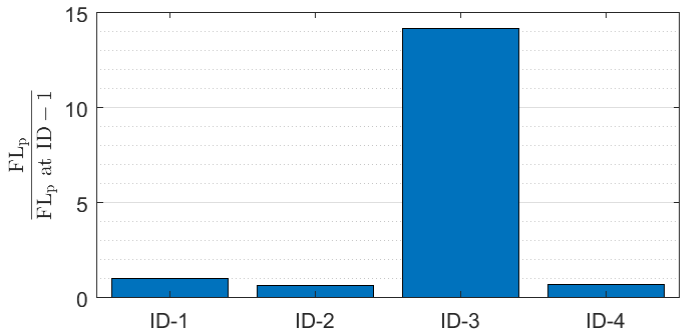

Figure 8-4: FL_p of details of interest, normalised by FL_p of detail ID-1

8.3.6 Validation

Both the validity and the significance of the fatigue life predictions can be characterised by the difference between FL_p and FL_m as a proportion of the design life FL_d of the patrol boat. The design life should be the minimum fatigue life of the structure. Figure 8-5 indicates that the differences between FL_m and FL_p are 8%, 7% and 22% of FL_d for details of interest ID-1, ID-2 and ID-4, respectively. The predicted fatigue life at location ID-3 is greater than the design life, and no defects have been reported at this location. There is also agreement between the order

of the FL_p values shown in Figure 8-4, and the order of the FL_m values (given in Table 4-3) by detail. Thus, the fatigue life predictions are considered to be valid.

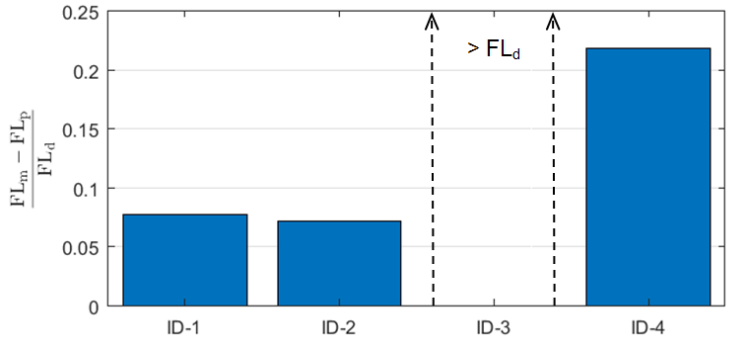

Figure 8-5: Difference between fatigue life values based on derived stress spectra and maintenance records as ratio of design fatigue life of patrol boat

8.3.7 Feedback to Platform Management

Options to achieve the desired service life of a ship include service restriction, repair design of joints to have better fatigue resistance, and improved weld dressing [26]. The effect of implementing these options on the service life can be quantified after modification of the FEA model and re-selection of the S-N curve as necessary. This is demonstrated in Figure 8, which shows the percentage change in FL_p of detail of interest ID-1 with changing K applied to the reference stress spectra. For example, a 10% decrease of K results in a 50% increase in the fatigue life. Conversely, if a nearby structural item fails and there is load shedding to the joint, the stresses would be expected to be greater. For instance, a 10% increase of K leads to a fatigue life penalty of 30%.

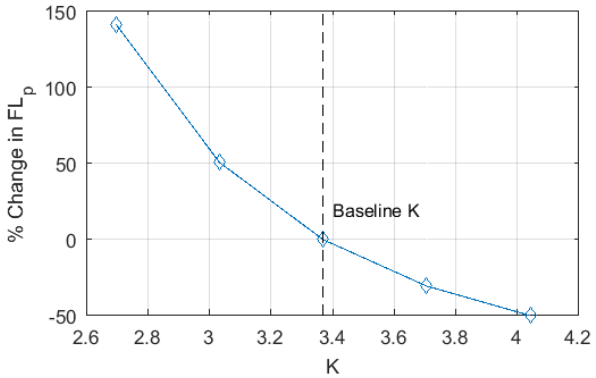

Figure 8-6: Change in FL_p with change in K applied to reference stress spectra at detail of interest ID-1

Although engineering design and mission requirements are not covered in detail in this thesis, examples of how the framework has/could incorporate feedback to inform the through-life management of a naval ship include:

- Fatigue damage polar plots for a targeted condition (refer to Section 7.6) as a useful supplement to a speed-wave height limiting curve on the bridge. This is because operational conditions are explicitly linked to structural fatigue damage.
- Improvement of the fatigue life of structural details by selection of a configuration with a smaller stress concentration factor (for example, replacement of straight brackets by curved brackets at the bottom and top of pillars).
- Demonstration of the significant variation of the fatigue life of the patrol boat depending upon the operational profile and the effect of the change of displacement due technology upgrades [152, 153].

8.4 Discussion

Issues with the structural performance of the patrol boat are not unexpected due to its weight-optimised structure and the requirement to operate in harsh sea conditions when a commercial vessel would otherwise seek shelter. The USN also reviewed hull girder, slamming and vehicle deck design loads for the Littoral Combat Ship because of hull cracking [67]. Even in conventional steel ships, cracks can initiate and propagate before the required service life [55, 186]. However, feedback from operations provides knowledge on fatigue-critical details typical of HSLC.

The approach taken to translate a reference stress spectrum to a detail of interest is to use a single scaling factor. This approach is applicable when the strain gauge is located sufficiently close to the detail of interest, as it can be assumed that the response at the detail of interest is directly proportional to that at the strain gauge location. However, this assumption may not hold when the strain gauge is far from the detail of interest. In this case, a more complex transfer function should be formulated [187, 188].

The effects of weld repairs are not explored explicitly in this chapter. That is, FL_m is treated as the 'first' fatigue life of the details of interest. However, as the proposed through-life hybrid fatigue assessment method is a feedback loop it can be used to predict the time between completion of a repair to re-cracking, and to assess different repair solutions.

In resource-limited environments, there is a trade-off between the required accuracy and the cost of through-life fatigue management of an in-service, complex structure [189].

Recently, research has been conducted to determine cost-efficient HMS plans that provide crucial information regarding ship performance and optimum maintenance schedules [80, 190]. In the offshore industry codes exist to manage structural integrity, such as ISO 19902:2007 [191] and DNV GL's Offshore Standards [192]. These codes require an evaluation of the resistance against fatigue damage and, based on the results, establishment of inspection programmes both during construction and in-service. Such programmes are considered conservative and expensive, and ways to improve their efficiency are being researched [169, 193].

One issue in predicting the fatigue life is bias in the input data or validation dataset. For example, the uncertainty associated with a single record can be larger than the uncertainty associated with the average of many records [95] (refer to Section 3.4). In the field of survival analysis, samples are considered censored when: 1) the exact failure times are not known but it is known that the failure occurred sometime between inspection and time zero, and 2) the failures have not occurred and 'the waiting time' exceeds the observation time. Censored data can be taken into account by use of the maximum likelihood method [194]. However, the maximum likelihood method can yield biased estimates when the number of samples collected is small.

The quantification and management of uncertainty in the different sources of data, and models, required in effective ship life-cycle assessment are recognised challenges [95, 179, 189, 195]. Frangopol and Soliman [189, p 15] hypothesise that the most insurmountable future challenge may be 'related to efforts needed to reduce the gap between the theory and practice in the life-cycle analysis and management field. A large number of efficient and effective life-cycle management techniques exist; however, the real-world application of these methodologies does not exist.' The focus of this chapter is identifying, formulating, and building confidence in the necessary tools to put the framework in the hands of decision-makers and ship managers. In this respect, value-adds to the framework may be:

- Implementation of a methodology, such as that proposed by Hifi and Barltrop [95], to calibrate the prediction models of structural defects using data from experience-based methods and expert judgement.
- Frequentist or Bayesian methods that address the small number of cracking reports [134, 196].

8.5 Conclusion

A method to measure and monitor full-scale structural responses and the operational profile, combined with the maintenance history, to evaluate the fatigue life evaluation of a naval vessel is proposed. Four different aluminium welded details were studied. The fatigue damage was estimated by employing cumulative damage theory, combined with Eurocode 9 S-N curves, to stress spectra derived from in-service strain measurements. A stress spectrum was related to a detail by applying the ratio of the maximum stress ranges of the detail to the strain gauge location. The resulting fatigue life predictions correlate well to fleet maintenance data. The proposed method is efficient because it is properly linked to stress analysis, and is a trade-off between accuracy and effort. The present study can be extended by employing a probabilistic approach to take into account the parameters of influence in fatigue assessment.

Where to Next?

The through-life hybrid fatigue assessment method proposed in this chapter and the work presented in Chapters 2 through 7 are considered and integrated on the quantitative-qualitative dimension in Chapter 9. This forms the response to research question #3.

Chapter 9. Approach to Provide Advice Regarding Fatigue Life for Decision-makers

9.1 Introduction

The design, acquisition, and management of a naval ship are a balance between costs and threats, and performance objectives and opportunities [17, 80, 174, 197]. Therefore, there is a need to articulate the level of confidence that can be associated with a predicted fatigue life.

The aim of this chapter is to elucidate the optimum approach to provide evidence-based advice regarding the fatigue life of naval HSLC for decision-makers. The optimum approach, in this context, is one that features the best knowledge and minimisation of the uncertainty associated with variables in fatigue life assessment. This work can be used to inform Defence risk management and seaworthiness[xi], with respect to risk identification and mitigation planning. The risks can be due to uncertainties and knowledge gaps. That is, at the various stages of the CLC, stakeholders can better refine the likelihood and consequence of a risk or choose to gather additional information [198]. This chapter is partially a continuation of Sections 7.6 and 8.3.7, which show how underlying information can be synthesised to generate evidence-based advice. This is to support ship managers and executive authority with decision-making on structural impacts and operational matters.

The aim is achieved by integrating the knowledge gained throughout the PhD research through qualitative and quantitative analyses. Consideration and integration of data on the quantitative-qualitative dimension helps mitigate the use of inappropriate statistical techniques and related conclusions [199, 200].

The present chapter is divided into four main subsections:

- Section 9.2 presents a qualitative analysis of different fatigue life evaluation approaches.

[xi] The RAN seaworthiness outcome is the achievement of 'the maximum likelihood of a realised system being able to achieve the specified tasking where the OSI[xi] is clearly understood and articulated, hazards and risks are eliminated or minimised in context of the OSI [Operational and Support Intent] and the system is operated as intended' [14 , p.18].

- Section 9.3 presents a quantitative analysis of fatigue life variables based on both the ACPB HMS data and SFA.
- In Section 9.4, the need to generate S-N curves for the welded joints to reduce the uncertainty in the fatigue life answer is discussed.
- The overall conclusions of these analyses are presented in Section 9.5

9.2 Qualitative Analysis of Fatigue Life Evaluation Approaches

The objective of qualitative research is to build a larger knowledge base about a problem space. The empirical and theoretical resources needed to comprehend an idea are seen as interwoven within the context [201]. The type of inquiry is exploratory in nature.

To guide the qualitative analysis, the following problem questions are posed:

1. What are the key attributes that characterise a fatigue analysis of a welded ship structural detail?
2. To what extent do different fatigue analysis approaches achieve the key attributes?

The fatigue analysis approaches - or options - were identified in the technical review in Chapter 2 and in Chapter 3.

By posing and answering the above questions the intention is to build a decision-making aid regarding the most appropriate fatigue analysis option, to be contextualised by stakeholders in terms of availability of resources, budget, desired precision and validation, and schedule. The techniques used to perform the qualitative analysis are data review, codification, and a comparative analysis, as illustrated in Figure 9-1.

The process begins with a data review that is framed by the problem questions above. This step is followed by scrutiny and codification of the collected information, which involves reduction of the information into key attributes that describe the problem under investigation [202]. These attributes are then used to compare the fatigue analysis approaches.

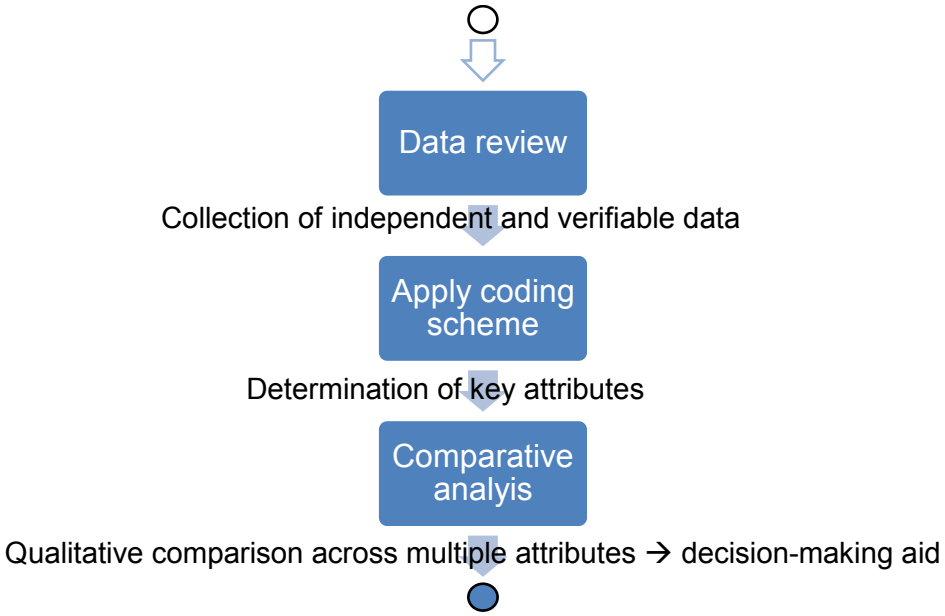

Figure 9-1: Qualitative analysis process and inputs and outputs at each step

9.2.1 Data Review

A data review comprises examination of a variety of sources to collect independently verifiable information [199]. In addition to the scope and limitations of the PhD defined in Section 1.5, the review was scoped by:

- Source: publications from academia, industry, and defence organisations.
- Keywords:
  - Ship AND fatigue
  - Steel OR aluminium
  - Naval OR navy OR “coast guard” OR patrol OR "high speed craft" OR "high speed light craft"

9.2.2 Codification

Codification of the collected data involves scrutinising and finding themes in the data [199]. In this study, the collected information was firstly scrutinised for relevance. For instance, though they appeared frequently in the data, topics such as improved welding techniques and use of composites in shipbuilding were deemed outside of scope. Secondly, topics in the data were clustered by commonality to discern the key themes or attributes as listed in Table 9-1.

It was assumed that single-source bias was sufficiently minimised by ensuring that a theme appeared in three or more sources.

Table 9-1: Identified key attributes of a fatigue analysis of a welded hull structure

#	Attribute	Reason/Need	Reference
I.	Probabilistic framework/ analysis	• Need to understand importance and interaction between various factors to fatigue damage, including operational profile, wave scatter diagrams, wave spectra, heading distributions. • Enable the limits of the structural performance to be accurately established. • Fatigue damage in ship structures is highly uncertain.	[145, 153, 203-208], Chapter 7
II.	Accounts for slamming	• Slamming can have a considerable influence on the fatigue life of HSLC and naval ships when compared to accounting for the global wave induced stresses alone.	[21, 22, 145, 209], Chapter 4
III	Can inform maintenance actions	• As fatigue cracking can lead to unanticipated costs and loss of availability of naval, effective inspection planning of naval ships under fatigue damage is needed.	[17, 95, 203], Chapter 8
IV	Allows assessment of remaining life	• Reduce maintenance and life-cycle management costs, and increase operational availability of ship. • May need to extend life of ship.	[15-17, 210]
V	Practical ('pragmatic')	• One of the main obstacles to the implementation of a fatigue analysis approach for marine structures is efficiency; for instance, is use of a commercial FEA package adequate or are specialised techniques required? • Approach should be able to be linked to other naval engineering/management systems. • Government ship acquisition directives may emphasise the use of industry practices.	[14, 211-214], Chapter 2

9.2.3 Comparative Analysis

In the comparative analysis, he options are rated using a six level ordinal scale (with ratings of None, Very Low, Low, Medium, High and Very High) by that represents the extent that they exhibit the attributes. This analysis takes aspects from Comparative Risk Assessment (CRA), which offers a systematic framework for evaluating variables that pose different risks in problem-solving [215]. However, the current procedure diverges from CRA in that the options are not weighted and overall rankings are not given as these activities should involve stakeholder engagement. This is because the attitudes of the different stakeholders can significantly affect the results of an assessment, and in turn decision making [216]. Each option is 'bound by implicit stakeholder constraints of cost, schedule and risk level' [217, p. 10].

The ratings were assigned to each option based on the Candidate's experience as well as the evidence gained during the PhD research. Thus, the analysis of the options is a mix of 'hard' (externally verifiable)[xii] and 'soft' (not externally verifiable)[xiii] techniques [199]. The ratings are presented in Table 9-2.

Table 9-2: Comparison of extents that different approaches to fatigue life analysis achieve key attributes

#	Approach	Attribute				
		I	**II**	**III**	**IV**	**V**
		Probabilistic analysis	**Accounts for slamming**	**Can inform maintenance actions**	**Allows assessment of remaining life**	**Practical / 'pragmatic'**
1	Rules-based approach (implicit)	None	None	None	None	Very high
2	Simplified fatigue analysis	None	Low[xiv]	None	Low	Very high
3	SFA using numerical tool	Very high	Low[xv]	Low	Medium	Medium
4	RC + CDT applied to full-scale data	High	Very high	Medium	High	Low
5	Analysis of maintenance data	Very low	Very high	High	Low	High
6	#3 + #5	Very high	Medium	High	Medium	Medium
7	#4 + #5	High	Very high	High	High	Low-Medium
8	#3 + #4[xvi]	Very high	Very high	High	High	Low

For example, it is submitted that Option #1 (assumption that a ship's design service life will be met if it is designed to a set of classification society rules) does not achieve attributes **I**

[xii] 'Hard' because data review is part of the process.
[xiii] 'Soft' because an ordinal scale and individual opinion are employed.
[xiv] Depends on stress distribution used - refer to Chapter 6.
[xv] Typically, hydrodynamic analysis is linear – refer to Chapter 7.
[xvi] An example realisation of combining Options #3 + #4 is virtual hull monitoring, which is a technique that combines the results from SFA with speed, heading, and position data (via GPS or a ship-board navigational system) and wave data (using measurements, ship logs, or hindcasts). Virtual hull monitoring is a potential means to 'monitor' ship stress states without strain gauge measurements.

to **IV** but is practical. In general, design to classification society rules provides the minimum standard for ship structural safety. However, classification societies may argue that design life variables are taken into account through their experience. Nevertheless, it is extremely difficult for the Candidate to gain an understanding of how the elements of class society experience directly link to attributes **I** to I**V**.

In contrast, Option #4 - rainflow counting plus CDT (RC + CDT) applied to long-term stress data - achieves attributes **I** to **IV** to a relatively high degree but features low practicality as it is time and resource intensive. Option #7 represents the through-life hybrid fatigue assessment framework presented in Chapter 8. Combining Options #4 + #5 offers achievement of key attributes **I** to **IV** to a greater level than that of the individual options. However, though it is practical to integrate available fleet maintenance data into a monitoring program, the resources needed to realise this option are relatively significant.

In Australian Defence, ship's seaworthiness includes 'appropriate structural integrity of physical elements including hull, structures …' [14, p. 191]. One approach to assure this aspect of seaworthiness, throughout the CLC, may be to explicitly link service life modelling and hull monitoring to seaworthiness management [83].

The actual labour and monetary costs of the different approaches are only superficially considered within the fifth attribute (practical/pragmatic) in Table 9-2. In addition to understanding seaworthiness and operational adaptability requirements, it is important to offer a costs-benefits analysis that can be used to decide if a particular approach is worth the investment [83, 218]. For instance, if a naval structure is designed using the 'safe life' philosophy so that it should not fail due to fatigue damage during its service life, why should it be monitored (Option #4)? Using this argument, the cost of choosing Option #4 is high but for little benefit. However, the key assumptions that underlie this argument (for example, that the ship is used in the same manner as that stipulated in the Operating and Support Intent (OSI), or that incorporation of safety factors in design is sufficient) can change or be untrue. For the adoption of an approach to fatigue life management to be justified, the sum of both the tangible and intangible[xvii] costs needs to be low relative to the benefits [218].

It is conceded that there is bias introduced by the Candidate's experience, which influences the ratings of the options in Table 9-2. For example, the installation and

[xvii] Intangible costs include those arising from project planning, training personnel, maintenance and repair, and disposal.

caretakership of the HMSs on *Glenelg* and *Maryborough* was considerably resource intensive. One lesson learned from this experience is that a HMS should incorporate low-cost and highly reliable instrumentation rather than be a broad instrument suite. Also, a HMS can be scaled to meet the constraints of the stakeholder. Furthermore, efforts are being directed to optimise resource allocation for whole-of-ship management (for example, by using an Integrated Platform Management System or the Digital Twin concept – refer to Appendices E.1 and E.2 - and to determine cost-efficient HMS plans [80, 219]. However, further work to improve HMSs is outside of the scope of the thesis.

9.3 Quantitative Analysis of Fatigue Life Variables

In this section, quantitative techniques are used to improve understanding of the confidence in the fatigue life answer when using different approaches and sources of information. In comparison to qualitative research, the type of inquiry in quantitative research is results-oriented. The objective is to examine the relationships between variables [220].

A confidence interval gives an estimated range of values which could reasonably be attributed to the analysed quantity. Uncertainties can be due to random effects, and the practical limits on correcting for systematic effects. Uncertainty can be quantified by combining various elements of uncertainty, which are based on the results of repeated analyses or measurements [95, 206]. For example, Garbatov and Guedes Soares [206] assessed the uncertainties introduced by discrete, closed-form and spectral approaches to analyse the fatigue damage of ship structural details. Also, the influence of ship main characteristics, loading condition, and wave environment were considered. The uncertainty, chosen on the basis of the desired level of confidence, was reported for each variable.

It is not a straight-forward process to ascertain the joint uncertainty of the variables in the fatigue life analysis of the ACPB because a single model or experiment of the ship cannot explicitly capture the observations/distributions of all of the input variables. Table 9-3 lists four of the approaches to fatigue life prediction considered in Section 9.2. For instance, SFA allows the wave scatter, wave spectrum, speed, headings distributions, and the S-N curve to be defined. However, slamming loads are typically not included in the analysis. In comparison, slamming loads are implicitly captured in the *Maryborough* HMS data; the number, and contribution to fatigue damage, of slams can be derived using the method reported in Chapter 5. However, a limitation of this HMS was that environmental parameters could not be measured (with the exception of dedicated sea trials).

Table 9-3: Known/definable variables[xviii] in fatigue life prediction for each approach

Variable	Rules-based approach (implicit)	Simplified fatigue analysis	SFA using numerical tool	RC + CDT applied to full-scale stress data (from *Maryborough* HMS)
$H_{1/3}$ [m] – T_z [s]	×	×	✓	×
v [kn]	×	×	✓	✓
χ [deg]	×	×	✓	×
Wave spectrum	×	×	✓	×
S-N curve	×	✓	✓	✓
N_{slam}	×	×	×	✓
Time at sea	✓	✓	✓	✓

In light of this issue, the following approach is taken to quantify the combined uncertainty of the fatigue life answer due to the uncertainties associated with the variables in Table 9-3:

1. Analyse *Maryborough* HMS data to -
    a. Establish the longer-term importance of slamming (extension of the analysis performed in Chapter 5).
    b. Determine the correlation between the hourly number of slams, vessel speed, significant stress, and fatigue damage.
    c. Investigate if there is a simplified way to include the slamming contribution to fatigue in SFA.
2. Based on the results of step 1, use SFA to conduct the sensitivity study of the variables listed in Table 9-3.

9.3.1 Analysis of Maryborough HMS Data

The uncertainty associated with the occurrence of slamming and its impact on the fatigue damage is investigated via analysis of the data acquired from the *Maryborough* HMS. Based on the available data at strain gauge s3.1.2 (3304 hours), and using the methods presented in Chapter 5, *Maryborough* sustained slamming during 50 hours. Also, she was at sea 30% of the

[xviii] The effect of the operating load, or displacement, on the fatigue life of the ACPB is not part of the analysis because it is minor compared to the effect of operations in different ocean environments and with a different speed profile [152].

monitored time. Therefore, *Maryborough* experienced slamming approximately 5% of the time at sea. It is assumed that the vessel encountered relatively heavy sea states and operated in bow quartering to heads seas during these times.

Table 9-5 presents the total fatigue damage D_{total} incurred at five strain gauge locations (listed in Table 9-4 and shown in Figure 9-2) during the entire monitoring period, during the periods in which slamming was detected, and the ratio between the two values. In addition to s3.1.2, strain gauges s2A.1.2, s2A.2.1, s2A.5.2, and s2A.5.3 were selected for analysis because there is good data availability from these sensors.

It is seen from Table 9-5 that the D_{total} ratio is 0.45 at s3.1.2. This result is significant, as almost half of the fatigue damage was accrued during a relatively small fraction of *Maryborough's* time at sea. The D_{total} ratios at strain gauge locations s2A.1.2, s2A.5.2, and s2A.5.3 are less than that at s3.1.2. This is attributed to the dissipation of energy, associated with the slam event, through the structure. Nevertheless, on average, approximately 40% of the fatigue damage was incurred during 5% of the time at sea.

Table 9-4: Analysed strain gauge locations on HMAS *Maryborough*

ID	Side	Approximate location	% L_{WL} forward of transom
s2A.1.2	Port	5000 mm above USK On middle of flange of stiffener 3340 mm off CL	72%
s2A.2.1	Port	5000 mm above USK On middle of flange of stiffener 2850 mm off CL	73%
s2A.5.2	Stbd	5000 mm above USK On plating approx. 2925 off CL	73%
s2A.5.3	Stbd	5000 mm above USK On middle of flange of stiffener 2850 mm off CL	74%
s3.1.2	CL	Centre of flange on keel	70%

Table 9-5: D_{total} during monitoring period and period in which slamming occurred

Strain gauge	E9 S-N curve	K	D_{total}		
			Monitoring time at sea	Slamming time	Ratio
s3.1.2	11.3	2.7	0.016	0.0072	0.45
s2A.1.2	5.6	1.5	0.0015	5.3×10^{-4}	0.34
s2A.2.1	5.6	1.5	8.7×10^{-4}	4.0×10^{-4}	0.45
s2A.5.2	5.6	1.5	0.019	0.0072	0.38
s2A.5.3	5.6	1.5	0.0088	0.0030	0.34

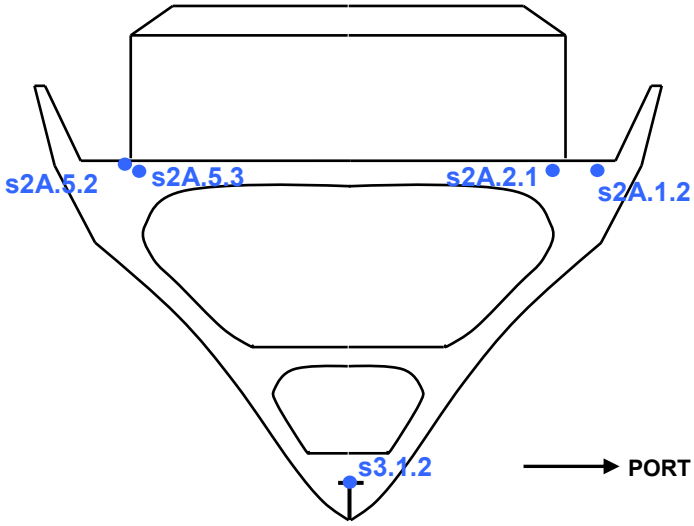

Figure 9-2: Schematic of hull cross-section showing *Maryborough* strain gauge locations listed in Table 9-4

Kendall's rank correlation coefficient is a measure of the statistical association between the rankings of two variables. It assesses how well the relationship between the two variables can be described by a monotonic function. The technique does not assume a distribution shape, rather only the difference between ranks is important. The rank correlation coefficient τ is calculated using Equation 24:

$$\tau = \frac{(\text{number of concordant pairs}) - (\text{number of discordant pairs})}{n_{obs}(n_{obs} - 1)/2} \qquad \textbf{Equation 24}$$

In Equation 24, n_{obs} is the number of observations. If the direction of the rankings is the same, the pairs are concordant. If the direction of the rankings is not the same, the pairs are discordant.

A limited subset of the HMS data is used in the correlation. This subset is comprised of 522 hours, and was created such that each observation of v_{ave} has a standard deviation of less than 1 kn to ensure minimal speed fluctuation during each hour. Heading changes are also relatively small. The normalised speed distribution based on the subset is given in Figure 9-3. For comparison the long-term speed profile, over 9200 hours, is shown in Figure 9-3.

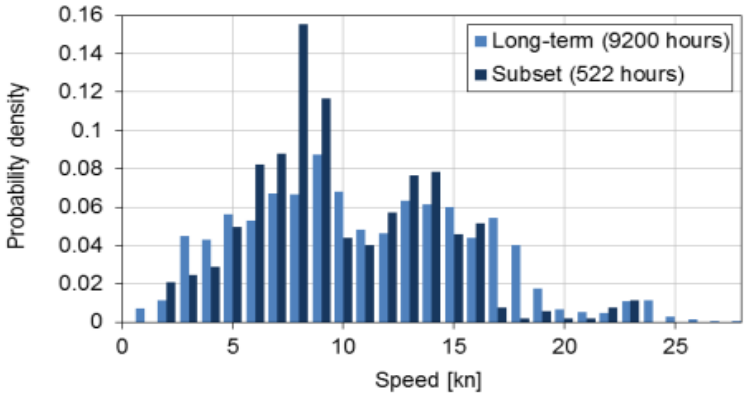

Figure 9-3: Comparison between normalised speed histograms from 522 hour subset and 9200 hours (speed greater than 1 kn)

The values of τ between pairings of N_{slam}, average vessel speed v_{ave}, and $\Delta\sigma_{1/3}$ and D_{total} per hour at s2A.5.2 and s3.1.2, over 522 hours (observations) is given in Table 9-6.

The statistical significance of a correlation is indicated by a probability value or p-value. P-values for the correlation coefficients are presented in Figure 9-7. N_{slam}, average vessel speed v_{ave}, and $\Delta\sigma_{1/3}$ and D_{total} per hour at s2A.5.2 and s3.1.2 are plotted against D_{total} per hour at s3.1.2 in Figure 9-4.

Table 9-6: τ correlation coefficients between hourly N_{slam}, average vessel speed at instances of slams v_{slam}, slam severity, D_{wave}, and D_{total} at s3.1.2 (522 observations)

				s2A.5.2			s.3.1.2		
		N_{slam}	v_{ave} [kn]	$\Delta\sigma_{1/3}$ [MPa]	D_{wave}	D_{total}	$\Delta\sigma_{1/3}$ [MPa]	D_{wave}	D_{total}
	N_{slam}	1							
	v_{ave} [kn]	0.076	1						
s2A.5.2	$\Delta\sigma_{1/3}$ [MPa]	0.232	-0.034	1					
s2A.5.2	D_{wave}	0.251	-0.057	0.880	1				
s2A.5.2	D_{total}	0.252	-0.042	0.888	0.933	1			
s.3.1.2	$\Delta\sigma_{1/3}$ [MPa]	0.220	-0.092	0.821	0.835	0.828	1		
s.3.1.2	D_{wave}	0.262	-0.077	0.750	0.821	0.795	0.813	1	
s.3.1.2	D_{total}	0.262	-0.087	0.759	0.840	0.822	0.830	0.939	1

Table 9-7: p-values for results in Table 9-6

				s2A.5.2			s.3.1.2		
		N_{slam}	v_{ave} [kn]	$\Delta\sigma_{1/3}$ [MPa]	D_{wave}	D_{total}	$\Delta\sigma_{1/3}$ [MPa]	D_{wave}	D_{total}
	N_{slam}	1							
	v_{ave} [kn]	0.519	1						
s2A.5.2	$\Delta\sigma_{1/3}$ [MPa]	$<10^{-3}$	0.089	1					
	D_{wave}	0.001	0.494	$<10^{-3}$	1				
	D_{total}	$<10^{-3}$	0.432	$<10^{-3}$	$<10^{-3}$	1			
s.3.1.2	$\Delta\sigma_{1/3}$ [MPa]	$<10^{-3}$	0.006	$<10^{-3}$	$<10^{-3}$	$<10^{-3}$	1		
	D_{wave}	0.007	0.351	$<10^{-3}$	$<10^{-3}$	$<10^{-3}$	$<10^{-3}$	1	
	D_{total}	0.006	0.331	$<10^{-3}$	$<10^{-3}$	$<10^{-3}$	$<10^{-3}$	$<10^{-3}$	1

Most of the p-values given in Table 9-7 are less than 0.05, indicating that the associated correlations are significant. The p-values between v_{ave} and D_{wave}, and D_{total}, at both s3.1.2 and s2A.5.2, are greater than 0.33. Thus, relative to other correlations, there is a greater probability that these correlation coefficients occur by chance rather than due to a causal relationship.

The results shown in Table 9-6 and Figure 9-4 indicate that, unsurprisingly, the values of τ between D_{wave} and D_{total} at the two strain gauge locations are the strongest. D_{total} as a function of D_{wave} can be modelled by Equation 25. Using the non-linear least squares approach in MATLAB [88] the coefficients c_1 and c_2, with confidence intervals, are found and are presented in Table 9-8.

$$D_{total} = c_1 \times D_{wave} + c_2 \qquad \textbf{Equation 25}$$

Table 9-8: Coefficients with confidence intervals for Equation 25

Strain Gauge	c_1	c_2	R^2
s2A.5.2	2.05 (2.04, 2.06)	$1.81\text{x}10^{-7}$ ($-1.54\text{x}10^{-7}$, $5.16\text{x}10^{-7}$)	0.997
s3.1.2	2.09 (2.08, 2.10)	$-4.55\text{x}10^{-7}$ ($-8.26\text{x}10^{-7}$, $-8.39\text{x}10^{-8}$)	0.998

The correlations between D_{total} at s3.1.2 and s2A.5.2, and $\Delta\sigma_{1/3}$ at s3.1.2 and s2A.5.2, are also strong (τ values of 0.822 and 0.821, respectively). The relationship between the latter two elements can be modelled by the following linear function (with R^2 of 0.95):

$$\Delta\sigma_{1/3} \text{ at s2A.5.2} = 1.7 \times \left(\Delta\sigma_{1/3} \text{ at s3.1.2}\right) + 1.6 \qquad \textbf{Equation 26}$$

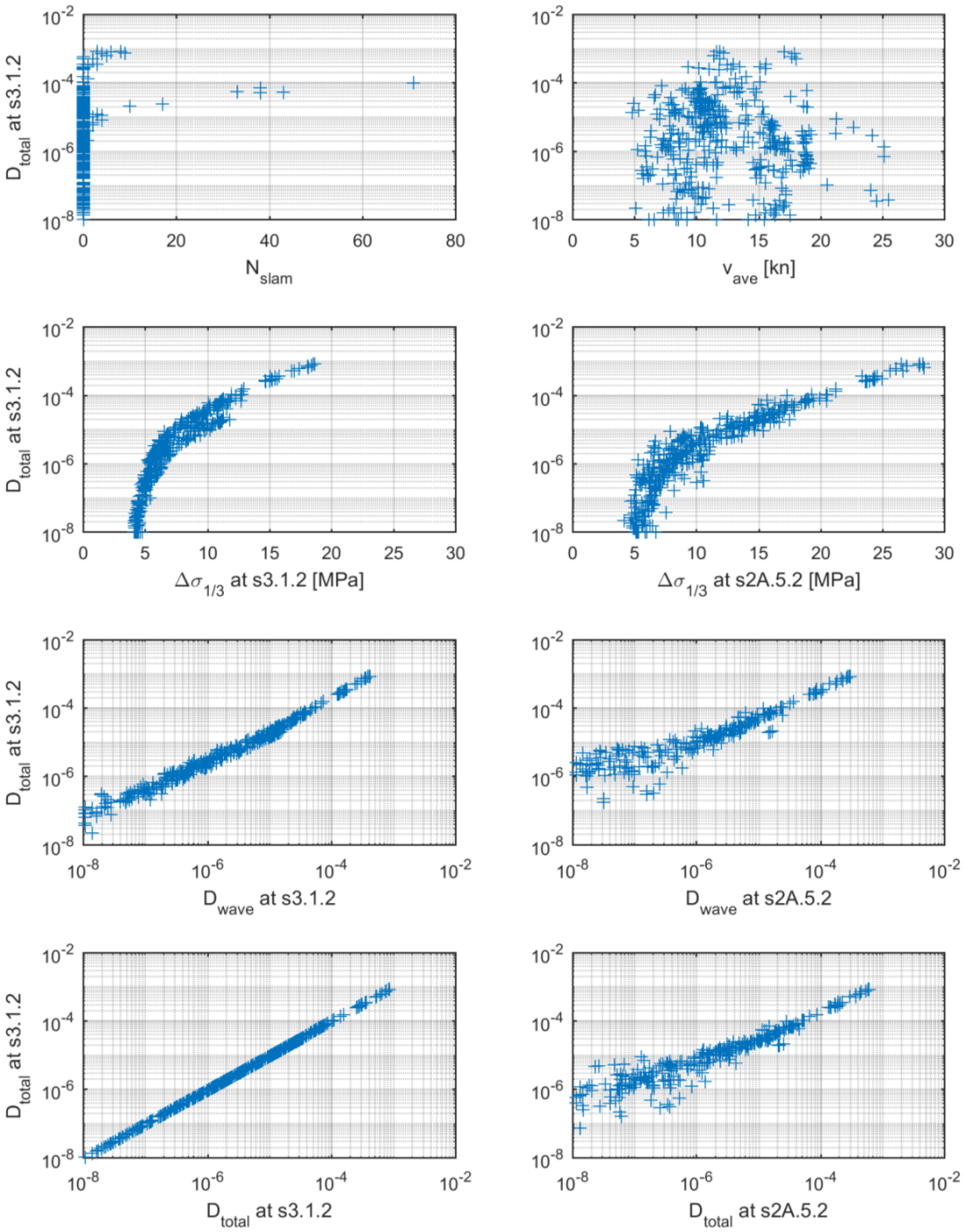

Figure 9-4: D_{total} at s3.1.2 versus N_{slam}, v_{ave}, $\Delta\sigma_{1/3}$ at s2A5.2, $\Delta\sigma_{1/3}$ at s3.1.2, D_{total} at s2A.5.2, and D_{total} at s3.1.2 over 522 hours in which *Maryborough* was at sea

The correlation between v_{ave} and the other variables is relatively weak, and negative. Although slamming occurred during a small percentage of the time at sea, N_{slam} is of greater significance to D_{total} than v_{ave} at the two structural locations considered. Prima facie, these observations are counter-intuitive as it would be expected that the stresses and in turn the fatigue damage increase with speed. As discussed in Section 7.5.2, based on SFA using linear

hydrodynamic analysis, the correlation between vessel speed and fatigue damage is positive. However, it is proposed that voluntary speed reduction[xix] and/or involuntary speed reduction[xx], due to the vessel encountering relatively high sea states, influences the fatigue damage incurred. Involuntary and voluntary speed reduction can depend on the significant wave height and the relative heading between the ship and waves [221, 222]. The ship master may also be following a speed-wave height limiting curve[xxi]. These factors are inherently captured in the measured data, but not in the SFA. The results of the sensitivity analysis based on SFA showed that the fatigue damage is most sensitive to increasing significant wave height when applying a uniform distribution to all parameters (refer to Table 7-6 and Table 7-7). Yet, when distributions representative of operational conditions are considered, the significance of $H_{1/3}$ is smaller (refer to Table 7-8 and Table 7-9). Furthermore, there is negligible correlation between speed and the significant wave height as inferred from Table 7-6 through Table 7-9. As such, it is suggested that use of long-term distributions of $H_{1/3} - T_z$ and v, which are assumed in numerical fatigue analysis, may mask the interdependencies between the variables that affect the probability of the vessel experiencing slamming.

It may be possible to combine the slamming contribution to the fatigue damage with that estimated via SFA by applying Equation 25 to the latter. This may enable the slamming contribution to be treated as a variable in an expanded sensitivity analysis (to that presented in Sections 4.6 and 7.5).

9.3.2 Multi-Factorial Numerical Experiment Based on SFA Results

A multi-factorial numerical experiment is performed based on the results of SFA of the ACPB. Three each of wave scatter diagram, speed distribution, heading distribution, and wave energy spectra are considered in the experiment, as listed in Table 9-9. Each element of the experiment calculates the accumulated fatigue damage over one year at sea.

[xix] Voluntary speed reduction occurs when the ship operator reduces the speed of the ship due to severe slamming or large accelerations.

[xx] Involuntary speed reduction is due to the added resistance of the ship, and changes to the propeller efficiency, due to waves and wind.

[xxi] From DNV HSLC rules [44, Pt.3 Ch.1 Sec.2, p. 13]: 'the craft may, from a structural point of view, operate within the boundaries of the specified operational envelope "Speed vs. Wave Height Curve". The heading of the craft has to be carefully adjusted to the wave pattern, and speed reduced, to prevent excessive loads on the hull. It is understood that a Speed vs. Wave Height Curve is stated in the Appendix to Classification Certification for the ACPB, but this information is not available to the public.

Table 9-9: Fatigue damage model input variables

Variable	Distribution		
Wave scatter $H_{1/3}$ [m] – T_z [s]	Northern Australian Waters (NAW)	Southern Ocean (SO)	South East Indian Ocean (SEIO)
v [kn]	GLE in Figure 4-3	MAR 'subset' - over 522 hours - Figure 9-3	MAR 'full' - over 9200 hours - in Figure 9-3
χ [deg]	Uniform	Non-uniform1 shown in Figure 9-5	Non-uniform2 shown in Figure 9-5
Wave energy spectrum	Bretschneider [167]	JONSWAP [223]	Pierson-Moskowitz (P-M) [224]

MAR = *Maryborough*
GLE = *Glenelg*

The heading distributions shown in Figure 9-5 are uniform, 'non-uniform1', and 'non-uniform2'. A uniform distribution is considered because it is typically assumed in fatigue strength assessment [225]. Usually, course changes in heavy weather are made to avoid the ship capsizing or excessive ship rolling. Thus, the probability of head and/or following seas is much higher than beam seas in heavy weather than in smaller sea states [155], which is reflected in the non-uniform1 distribution. The non-uniform2 distribution is formed on the assumption that *Maryborough* operated in bow quartering to heads seas during the periods in which she experienced slamming (refer to previous section). By analysing different heading distributions, the effect of changing course on the fatigue damage can also be investigated.

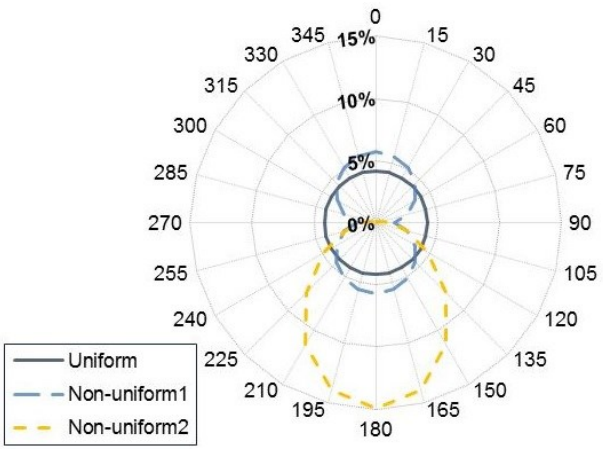

Figure 9-5: Uniform, non-uniform1, and non-uniform2 heading distributions

Figure 9-6 and Figure 9-7 display boxplots of fatigue damage versus wave scatter diagram and wave energy spectrum, respectively. Also presented are boxplots of fatigue damage versus speed distribution and heading distribution in Figure 9-8 and Figure 9-9. On

each box, the central line indicates the median, and the bottom and top edges of the box indicate the 25th and 75th percentiles, respectively. The whiskers extend to the most extreme data points excluding outliers, which are greater than 1.5 times the interquartile range (IQR) away from the top or bottom edge of the box. Outliers are denoted by the '+' symbol.

The pertinent observations from Figure 9-6 through Figure 9-9 are as follows:

- Operation in the Southern Ocean with the Pierson-Moskowitz spectrum, MAR 'full' speed profile, and non-uniform2 heading distribution leads to the highest fatigue damage at both strain gauge locations.
- Of the variables considered in the experiment, the largest spread in the medians of D is produced by the wave energy spectra. In comparison, the smallest spread in the medians of D is seen across the speed distributions.
- The maximum difference in the medians of D for the three speed distributions considered is approximately 9%.
- The maximum difference in the medians of D for the three heading distributions is approximately 38%.
- There are potential outliers in some of the groupings of the data (based on 1.5 x IQR). For instance, there are no outliers in the data group for the Pierson-Moskowitz wave spectrum (refer to Figure 9-7), but the speed distribution data groups contain at least one potential outlier (refer to Figure 9-8). These potential outliers can be explained by the strong influence of operation in the Southern Ocean and/or the Pierson-Moskowitz wave spectrum on the damage incurred. Figure 9-10 displays a comparison between histograms of D when grouped by the MAR 'full' speed profile and the Pierson-Moskowitz wave spectrum. There is one count in the 0.2 - 0.25 bin that is present in both data groupings. This count is a potential outlier in the MAR 'full' speed profile grouping but not in the Pierson-Moskowitz wave spectrum grouping.

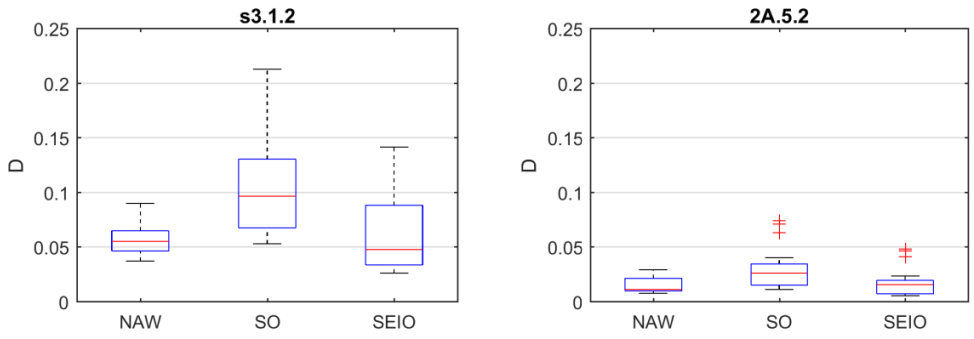

Figure 9-6: Boxplot of fatigue damage versus wave scatter at s3.1.2 and s2.5.2

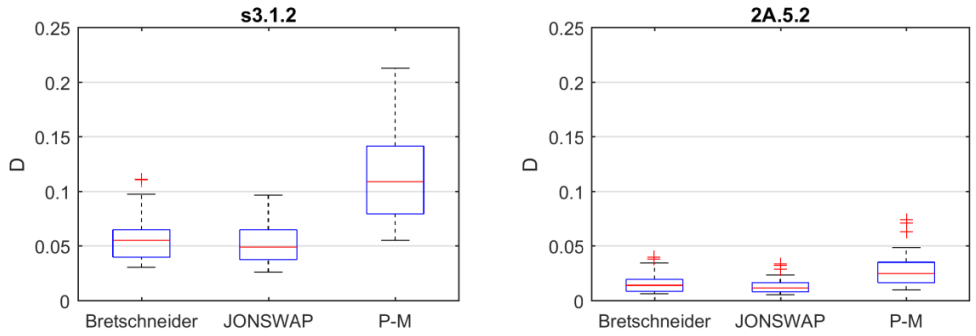

Figure 9-7: Boxplot of fatigue damage versus wave energy spectrum at s3.1.2 and s2.5.2

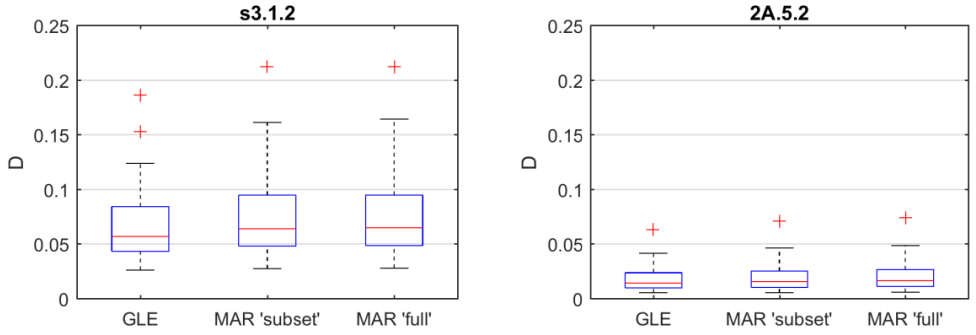

Figure 9-8: Boxplot of fatigue damage versus speed distribution at s3.1.2 and s2.5.2

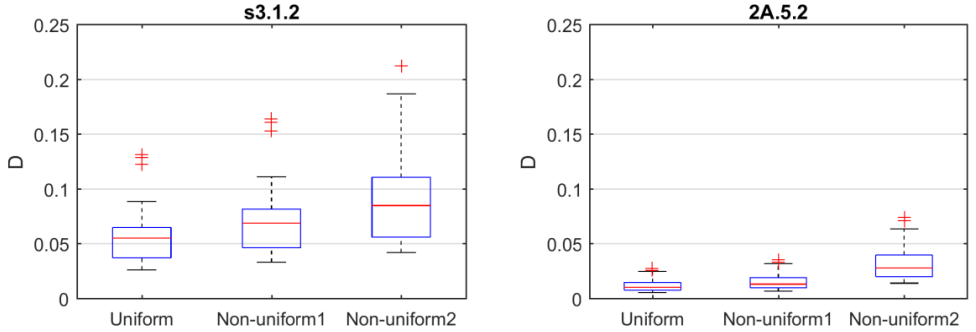

Figure 9-9: Boxplot of fatigue damage versus heading distribution at s3.1.2 and s2.5.2

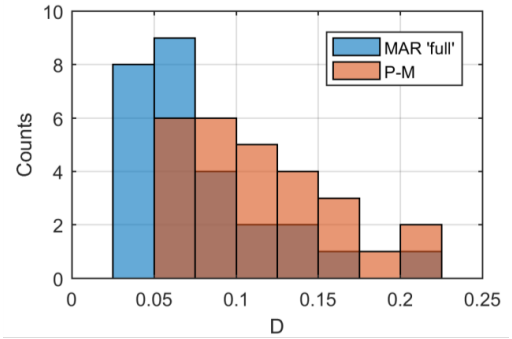

Figure 9-10: Comparison between histograms of D for *Maryborough* 'full' speed profile and Pierson-Moskowitz wave spectrum

The confidence interval (CI) about the mean (μ) of D can be calculated using Equation 27, where t* is an appropriate t-score from the t-distribution[xxii]:

$$\mu_D \pm t^* \frac{SD(D)}{\sqrt{N\_samples}} \qquad \textbf{Equation 27}$$

Equation 27 is used to calculate the lower CI at 90%, mean, and upper CI of D at s3.1.2 and s2A.5.2, ordered by the mean, are shown in Figure 9-11 and Figure 9-12, respectively. Based on SFA and the design of the multi-factorial experiment, with 90% confidence, the Pierson-Moskowitz wave spectrum is associated with the largest accumulated fatigue damage at s3.1.2 though the greatest uncertainty is connected to the non-uniform2 heading distribution. In comparison, at s2A.5.2 the non-uniform2 heading distribution is associated with the largest value of D, though followed by the Pierson-Moskowitz spectrum. The largest uncertainty at this location is also related to the Pierson-Moskowitz spectrum.

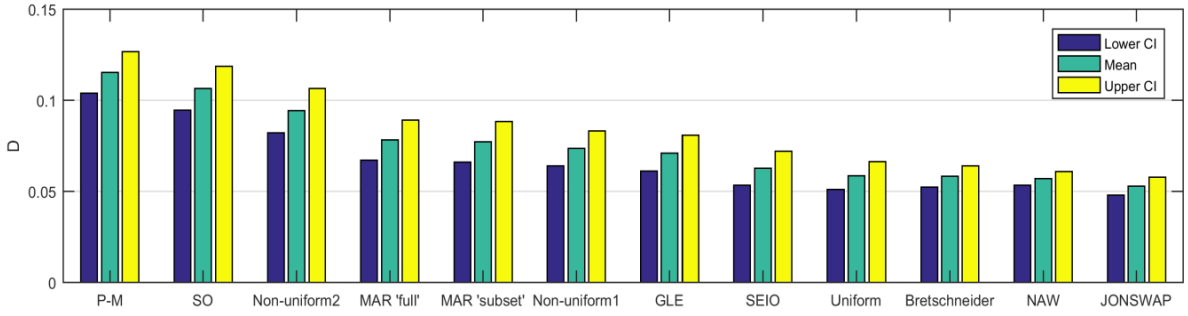

Figure 9-11: Lower CI, mean, and upper CI (90%) of D for wave scatter, wave spectrum, and heading-speed distributions for s3.1.2

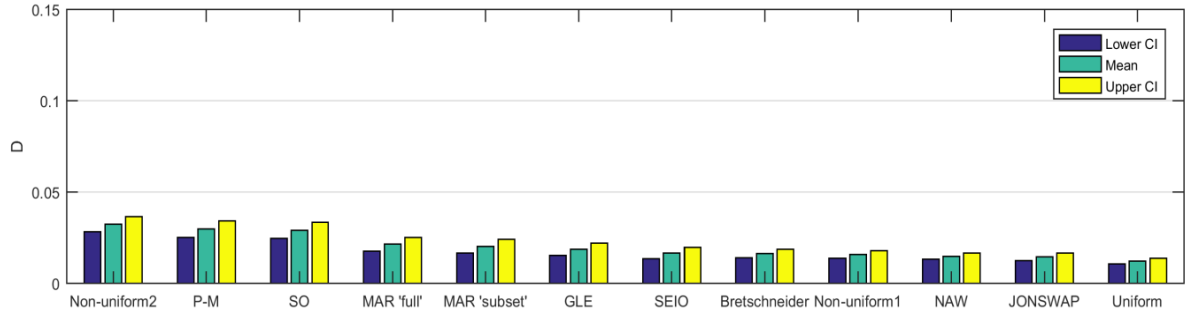

Figure 9-12: Lower CI, mean, and upper CI (90%) of D for wave scatter, wave spectrum, and heading-speed distributions for s2A.5.2

[xxii] The t distribution, rather than the normal distribution, is used because the number of samples per category is less than 30.

9.3.3 Sensitivity Analysis with Inclusion of Slam Correction

A limitation of the multi-factorial experiment is that the structural responses to slamming loads are not included in the fatigue assessment. As discussed in Section 9.3.1, it may be possible to apply a correction factor to the results of the SFA via Equation 25 to enable a multivariate sensitivity of fatigue damage that includes slamming as a variable.

SFA involves discretisation of a vessel's lifetime exposure at sea into 'cells', whereby each cell represents a particular combination of $H_{1/3}$, χ, and v. For the sensitivity study, the fatigue damage per cell (total of 3120 cells/samples) is calculated for conditions that are believed to best match the HMS data analysed in the previous section at s3.1.2, as follows:

- Northern Australian Waters.
- MAR 'subset' speed distribution.
- Non-uniform1 heading distribution.
- Bretschneider wave energy spectrum (prescribed for seakeeping analysis in [226]).

Application of the slam correction is treated as binary data (0 or 1). This is deemed appropriate as the small confidence intervals and high value of R^2, given in Table 9-8, indicate that the coefficients in Equation 25 are accurate *for the given data*.

The correction is applied to a certain number of cells, which have been ranked in descending order by D, such that the ratio between the 'uncorrected' D to the 'corrected' D summed over the given cells is 0.45 (as found in Table 9-5). The result of this process is illustrated in Figure 9-13, which shows a 3D scatter plot of v, χ, and $H_{1/3}$ with colourbar scaled by D. The unfilled and filled circles denote cells without and with the slam correction, respectively. Approximately 14% of the cells are corrected. This corresponds to almost 7% of the operational time, which is comparable to that observed from the *Maryborough* HMS data (refer to Section 9.3.1).

Using Equation 24, the τ and p-values between pairings of slam correction, v, χ, $H_{1/3}$, T_z and D at s3.1.2 are calculated and are given in Table 9-10 and Table 9-11, respectively. The results indicate that the slam correction, followed by $H_{1/3}$, has the largest relative influence on the fatigue damage sustained. Most of the other correlations are very mild.

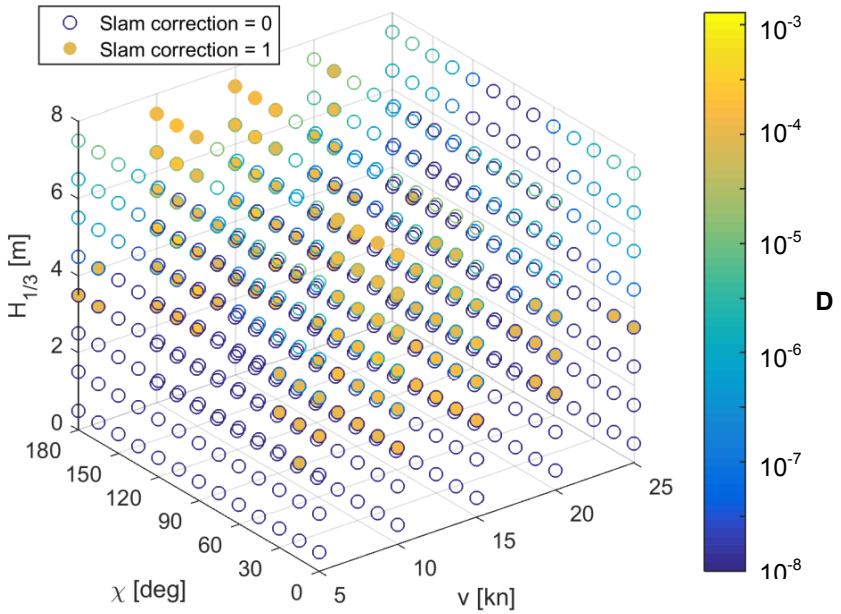

Figure 9-13: Scatter plot of v, χ, and $H_{1/3}$ with colourbar scaled by D. Unfilled circles denote samples without slam correction, and filled circles denote samples with slam correction

Table 9-10: τ correlation coefficients between slam correction, v, χ, $H_{1/3}$, T_z and D at s3.1.2

	Slam correction	v [kn]	χ [deg]	$H_{1/3}$ [m]	T_z [s]	D
Slam correction	1					
v [kn]	-0.089	1				
χ [deg]	0.033	0	1			
$H_{1/3}$ [m]	0.149	0	0	1		
T_z [s]	-0.139	0	0	0.217	1	
D	0.447	-0.053	-0.048	0.384	-0.174	1

Table 9-11: p-values of results in Table 9-10

	Slam correction	v [kn]	χ [deg]	$H_{1/3}$ [m]	T_z [s]	D
Slam correction	1					
v [kn]	$<10^{-3}$	1				
χ [deg]	0.030	1	1			
$H_{1/3}$ [m]	$<10^{-3}$	1	1	1		
T_z [s]	$<10^{-3}$	1	1	$<10^{-3}$	1	
D	$<10^{-3}$	$<10^{-3}$	$<10^{-3}$	$<10^{-3}$	$<10^{-3}$	1

9.3.4 Discussion

The results from the quantitative analysis can be used to provide advice to stakeholders regarding fatigue life management of naval HSLC.

The fatigue damage sustained by the ACPB, and associated uncertainty in the answer, would increase if the ACPB operational environment was to include the Southern Ocean or the North East Indian Ocean. Although this circumstance is unlikely for the ACPB, it is an important consideration for future combatants. This is because there is a need for navies to have operational flexibility to deal with continuous mission changes [1-3]. In addition, the New Zealand Defence Force and LR are undertaking a project to better define sea states encountered in the Southern Ocean with the potential for amendments to LR Rules and procedures to better reflect the encountered environment. There is currently a lack of wave data for the Southern Ocean, resulting in Classification Society structural requirements being based on sea conditions in the northern hemisphere [227].

There is greater uncertainty associated in a fatigue life prediction when the Pierson-Moskowitz wave spectrum is assumed rather than the Bretschneider or JONSWAP spectra. This can inform requirements setting (for example, DEF(AUST)5000 [226]).

In the absence of a long-term hull monitoring campaign using an extensive HMS, it is judicious to implement some type of slam monitor. For example, Colwell and Stredulinsky [142] discussed the development of a real-time indicator of slam severity on the KINGSTON Class Maritime Coastal Defence Vessel. From sea trial measurements, a strong correlation between the centreline vertical bow acceleration and the probability of slamming occurrence was found. Similarly, the slamming detection method described in Chapter 5 could be utilised in the construction of a slam monitor.

For the two strain gauge locations considered, the hourly $\Delta\sigma_{1/3}$ and stress spectra derived at one location could be easily transferred to the other by applying a constant. Thus, it may be sufficient to instrument only one of the locations.

The results given in Figure 9-8 and in the correlation analyses demonstrate that different speed distributions, derived from GPS data from two ACPBs, do not result in statistically significant differences in the estimated fatigue damage. The implication of this result is that, particularly in a resource-constrained environment, it may be sufficient to instrument only one vessel in the fleet. This finding is consistent with that of Thompson [207][xxiii]. At the same time, instrumenting a second vessel in the fleet with a slam monitor

[xxiii] Thompson [207] assessed the variation of fatigue damage accumulation within a class of naval ships that operate in different geographical locations (two coastal fleets). The fatigue damage variation within each coastal fleet was found to be minor, but the difference between the two fleets was up to 50%. The author offered that the relative damage of ships within each coastal fleet may depend more on the total time at sea than the mix of geographic locations that had been visited.

and/or wave environment measuring device would augment the ability of stakeholders to manage the structural integrity of the fleet.

The slam correction technique employed in Section 9.3.3 is simplistic, though is consistent with techniques used in industry and reported in academia. For example, for the fatigue strength assessment of container ships, DNV GL [225] provide an empirical formula to calculate a 'vibration factor' to be applied to the wave-induced stress due to vertical bending. The vibration factor represents a correction of the wave-induced stress due to the additional damage from whipping for the intended operational area.

9.3.4.1 With More Data… Further Analysis of Slamming

Based on the analysis of available HMS data using the methods presented in Chapter 5, most of the slamming sustained by *Maryborough* during the hull monitoring campaign occurred during three different periods. These three periods are referred to as 'trip 1', 'trip 2', and 'trip 3'. Each trip is characterised by unique speed and heading distributions as well as encountered seaway. Figure 9-14 shows the number of slams versus D_{all} at s3.1.2 per hour, grouped by storm. Similarly, Figure 9-15 illustrates the number of slams versus D_{wave} at s3.1.2.

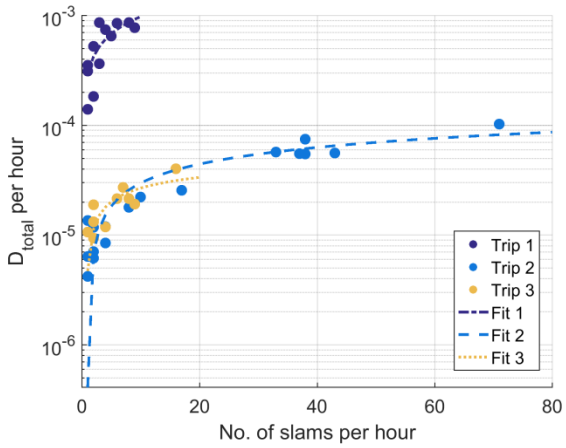

Figure 9-14: Number of slam events versus D_{total} at s3.1.2, grouped by trip, with two-term power curves of best fit

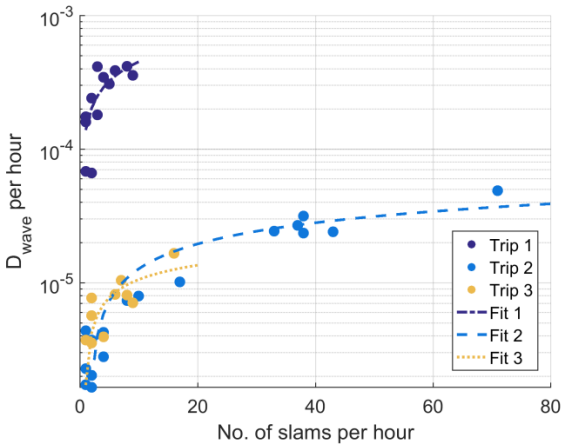

Figure 9-15: Number of slam events versus D_{wave} at s3.1.2, grouped by trip, with two-term power curves of best fit

The results shown in Figure 9-14 and Figure 9-15 demonstrate that fatigue damage is directly proportional to the number of slams experienced. This relationship can also be modelled by a power curve:

$$FD = \alpha\left(N_{slams}\right)^{\phi} + \eta \qquad \textbf{Equation 28}$$

The coefficients α, ϕ, and η in Equation 28, and values of R^2 for each curve of best fit, are given in Table 9-12. The difference between the D_{all} and D_{wave} power curves represents the contribution of slamming-induced whipping stresses to the fatigue damage.

An attempt was made to obtain wave height data from satellite measurements of the ACPB area of operations but, unfortunately, the vessel was not in the vicinity of the satellite sweep during these periods. However, there is value in trying to correlate or model the relationship between slam number with speed, significant wave height, and other variables. This would enable assessment of the effect of changes to these variables on the contribution of slamming to the fatigue damage, which is not possible using SFA based on the results of linear hydrodynamic simulation (as discussed in Chapter 7). To obtain the required environmental data, sea trials in higher sea states, a ship-board wave-height measuring device, or development and implementation of the 'ship-as-a-wave-buoy' concept is needed.

Table 9-12: Coefficients and R^2 values for best fits of N_{slam} versus D_{total} and D_{wave}

Trip	Duration	Date	D	α	ϕ	η	R^2
1	~29 hrs	June 2015	D_{total}	28.8×10^{-5}	0.527	1.06×10^{-5}	0.65
			D_{wave}	18.3×10^{-5}	0.432	-4.39×10^{-5}	0.62
2	~20 hrs	May 2016	D_{total}	2.37×10^{-5}	0.351	-2.33×10^{-5}	0.90
			D_{wave}	1.20×10^{-5}	0.336	-1.33×10^{-5}	0.87
3	~15 hrs	June 2016	D_{total}	111×10^{-5}	0.00858	-111×10^{-5}	0.64
			D_{wave}	4.96×10^{-5}	0.0716	-4.79×10^{-5}	0.61

9.4 Material Factors

In addition to operational parameters the choice and accuracy of S-N curves affects the fatigue life prediction. In Chapter 4, a refinement of the nominal stress approach for joints typical of aluminium welded ship details was proposed, though it was acknowledged that it is reliant on the appropriate selection of the E9 detail. In Chapter 7 the relatively low correlation between the fatigue limit, as the characteristic value of the S-N curve, to the fatigue damage relative to operational parameters was demonstrated. However, is there a need to generate S-N curve for the welded joints found on an aluminium naval ship to reduce the uncertainty in the fatigue life answer?

In military aviation, the analysis of an aircraft's fatigue life is normally accompanied by coupon, component and/or full-scale testing [228]. This level of material testing for a new ship is uncommon. A possible explanation is that, in comparison to airworthiness requirements,

seaworthiness requirements are less rigid and a greater level of risk is accepted. Also, there is less financial incentive for operators to extract as much life out of their ships as possible.

It has been observed that some structural details found on aluminium ships cannot be found in design codes, which may in part be due to the lack of information on the fatigue strength of typical structural details [48, 55]. In reference to simulation and accuracy of input data, Kramer *et al.* [107, pp. 25-26] state that 'costs … need to be justified by the life cycle maintenance and operational savings that will be realised through a more accurate fatigue analysis'. However, cost-benefits analyses for conducting component fatigue testing relevant to marine structures, particularly those constructed from aluminium, are sparse in the literature. For instance, Ravi Chandran *et al.* [105] assert that a large number of suitably sized specimens should be tested to adequately cover the breadth of S–N curve shapes, though do not specify the number and size.

If using the safe life philosophy and representative S-N curves in a design standard cannot be found, then component testing is required. This includes different welding processes, as the bulk of the test data refer to arc welded joints [26].

As shown in Table 4-4 in Chapter 4, there was some inconsistency between the detail of interest ID-1 (a circumferential joint at the top of a pillar) and the selected S-N curve. This issue could be remediated by conducting component fatigue testing of this type of welded joint to obtain truly representative S-N curve data. This would be particularly advantageous if through-life structural monitoring was not part of the LOT management of the ship, as it would be a means to reduce the uncertainty of the fatigue life answer when it cannot be achieved through the collection of operational information (as proposed in Chapter 8). Nonetheless, even if a structural detail is not found to be critical during a stress analysis or fatigue screening, but the related confidence limits on the answer are large, it may be sensible to include the detail in a targeted hull inspection regime.

9.5 Conclusion

Structural LOT management of a naval ship is a balance between costs and performance objectives. In this chapter, the provision of evidence-based advice regarding the fatigue life of naval HSLC for decision-makers has been explored by integrating the knowledge gained throughout the PhD research in qualitative and quantitative analyses. The intention of this chapter is to offer a decision-making aid regarding the most appropriate fatigue analysis option, to be contextualised by stakeholders.

A qualitative analysis of different fatigue analysis options, using data review, codification, and comparative analysis, was useful as a structured approach to comparing the options with respect to the identified key attributes. The comparative analysis indicated that the assumption that a ship's design service life will be met if it is designed to a set of classification society rules does not achieve most of the key attributes of a fatigue analysis but is cheap to implement. In contrast, the option that represents the through-life hybrid fatigue assessment framework presented in Chapter 8 covers the key attributes to a high level but requires more resources.

Quantitative analysis based on the HMS data and SFA demonstrated that the fatigue life of the analysed structural details varies significantly with the variation of the input data. In addition, the importance of a particular variable changes with the usage of the vessel and with structural location. However, for naval HSLC, management of the structural fatigue life is considerably aided by measuring the ship speed and the encountered wave environment as coupled observations, and by implementing a slam monitor.

A summary of some of the variables in structural fatigue analysis and ways to obtain information to reduce the related uncertainty is provided in Table 9-13.

Table 9-13: Summary of variables in fatigue analysis, and ways to obtain information to reduce related uncertainty

Variable	Ways to obtain larger volume and/or accurate information to reduce confidence limits of answer	Effort required*	Reference in thesis
Wave scatter ($H_{1/3}$ [m] - T_z [s])	Implement 'ship-as-a-wave-buoy' system or install wave-height measurement instrument	Low-medium	Sections 7.5.2 and 9.3.2
v [kn]	Obtain speed data from onboard navigation system or install GPS as part of a HMS	Low	Sections 7.5.2, 9.3.1, and 9.3.2
χ [deg]	Implement wave-height measurement instrument, or capture in ship's log	Low-medium	Sections 7.5.2 and 9.3.2
Wave spectrum	Long-term campaign to better define sea states in different ocean environments	Very high	Section 9.3.2
S-N curve	Do full-scale fatigue testing of welded details	Very high	Sections 4.6 and 7.5.2
N_{slam}	Slam monitor	High	Chapter 5 and section 9.3

*Effort scale: Low, Medium, High, Very high

9.6 Acknowledgements

The assistance provided by Mr Mario Selvestrel, Dr Peter Dennis, and Dr Stuart Cannon is greatly appreciated.

Chapter 10. Main Conclusions and Further Work

Navies around the world are carrying out fleet modernisation. In Australia, there is a need for the RAN to have operational flexibility to deal with evolving requirements. The significant acquisition costs of naval ships and budgetary constraints necessitate the effective management of the structural LOT of the fleet-in-being to maintain maritime capability. Furthermore, it is imperative that lessons learned from both domestic and international experience are implemented.

The structural LOT of a naval ship can be dictated by the fatigue life. As the LOT is often extended beyond the original design life, and fatigue cracking of the structure can lead to costly repairs and reduction of availability of the ship, it is critical to improve understanding of the accuracy, influence, and uncertainty related to fatigue life assessment approaches and the required input variables. This is particularly the case for naval HSLC as the applied loads can feature a high degree of non-linearity, and slamming loads and associated responses can have a significant impact on the stress magnitudes experienced in the structure.

Therefore, this thesis has presented a framework for efficient structural fatigue life assessment for high-performance naval ships. The framework helps to inform risks through-life to decision-makers, by integrating real-world data and optimised tool selection.

The thesis summary, major conclusions, value proposition, and recommendations for further work are presented below.

10.1 Summary of Work Completed

The processes carried out during the PhD candidature are summarised below:

- Identification of challenges in applying existing methods of fatigue assessment to HSLC.
- Modification of a FE model of the ACPB, built by the Candidate before the commencement of the PhD, to be suitable for detailed stress analysis and fatigue assessment.
- Planning and conducting dedicated sea trials with the ACPB HMAS *Maryborough*.

- Development of a systematic approach to analyse data acquired from the *Glenelg* and *Maryborough* HMS. This includes data retrieval, unpacking, conditioning, interrogation, health checking and calculations for structural stress analysis.
- Establishment of factors in determining sufficiency a full-scale dataset for valid fatigue analysis and conclusions.
- Verification of strain gauges and pressure sensors installed on *Maryborough*.
- Investigation into different approaches to identify slam events using strain measurement data of an in-service naval HSLC.
- Proposal of a refinement of the nominal stress approach for joints typical of aluminium welded ship details
- Investigation of the validity of stress spectra assumptions required in simplified fatigue analysis, based on data obtained from the *Glenelg* HMS.
- Part validation of Spectral Fatigue Analysis (SFA), implemented in MAESTRO, against *Maryborough* sea trials data during which linear motions and loads dominated.
- Performance of sensitivity analysis between the significant wave height, wave period, ship heading, fatigue resistance, and fatigue damage at two structural locations on ACPB.
- Proposal of a method to measure and monitor full-scale structural responses and the operational profile, combined with the maintenance history, to evaluate the fatigue life of a naval HSLC.
- Exploration of the optimum provision of evidence-based advice regarding the fatigue life of naval HSLC for decision-makers, by integrating the knowledge gained throughout the PhD research in qualitative and quantitative analyses.

10.2 Main Conclusions

As per the Introduction of the thesis (Chapter 1), three research questions were posed. The findings of the PhD lead to the following major conclusions:

1. *Which available tools can be combined to progress structural LOT assessment of naval HSLC?*

   Selection of options such as frequency-domain versus time-domain load calculations, use of measured strains versus computed stress, and detailed versus simplified load

characterisation is a balance between the maturity of the method, available resources, need for accuracy and schedule. This implies that a new balanced or hybrid approach to fatigue analysis, that leverages the benefits of different methods and sources of data, can be more universally effective. Hull monitoring data, fleet maintenance data, finite element modelling, spectral fatigue analysis, and expert judgement can be successfully combined in a through-life framework.

2. *What are suitable enhancements to fatigue life assessment methods applied to naval HSLC?*

The through-life hybrid fatigue assessment method proposed in Chapter 8 combines measured full-scale data, survey reports, and numerical tools in a practical manner. It includes enhancements to fatigue life assessment methods applied to naval HSLC, as follows:

- A refinement of the nominal stress approach for joints typical of aluminium welded ship details, plus a modified nominal stress extraction process which extends the guidance provided by Eurocode 9.
- A method to identify slam events experienced by naval HSLC, and to determine the slamming contribution to fatigue damage.
- Provision of operational guidance, as part of the management of the structural integrity of the fleet, based on sensitivity analysis of the fatigue damage to the significant wave height, wave period, ship heading, ship speed, and fatigue resistance of a detail.

3. *What is the optimum approach to provide advice regarding the structural LOT of naval HSLC for decision-makers?*

The optimum approach to provide evidence-based advice regarding the fatigue life of naval HSLC for decision-makers is one that features minimisation of uncertainty and knowledge gaps. Consideration and integration of data on the quantitative-qualitative dimension is means to build a decision-making aid regarding the most appropriate fatigue analysis option, to be contextualised by stakeholders.

The assumption that a ship's design service life will be met if it is designed to a set of classification society rules does not achieve most of the key attributes of a fatigue analysis but is cheap to implement. In contrast, the option that represents the through-life hybrid fatigue assessment framework covers the key attributes to a high level but

requires more resources.

The fatigue life of the analysed structural details varies significantly with the variation of the input data. In addition, the importance of a particular variable changes with the usage of the vessel and with structural location. However, for naval HSLC, management of the structural fatigue life is considerably aided by measuring the ship speed and the encountered wave environment as coupled observations, and by implementing a slam monitor.

10.3 Value Proposition

The beneficiaries of the findings of investigation include Government, navies, classification societies, and maintenance providers. The body of work carried out during the candidature has already been utilised in other applications and to provide evidence-based advice to the Australian Defence Organisation (ADO), as follows:

- Improved understanding of the uncertainties and interdependencies between the fatigue life and capability aspects of naval ships [153] (refer to Appendix D). This work supports the Australian Government's NSP [1].
- Improved understanding of the key consequences to the RAN's ability to manage the LOT of ships without the use of hull monitoring systems [83] (refer to Appendix E). This work supports continuous shipbuilding strategies, particularly continuous improvement between batches [214] by having accurate data on the ship's usage.
- Provision of evidence-based advice to the ADO regarding the structural integrity of the ACPBs [229].
- Provision of advice to the ADO regarding setting testable structural LOT requirements during the Risk Mitigation and Requirement Setting stage of a new ship.
- Transfer of technologies and methods to industry – advice provided to Australian industry has been used to appropriately specify and commission, and analyse the acquired data from, a HMS on another RAN ship.
- Though not directly reported in the thesis, preliminary correlation of different parameters during a slam event was performed from the *Maryborough* sea trials data. The propagation of the pressure pulse from the keel to the chine, relatively large ship motions and structural responses, and excitation of the longitudinal bending modes were revealed [77]. This information supports the development of numerical

seakeeping tools that can lead to improved fatigue life prediction tools (this is discussed further in Appendix A.1).

10.4 Further Work

The work presented in this thesis can be expanded as follows:

- The proposed implementation of the nominal stress approach described in Chapter 4 can be supported through undertaking a controlled experimental and/or simulation program.
- To provide near real-time slam event information to the operator, use of either the whipping stress magnitude or rate criteria appears to be favourable. However, for a particular vessel future users should find and verify the appropriate criterion and sensor locations. To use the proposed method for decision support, its robustness in all conditions encountered needs to be established. This would involve determining the sensitivity of both slam occurrence and severity to encounter frequency, speed, and significant wave height.
- If simplified fatigue analysis is used strategies to better describe stress spectra, such as determining the characteristic fatigue loads and probabilities in the area of operations, are needed.
- A simplified way to include the contribution of non-linear loads in SFA may be to identify the missing 'non-linear loads variable' through regression analysis between the measured strain and other parameters. Long-term strain measurements acquired from the HMS onboard *Maryborough* are available. The 'non-linear loads variable' could then be used to calibrate the results of the SFA. Such an approach may be in a similar vein to a correlation analysis between wave and whipping bending moments [155], and that used in Section 9.3.3.
- Methods to include slamming loads in spectral approaches to fatigue analysis have been proposed [175, 176]. There is merit in incorporating such a method in future analyses.
- Fatigue analysis of an in-service, complex structure is very often a balance between practical considerations including the availability of data, time and resource limitations, and the required accuracy. A trade-off study between the required accuracy and cost of through-life fatigue management is part of future research.
- To better manage uncertainties reliability-based fatigue assessment is worthy of future investigation [55, 71, 230].

- As noted in Section 1.5, corrosion, metal sensitisation, the heat affected zone, and welding-induced plate and stiffener imperfections can impact the structural integrity of a ship. A sensitivity study on the impact of these types of degradation, combined with fatigue damage, would be beneficial.
- Implementation of a methodology to calibrate the fatigue life models using data from experience-based methods and expert judgement.

Chapter 11. References

1. Department of Defence, *Naval Shipbuilding Plan*. 2017, Commonwealth of Australia: Canberra, Australia.

2. Public Works and Government Services Canada, *The 2016 National Shipbuilding Strategy Annual Report*. 2016.

3. Ministry of Defence, *National Shipbuilding Strategy: The Future of Naval Shipbuilding in the UK*. 2017: Government of the United Kingdom.

4. United States Government Accountability Office, *Navy Shipbuilding: Past Performance Provides Valuable Lessons for Future Investments*. 2018, GAO-18-238SP, United States Government: United States.

5. Dean, A.W., Reina, J.J., and Bao, H.P., *Identification of Supplementary Metrics to Sustain Fleet Readiness from a Maintenance Perspective.* Naval Engineers Journal, 2008. **120**(2): p. 81-88.

6. Temple, D. and Collette, M., *Minimizing lifetime structural costs: Optimizing for production and maintenance under service life uncertainty.* Marine Structures, 2015. **40**: p. 60-72.

7. Schank, J., Arena, M., Kamarck, K., Lee, G., Birkler, J., Murphy, R., and Lough, R., *Keeping Major Naval Ship Acquisitions on Course*. 2014: Santa Monica.

8. Rizzo, P., *Plan to Reform Support Ship Repair and Management Practices*. 2011, Canberra, Australia: Ministerial and Executive Coordination and Communication Division.

9. Department of Defence, *Interim Capability Lifecycle Manual*. 2017, Commonwealth of Australia: Canberra, Australia.

10. Blanchard, B. and Fabrycky, W., *Systems Engineering and Analysis*. 1998, Upper Saddle River, United States: Prentice-Hall.

11. Hughes, O. and Paik, J., *Ship Structural Analysis and Design*. 2010, Jersey City, USA: The Society of Naval Architects and Marine Engineers.

12. Crupi, V., Guglielmino, E., Risitano, A., and Taylor, D., *Different Methods for Fatigue Assessment of T Welded Joints Used in Ship Structures.* Journal of Ship Research, 2007. **51**(2): p. 150-159.

13. Fricke, W., Cui, W., Kierkegaard, H., Kihl, D., Koval, M., Mikkola, T., Parmentier, G., Toyosada, M., and Yoon, J.-H., *Comparative fatigue strength assessment of a structural detail in a containership using various approaches of classification societies.* Marine Structures, 2002. **15**: p. 1-13.

14. Department of Defence, *Defence Seaworthiness Management System Manual (DSwMSMAN)*. 2017, Australian Government: Canberra, Australia.

15. Groden, M. and Collette, M., *Fusing fleet in-service measurements using Bayesian networks.* Marine Structures, 2017. **54**: p. 38-49.

16. Hess, P., Aksu, S., Blake, J., Boote, D., Caridis, P., Egorov, A., Fjeldstad, A., Hoogeland, M., Murayama, H., Anderson, M.R., and Tammer, M., *Structural Longevity*, in *Proceedings of the 19th International Ship and Offshore Structures Congress*. 2015: Cascais, Portugal. p. 211-287.

17. Eccles, T.J., Ashe, G., and Albrecht, S., *The achieving service life program.* Naval Engineers Journal, 2010. **122**(3): p. 103-112.

18. Gudze, M., Flockhart, C., and Cannon, S., *Short Term Damage Assessment in Naval Ship Structures*, in *Pacific 2006 International Maritime Conference*. 2006: Sydney, Australia.

19. Kramer, R., Haugan, G., and Fredriksen, A., *US navy high speed craft - Comparison of ABS and DNV structural requirements.* Transactions - Society of Naval Architects and Marine Engineers, 2006. **113**: p. 340-366.

20. Thomas, G., Davis, M., Holloway, D., and Roberts, T., *The Effect of Slamming and Whipping on the Fatigue Life of a High-Speed Catamaran.* Australian Journal of Mechanical Engineering, 2006. **3**(2): p. 165-174.

21. Zhu, J. and Collette, M., *Lifecycle Fatigue Management for High-Speed Vessels Using Local Approaches*, in *11th International Conference on Fast Sea Transportation*. 2011: Honolulu, USA.

22. Thomas, G., Davis, M., Holloway, D., Watson, N., and Roberts, T., *Slamming Response of a Large High-Speed Wave-Piercer Catamaran.* Marine Technology, 2003. **40**(2): p. 126-140.

23. Tuitman, J. and Hoogendoorn, D., *Fatigue in High-Speed Aluminium Craft: A Design Methodology for Predicting the Fatigue Life*, in *12th International Conference on Fast Sea Transportation*. 2013: Amsterdam, the Netherlands.

24. Du, J., Li, H., Zhang, M., and Wang, S., *A novel hybrid frequency-time domain method for the fatigue damage assessment of offshore structures.* Ocean Engineering, 2015. **98**: p. 57-65.

25. Hodapp, D., Collette, M., and Troesch, A., *Nonlinear Fatigue Crack Growth Predictions for Simple Specimens Subject to Time-Dependant Ship Structural Loading Sequences* Trans Soc Naval Archit Marine Eng, 2013. **121**.

26. Maddox, S.J., *Review of fatigue assessment procedures for welded aluminium structures.* International Journal of Fatigue, 2003. **25**(12): p. 1359-1378.

27. Mart, P.L., Pescott, E., Russo, S., and Pedrina, L.M., *Marine corrosion of 5XXX aluminium alloys*, in *International Maritime Conference 2010, Pacific 2010*. 2010: Sydney, Australia. p. 267-277.

28. Melchers, R.E. and Jeffrey, R.J., *Probabilistic models for steel corrosion loss and pitting of marine infrastructure.* Reliability Engineering and System Safety, 2008. **93**(3): p. 423-432.

29. Paik, J. and Melchers, R., eds. *Condition assessment of aged structures*. 2008, Woodhead Publishing Limited: Cambridge.

30. Benedictus-deVries, S., *Fatigue Crack Initiation Behavior of Welded AA5083 in a Seawater Environment.* Journal of Engineering Materials and Technology, 2004. **126**(2): p. 199-203.

31. Sensharma, P., Collette, M., and Harrington, J., *Effect of Welded Properties on Aluminium Structures*. 2011, Ship Structures Committee: Washington, United States.

32. Paik, J., Thayamballi, A., Ryu, J., Jang, J., Seo, J., Park, S., Seo, S., Renaud, C., Cojeen, H., and Kim, N., *The Statistics of Weld Induced Initial Imperfections in Aluminium Stiffened Plate Structures for Marine Applications.* Transactions of the Royal Institution of Naval Architects Part A: International Journal of Maritime Engineering, 2006. **148**(4): p. 19-62.

33. Magoga, T. and Flockhart, C., *Effect of Weld-induced Imperfections on the Ultimate Strength of an Aluminium Patrol Boat determined by the ISFEM Rapid Assessment Method.* Ships and Offshore Structures, 2013.

34. Benson, S., Downes, J., and Dow, R., *Ultimate Strength Characteristics of Aluminium Plates for High-speed Vessels.* Ships and Offshore Structures, 2011. **6**(1-2): p. 67-80.

35. Benson, S., Downes, J., and Dow, R., *Compartment Level Progressive Collapse Analysis of Lightweight Ship Structures.* Marine Structures, 2013. **31**: p. 44-62.

36. Fricke, W. and Paetzold, H., *Full-scale fatigue tests of ship structures to validate the S-N approaches for fatigue strength assessment.* Marine Structures, 2010. **23**(1): p. 115-130.

37. Okawa, T., Sumi, Y., and Mohri, M., *Simulation-based fatigue crack management of ship structural details applied to longitudinal and transverse connections.* Marine Structures, 2006. **19**(4): p. 217-240.

38. American Bureau of Shipping, *Guidance Notes Structural Direct Analysis for High-Speed Craft*. 2011, American Bureau of Shipping: Houston, USA.

39. Mansour, A. and Liu, D., *Strength of Ships and Ocean Structures*. 2008, The Society of Naval Architects and Marine Engineers: Jersey City, USA.

40. Austal Ships. *Royal Australian Navy 56m*. 2015 25/1/2015]; Available from: http://www.austal.com/en/products-and-services/defence-products/patrol-boats/royal-australian-navy-56m.aspx?source=category.

41. Nielsen, U., Jensen, J., Pedersen, P., and Ito, Y., *Onboard monitoring of fatigue damage rates in the hull girder.* Marine Structures, 2011. **24**: p. 182-206.

42. Sheinberg, R., Cleary, C., Stambaugh, K., and Storhaug, G., *Investigation of Wave Impact and Whipping Response on the Fatigue Life and Ultimate Strength of a Semi-Displacement Patrol Boat*, in *11th International Conference on Fast Sea Transportation FAST 2011*. 2011: Honolulu, Hawaii, USA.

43. Bureau Veritas, *Rules for the Classification of High Speed Craft*. 2002, Bureau Veritas,: Courbevoie, France.

44. Det Norske Veritas, *Rules for Classification of High Speed, Light Craft and Naval Surface Craft*. 2011: Høvik, Norway.

45. Lloyd's Register, *Rules and Regulations for the Classification of Special Service Craft*. 2013, Lloyd's Register: London, UK.

46. ClassNK, *Rules for High Speed Craft*. 2013, ClassNK: Tokyo, Japan.

47. Germanischer Lloyd, *Special Craft, High Speed Craft*, in *Rules for Classification and Construction, Ship Technology*. 2013, Germanischer Lloyd: Hamburg, Germany.

48. Sielski, R., *Research Needs in Aluminum Structures.* Ships and Offshore Structures, 2008. **3**(1): p. 57-65.

49. Paris, P., Gomez, M., and Anderson, W., *A Rational Analytic Theory of Fatigue.* Trend in Engineering, 1961. **13**: p. 281-285.

50. Lotsberg, I., Sigurdsson, G., and Terje Wold, P., *Probabilistic Inspection Planning of the Åsgard A FPSO Hull Structure With Respect to Fatigue.* Journal of Offshore Mechanics and Arctic Engineering-transactions of The Asme - J OFFSHORE MECH ARCTIC ENG, 2000. **122**.

51. Kim, S. and Frangopol, D.M., *Optimum inspection planning for minimizing fatigue damage detection delay of ship hull structures.* International Journal of Fatigue, 2011. **33**(3): p. 448-459.

52. Kim, P.Y., Park, J., Choi, B.K., and Kim, O.H. *Fatigue Life Calculation for a Ship Subjected to Hull Girder Vibration*. in *Proceedings of the International Offshore and Polar Engineering Conference*. 2002.

53. Heggelund, S.E., Storhaug, G., and Choi, B.K., *Full scale measurements of fatigue and extreme loading including whipping on an 8600TEU post panamax container vessel in the asia to Europe trade*, in *30th International Conference on Ocean, Offshore and Arctic Engineering*. 2011: Rotterdam, The Netherlands. p. 273-282.

54. Barhoumi, M. and Storhaug, G., *Assessment of Whipping and Springing on a Large Container Vessel*, in *12th International Symposium on Practical Design of Ships and Other Floating Structures*. 2013: Changwon City, South Korea.

55. Soliman, M., Barone, G., and Frangopol, D.M., *Fatigue reliability and service life prediction of aluminum naval ship details based on monitoring data.* Structural Health Monitoring, 2015. **14**(1): p. 3-19.

56. Kapsenberg, G.K., *Slamming of ships: Where are we now?* Philosophical Transactions of the Royal Society A: Mathematical, Physical and Engineering Sciences, 2011. **369**(1947): p. 2892-2919.

57. Li, Z., Ringsberg, J.W., and Storhaug, G., *Time-domain fatigue assessment of ship side-shell structures.* International Journal of Fatigue, 2013. **55**: p. 276-290.

58. French, B., *Slamming of Large High-Speed Catamarans in Irregular Seas. PhD thesis.* 2012, University of Tasmania: Launceston, Australia.

59. American Bureau of Shipping, *Guidance Notes on Spectral-Based Fatigue Analysis For Vessels*. 2012, American Bureau of Shipping: Houston, USA.

60. Det Norske Veritas, *Fatigue Assessment of Ship Structures*. 2010, Classification Notes 30.7, Det Norske Veritas: Høvik.

61. Gao, Z. and Moan, T., *Frequency-domain fatigue analysis of wide-band stationary Gaussian processes using a trimodal spectral formulation.* International Journal of Fatigue, 2008. **30**(10-11): p. 1944-1955.

62. Sgarioto, D., Turner, T., van Walree, F., and Macfarlane, G., *Development and Validation of a Non-Linear Seakeeping Tool For High Speed Craft*, in *Pacific 2015 International Maritime Conference*. 2015: Sydney, Australia.

63. Dessi, D. and Ciappi, E., *Slamming clustering on fast ships: From impact dynamics to global response analysis.* Ocean Engineering, 2013. **62**: p. 110-122.

64. McNamara, J. and Connolly, J., *Prediction of Global Loads and Vessel Response to Wave Impact Loading*, in *20th International Conference on Offshore Mechanics and Arctic Engineering*. 2001: Rio de Janeiro, Brazil.

65. Thomas, G., Winkler, S., Davis, M., Holloway, D., Matsubara, S., Lavroff, J., and French, B., *Slam events of high-speed catamarans in irregular waves.* Journal of Marine Science and Technology, 2011. **16**(1): p. 8-21.

66. Kapsenberg, G.K., Van't Veer, A.P., Hackett, J.P., and Levadou, M.M.D., *Aftbody slamming and whipping loads.* Transactions - Society of Naval Architects and Marine Engineers, 2003. **111**: p. 213-231.

67. Zimmerman, G., *The U.S. Navy Littoral Combat Ship: Current Issues and How to Employ it in the Future*. 2012, United States Marine Corps: Virginia, United States.

68. Stewart, C., *Patrol boats can't stay shipshape*, in *The Australian*. 2012, News Corp Australia: Sydney, Australia.

69. Stewart, C., *Cracks curtail border patrols*, in *The Australian*. 2014, News Corp Australia: Sydney, Australia.

70. Stewart, C. and Taylor, P., *Border patrols at breaking point over asylum boats*, in *The Australian*. 2013, News Corp Australia: Sydney, Australia.

71. Collette, M. and Incecik, A., *An approach for reliability-based fatigue design of welded joints on aluminium high-speed vessels.* Journal of Ship Research, 2006. **50**(1): p. 85-98.

72. Tuitman, J., Bosman, T., and Harmsen, E., *Local structural response to seakeeping and slamming loads*, in *Marine Structures*. 2013. p. 214-237.

73. Khedmati, M.R. and Pedram, M., *A numerical investigation into the effects of slamming impulsive loads on the elastic-plastic response of imperfect stiffened aluminium plates.* Thin-Walled Structures, 2014. **76**: p. 118-144.

74. Kim, J., Kim, Y., Yuck, R., and Lee, D., *Comparison of slamming and whipping loads by fully coupled hydroelastic analysis and experimental measurement.* Journal of Fluids and Structures, 2015. **52**: p. 145-165.

75. *Defence Capability Development Handbook 2012*, Department of Defence, Editor. 2012, Capability Development Group: Canberra, Australia.

76. Sea Power Centre – Australia, *Welcome to the Armidale Class*. 2006: Canberra, Australia.

77. Magoga, T., *Trials and Tribulations: Load and Structural Response Measurements of a Naval Semi-Planing Craft*, in *Pacific 2017 International Maritime Conference*. 2017: Sydney, Australia.

78. Hind, R. *Defence Minister David Johnstone defends the Armidale Class Patrol Boat after HMAS Bundaberg fire*. ABC News, 2014.

79. Department of Defence *Approved Major Capital Equipment Projects: Top 30 Projects by 2004-05 Expenditure*. SEA 1444 Armidale-class Patrol Boat, 2005.

80. Sabatino, S. and Frangopol, D.M., *Decision making framework for optimal SHM planning of ship structures considering availability and utility.* Ocean Engineering, 2017. **135**: p. 194-206.

81. Stambaugh, K., Drummen, I., Cleary, C., Sheinberg, R., and Kaminski, M., *Structural fatigue life assessment and sustainment implications for a new class of US coast guard cutters.* Transactions - Society of Naval Architects and Marine Engineers, 2014. **122**: p. 434-444.

82. DNV GL. *Stress measurement and monitoring*. [website] 2018 20/11/18]; Available from: https://www.dnvgl.com/services/stress-measurement-and-monitoring-2447.

83. Magoga, T. and Morris, B., *An Investigation into RAN Ship Structural Life-of-Type Management without Hull Monitoring Systems*. 2019, DST-Group-TN-1826, Defence Science and Technology Group: Melbourne, Australia.

84. Phelps, B. and Morris, B., *Review of Hull Structural Monitoring Systems for Navy Ships*. 2013, DSTO-TR-2818: Melbourne, Australia.

85. Okasha, N.M., Frangopol, D.M., Saydam, D., and Salvino, L.W., *Reliability analysis and damage detection in high-speed naval craft based on structural health monitoring data.* Structural Health Monitoring, 2011. **10**(4): p. 361-379.

86. Gardiner, C., Vincent, P., Wilson, A., Ellery, D., and Armstrong, T., *A trial sensor network for the Armidale Class patrol boat*, in *International Maritime Conference, Pacific 2008*. 2008: Sydney, Australia. p. 504-514.

87. Magoga, T., Riding, B., and Aksu, S., *Fatigue Assessment of the Armidale Class Patrol Boat using the S-N Approach Applied to Full-Scale Measurements* 2016, DST Group-TR-3298, Defence Science and Technology Group: Melbourne, Australia.

88. MathWorks, *MATLAB R2015b*. 2015, Natick, United States of America.

89. Magoga, T., Aksu, S., Cannon, S., Ojeda, R., and Thomas, G., *Identification of Slam Events Experienced by a High-Speed Craft.* Ocean Engineering, 2017. **140**: p. 309-321.

90. Dawes-Lynch, J. and Magoga, T., *HMAS Maryborough Hull Monitoring System: Data Processing and Analysis Methods*. 2017, DST Group-GD-0952, Defence Science and Technology Group: Melbourne, Australia.

91. *Armidale Class Patrol Boat Assest Management and Planning System Data*. 2012, Defence Materiel Organisation.

92. Garbatov, Y. and Guedes Soares, C., *Structural maintenance planning based on historical data of corroded deck plates of tankers.* Reliability Engineering & System Safety, 2009. **94**(11): p. 1806-1817.

93. Bharadwaj, U. and Wintle, J., *Risk-based optimization of inspection planning in ships.* Journal of Ship Production, 2011. **27**(3): p. 111-117.

94. Hodkiewicz, M. and Tien-Wei Ho , M., *Cleaning historical maintenance work order data for reliability analysis.* Journal of Quality in Maintenance Engineering, 2016. **22**(2): p. 146-163.

95. Hifi, N. and Barltrop, N., *Correction of prediction model output for structural design and risk-based inspection and maintenance planning.* Ocean Engineering, 2015. **97**: p. 114-125.

96. DRS Defense Solutions, *MAESTRO 11.0.0*. 2013: Stevensville.

97. Magoga, T., *Development and Verification of a Finite Element Model of the Armidale Class Patrol Boat*. 2013, DSTO-TR-2811, Defence Science and Technology Organisation: Melbourne, Australia.

98. Basu, R., Kirkhope, J., and Srinivasan, J., *Guideline for Evaluation of Finite Elements and Results*. 1996, Ship Structure Committee, US Coast Guard: Washington, DC, USA.

99. Miner, M., *Cumulative damage in fatigue.* Journal of Applied Mechanics, 1945. **12**: p. 159-164.

100. Yeter, B., Garbatov, Y., and Guedes Soares, C., *Evaluation of fatigue damage model predictions for fixed offshore wind turbine support structures.* International Journal of Fatigue, 2016. **87**: p. 71-80.

101. Hobbacher, A., *Recommendations for fatigue design of welded joints and components*. 2008, XIII-1539-96 / XV-845-96, International Institute of Welding: Paris, France.

102. Technical Committee CEN/TC 250, *Eurocode 9: Design of aluminium structures*. 1999, British Standards: Brussels, Belgium.

103. Zhang, Y.-H. and Maddox, S.J., *Investigation of fatigue damage to welded joints under variable amplitude loading spectra.* International Journal of Fatigue, 2009. **31**(1): p. 138-152.

104. Cui, W., Wang, F., and Huang, X., *A unified fatigue life prediction method for marine structures.* Marine Structures, 2011. **24**(2): p. 153-181.

105. Ravi Chandran, K.S., Chang, P., and Cashman, G.T., *Competing failure modes and complex S–N curves in fatigue of structural materials.* International Journal of Fatigue, 2010. **32**(3): p. 482-491.

106. Cosso, G.L., Rizzo, C.M., and Servetto, C., *Fitness-for-service assessment of defected welded structural details by experimental evaluation of the fatigue resistance S-N curve.* Welding in the World, 2016. **60**(5): p. 847-858.

107. Kramer, R., Rampolla, B., and Magnussen, A., *Fatigue of Aluminum Structural Weldments*. 2000, SSC-410, Ship Structure Committee,: Washington, United States.

108. Johnson, N.R., Lynch, J.P., and Collette, M.D., *Response and fatigue assessment of high speed aluminium hulls using short-term wireless hull monitoring.* Structure and Infrastructure Engineering, 2018. **14**(5): p. 634-651.

109. Drummen, I., Hageman, R., and Stambaugh, K., *Structural fatigue life assessment and maintenance needs for a new class of US Coast Guard Cutters*, in *Life-Cycle of Engineering Systems: Emphasis on Sustainable Civil Infrastructure*. 2017. p. 1919-1926.

110. Neuberg, O. and Drimer, N., *Fatigue limit state design of fast boats.* Marine Structures, 2017. **55**: p. 17-36.

111. Horn, A., Andersen, M., Biot, M., Bohlmann, B., Mahérault-Mougin, S., Kozak, J., Osawa, N., Jang, Y., Remes, H., Ringsberg, J., and van der Cammen, J., *TCIII.2: Fatigue and Fracture*, in *Proceedings of the 17th International Ship and Offshore Structures Congress*. 2009, Seoul National University: Seoul, South Korea. p. 211-287.

112. Du Toit, M. and Mutombo, K., *Reduction in fatigue strength of arc welded aluminium 5083-H111 on immersion in NaCl.* Advanced Materials Research, 2014(891-892): p. 1469.

113. Blagojevic, B., Domazet, Z., and Kalman, Z., *Productional, Operational, and Theoretical Sensitivities of Fatigue Damage Assessment in Shipbuilding.* Journal of Ship Production, 2002. **18**(4): p. 185-194.

114. Tveiten, B., Wang, X., and Berge, S., *Fatigue assessment of aluminum ship details by hot-spot stress approach.* Transactions - Society of Naval Architects and Marine Engineers, 2007. **115**: p. 31-49.

115. Shen, W., Yan, R., Barltrop, N., Liu, E., and Song, L., *A method of determining structural stress for fatigue strength evaluation of welded joints based on notch stress strength theory.* International Journal of Fatigue, 2016. **90**: p. 87-98.

116. Xiao, Z.-G. and Yamada, K., *A method of determining geometric stress for fatigue strength evaluation of steel welded joints.* International Journal of Fatigue, 2004. **26**(12): p. 1277-1293.

117. Fricke, W., *Fatigue analysis of welded joints: state of development.* Marine Structures, 2003. **16**(3): p. 185-200.

118. Matic, T. and Domazet, Z., *Determination of structural stress for fatigue analysis of welded aluminium components subjected to bending.* Fatigue & Fracture of Engineering Materials & Structures, 2005. **28**(9): p. 835-844.

119. Jensen, J., *Load and global response of ships*. 2001, Oxford: Elsevier Science.

120. Matsuishi, M. and Endo, T., *Fatigue of metals subjected to varying stress*, in *Japan Society of Mechanical Engineers*. 1968: Fukuoka, Japan.

121. Lee, Y., Barkey, M., and Hong-Tae, K., *Metal Fatigue Analysis Handbook Practical Problem-Solving Techniques for Computer-Aided Engineering*. 2012, Sydney: Butterworth-Heinemann

122. Kecsmar, J. and Shenoi, R.A., *Some notes on the influence of manufacturing on the fatigue life of welded aluminum marine structures.* Journal of Ship Production, 2004. **20**(3): p. 164-175.

123. Syahroni, N. and Berge, S., *Fatigue Assessment of Welded Joints Taking Into Account Effects of Residual Stress.* Journal of Offshore Mechanics and Arctic Engineering 2010. **134**(2).

124. Al Zamzami, I. and Susmel, L., *On the accuracy of nominal, structural, and local stress based approaches in designing aluminium welded joints against fatigue.* International Journal of Fatigue, 2017. **101**: p. 137-158.

125. Radaj, D., Sonsino, C.M., and Fricke, W., *Recent developments in local concepts of fatigue assessment of welded joints.* International Journal of Fatigue, 2009. **31**(1): p. 2-11.

126. Magoga, T., Aksu, S., Cannon, S., Ojeda, R., and Thomas, G., *Comparison between Fatigue Life Values Calculated Using Standardised and Measured Stress Spectra of a Naval High Speed Light Craft*, in *13th International Symposium on the Practical Design of Ships and Other Floating Structures*. 2016: Copenhagen, Denmark.

127. International Association of Classification Societies, *Common Structural Rules for Bulk Carriers and Oil Tankers*. 2010: London, United Kingdom.

128. Wolberg, J., *Designing Quantitative Experiments: Prediction Analysis*. 2010, Berlin, Germany: Springer.

129. Hess, P., Aksu, S., Blake, J.I.R., Boote, D., Caridis, P., Egorov, A., Fjeldstad, A., Hoogeland, M., Murayama, H., Anderson, M.R., and Tammer, M., *Structural Longevity*, in *Proceedings of the 19th International Ship and Offshore Structures Congress*. 2015: Cascais, Portugal. p. 211-287.

130. Moan, T., *Life cycle structural integrity management of offshore structures.* Structure and Infrastructure Engineering, 2018. **14**(7): p. 911-927.

131. International Organization for Standardization, *Welding - Arc-welded joints in aluminium and its alloys - Quality levels for imperfections*. 2005, ISO 10042:2005.

132. Garbatov, Y., Rudan, S., and Guedes Soares, C., *Fatigue assessment of welded trapezoidal joints of a very fast ferry subjected to combined load.* Engineering Structures, 2010. **32**: p. 800-807.

133. Det Norske Veritas, *Fatigue Assessment of Ship Structures, Classification Note No. 30.7*. 2010: Høvik, Norway.

134. Beer, M., Ferson, S., and Kreinovich, V., *Imprecise probabilities in engineering analyses.* Mechanical Systems and Signal Processing, 2013. **37**(1-2): p. 4-29.

135. Maljaars, J. and Vrouwenvelder, A.C.W.M., *Probabilistic fatigue life updating accounting for inspections of multiple critical locations.* International Journal of Fatigue, 2014. **68**: p. 24-37.

136. Wang, Y., *Spectral fatigue analysis of a ship structural detail – A practical case study.* International Journal of Fatigue, 2010. **32**: p. 310-317.

137. Horn, A., Anderson, M., Biot, M., Bohlmann, B., Mahérault-Mougin, S., Kozak, J., Osawa, N., Jang, Y., Remes, H., Ringsberg, J., and van der Cammen, J. *Committee III.2 Fatigue and Fracture*. in *17th International Ship and Offshore Structures Congress*. 2009. Seoul, Korea.

138. Guo, T., Li, A., and Wang, H., *Influence of ambient temperature on the fatigue damage of welded bridge decks.* International Journal of Fatigue, 2008. **30**: p. 1092-1102.

139. Engesvik, K.M. and Moan, T., *Probabilistic analysis of the uncertainty in the fatigue capacity of welded joints.* Engineering Fracture Mechanics, 1983. **18**(4): p. 743-762.

140. Wirsching, P.H., *Fatigue reliability for offshore structures.* Journal of Structural Engineering (United States), 1984. **110**(10): p. 2340-2356.

141. Ćorak, M., Parunov, J., and Guedes Soares, C., *Long-term prediction of combined wave and whipping bending moments of container ships.* Ships and Offshore Structures, 2013.

142. Colwell, J. and Stredulinsky, D., *Seakeeping Operator Guidance*, in *Pacific 2012 International Maritime Conference*. 2008: Sydney, Australia.

143. Aksu, S., Magoga, T., and Riding, B., *Analysis of HMAS GLENELG's Onboard Structural Monitoring Data*, in *Pacific 2015 International Maritime Conference*. 2015: Sydney, Australia.

144. Carrera, G. and Rizzo, C., *Measurements of Motions, Loads and Structural Response on a Fast FRP Pleasure Craft*, in *International Conference on Fast Sea Transportation, FAST'2005*. 2005: St. Petersburg, Russia.

145. Kwon, K., Frangopol, D., and Kim, S., *Fatigue performance assessment and service life prediction of high-speed ship structures based on probabilistic lifetime sea loads.* Structure and Infrastructure Engineering, 2013. **9**(2): p. 102-115.

146. *MAESTRO 11.2.2*. 2015, DRS Defense Solutions: Stevensville, USA.

147. Ito, Y., Nielsen, U., and Jensen, J., *Estimation of Fatigue Damage from Full-Scale Measurements of Hull Girder Stresses*, in *11th International Symposium on Practical Design of Ships and Other Floating Structures*. 2010: Rio de Janeiro, Brazil.

148. Ochi, M., *Prediction of the occurrence and severity of ship slamming at sea*, in *5th Symposium on Naval Hydrodynamics*. 1964: Bergen, Norway.

149. Engle, A., Lin, W., Salvesen, N., and Shin, Y., *Application of 3-D nonlinear wave-load and structural-response simulations in naval ship design.* Naval Engineers Journal, 1997. **109**(3): p. 253-265.

150. Fricke, W. and von Lilienfeld-Toal, A., *Annahmen von Beanspruchungskollektiven für Schiffskonstruktionen und deren Absicherung durch Messung.* Materials Testing, 2008. **50**(11-12): p. 721-728.

151. Germanischer Lloyd, *Rules for Classification and Construction Ship Technology, Seagoing Ships*. 2013, Germanischer Lloyd: Hamburg, Germany.

152. Dwyer, D., Magoga, T., and Morris, B., *Fatigue life as a factor in assessing warship design flexibility to support batch-building programs*, in *7th International Conference on Marine Structures (MARSTRUCT 2019)*. 2019.

153. Magoga, T. and Dwyer, D., *Fatigue Life as a Variable in Assessing Naval Ship Flexibility.* Naval Engineers Journal, 2018. **130**(3).

154. Wirsching, P.H., *Fatigue reliability in welded joints of offshore structures.* International Journal of Fatigue, 1980. **2**(2): p. 77-83.

155. Ćorak, M., Parunov, J., and Guedes Soares, C., *Probabilistic load combination factors of wave and whipping bending moments.* Journal of Ship Research, 2015. **59**(1): p. 11-30.

156. Tran Nguyen, K., Garbatov, Y., and Guedes Soares, C., *Spectral fatigue damage assessment of tanker deck structural detail subjected to time-dependent corrosion.* International Journal of Fatigue, 2013. **48**: p. 147-155.

157. Zhu, J. and Collette, M., *A Bayesian approach for shipboard lifetime wave load spectrum updating.* Structure and Infrastructure Engineering, 2017. **13**(2): p. 298-312.

158. Chiu, F.-C., Tiao, W.-C., and Guo, J., *Experimental study on the nonlinear pressure acting on a high-speed vessel in irregular waves.* Journal of Marine Science and Technology, 2009. **14**(2): p. 228-239.

159. Guzsvany, G., Flockhart, C., and Cannon, S., *Operational profile of naval surface ships and lifetime structural load analysis*, in *Pacific 2006 International Maritime Conference*. 2006: Sydney, Australia.

160. Thompson, I., *Validation of naval vessel spectral fatigue analysis using full-scale measurements.* Marine Structures, 2016. **49**: p. 256-268.

161. Aldous, L., Smith, T., Bucknall, R., and Thompson, P., *Uncertainty analysis in ship performance monitoring.* Ocean Engineering, 2015. **110**(Part B): p. 29-38.

162. Ma, M., Zhao, C., and Hughes, O., *A practical method to apply hull girder sectional loads to full-ship 3D finite-element models using quadratic programming.* Ships and Offshore Structures, 2014. **9**(3): p. 257-265.

163. Zhao, C. and Ma, M., *A hybrid 2.5-dimensional high-speed strip theory method and its application to apply pressure loads to 3-dimensional full ship finite element models.* Journal of Ship Production and Design, 2016. **32**(4): p. 216-225.

164. Rychlik, I., *Note on Cycle Counts in Irregular Loads.* Fatigue & Fracture of Engineering Materials & Structures, 1993. **16**(4): p. 377-390.

165. Magoga, T., Brincat, M., and Dawes-Lynch, J., *Verification of Pressure Sensors and Strain Gauges Installed Onboard HMAS Maryborough*. 2016, DST-Group-TN-1576, Defence Science and Technology Group: Melbourne, Australia.

166. QinetiQ North America, *Micro Air-launched Expendable Wave Buoy Operators Manual*. no date, QinetiQ North America: Slidell, USA.

167. Bretschneider, C., *Wave variability and wave spectra for wind generated gravity waves*. 1959, Tech. Memo. No. 118, Beach Erosion Board, US Army Corps of Eng: Washington DC, United States.

168. Li, Z., Mao, W., Ringsberg, J.W., Johnson, E., and Storhaug, G., *A comparative study of fatigue assessments of container ship structures using various direct calculation approaches.* Ocean Engineering, 2014. **82**: p. 65-74.

169. Mohammadi, S.F., Galgoul, N.S., Starossek, U., and Videiro, P.M., *An efficient time domain fatigue analysis and its comparison to spectral fatigue assessment for an offshore jacket structure.* Marine Structures, 2016. **49**: p. 97-115.

170. Magoga, T., Aksu, S., and Slater, K., *Proposed Implementation of Nominal Stress Approach for Fatigue Assessment of Aluminium Naval Ships.* Part M: Journal of Engineering for the Maritime Environment, submitted for publication.

171. *Recommended Procedures and Guidelines: Seakeeping Tests*. 2014, 7.5-02-05-04, International Towing Tank Conference: Denmark.

172. Saltelli, A., Chan, K., and Scott, E.M., eds. *Sensitivity Analysis*. 2008, John Wiley & Sons: Chichester.

173. Cannon, S., Guzsvany, G., and Turner, T., *A Study of the Effect of Wave Loading on a Frigate Operating in the Southern Ocean Versus the North Atlantic*, in *Pacific 2004 International Maritime Conference*. 2004: Sydney, Australia.

174. Molent, L. and Aktepe, B., *Review of fatigue monitoring of agile military aircraft.* Fatigue & Fracture of Engineering Materials & Structures, 2000. **23**: p. 767-785.

175. Jiao, G. and Moan, T., *Probabilistic analysis of fatigue due to Gaussian load processes.* Probabilistic Engineering Mechanics, 1990. **5**(2): p. 76-83.

176. Benasciutti, D. and Tovo, R., *Comparison of spectral methods for fatigue analysis of broad-band Gaussian random processes.* Probabilistic Engineering Mechanics, 2006. **21**(4): p. 287-299.

177. Magoga, T., Aksu, S., Cannon, S., Ojeda, R., and Thomas, G., *Through-Life Hybrid Fatigue Assessment of Naval Ships.* Ships and Offshore Structures, 2019. **14**(7).

178. Doshi, K. and Vhanmane, S., *Probabilistic fracture mechanics based fatigue evaluation of ship structural details.* Ocean Engineering, 2013. **61**(0): p. 26-38.

179. Ibrahim, R.A., *Overview of structural life assessment and reliability, part II: Fatigue life and reliability assessment of naval ship structures.* Journal of Ship Production and Design, 2015. **31**(2): p. 100-128.

180. Koenig, P., Nalchajian, D., and Hootman, J., *Ship Service Life and Naval Force Structure.* Naval Engineers Journal, 2009. **121**(1): p. 69-77.

181. Directorate General Technical Airworthiness. *Airworthiness Design Requirements Manual*. 2014 27/1/15]; Available from: http://www.defence.gov.au/DGTA/Documents/Publications/7001054/eADRM%20web/7117.htm.

182. Military Aviation Authority. *Structural Integrity Handbook*. 2015 14/01/17]; Available from: https://www.gov.uk/government/uploads/system/uploads/attachment_data/file/426205/Structural_Integrity_Handbook.pdf.

183. Chakarov, K., Garbatov, Y., and Guedes Soares, C., *Hot spot stress and stress concentration factors due to different fabrication imperfections in deck structures.* International Shipbuilding Progress, 2008. **55**(1-2): p. 47-62.

184. Meneghetti, G., *The peak stress method applied to fatigue assessments of steel and aluminium fillet-welded joints subjected to mode I loading.* Fatigue and Fracture of Engineering Materials and Structures, 2008. **31**(5): p. 346-369.

185. Thévenet, D., Ghanameh, M.F., and Zeghloul, A., *Fatigue strength assessment of tubular welded joints by an alternative structural stress approach.* International Journal of Fatigue, 2013. **51**: p. 74-82.

186. Ma, K. and Bea, R., *A Repair Management System for Fatigue Cracks in Ships.* SNAME Transactions, 1995. **103**: p. 343 - 396.

187. Swanton, G. and Walker, K., *Development of a Transfer function to Relate F-111 Aircraft Fatigue Data Analysis System (AFDAS) Strain Outputs to Loads and Control*

Point Stresses. 1997, DSTO-TR-0563, Defence Science and Technology Organisation: Melbourne, Australia.

188. Molent, L., *A unified approach to fatigue usage monitoring of fighter aircraft based on F/A-18 experience*, in *ICAS98, International Council of the Aeronautical Sciences*. 1998: Melbourne, Australia.

189. Frangopol, D.M. and Soliman, M., *Life-cycle of structural systems: recent achievements and future directions.* Structure and Infrastructure Engineering, 2016. **12**(1): p. 1-20.

190. Koboević, Ž., Bebić, D., and Kurtela, Ž., *New approach to monitoring hull condition of ships as objective for selecting optimal docking period.* Ships and Offshore Structures, 2018: p. 1-9.

191. International Organization for Standardization, *Petroleum and natural gas industries - fixed steel offshore structures*. 2014, ISO 19902:2007 + Amd 1:2013.

192. DNV GL, *Offshore Standards*. 2017, DNVGL-OS, DNV GL AS.: Oslo, Norway.

193. Aeran, A., Siriwardane, S.C., Mikkelsen, O., and Langen, I., *A framework to assess structural integrity of ageing offshore jacket structures for life extension.* Marine Structures, 2017. **56**: p. 237-259.

194. Hu, W., Tong, Y., Walker, K., Mongru, D., Amaratunga, R., and Jackson, P., *A Review and Assessment of Current Airframe Lifing Methodologies and Tools in Air Vehicles Division*. 2006, DSTO-RR-0321, Defence Science and Technology Organisation: Melbourne, Australia.

195. Bitner-Gregersen, E.M., Vanem, E., Gramstad, O., Hørte, T., Aarnes, O.J., Reistad, M., Breivik, Ø., Magnusson, A.K., and Natvig, B., *Climate change and safe design of ship structures.* Ocean Engineering, 2018. **149**: p. 226-237.

196. McNeish, D., *On Using Bayesian Methods to Address Small Sample Problems.* Structural Equation Modeling: A Multidisciplinary Journal, 2016. **23**(5): p. 750-773.

197. Magoga, T., Aksu, S., Cannon, S., Ojeda, R., and Thomas, G., *The Need for Fatigue Life Prediction Methods Tailored to High-Speed Craft: A Technical Review*, in *Pacific 2015 International Maritime Conference*. 2015: Sydney, Australia.

198. Doerry, N., *Making Risk Management Work*, in *Technology, Systems & Ships 2018*. 2018: Washington DC, United States.

199. Watkins, R., Meiers, M.W., and Visser, Y.L., *A Guide to Assessing Needs: Essential Tools for Collecting Information, Making Decisions and Achieving Development Results*. 2012, Washington DC: The World Bank.

200. Bryman, A., *Integrating quantitative and qualitative research: how is it done?* Qualitative Research, 2006. **6**(1): p. 97-113.

201. Tracy, S., *Qualitative Research Methods: Collecting Evidence, Crafting Analysis, Communicating Impact*. 2013, Chichester, UK: Wiley-Blackwell.

202. Leedy, P.D. and Ormrod, J.E., *Practical Research: Planning and Design*. 7th ed. 2001, Upper Saddle River, N.J.: Pearson Prentice Hall.

203. Dong, Y. and Frangopol, D.M., *Incorporation of risk and updating in inspection of fatigue-sensitive details of ship structures.* International Journal of Fatigue, 2016. **82**: p. 676-688.

204. Liu, Y., Frangopol, D.M., and Cheng, M., *Risk-informed structural repair decision making for service life extension of aging naval ships.* Marine Structures, 2019. **64**: p. 305-321.

205. Yang, D.Y. and Frangopol, D.M., *Evidence-based framework for real-time life-cycle management of fatigue-critical details of structures.* Structure and Infrastructure Engineering, 2018. **14**(5): p. 509-522.

206. Garbatov, Y. and Guedes Soares, C., *Uncertainty assessment of fatigue damage of welded ship structural joints.* Engineering Structures, 2012. **44**: p. 322-333.

207. Thompson, I., *Fatigue damage variation within a class of naval ships.* Ocean Engineering, 2018. **165**: p. 123-130.

208. Knight, J.T., Collette, M.D., and Singer, D.J., *Design for flexibility: Evaluating the option to extend service life in preliminary structural design.* Ocean Engineering, 2015. **96**: p. 68-78.

209. Drummen, I., Storhaug, G., and Moan, T., *Experimental and numerical investigation of fatigue damage due to wave-induced vibrations in a containership in head seas.* Journal of Marine Science and Technology, 2008. **13**(4): p. 428-445.

210. Diez-Olivan, A., Del Ser, J., Galar, D., and Sierra, B., *Data fusion and machine learning for industrial prognosis: Trends and perspectives towards Industry 4.0.* Information Fusion, 2019. **50**: p. 92-111.

211. Cui, W.C., *A feasibility study of fatigue life prediction for marine structures based on crack propagation analysis.* Proceedings of the Institution of Mechanical Engineers Part M: Journal of Engineering for the Maritime Environment, 2003. **217**(1): p. 11-23.

212. Baltrop, N. *Final Report Summary - RISPECT (Risk-Based Expert System for Through–Life Ship Structural Inspection and Maintenance and New-Build Ship Structural Design)*. 2013 6 December 2018]; Available from: https://cordis.europa.eu/docs/results/218499/final1-rispect-final-publishable-report.pdf.

213. Sielski, R., Wilkins, J.R., and Hults, J.A., *Supplemental Commercial Design Guidance for Fatigue*. 2002, SSC - 419: Washington, USA.

214. Department of Defence, *Navy's Operationalisation of the Naval Shipbuilding Plan*. 2017, Commonwealth of Australia: Canberra, Australia.

215. Morgenstern, R.D., Shih, J.-S., and Sessions, S.L., *Comparative risk assessment: an international comparison of methodologies and results.* Journal of Hazardous Materials, 2000. **78**(1): p. 19-39.

216. Dong, Y., Frangopol, D.M., and Sabatino, S., *A decision support system for mission-based ship routing considering multiple performance criteria.* Reliability Engineering & System Safety, 2016. **150**: p. 190-201.

217. Dawson, E., Morris, B., and Duffy, J., *Developing Australia's Indigenous Marine Vehicle Manoeuvring Analysis and Evaluation Capability*, in *Pacific 2012 International Maritime Conference*. 2012: Sydney, Australia.

218. Perez, I., DiUlio, M., Maley, S., and Phan, N., *Structural health management in the Navy.* Structural Health Monitoring, 2010. **9**(3): p. 199-207.

219. Koboević, Ž., Bebić, D., and Kurtela, Ž., *New approach to monitoring hull condition of ships as objective for selecting optimal docking period.* Ships and Offshore Structures, 2018. **14**(1): p. 1-9.

220. Johnson, R. and Christensen, L., *Educational Research Quantitative, Qualitative, and Mixed Approaches*. 2014, Thousand Oaks, United States: Sage.

221. Petricic, M. and Mansour, A.E., *Long-term correlation structure of wave loads using simulation.* Marine Structures, 2011. **24**(2): p. 97-116.

222. Faltinsen, O., *Sea Loads on Ships and Offshore Structures*. 1990, Cambridge, United Kingdom: Cambridge University Press.

223. Hasselmann, K., Barnett, T.P., Bouws, E., Carlson, H., Cartwright, D.E., Enke, K., Ewing, J.A., Gienapp, H., Hasselmann, D.E., Kruseman, P., Meerburg, A., Müller, P., Olbers, D.J., Richter, K., Sell, W., and Walden, H., *Measurements of wind-wave growth and swell decay during the Joint North Sea Wave Project (JONSWAP)*. 1973, Deutches Hydrographisches Institut.

224. Pierson, W. and Moskowitz, L., *A Proposed Spectral Form for Fully Developed Wind Seas Based on the Similarity Theory of S. A. Kitaigorodskii.* Journal of Geophysical Research, 1964. **69**(24): p. 5181-5190.

225. DNV GL, *Fatigue and ultimate strength assessment of container ships including whipping and springing*. 2015, DNVGL-CG-0153, DNV GL AS.: Oslo, Norway.

226. Director of Navy Platform Systems (DNPS), *DEF(AUST)5000 ADF Maritime Materiel Requirement Set*. Vol. 3: Hull System Requirements, Part 6: Seakeeping. 2003, Canberra, Australia: Department of Defence.

227. Garrett, S., *Southern Ocean operating area: The hunt for liquid Himalayas*. 2018, [presentation]. New Zealand Defence Force: New Zealand.

228. McDonald, M., Barter, S., Jones, R., and Molent, L., *Spectrum Fatigue Crack Growth Evaluation Using Variable Amplitude Data*. 2007, Engineers Australia. p. [180]-[205].

229. Magoga, T. and Aksu, S., *Progressive Failure Analysis of the Armidale Class Patrol Boat*. 2015, DSTO-TR-2813, Defence Science and Technology Organisation: Melbourne, Australia.

230. Lotsberg, I., Sigurdsson, G., Fjeldstad, A., and Moan, T., *Probabilistic methods for planning of inspection for fatigue cracks in offshore structures.* Marine Structures, 2016. **46**: p. 167-192.

231. Rosén, A. and Garme, K., *Slamming Studies on High-Speed Planing Craft through Full-Scale Trials and Simulations*, in *International Conference on Fast Sea Transportation (FAST'99)*. 1999: Seattle, USA.

232. Paik, J., Lee, J., Shin, Y., and Wang, G., *Design Principles and Criteria for Ship structures under Impact Pressure Loads Arising from Sloshing, Slamming and Green Seas.* Transactions - Society of Naval Architects and Marine Engineers, 2004. **112**.

233. *Actions and Action Effects*. 1999, Norwegian Standard N003, NORSOK: Norway.

234. Rosén, A., Garme, K., and Kuttenkeuler, J., *Full-Scale Design Evaluation of the Visby Class Corvette*, in *International Conference on Fast Sea Transportation, Fast'2007*. 2007: Shanghai, China.

235. Geertsma, R.D., Negenborn, R.R., Visser, K., and Hopman, J.J., *Design and control of hybrid power and propulsion systems for smart ships: A review of developments.* Applied Energy, 2017. **194**: p. 30-54.

236. *IPMS - Integrated Platform Management System*. 2018; Available from: https://www.logimatic.com/automation/maritime-automation/ipms-1.

237. Bøgh, S., *FW: Please contact me regarding IPMS from Logimatic [email]*, T. Magoga, Editor. 2018: Aalborg, Denmark.

238. Zimmerman, P., Gilbert, T., and Salvatore, F., *Digital engineering transformation across the Department of Defense.* The Journal of Defense Modeling and Simulation: Applications, Methodology, Technology, 2017: p. 1-11.

239. Alam, K.M. and El Saddik, A., *C2PS: A Digital Twin Architecture Reference Model for the Cloud-based Cyber-Physical Systems*. Vol. PP. 2017. 1-1.

240. Royal Australian Navy, *Navy's Operationalisation of the Naval Shipbuilding Plan*. 2017, Commonwealth of Australia: Canberra.

241. Lewis, G., *ABS to pilot bow-to-stern Condition-Based Class for U.S. Navy's MSC*. 2018, American Bureau of Shipping (ABS): Houston, United States.

242. Kraft, E.M., *The Air Force Digital Thread/Digital Twin - Life Cycle Integration and Use of Computational and Experimental Knowledge*, in *54th AIAA Aerospace Sciences Meeting*. 2016, American Institute of Aeronautics and Astronautics.

243. Fu, T. *Navy Platform Digital Twin*. 2017 17/12/2018]; Available from: http://onlinepubs.trb.org/onlinepubs/mb/2017Spring/fu.pdf.

244. Ye, X.W., Ni, Y.Q., Wong, K.Y., and Ko, J.M., *Statistical analysis of stress spectra for fatigue life assessment of steel bridges with structural health monitoring data.* Engineering Structures, 2012. **45**: p. 166-176.

245. Farreras-Alcover, I., Chryssanthopoulos, M.K., and Andersen, J.E., *Data-based models for fatigue reliability of orthotropic steel bridge decks based on temperature, traffic and strain monitoring.* International Journal of Fatigue, 2017. **95**: p. 104-119.

246. Deng, Y., Liu, Y., Feng, D.M., and Li, A.Q., *Investigation of fatigue performance of welded details in long-span steel bridges using long-term monitoring strain data.* Structural Control and Health Monitoring, 2015. **22**(11): p. 1343-1358.

247. Kim, Y., Kim, B.H., Choi, B.K., Park, S.G., and Malenica, S., *Analysis on the full scale measurement data of 9400TEU container Carrier with hydroelastic response.* Marine Structures, 2018. **61**: p. 25-45.

248. Leira, B.J., *Reliability updating based on monitoring of structural response parameters.* Reliability Engineering and System Safety, 2016. **155**: p. 212-223.

[Page intentionally left blank]

Appendix A

Trials and Tribulations: Load and Structural Response Measurements of a Naval Semi-Planing Craft

This refereed conference paper was presented at the Pacific 2017 International Maritime Conference in Sydney, Australia. The citation is:

Magoga, T., *Trials and Tribulations: Load and Structural Response Measurements of a Naval Semi-Planing Craft*, in Pacific 2017 International Maritime Conference. 2017: Sydney, Australia.

Abstract

In mid-2016 sea trials were undertaken on the Royal Australian Navy Armidale Class Patrol Boat HMAS *Maryborough*. This vessel was instrumented with a hull monitoring system, which included strain gauges, a motion reference unit, a Global Positioning System, and an array of pressure transducers at a forward section of the hull. The objective of the trials was to extend the knowledge base on the loads and structural responses of the vessel, coupled to the wave environment, at specific headings and speeds. The work forms part of a larger effort to improve hydrodynamic, structural, and service life assessment methodologies of naval craft. Although relatively low sea states were encountered, the capability to acquire real-time environmental, loads, and response data was demonstrated. This achievement is non-trivial, as measurement of pressure at full-scale is relatively rare and is used to validate numerical hydrodynamic tools. The pressure at locations below and near the mean waterline tended to be harmonic, though the latter featured a one-sided cut-off due to the free surface crossing the hull. Above the waterline, in the bow flare region, the pressure featured a larger degree of non-linearity. The stress and pressure records were correlated, allowing their relationship to be qualitatively examined. The implications of the results on structural assessment procedures are discussed, and recommendations for further analysis are made.

A.1 Recommendations

The findings presented in this paper can be used in further work, as follows:

- It may be possible to expand and validate a quasi-static approach to applying both the wave and slam loads in FEA; that is, to idealise slam loading for application in FEA. This is important because the pressure impulse, or pressure integrated over a given area or time, is important in structural design [231, 232]. As the pulse length of the analysed slam event was 2.6 to 4.6 times the fundamental period of vibration of the ACPB with added mass [89], it can be assumed that the impulse behaves in the quasi-static domain [232, 233].
- To help improve existing semi-empirical design pressure formulae to cover naval ships. This could augment the work of Rosén *et al.* [234] that showed that the panel loads experienced by the Visby Class corvette were distinctly higher than the minimum requirements set by the classification society.

Appendix B

HMAS *Maryborough* Hull Monitoring System: Data Processing and Analysis Methods

This DST Group report was reviewed internally. The citation is:

Dawes-Lynch, J. and Magoga, T., *HMAS Maryborough Hull Monitoring System: Data Processing and Analysis Methods*. 2017, Defence Science and Technology Group: Melbourne, Australia.

Abstract

This report describes a systematic approach developed by DST Group to analyse usage monitoring data acquired from HMAS *Maryborough*. In the first section of the report, the required data analysis processes and their associated objectives are explained. This includes data retrieval, unpacking, conditioning, interrogation, health checking and calculations for structural stress analysis. Presented in the second section of the report is a user's guide for software tools that have been developed for the purpose of carrying out the required data analysis.

Appendix C

Verification of Pressure Sensors and Strain Gauges Installed Onboard HMAS *Maryborough*

This DST Group report was reviewed internally. The citation is:

Magoga, T., Brincat, M., and Dawes-Lynch, J., *Verification of Pressure Sensors and Strain Gauges Installed Onboard HMAS Maryborough*. 2016, Defence Science and Technology Group: Melbourne, Australia.

Abstract

In support of the operational availability and sustainment of the Armidale Class Patrol Boats, the Defence Science and Technology Group is undertaking research to improve structural integrity assessment of aluminium semi-planing vessels. As part of the program, HMAS *Maryborough* was instrumented with a Hull Monitoring System. To check the accuracy of strain and pressure measurements, verification of installed strain gauges and pressure sensors was undertaken. This report describes the method, collection of data, and results of the verification.

Appendix D

Fatigue Life as a Variable in Assessing Naval Ship Flexibility

The work presented in this appendix was published in the *Naval Engineers Journal*. The citation is:

Magoga, T. and Dwyer, D., *Fatigue Life as a Variable in Assessing Naval Ship Flexibility*. Naval Engineers Journal, 2018. 130(3).

Abstract

Recently established naval shipbuilding initiatives aim to grow national industry and facilitate ready technology insertion during different phases of the capability life cycle. In this landscape, combined with budgetary constraints and the complexities associated with ensuring the enduring capability of the fleet, a ship's structural performance is of importance. Ships should be sufficiently flexible to allow system upgrades and changes to operations. To assess the costs and benefits of options to meet evolving demands, it is critical to understand the contribution of a ship's structural performance to its capabilities. This is underscored by fatigue life prediction tools capable of linking structural parameters with other performance requirements. However, there is only a relatively small body of literature concerned with these elements. This paper presents a way to improve understanding of the uncertainties and interdependencies between the fatigue life and capability aspects of naval ships. Two case studies are presented: the first focuses on the effect of a potential technology upgrade on the fatigue life of two candidate ships for acquisition, the second on the effect of operational profile changes on the fatigue life of an in-service ship. The case studies evaluate the fatigue damage incurred at critical details of the different ships, which is significantly dependant on the operational profile and the added displacement due a technology upgrade. Finally, future work is discussed.

Appendix E

An Investigation into RAN Ship Structural Life-of-Type Management without Hull Monitoring Systems

This DST Group report was reviewed internally. The citation is:

Magoga, T. and Morris, B., *An Investigation into RAN Ship Structural Life-of-Type Management without Hull Monitoring Systems*. 2019, DST-Group-TN-1826, Defence Science and Technology Group: Melbourne, Australia.

Abstract

A preliminary study was conducted on the considerations, assumptions, and options for managing the structural Life of Type (LOT) of new Royal Australian Navy (RAN) ships without ship Hull Monitoring Systems (HMS). The study used critical thinking, or 'red teaming' techniques to identify the consequences of not implementing HMS on board RAN ships, as well as to identify LOT management strategies that do not use HMS. The key consequence is that the RAN's ability to manage LOT risks and fleet availability will be impacted. Three alternative LOT management strategies were identified. The study found that the three categories of approaches for LOT management without a HMS would lead to a lower level of confidence in the management of RAN ship LOT risks. This is mainly due to the need for accurate data on the ship's operational usage to manage its LOT risks with a high degree of confidence. This data, in combination with emerging technologies such as the Digital Twin, provides opportunities for condition-based maintenance and support for the RAN to be a 'smart owner'. Implementing HMS on board RAN ships will however incur through-life financial and human resource costs and decision-makers will need to trade off these costs with the LOT management and other benefits.

E.1 Integrated Platform Management System

An Integrated Platform Management System (IPMS) is a distributed control and monitoring system for a ship or submarine's mechanical, electrical and damage control machinery systems. This type of system architecture may be a possible option for hull monitoring synchronised with other shipboard systems that are already part of the IPMS (for example, navigation and propeller shaft speed).

A recent trend in both commercial and naval applications is the design of versatile ships. This has led to, for instance, an increase in the variety of hybrid propulsion and power supply architectures [235]. Increasing the sophistication and number of management/control/monitoring 'sub-systems' at the whole-of-ship level may enable links to functional specifications such as fleet availability and maintenance. Implementation of an IPMS that includes hull monitoring is a promising approach to assess and improve platform performance against multiple requirements for future 'smart ships' [145, 235].

IPMS technology has been implemented on many surface combatants and submarines, including Navantia's IPMS on the RAN Landing Helicopter Docks and Hobart Class and the Logimatic IPMS [236] on Danish warships. Logimatic advise that their system is capable of incorporating real-time data acquisition and monitoring of virtually any kind of equipment where sensors can be installed. Although to date they have not interfaced strain gauges and other hull monitoring hardware to their IPMS, it would be straight-forward to implement [237].

E.2 Digital Twin

The Digital Twin refers to a digital representation of a physical asset or system. It is a framework that integrates technical data, software, and knowledge into actionable information, to inform decision makers throughout a system's lifecycle [238]. The Digital Twin should represent all of the functionalities of the physical system [239].

The Digital Twin concept is currently a topic of interest in the research community. The requirement for digital engineering concepts has been driven by the need to adapt quickly to changing operational and threat environments, fiscal constraints, and the rapid pace of technology advancement [238, 240]. In addition, sensors and computer networks have become omnipresent; the analysis of acquired data from the physical environment is possible more than ever before [239]. For ship structural management the Digital Twin can facilitate condition based maintenance, rather than calendar-based hull surveys, to potentially increase a ship's operational availability and flexibility [241] and reduce the through-life cost of ownership.

The volume and type of data, and nature of decisions, vary throughout the lifecycle of the system. Therefore, a wide range of analytical tools need to be available in the Digital Twin for it to be effective [238].

Recent studies and uses of the Digital Twin concept include:

- The United States Air Force deployment of the Digital Twin concept, via a pilot study and development of an engineering knowledge management system [242].
- Fusion of measured data and physics-based models of naval vessels, in the form of the United States Navy Digital Twin. The aim of this research is to predict the optimum performance, materiel state, and susceptibility of a naval vessel. The anticipated outcome is enhanced resource allocation, logistics planning, and in-situ decision-making [243].
- ABS is building a Digital Twin for each vessel of the United States Navy's Military Sealift Command. The aim of the Digital Twin is to detect abnormal behaviour, thus acting as an early warning system for problems [241].

Appendix F Measurement Period for Fatigue Life Prediction

One of the underlying premises in this thesis is that the HMS data can be used to reduce uncertainties associated with long-term loads applied to a ship and, in turn, to perform improved structural performance assessment.

In order to conduct effective fatigue performance evaluation, representative stress histories should be applied. A relatively small amount of data may fail to cover the complexity and diversity of fatigue loading effects caused by environmental conditions. The question arises; how much data is enough? This question appears to be more directly addressed in literature pertaining to bridges than to ship structures. A measurement period of one year is considered to allow accurate strain-based fatigue and condition assessment of bridges because seasonal effects on traffic intensities are captured [138, 244-246]. For ships, a consensus on the required measurement period does not appear to exist. Whereas Kim *et al.* [247] used ten months of monitoring data to estimate the fatigue damage for a 20 year service life of a 9400TEU container carrier, Leira [248] based an investigation on the effect of ice loading on the fatigue damage of an icebreaker on a single expedition. Leira [248] also found that the short-term stress distribution could be well described by an exponential distribution.

The operational profile of a ship can be characterised by its area of operations (encountered wave environment), speed profile, and time at sea. HMAS *Glenelg* is considered representative of the Armidale class and it is assumed that the dataset obtained from the HMS is sufficiently extensive to permit valid analysis and conclusions to be drawn (refer to Section 6.2). The factors in determining if the dataset is long enough to appropriately quantify the distribution of stress ranges are given in Table F-1. These factors are based on experience reported in the literature and that of the Candidate.

Table F-1: Factors in determining if full-scale dataset is sufficiently extensive to derive long-term stress distribution (for example case of HMAS *Glenelg*)

Area of Operations	Based on the GPS data, it was determined that *Glenelg's* main area of operations was the Timor Sea and the parts of the Indian Ocean between Australia and Christmas Island. This is consistent with the activities of the fleet.
Annual Distribution of Operational Time	Figure F-1 presents the distribution of *Glenelg's* operational time per year over a 3.5 year period, based on GPS data. In northern Australia the wet season usually starts in November and ends in April, and is associated with greater storm activity than in the dry season. Figure F-1 indicates that there is reasonable coverage of both the wet and dry seasons in the HMS data.
Time at sea	*Glenelg* was at sea 43% of the time, which is comparable to the historical time at sea per year averaged across the fleet.
Stress spectra	The derived stress spectra can be fit to distributions (refer to Section 6.2).
Frequency domain representation	The modes of interest over the frequency range are evident in the data (spectral density estimation of the strain time records are presented in Section 5.3).

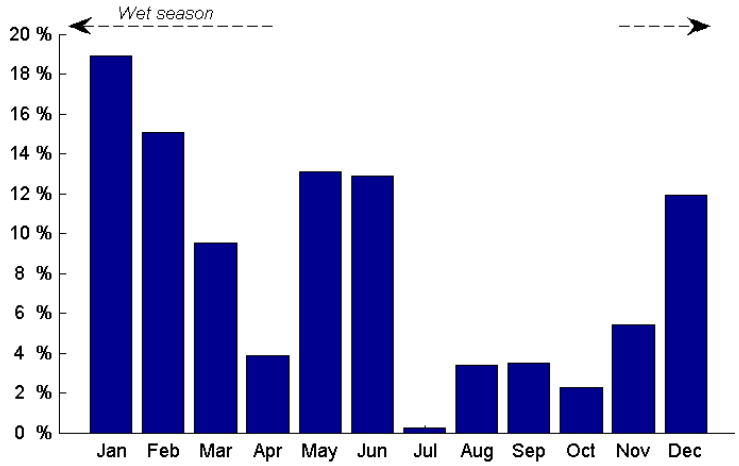

Figure F-1: Annual distribution of *Glenelg* operational time over 3.5 year period [87]

[Page intentionally left blank]